# Enhancing Accuracy and Reliability of Spinal Load Estimation in Lifting/Lowering Tasks: Insights from Inverse Dynamics-Based Multibody Modelling in OpenSim

**Mohammadhossein Akhavanfar**

Thesis submitted to the University of Ottawa
in partial Fulfillment of the requirements for the
Doctorate of Philosophy in Human Kinetics

School of Human Kinetics
Faculty of Health Sciences
University of Ottawa

# Table of Contents

# Dedication

I wish to dedicate this dissertation to the people of my homeland, Iran—those whose history, poetry, music, and culture have been rich with a desire for goodness towards their fellow human beings. Their kindness has nourished the roots of my existence, allowing me to grow and strive to take even small steps towards improving the health of people around the world.

I would like to dedicate this dissertation in a more particular way to the Women–Life–Freedom movement and the women of Iran, those who, through their resistance against injustice, have taught me profound lessons of life. They have kept hope alive in our hearts, reminding us that Iran will be saved from the corruption of those with malicious intentions.

## Acknowledgements

I extend my sincere gratitude to my thesis supervisor, Dr. Ryan Graham. Ryan, your invaluable guidance helped me navigate the peaks and valleys of the roller coaster ride of doctoral studies, and your encouragement and unwavering support were the reasons I enjoyed the ride as much as I did. Thank you not only for being such a great mentor for my academic growth, but also for looking out for my mental well-being and other aspects of life.

A heartfelt thank you to my co-authors and the members of the evaluation committee, whose guidance enriched the present thesis. I would like to especially thank Dr. Thomas Uchida, whose collaboration has been one of the highlights of my academic life. Thomas, your thoughtful and meticulous feedback significantly enhanced my skills as a researcher.

I am thankful for all my colleagues in Dr. Graham's laboratory. Working with all of you has been an amazing experience, and I take pride in our friendship. Alexandre and Matthew, your exceptional help greatly enhanced this dissertation and broadened my horizons as a researcher.

My dear Maman and Baba, writing this thesis would not have been possible without your efforts throughout my life. Although we have been physically apart for several years, your patience, encouragement, and unconditional love continue to help me grow every day. I will always be inspired by your approach to life.

My dear wife and best friend, Fatemeh, words cannot express my love and gratitude for you. I would say that your contribution to this work has been greater than mine. Without your love and kindness, your patience and support, your resilience and efforts, or simply, without you, I could not have done it. You complete me, you are my better half, and I love you.

# Co-Authorship

This dissertation contains material from four published manuscripts (Chapters 3–6). The authorship is as follows:

Chapter 3: Akhavanfar, M., Brandon, S.C.E., Brown, S.H.M., Graham, R.B., 2019. Development of a novel MATLAB-based framework for implementing mechanical joint stability constraints within OpenSim musculoskeletal models. J. Biomech. 91, 61–68.

Chapter 4: Akhavanfar, M., Uchida, T.K., Clouthier, A.L., Graham, R.B., 2022. Sharing the load: modelling loads in OpenSim to simulate two-handed lifting. Multibody Syst. Dyn. 54, 213–234.

Chapter 5: Akhavanfar, M., Uchida, T.K., Graham, R.B., 2023. Evaluation of spinal force normalization techniques. J. Biomech. 147, 111441.

Chapter 6: Akhavanfar, M., Mir-Orefice, A., Uchida, T.K., Graham, R.B., 2024. An enhanced spine model validated for simulating dynamic lifting tasks in OpenSim. Ann. Biomed. Eng. 52, 259–269.

For each manuscript, M. Akhavanfar completed the tasks of conceptualization and design of the research, acquisition of the data, analysis and interpretation of the data, writing the manuscripts, and critical revision of the manuscripts before publication.

# Abstract

This thesis aims to enhance the accuracy, reliability, and accessibility of estimating intervertebral forces during lifting/lowering tasks, with implications for improving back health in diverse settings, including workplaces. Four musculoskeletal multibody modelling studies using OpenSim were conducted to achieve these objectives.

First, a novel Stability-Constrained Static Optimization framework (SCSO) was developed for OpenSim to improve reliability in estimating spinal loads during static lifting tasks. The muscle activities predicted by the SCSO framework demonstrated closer agreement with electromyography data compared to those obtained by the default optimization solver in OpenSim, making it more suitable for estimating muscle forces and spinal joint loads during static tasks.

Next, the impact of five approaches for modelling hand–mass interaction on estimated spinal joint loads during dynamic lifting tasks was evaluated. Results indicated substantial differences in predicted spinal loads, particularly with increasing movement speed.

A new fully articulated thoracolumbar spine (FATLS) model was developed for Studies 3 and 4. Study 3 assessed techniques for normalizing spinal forces, aiming to remove body weight variation effects on spinal force estimates. The discussions of this study facilitated better result comparisons against experimental data in the final study.

The newly developed FATLS model's estimation of spinal forces was validated against experimental data during dynamic lifting/lowering tasks in Study 4. The results of Study 4 demonstrated accurate capture of changes in maximum forces across various dynamic lifting tasks as well as effectively predicting time-varying spinal forces using the FATLS model.

Key recommendations of the present thesis include using the FATLS model for estimating intervertebral forces during lifting tasks due to its high biofidelity, accessibility, and validation to a greater extent than previous models. Additionally, employing the SCSO framework is advised for estimating muscle activation patterns during static lifting tasks. Lastly, it is suggested to report uncertainty of spinal force estimates associated with the employed modelling approach for external hand forces and moments.

Adhering to these recommendations can empower researchers and practitioners in occupational biomechanics, enabling more effective use of musculoskeletal modelling and contributing to improved back health.

# List of Figures

# List of Tables

## Definition of Terms

| | |
|---|---|
| **API** | Application Programming Interface |
| **BW** | Body Weight |
| **BWDN** | Body Weight Division Normalization |
| **BWON** | Body Weight Offset Normalization |
| **BWPCN** | Body Weight Power Curve Normalization |
| **COM** | Centre of Mass |
| **COP** | Centre of Pressure |
| **DOF** | Degrees of Freedom |
| **EHF&M** | External Hand Forces and Moments |
| **EMG** | Electromyography |
| **FATLS** | Fully Articulated Thoracolumbar Spine |
| **FD** | Forward Dynamics |
| **FE** | Finite Element |
| **FLV** | Force–Length–Velocity |
| **GRF** | Ground Reaction Forces |
| **GRF&M** | Ground Reaction Forces and Moments |
| **ICC** | Intraclass Correlation Coefficient |
| **ID** | Inverse Dynamics |
| **IDP** | Intradiscal Pressure |
| **IK** | Inverse Kinematics |
| **IVD** | Intervertebral Disc |
| **JRA** | Joint Reaction Analysis |
| **LFB** | Lifting Full-Body |
| **MA** | Muscle Analysis |
| **MSK** | Musculoskeletal |
| **MVC** | Maximum Voluntary Contraction |
| **OPT** | Optimization |
| **PK** | Point Kinematics |
| **RA** | Rectus Abdominis |
| **RMSE** | Root Mean Square Error |
| **RRA** | Residual Reduction Algorithm |
| **SCSO** | Stability-Constrained Static Optimization |
| **SDN** | Standing Division Normalization |
| **SO** | Static Optimization |
| **WMSD** | Work-Related Musculoskeletal Disorder |

# Chapter 1: General Introduction

## 1.1 Work-Related Musculoskeletal Disorders of the Spine

Work-related musculoskeletal disorders (WMSDs), and more specifically back disorders, are highly prevalent and represent a major worldwide health problem (Bonfiglioli et al., 2022; Cieza et al., 2020). For instance, WMSDs accounted for 29–35% and 50% of all occupational injuries and illnesses causing absence from work in the United States and Europe, respectively (Bevan, 2015; Bhattacharya, 2014). Based on Workplace Safety and Insurance Board reports, the total cost of work-related back disorders in 2021 was more than $90 million in Ontario alone.

The risk factors in the etiology of WMSDs can be characterized into three broad categories: 1) physical and biomechanical (e.g., inappropriate postures and repetitive movements), 2) psychosocial (e.g., low social support and stressful work), and 3) individual (e.g., gender and age) (Afsharian et al., 2023). These risk factors separately or through their interactions may lead to the development of WMSDs (Hernandez and Peterson, 2012). The present thesis is focusing on the physical and biomechanical aspect in the etiology of work-related back disorders. Injuries due to manual lifting play a major role in the etiology of back disorders, where statistical findings suggest about half of all back pain is related to manual lifting tasks (Ahmad and Muzammil, 2023). Therefore, more specifically, this thesis examines a specific aspect (i.e., biomechanical factors) of the etiology of work-related back disorders during lifting/lowering tasks, which paves the way for improving back health in workplaces.

## 1.2 Biomechanical Perspectives on Back Injuries

When investigating the risk of injuries from a biomechanical perspective, the assessment focuses on whether the internal loads on affected tissues exceed their internal tolerances. The term ‘load’ can refer to physical stresses with kinetic, kinematic, oscillatory, or thermal energy sources

(Radwin et al., 2002). In this thesis, the term 'internal loads' specifically refers to physical stresses with kinetic sources. Tissue failure or damage, which may result in pain, discomfort, impairment, and possibly disability, can be due to acute or repetitive loading (Kumar, 1994). In an acute trauma, a single identifiable event causes the internal loads to exceed tissue tolerance. In a cumulative trauma, repetitive loading (such as repeated exposures or exposures of sufficiently long duration) reduces the tissue's tolerance to the point where previously acceptable loads can now result in injury (Kumar, 1990; Potvin, 2008; Radwin et al., 2002). Therefore, determining internal loads is necessary for the biomechanical investigation of work-related back injuries.

Intervertebral loads have been measured *in vivo* by inserting needles equipped with pressure transducer tips into the intervertebral discs (Polga et al., 2004; Schultz et al., 1982; Wilke et al., 2001), or by inserting instrumented implants into patients who had received vertebral body replacement (Rohlmann et al., 2013). Due to the invasiveness associated with direct measurement of intervertebral loads, computational biomechanical models have been widely used to estimate intervertebral loads for various applications, including occupational biomechanics. These models aim to apply mechanical principles to analyze biological tissues, specifically the human spine in this thesis, and find the solution to mathematical equations that incorporate the geometry, physical attributes, and biomechanical properties of the modelled structure.

### 1.3 Computational Modelling of the Spine

Numerous computational models of the spine, varying in complexity, have been developed and used to estimate intervertebral forces during lifting/lowering tasks (Alizadeh et al., 2020; Bassani and Galbusera, 2018; Dreischarf et al., 2016; Lerchl et al., 2023). These models can be differentiated from each other based on various factors, including i) the biomechanical modelling approach (e.g., multibody vs. finite element models), ii) the motion-solving approach (e.g., inverse

vs. forward dynamics), iii) the constitutive elements of the model (e.g., properties and numbers of body segments, muscles, and ligaments), iv) the extent to which these models were validated, and v) the musculoskeletal modelling tool used for the simulation. All studies in the present thesis are focusing on estimating intervertebral forces using multibody dynamics–based musculoskeletal models along with inverse dynamic analyses in OpenSim. The rationale for this concentration will be briefly reviewed as follows.

In classic musculoskeletal multibody modelling of the spine, vertebral bones are idealized as rigid bodies (segments), and intervertebral discs are represented as mechanical joints (e.g., spherical joints), which restrict the relative motion between segments (Simeon, 2013). Muscles are modelled as actuators, and depending on the model complexity, additional mechanical elements such as springs, dampers, and bushings might be employed to simulate ligaments and other connective tissues (Bassani and Galbusera, 2018). Multibody modelling is well-suited for investigating macroscopic biomechanics and addressing fundamental questions regarding human motion (Stops et al., 2012). However, to gain insight into the microstructural, nonlinear material properties of tissues, and complex deformations of intervertebral discs, finite element models offer greater suitability. Finite element models discretize the domain into finite sub-domains or elements, based on continuum mechanics. Therefore, these models can analyze strain and stress distributions within different components of the spine, providing valuable information on phenomena such as remodelling, degradation, failure, and multi-physics couplings (Schmidt et al., 2013). While finite element models offer detailed insights, they are computationally demanding due to their higher level of complexity. Therefore, in the context of analyzing intervertebral loads at a holistic level, multibody modelling is more appropriate for the studies in this thesis. Its

simplified representation allows for efficient analysis and aligns with the research objectives of understanding intervertebral loads within a broader context.

Multibody spine models have been developed using various tools, including in-house codes as well as commercial and open-source software packages. The commercial software packages include, but are not limited to, AnyBody (AnyBody Technology, Aalborg, Denmark), ADAMS (Hexagon AB, Newport Beach, United States), SIMM (Musculographics Inc., Santa Rosa, United States), SIMPACK (Dassault systèmes, France), RECURDYN$^{TM}$ (Function Bay Inc., Seongnam, Korea), and LifeMOD$^{TM}$ (LifeModeler Inc., San Clemente, United States). The two notable open-source software packages utilized in the development of multibody spine models are OpenSim (SimTK, Stanford, United States) and ArtiSynth (University of British Columbia, Vancouver, Canada). OpenSim (Delp et al., 2007) is the most widely used multibody musculoskeletal modelling platform, offering a comprehensive set of extensible tools and libraries designed for musculoskeletal modelling and simulation (Seth et al., 2018). Considering the versatility, reliability, and extensive documentation of OpenSim, as well as its widespread adoption in the field of biomechanics, it was selected as the primary software platform for all the studies conducted in this thesis.

In multibody modelling, the motion of constrained bodies and the forces acting on them are described using equations derived from Newton's second law. These equations can be solved using inverse or forward dynamics approaches. In inverse dynamics simulations, internal forces and moments (e.g., muscle forces and moments) are calculated based on known (measured or estimated) movements and external forces (Otten, 2003). On the other hand, in the forward dynamics motion-solving approach, internal forces and moments are first derived without assuming known kinematics, and then the motion is calculated from the known internal forces and

moments (Otten, 2003). The overarching purpose of this thesis is to provide insights into the safety of lifting/lowering tasks by estimating intervertebral loads based on known movements and external forces, thus requiring a descriptive motion-solving approach rather than a predictive one. Therefore, the modelling studies in this thesis focus on inverse dynamics analysis.

In the inverse dynamics motion-solving approach, the calculation of net external forces and torques at each joint becomes possible once the kinematic data and known external forces and moments are available. The subsequent step involves computing muscle forces using dynamic equilibrium equations, enabling the determination of intervertebral forces that represent the internal loads borne by the joint structure. However, it is essential to note that biofidelic spine models pose a challenge, as the number of unknown muscle forces exceeds the available equilibrium equations, resulting in a highly redundant muscle recruitment problem. To address this redundancy, various methods can be employed, including mathematical optimization, electromyography (EMG), or hybrid approaches. EMG and hybrid approaches, by leveraging EMG signals, possess a physiological foundation that accounts for inter- and intra-subject variability, potentially enabling a more comprehensive capture of various patterns of agonistic synergy and antagonistic co-contraction in solving the muscle recruitment problem compared to optimization-based models (Banks et al., 2022; Gagnon et al., 2001). However, optimization-based models are commonly utilized in spine modelling due to limitations associated with EMG, such as numerous assumptions related to cross-talk issues (recording nearby muscle activity) and the challenge of determining appropriate gains for muscles to satisfy equilibrium equations (Dreischarf et al., 2016; Lerchl et al., 2023). Hence, this thesis employed mathematical optimization in all studies to solve for muscle forces, making it a more ecologically suitable choice for applications outside of laboratory settings, such as in workplaces.

## 1.4 Thesis Statement

The global objective of this thesis is to estimate intervertebral forces during lifting and lowering tasks with improved accuracy, reliability, and accessibility compared to previous studies. Achieving this goal ultimately enhances our knowledge of identifying hazardous lifting and lowering conditions in workplaces and enables the design of new ergonomic interventions to reduce the risk of occupational back injuries. This overarching objective was achieved through the execution of the following four studies.

## 1.5 Study 1

The common optimization-based models used in musculoskeletal modelling software packages, including OpenSim, have a major shortcoming: they do not account for the realistic activations of antagonist muscles (Bassani and Galbusera, 2018; Le et al., 2017; Lerchl et al., 2023). This limitation arises from the optimization goal of minimizing a cost function which avoids increasing the joint demand, thus disregarding the co-contraction of antagonist muscles. Consequently, the muscle activation patterns assessed by common optimization-based models may not accurately reflect reality, thereby limiting the accurate prediction of intervertebral forces. Recognizing this inherent limitation, a few studies have tackled this issue by incorporating mechanical joint stability as an additional constraint in their in-house codes and captured more realistic muscle activation patterns during static tasks (Hajihosseinali et al., 2014). In line with these efforts, Study 1 presents an open-source framework which incorporates stability constraints within the default optimization solver in OpenSim. This framework is designed to be generalizable to a wide range of OpenSim models, regardless of their complexity.

### 1.6 Study 2

While Study 1 made significant advancements in predicting the synergy of antagonist and agonist muscle activations during static and quasi-static tasks, the validation of spinal forces estimated by the previously developed models during such tasks has generally demonstrated good agreement with experimental data (Bayoglu et al., 2017; Bruno et al., 2015). On the other hand, the importance of analysis of dynamic lifting tasks and its substantial influence on spinal forces are well understood (Fathallah et al., 1998; McGill and Norman, 1985). For instance, it has been shown that the risk of back injuries considerably increases with greater trunk velocities (Bazrgari et al., 2008; Marras et al., 1995). Nevertheless, few validation efforts have been conducted on spine models in the context of dynamic lifting/lowering tasks. Therefore, presenting and validating a spine model to a greater extent during dynamic lifting/lowering tasks will enhance the practical impact and applicability of the model.

The forces and moments that interact between the lifted mass and the hands, referred to as external hand forces and moments (EHF&M), play a critical role in estimating intervertebral forces as they are known quantities in the dynamic equilibrium problem within the inverse dynamics simulation workflow. In spine-modelling studies, two common approaches are used to model EHF&M during dynamic lifting tasks: considering them as static loads (i.e., applying gravity-oriented loads to the hands) or increasing the mass of the hands themselves. However, these common approaches greatly simplify the effect of EHF&M during dynamic lifting tasks, and the effect of these simplifications on the estimated intervertebral loads have not been investigated. Study 2 of this thesis introduces and thoroughly discusses five approaches (i.e., the two common approaches and three other proposed approaches) to model the interaction between the lifted mass and the hands during two-handed lifting tasks. Additionally, Study 2 is the first investigation that

explores the impact of different modelling decisions for hand–mass interaction on the estimated spinal joint loads.

### 1.7 Study 3

As stated earlier, numerous computational models of the spine have been developed, greatly contributing to our knowledge of spine biomechanics. However, the main goal of this thesis is to build upon the strengths of previous spine modelling studies while addressing their important limitations in modelling and validation. To address the modelling limitations, a new model was developed by enhancing a previously developed fully articulated thoracolumbar spine model in OpenSim. During the validation of estimated intervertebral forces by the new model in dynamic lifting tasks, it became apparent that to account for anthropometric differences, previous studies often divided spinal forces by body weight or by intervertebral loads during a neutral, unloaded standing posture. However, it has been recognized in the literature that these normalization techniques may not be adequate for other kinetic variables or tasks, such as ground reaction forces in walking (Stickley et al., 2018; Wannop et al., 2012). Therefore, Study 3 was conducted to investigate, for the first time, the effectiveness of four techniques for normalizing spinal forces and removing the effect of body weight.

### 1.8 Study 4

Building upon the developed methods and findings in Studies 2 and 3, Study 4 serves two main purposes. Firstly, it aims to validate the new model across a broader range of dynamic lifting/lowering tasks compared to previous spine musculoskeletal models. Secondly, it seeks to investigate the accuracy of the resulting spinal forces using each EHF&M approach. Ultimately, the author hopes that the findings from this thesis will pave the way towards achieving a consensus on the most suitable multibody model for estimating intervertebral loads during lifting/lowering

tasks, enabling the more effective use of musculoskeletal modelling in practice, and more specifically with occupational biomechanics. Therefore, all models and coding scripts are made freely available on our SimTK pages: https://simtk.org/projects/handloadinterac and https://simtk.org/projects/stab-so.

### 1.9 References


Afsharian, A., Dollard, M.F., Glozier, N., Morris, R.W., Bailey, T.S., Nguyen, H., Crispin, C., 2023. Work-related psychosocial and physical paths to future musculoskeletal disorders (MSDs). Saf. Sci. 164, 106177.

Ahmad, S., Muzammil, M., 2023. Revised NIOSH lifting equation: a critical evaluation. Int. J. Occup. Saf. Ergon. 29, 358–365.

Alizadeh, M., Knapik, G.G., Mageswaran, P., Mendel, E., Bourekas, E., Marras, W.S., 2020. Biomechanical musculoskeletal models of the cervical spine: A systematic literature review. Clin. Biomech. 71, 115–124.

Banks, J.J., Umberger, B.R., Caldwell, G.E., 2022. EMG optimization in OpenSim: A model for estimating lower back kinetics in gait. Med. Eng. Phys. 103, 103790.

Bassani, T., Galbusera, F., 2018. Musculoskeletal modelling. In: Galbusera, F., Wilke, H. (Eds.), Biomechanics of the Spine: Basic Concepts, Spinal Disorders and Treatments. Academic Press, Cambridge, pp. 257–277.

Bayoglu, R., Geeraedts, L., Groenen, K.H.J., Verdonschot, N., Koopman, B., Homminga, J., 2017. Twente spine model: A complete and coherent dataset for musculo-skeletal modelling of the lumbar region of the human spine. J. Biomech. 58, 52–63.

Bazrgari, B., Shirazi-Adl, A., Trottier, M., Mathieu, P., 2008. Computation of trunk equilibrium and stability in free flexion–extension movements at different velocities. J. Biomech. 41, 412–421.

Bevan, S., 2015. Economic impact of musculoskeletal disorders (MSDs) on work in Europe. Best Pract. Res. Clin. Rheumatol. 29, 356–373.

Bhattacharya, A., 2014. Costs of occupational musculoskeletal disorders (MSDs) in the United States. Int. J. Ind. Ergon. 44, 448–454.

Bonfiglioli, R., Caraballo-Arias, Y., Salmen-Navarro, A., 2022. Epidemiology of work-related musculoskeletal disorders. Curr. Opin. Epidemiol. Public Heal. 1, 18–24.

Bruno, A.G., Bouxsein, M.L., Anderson, D.E., 2015. Development and validation of a musculoskeletal model of the fully articulated thoracolumbar spine and rib cage. J. Biomech. Eng. 137, 081003.

Cieza, A., Causey, K., Kamenov, K., Hanson, S.W., Chatterji, S., Vos, T., 2020. Global estimates of the need for rehabilitation based on the Global Burden of Disease study 2019: a systematic

analysis for the Global Burden of Disease Study 2019. Lancet 396, 2006–2017.

Delp, S.L., Anderson, F.C., Arnold, A.S., Loan, P., Habib, A., John, C.T., Guendelman, E., Thelen, D.G., 2007. OpenSim: Open-source software to create and analyze dynamic simulations of movement. IEEE Trans. Biomed. Eng. 54, 1940–1950.

Dreischarf, M., Shirazi-Adl, A., Arjmand, N., Rohlmann, A., Schmidt, H., 2016. Estimation of loads on human lumbar spine: A review of in vivo and computational model studies. J. Biomech. 49, 833–845.

Fathallah, F.A., Marras, W.S., Parnianpour, M., 1998. An assessment of complex spinal loads during dynamic lifting tasks. Spine 23, 706–716.

Gagnon, D., Larivière, C., Loisel, P., 2001. Comparative ability of EMG, optimization, and hybrid modelling approaches to predict trunk muscle forces and lumbar spine loading during dynamic sagittal plane lifting. Clin. Biomech. 16, 359–372.

Hajihosseinali, M., Arjmand, N., Shirazi-Adl, A., Farahmand, F., Ghiasi, M.S., 2014. A novel stability and kinematics-driven trunk biomechanical model to estimate muscle and spinal forces. Med. Eng. Phys. 36, 1296–1304.

Hernandez, A.M., Peterson, A.L., 2012. Work-related musculoskeletal disorders and pain. In: Gatchel, R., Schultz I. (Eds.), Handbook of Occupational Health and Wellness. Springer, New York, pp. 63–85.

Kumar, S., 1990. Cumulative load as a risk factor for back pain. Spine 15, 1311–1316.

Kumar, S., 1994. A conceptual model of overexertion, safety, and risk of injury in occupational settings. Hum. Factors 36, 197–209.

Le, P., Best, T.M., Khan, S.N., Mendel, E., Marras, W.S., 2017. A review of methods to assess coactivation in the spine. J. Electromyogr. Kinesiol. 32, 51–60.

Lerchl, T., Nispel, K., Baum, T., Bodden, J., Senner, V., Kirschke, J.S., 2023. Multibody models of the thoracolumbar spine: A review on applications, limitations, and challenges. Bioengineering 10, 202.

Marras, W. S., Lavender, S. A., Leurgans, S. E., Fathallah, F. A., Ferguson, S. A., Gary Allread, W., Rajulu, S. L., 1995. Biomechanical risk factors for occupationally related low back disorders. Ergonomics 38, 377–410.

McGill, S.M., Norman, R.W., 1985. Dynamically and statically determined low back moments during lifting. J. Biomech. 18, 877–885.

Otten, E., 2003. Inverse and forward dynamics: models of multi-body systems. Philos. Trans. R. Soc. Lond. B. Biol. Sci. 358, 1493–1500.

Polga, D.J., Beaubien, B.P., Kallemeier, P.M., Schellhas, K.P., Lew, W.D., Buttermann, G.R., Wood, K.B., 2004. Measurement of in vivo intradiscal pressure in healthy thoracic intervertebral discs. Spine 29, 1320–1324.

Potvin, J.R., 2008. Occupational spine biomechanics: A journey to the spinal frontier. J. Electromyogr. Kinesiol. 18, 891–899.

Radwin, R.G., Marras, W.S., Lavender, S.A., 2002. Biomechanical aspects of work-related musculoskeletal disorders. Theor. Issues Ergon. Sci. 2, 153–217.

Rohlmann, A., Dreischarf, M., Zander, T., Graichen, F., Strube, P., Schmidt, H., Bergmann, G., 2013. Monitoring the load on a telemeterised vertebral body replacement for a period of up to 65 months. Eur. Spine J. 22, 2575–2581.

Schmidt, H., Galbusera, F., Rohlmann, A., Shirazi-Adl, A., 2013. What have we learned from finite element model studies of lumbar intervertebral discs in the past four decades? J. Biomech. 46, 2342–2355.

Schultz, A., Andersson, G., Ortengren, R., Haderspeck, K., Nachemson, A., 1982. Loads on the lumbar spine. Validation of a biomechanical analysis by measurements of intradiscal pressures and myoelectric signals. J. Bone Joint Surg. Am. 64, 713–720.

Seth, A., Hicks, J.L., Uchida, T.K., Habib, A., Dembia, C.L., Dunne, J.J., Ong, C.F., DeMers, M.S., Rajagopal, A., Millard, M., 2018. OpenSim: Simulating musculoskeletal dynamics and neuromuscular control to study human and animal movement. PLoS Comput. Biol. 14, e1006223.

Simeon, B., 2013. Computational flexible multibody dynamics: A differential-algebraic approach. Springer, Berlin.

Stickley, C.D., Andrews, S.N., Parke, E.A., Hetzler, R.K., 2018. The effectiveness of scaling procedures for comparing ground reaction forces. J. Biomech. 77, 55–61.

Stops, A., Wilcox, R., Jin, Z., 2012. Computational modelling of the natural hip: a review of finite element and multibody simulations. Comput. Methods Biomech. Biomed. Engin. 15, 963–979.

Wannop, J.W., Worobets, J.T., Stefanyshyn, D.J., 2012. Normalization of ground reaction forces, joint moments, and free moments in human locomotion. J. Appl. Biomech. 28, 665–676.

Wilke, H.J., Neef, P., Hinz, B., Seidel, H., Claes, L., 2001. Intradiscal pressure together with anthropometric data–a data set for the validation of models. Clin. Biomech. 16, 111–126.

# Chapter 2: Literature Review

## 2.1 Work-Related Musculoskeletal Disorders of the Spine

Vos et al. (2020) conducted a comprehensive assessment of disease incidence, prevalence, and several other population health metrics, covering 369 diseases and injuries across 204 countries and territories from 1990 to 2019. Using data from this extensive global burden study, Cieza and colleagues (2020) identified and analyzed 25 health conditions characterized by high prevalence, substantial disability burdens, and the potential for rehabilitation intervention during the course of the disease. Among these conditions, musculoskeletal disorders were identified as the most prevalent, affecting approximately 1.71 billion individuals out of a total of 2.45 billion worldwide. Musculoskeletal disorders encompass a range of injuries, including sprains, strains, and tears of muscles, tendons, ligaments, and damage to joints and bones (Bonfiglioli et al., 2022). In Canada, musculoskeletal disorders represent the most prevalent category among all chronic conditions and incur approximately $15 billion annually in disability-related costs (Maas et al., 2020).

Occupational (work-related) risk factors play a crucial role in the development, exacerbation, and persistence of musculoskeletal disorders. Work-related musculoskeletal disorders (WMSDs) pose a substantial public health challenge and impose a significant economic burden on healthcare systems. Across European industries, more than 50% of employees affected by WMSDs report work absenteeism, a rate notably higher than those affected by the influenza virus (10–12%) (Govaerts et al., 2021). The annual financial costs attributable to WMSDs in Europe are estimated at 240 billion euros, equivalent to nearly 2% of the Gross Domestic Product (Rosado et al., 2022). A provincial survey conducted in 2007–2008 in Québec, Canada, revealed

that one in five workers in the province had experienced non-traumatic WMSDs in at least one body region during the preceding 12 months (Sultan-Taieb et al., 2017).

Among musculoskeletal disorders, back disorders stand out as the leading cause of disability on a global scale. A recent meta-analysis focusing on the prevalence and incidence of WMSDs in Europe's secondary industries, known for their role in converting raw materials into consumer products, underscored that the back is the most common site for WMSDs (Govaerts et al., 2021). According to data from the Bureau of Labor Statistics, back injuries constitute the largest share of cases involving days away from work in the U.S. private sector, with back musculoskeletal injuries representing 38.5% of all reported WMSDs in 2016.

The causation of WMSDs is multifactorial, with various physical, psychosocial, and personal risk factors extensively explored in the literature. Researchers from diverse disciplinary backgrounds have examined different risk factors, focusing on various body regions and occupations. Consequently, numerous ergonomic tools and interventions have been developed to reduce work-related musculoskeletal injury rates. Strong associations between back injuries and occupational tasks involving lifting and lowering have been reported. Some examples include nurses lifting patients (Soylar and Ozer, 2018), heavy lifting in agriculture activities (Benos et al., 2020), and lifting objects such as wall sections and trusses in construction (Wang et al., 2015). From a biomechanical perspective, excessive mechanical loads on spinal joints during lifting and lowering tasks have been identified as one of the most important physical risk factors for work-related back injuries (Coenen et al., 2014a; Parreira et al., 2018). Therefore, the primary focus of the studies in this thesis is to enhance the evaluation of spinal joint loads during lifting and lowering tasks using biomechanical methods.

## 2.2 Biomechanical Perspectives on Back Injuries

Tissue injuries or mechanical failures occur when applied mechanical loads surpass the tissue's failure tolerance or strength (Bahr and Krosshaug, 2005). Tissue failure pathways generally fall into two categories: instantaneous and cumulative (Coenen et al., 2014b; McGill, 1997; Potvin, 2008). In the former, an event imposes a load on the tissue that exceeds its tolerance, leading to mechanical failure (Marras, 2000). In contrast, the cumulative failure scenario involves the repeated application of relatively low loads or the sustained application of loads over extended durations, resulting in trauma accumulation, reduced tissue recovery rates, and diminished tolerance limits, ultimately leading to injury (Kazemi et al., 2023; Waters et al., 2006).

Among various spinal tissues, the evaluation of mechanical loads on intervertebral discs (IVDs) is a subject of great interest in numerous studies. IVDs serve as the principal joints of the spine and play a vital role in distributing mechanical loads across vertebral bodies (Clouet et al., 2009; Desmoulin et al., 2020). Moreover, injuries related to IVDs, such as disc degeneration, are recognized as the primary cause of severe and chronic back pain and disorders (Adams and Dolan, 2005; Petit and Roquelaure, 2015). Therefore, the outcomes and discussions in the four studies of this thesis focus on the improved evaluation of intervertebral joint loads.

Desmoulin and colleagues (2020) conducted a review of various types of IVD injuries and, using data from in vitro studies, provided insights into various types of structural failures in IVDs, such as annulus tears and disc degeneration, and how these failures are associated with different types of mechanical loading (instantaneous and cumulative loading). However, regardless of the mechanical failure type, it is essential first to obtain spinal loads in *in vivo* conditions to comprehensively assess individuals' susceptibility to injury and effectively mitigate the incidence of work-related back injuries. Hence, in the following sections (2.3 and 2.4), measurement and

computational modelling methods employed to quantify intervertebral loads *in vivo* will be reviewed.

### 2.3 *In Vivo* Measurement of Spinal Joint Loads

Intradiscal pressure (IDP) measurement and measuring forces and moments using instrumented implants are two methods that can provide direct *in vivo* measurements of physical stresses with kinetic sources in the spine. IDP measurements involve measuring the hydrostatic pressure of the nucleus pulposus of the intervertebral disc using needle-mounted strain gauge pressure sensors (Li et al., 2022). Nachemson and Morris (1964) were the first to measure IDP *in vivo* using liquid-filled sensors, and Nachemson's pressure measurements in the 1960s and 1970s significantly advanced our knowledge of the loads acting on the human spine (Dreischarf et al., 2016). With the increased accuracy and advancements of pressure transducers, from liquid-filled sensors to piezoresistive ones, two important IDP measurement studies were published at the end of the 1990s. Sato et al. (1999) measured $L_4L_5$ IDP for eight healthy individuals and 28 patients in a total of eight different body positions, which included various lying, sitting, and standing postures. Wilke and colleagues provided a comprehensive set of $L_4L_5$ IDP data for many activities, eight of which involved lifting, yet for a single subject (Wilke et al., 2001, 1999). Most of the IDP measurements are reported for the lumbar spine (Andersson et al., 1977; Schultz et al., 1982; Takahashi et al., 2006). Polga et al. (2004) are the only group to report *in vivo* thoracic IDP measurements. They measured IDP in the middle ($T_6T_7$ or $T_7T_8$) and lower ($T_9T_{10}$ or $T_{10}T_{11}$) thoracic discs of six healthy volunteers for 18 static body positions, four of which involved static lifting.

The second method for measuring internal spinal loads is through instrumented implants, which record the temporal course of transmitted forces and moments within the spine (Rohlmann

et al., 2014b; Rohlmann et al., 2000). Internal spinal fixation devices and vertebral body replacement implants are often used to stabilize a severely injured and unstable spine, posteriorly and anteriorly, respectively (Rohlmann et al., 2013). Telemeterized internal spinal fixation devices and vertebral body replacement implants have been used by the Julius Wolff Institute team (https://orthoload.com/) to measure the loads acting on the human spine. The loads on telemeterized internal spinal fixation implants for 10 patients and vertebral body replacement implants for five patients were monitored and reported for numerous activities (Damm et al., 2020; Rohlmann et al., 2014e, 2014d, 2014c, 2014b, 2014a; Rohlmann et al., 2002, 2001).

The measured forces and moments in the implant data provide valuable information for addressing clinical questions related to vertebral body fusion, gaining a better understanding of remodelling processes, and advising patients on post-surgery exercises (Rohlmann et al., 2013). However, implant data are available in a small cohort, and interpreting loading patterns for the healthy population from implant data requires further care. On the other hand, IDP data can provide insight into the spinal loading of healthy individuals with non-degenerated discs, but the IDP measurement is also invasive, resulting in a limited number of *in vivo* IDP measurement studies. Additionally, to evaluate intervertebral compression forces, these forces should be estimated from IDP measurements, necessitating measuring the cross-sectional area of the disc and assuming a correction factor accounting for the heterogeneous material composition and non-uniform load transfer within the disc (Dreischarf et al., 2013). In summary, due to the invasive nature, complexity, and the limited number of available volunteers for *in vivo* measurement of spinal loads, computational models have been widely employed to estimate spinal loads in various conditions, as will be reviewed in the following sections.

## 2.4. Computational Modelling of the Spine

Numerous computational models have been developed, ranging from simple 2D link-segment models with a single-equivalent trunk extensor muscle (Chaffin, 1969) to models that consider the detailed geometries and nonlinear mechanical properties of spinal joint components (Khoddam-Khorasani et al., 2018). The existing modelling studies exhibit significant variation in several aspects, including the simplifications and assumptions made about geometry, the number and properties of components, the methodology used to estimate motion, and the biomechanical formulation of the problem, among others. Consequently, these modelling studies can be categorized and reviewed in multiple ways. One primary classification method for the existing spine models is to differentiate between finite element (FE) models and multibody models (Knapik et al., 2022). This classification serves as the basis for the subsequent review, shedding light on why the present thesis focuses on multibody modelling.

### *2.4.1 Finite Element Models*

FE analysis is a computational technique employed for solving differential equations that are used to describe various phenomena in diverse fields, such as mechanical stress analysis, fluid flow, and heat transfer. An FE model is created based on the system's geometry and divided into a multitude of discrete/finite elements. These elements can have varying materials and structural properties and are interconnected through nodes (Welch-Phillips et al., 2020). To predict the mechanical behaviour of a structure, apart from defining the geometry and material properties of the mechanical system, it is essential to specify loading conditions. In FE analysis, loading conditions and other constraints that have external influences on the structure are referred to as boundary conditions (Kramer et al., 2019). Once the mechanical system and boundary conditions are established, numerical methods are employed to solve the differential equations for each

element. This enables the determination of key quantities such as displacements at nodal points and strains and stresses within each element. Subsequently, a comprehensive understanding of the entire system's behaviour can be derived through the integration of these individual elements (Brekelmans et al., 1972).

The capability to represent intricate systems with geometric and material nonlinearities makes FE models invaluable for gaining insights into a diverse range of phenomena, such as remodelling, degradation, and failure in various spinal structures, including intervertebral discs (Khuyagbaatar et al., 2023; Schmidt et al., 2013). Despite the increased accessibility of imaging techniques for creating FE models and the affordability of computational costs for FE simulations over the past four decades, the calibration of detailed and accurate FE models remains a challenging and time-consuming task. Defining realistic boundary conditions for FE models, for example, continues to be a major challenge due to the limited possibilities for *in vivo* measurements (Nispel et al., 2023). In certain applications, the complexity of calibration and computational costs associated with FE models is indispensable. FE models find their predominant application in the field of orthopedics (Welch-Phillips et al., 2020), particularly in investigating the impacts of various surgical procedures (Wang and Guo, 2021; Xu et al., 2019) and designing new surgical instrumentations (Chen et al., 2015; Guo and Wang, 2020). However, the detailed investigation of structural behaviour and the mechanical load-sharing and distribution among various spine tissues were not the focus of the present thesis. On the contrary, the overarching purpose of this thesis was to provide a model that could be scaled within the simulation workflow relatively quickly for large populations, used easily for both static and dynamic lifting tasks, and plausibly predict intervertebral loads at the holistic level to gain insight into the potential biomechanical risk factors associated with lifting and lowering tasks in various workplaces. To achieve this purpose,

multibody models were deemed more appropriate and were thus employed in all studies within the current thesis, as will be reviewed in the following sections.

### *2.4.2 Multibody Modelling Components – Bodies and Joints*

In multibody modelling of the spine, vertebral bodies are treated as rigid segments, and intervertebral discs are commonly represented as spherical or ball joints, connecting the rigid segments together and allowing three rotational degrees of freedom (DOF) between them (Bruno et al., 2015; Christophy et al., 2012; De Zee et al., 2007; Favier et al., 2021; Huynh et al., 2015). In a few modelling studies, six DOF (three translational and three rotational DOF) were defined for modelling intervertebral joints (Ignasiak et al., 2016; Khurelbaatar et al., 2015; Malakoutian et al., 2018). While it is feasible to measure the motion of individual intervertebral joints using medical imaging techniques (Aiyangar et al., 2014; Li et al., 2009), for practical and widespread application of musculoskeletal models, optoelectronic and inertial sensors are commonly utilized to record motion. Subsequently, an optimization process is employed to estimate human joint kinematics (Begon et al., 2018; Duprey et al., 2017). When obtaining joint kinematics using skin-surface markers or inertial sensors, certain assumptions become necessary. For instance, coupling the rotations of the vertebral bodies (reducing independent DOF) is required to account for all rotational DOF of the entire thoracolumbar spine (51 DOF = 17 segments × 3 degrees of freedom). This helps avoid calculating unrealistic spine angles or encountering discontinuities in spinal motion (Alemi et al., 2021). If the complexity of a spine musculoskeletal model is further increased by introducing translational DOF between vertebral bodies, additional assumptions are needed to elucidate the joint kinematics of the model during the motion of interest and these assumptions require further validation (Hicks et al., 2015).

### *2.4.3 Multibody Modelling Components – Muscles*

To obtain spinal forces through multibody modelling, following the definition of skeletal geometry (bodies and joints), it is crucial to delineate the muscle structure. The role of muscles during motion can be implicitly modelled within a simulation pipeline by incorporating information on muscle moment arms (McGill and Norman, 1987), which can be sourced from cadaveric or imaging studies (Jorgensen et al., 2003, 2001). An alternative method involves explicit modelling of muscles, wherein their geometry is defined based on attachment points relative to segments (e.g., vertebral bodies and pelvis). Subsequently, the model takes into account muscle dynamics throughout the motion. Explicitly modelling muscles has become a prevailing approach, particularly with the advancement of multibody software packages, affording the opportunity to construct detailed anatomically based models of musculoskeletal geometry.

In earlier models, all torso muscles were represented as straight-line force vectors (Granata and Marras, 1993; McGill and Norman, 1986; Schultz and Andersson, 1981). However, this assumption may not align well with the reality of anatomical structures during certain movements. For instance, in flexed trunk postures, the modelled straight-line long back muscles might penetrate into the vertebral bodies (Arjmand et al., 2006; Garner and Pandy, 2000). The realistic definition of muscle geometry is crucial for estimating internal loads in biomechanical models. For example, Arjmand and colleagues (2006) demonstrated that modelling global erector spinae muscles (i.e., with upper attachments at the rib cage) using curved paths significantly influences the estimated muscle and spinal forces at all lumbar levels during static lifting tasks.

Various methods exist for considering the curvature of muscles, broadly categorized into two approaches (Hwang et al., 2017): i) the ‘via-points’ approach (Delp and Loan, 1995), where fixed or moving intermediate points (Suderman and Vasavada, 2012) defined along the muscle

path allow for the generation of realistic curved muscle paths as the joint moves, and ii) the 'wrapping surface' approach, in which the muscles wrap around pre-defined shapes or rigid bodies (Garner and Pandy, 2000). The 'via-points' approach is more common in spine biomechanics, especially for modelling back muscles, due to the inherent challenges in developing effective wrapping surfaces. Moreover, the predicted spinal forces were more accurate when the 'via-points' approach was used (Hwang et al., 2017).

The fundamental components of musculoskeletal multibody modelling—bodies, joints, and muscles—were briefly outlined and reviewed above. However, a musculoskeletal model can represent various biological structures, and there exists a spectrum of choices ranging from simple to complex for each structure (Hicks et al., 2015). For instance, in some spine modelling studies, the role of passive structures was neglected (Beaucage-Gauvreau et al., 2019; Bruno et al., 2015), whereas others incorporated passive stiffness properties using bushing elements to represent the entire passive joint structure (Christophy et al., 2013; Favier et al., 2021; Senteler et al., 2016), and some others explicitly modelled passive structures such as ligaments (Khurelbaatar et al., 2015).

### 2.5 Estimating Spinal Forces using Multibody Modelling

Irrespective of the model's complexity in terms of the number, geometry, and features of biological tissues, dynamic equations of motion must be solved in all biomechanical models when the aim is to derive kinetic variables, such as intervertebral forces. These dynamic equations of motion establish and maintain dynamic equilibrium between external and internal forces (Dreischarf et al., 2016). In their general vector format, they can be expressed as Equation 2.1 (Pandy, 2001), where $\mathbf{q}$, $\dot{\mathbf{q}}$, and $\ddot{\mathbf{q}}$ are vectors of the generalized positions, velocities, and accelerations, respectively, $\mathbf{M}(\mathbf{q})$ is the system mass matrix, $\mathbf{C}(\mathbf{q}, \dot{\mathbf{q}})$ is the vector of coriolis and centrifugal forces and torques; $\mathbf{G}(\mathbf{q})$ is the vector of gravitational forces and torques; $\mathbf{R}(\mathbf{q})$ is the

matrix of muscle moment arms, $\mathbf{F}^{\mathrm{MT}}$ is the vector of musculotendon forces, and $\mathbf{E}$ is the vector of external forces and torques.

$$\mathbf{M}(\mathbf{q})\ddot{\mathbf{q}} + \mathbf{C}(\mathbf{q})\dot{\mathbf{q}}^2 + \mathbf{G}(\mathbf{q}) + \mathbf{R}(\mathbf{q})\mathbf{F}^{\mathrm{MT}} + \mathbf{E}(\mathbf{q}, \dot{\mathbf{q}}) = 0 \qquad \text{(Eq. 2.1)}$$

### *2.5.1 Motion Solving Approaches (Forward vs. Inverse Dynamics)*

The equations of motion (Eq. 2.1) can be solved using either a forward or an inverse approach. Various methods can be employed in both forward and inverse dynamics simulations of musculoskeletal systems (Shourijeh et al., 2016), but fundamentally, in forward dynamics simulations, the inputs consist of muscle activations/forces or joint torques, and the equations of motion are integrated forward in time to determine the resulting human body movement from the applied forces and moments (Shourijeh and McPhee, 2014a). In contrast, the inverse dynamics approach utilizes measured or specified kinematics as inputs to compute essential kinetic data, such as net joint moments, muscle forces, and contact forces (Ackermann and Schiehlen, 2009).

The complexity and computational costs of simulations depend on many factors, including the model components and the chosen algorithm for either forward or inverse dynamics. Nonetheless, forward dynamics simulations of human movements tend to be more intricate and computationally demanding compared to inverse dynamics simulations (Damsgaard et al., 2006). This heightened complexity arises because prior knowledge of muscle excitations or joint torques is typically scarce. Consequently, determining a set of muscle excitations/forces that produce a desired movement in forward dynamics simulations becomes a more challenging task, necessitating an iterative process with feedback or correction mechanisms (Shourijeh and McPhee, 2014a; Thelen et al., 2003).

Forward dynamic simulations prove valuable in predictive scenarios and are particularly well-suited for answering 'what-if' questions, such as exploring the outcomes when control of muscles or muscle forces undergoes alterations (Shourijeh and McPhee, 2014b). On the other hand, the inverse dynamics approach finds applications in descriptive studies and is comparatively more straightforward to implement in the examination of human musculoskeletal dynamics, especially when motion data is readily available (Erdemir et al., 2007). In the context of this thesis, all studies involve inverse dynamics musculoskeletal modelling. Consequently, the subsequent sections delve into various methods within the inverse dynamics simulation pipeline, focusing on the estimation of spinal muscle forces and joint loads.

### 2.6 Inverse Dynamics–based Simulations

As highlighted earlier, irrespective of the chosen motion-solving approach, equations of motions should be solved in biomechanical models to maintain dynamic equilibrium between external and internal forces and moments. Certain biomechanical models adhere to dynamic equilibrium equations at a single spine level, typically $L_4L_5$ or $L_5S_1$ (Merryweather et al., 2009; Potvin, 1997). These models have gained popularity in ergonomics applications due to their simplicity in setup and usage (Rajaee et al., 2015). However, Arjmand et al. (2007) demonstrated that, for identical kinematics and external force inputs during lifting activities, muscle forces and intervertebral forces estimated based on single-level equilibrium models exhibit a significant level dependence. Furthermore, muscle forces estimated from these models can substantially violate equilibrium at levels other than the one considered in the model (Arjmand et al., 2007). Therefore, for more reliable estimations of muscle forces and intervertebral loads, it has been recommended to employ models and software packages capable of satisfying equilibrium equations at all joint levels (Arjmand et al., 2010).

In physical reality, the skeletal system is redundantly actuated by muscles, meaning that the number of muscles exceeds the degrees of freedom, and many muscles are multi-articular, spanning more than one joint (Ackermann and Schiehlen, 2009). Consequently, the number of unknown muscle forces surpasses the available equilibrium equations, resulting in the problem of solving equations of motion for muscle forces being mathematically indeterminate (with more unknowns than equations). To tackle this challenge in the context of inverse dynamics–based simulations of spine musculoskeletal models, various approaches have been introduced. These approaches can be broadly categorized into four groups: single-equivalent muscle models, optimization-driven models, electromyography (EMG)-driven models, and hybrid (EMG-assisted optimization) models (Dreischarf et al., 2016).

### *2.6.1 Single-Equivalent Muscle Modelling Approach*

The single-equivalent muscle models group agonistic muscles into a single equivalent muscle, disregarding antagonistic muscles to overcome kinetic redundancy. For instance, a single muscle is considered to represent the erector spinae muscle group, balancing the flexion moments exerted on the $L_5S_1$ joint by inertial and external forces (Chaffin, 1969; Merryweather et al., 2009). Single-equivalent muscle models are limited to estimating intervertebral forces and cannot be employed to assess individual trunk muscle activations and forces. In some modelling studies that utilized a single-equivalent muscle model, adjustments to the net muscle moment arm and its angle relative to the axis of rotation have been made during the movement to account for various factors, such as the coactivation between the erector spinae and external abdominal obliques determined from EMG data (Howarth et al., 2009). Nevertheless, the efficacy of these models is heavily contingent on the assumed single equivalent muscle moment arm, with a wide range of reported values for the line of action and moment arm of the single equivalent back muscle in the literature

(Nussbaum et al., 1995). While these models are commonly used in routine ergonomics evaluations to assess hazardous lifting situations due to their ease of use, their accuracy remains highly debatable (Dehghan and Arjmand, 2022; Rajaee et al., 2015).

### *2.6.2 Optimization-based vs. EMG-based Modelling Approaches*

The optimization-based approach is most commonly employed in spine musculoskeletal multibody modelling (Lerchl et al., 2023), where a single or multiple cost functions (such as the sum of muscle stresses or the sum of squared muscle activations) are minimized while simultaneously solving for the equations of motion (Dreischarf et al., 2016). The optimization approach provides a purely mathematical solution to the muscle redundancy problem and may, therefore, suffer from a lack of physiological content and inter-/intra-individual variations in muscle recruitment patterns, such as those observed between symptomatic and asymptomatic cases (Mohammadi et al., 2015).

Alternatively, the incorporation of electrical signals from muscles, collected using surface EMG electrodes, into musculoskeletal modelling has been advocated to account for inter- and intra-subject variability in muscle recruitment and overcome the redundancy present in biomechanical models. Although surface EMG signals are highly correlated with muscle forces, the exact relationship between muscle tensions and EMG signals remains undetermined due to the inability to directly measure muscle forces non-invasively. Many assumptions are required to estimate muscle forces from EMG signals, especially during dynamic movements (Disselhorst-Klug et al., 2009). Given the physiological complexities in estimating muscle forces from measured EMG activities and experimental challenges, such as cross-talk (Farina et al., 2004) or recording activity from deep and wide muscles (Staudenmann et al., 2005; Stokes et al., 2003), muscle forces derived solely from EMG data cannot satisfy equilibrium equations. Consequently,

hybrid or EMG-assisted optimization approaches have been introduced to simultaneously consider both EMG signals and equilibrium requirements.

### *2.6.3 EMG-assisted Optimization Approach*

Cholewicki and McGill (1994) pioneered one of the initial EMG-assisted optimization approaches in spine biomechanics. Their method (Cholewicki et al., 1995; Cholewicki and McGill, 1994), or variations thereof with the same underlying concept (Gagnon et al., 2011; Vigouroux et al., 2007), has found application in various spine modelling studies (Banks et al., 2022; Mohammadi et al., 2015). In this approach, muscle forces are initially estimated based on EMG activities using Eq. 2.2:

$$F_i = \left(\frac{EMG_i}{EMG_{max,i}}\right)^{0.769} \times A_i \times \sigma_{max} + F_{p,i} \qquad \text{(Eq. 2.2)}$$

Here, $F_i$ represents the total force of the $i^{\text{th}}$ muscle, $EMG_i$ and $EMG_{max,i}$ are the $i^{\text{th}}$ muscle's activation during the performed task and the maximum voluntary isometric contraction task, respectively, $A_i$ is the $i^{\text{th}}$ muscle cross-sectional area, $\sigma_{max}$ is the maximum allowable muscle stress, and $F_{p,i}$ accounts for the passive force in muscle $i$.

As mentioned earlier, these initially estimated muscle forces do not satisfy equilibrium requirements. Consequently, hybrid algorithms aim to fulfill equilibrium equations around the joints by making the least possible adjustments to individual muscle forces calculated using EMG. These adjustments to muscle forces are applied through coefficients known as the gains. During each instant of the inverse dynamics simulation, the optimization problem presented in Eq. 2.3 needs to be solved:

$$\text{Minimize } \sum_{i=1}^{N} M_{i,j} \cdot (1 - g_i)^2 \quad where\ M_{i,j} = \sqrt{M_{x(i,j)}^2 + M_{y(i,j)}^2 + M_{z(i,j)}^2}$$

Subject to $\sum_{i=1}^{N} g_i \cdot M_{x(i,j)} = M_{xj}$

$$\sum_{i=1}^{N} g_i \cdot M_{y(i,j)} = M_{yj} \quad \text{(Eq. 2.3)}$$

$$\sum_{i=1}^{N} g_i \cdot M_{z(i,j)} = M_{zj}$$

$$g_i \geq 0 \quad i = 1, 2, \dots, N$$

In Eq. 2.3, $M_{i,j}$ represents the moment of muscle *i* (of which there are *N*) acting at joint *j*. The objective function ensures that the muscle gains ($g_i$) do not deviate significantly from unity, and the equality constraints in the optimization problem work to balance the internal and net external moment components (i.e., $M_{xj}$, $M_{yj}$, $M_{zj}$) at each joint in three planes.

Although the hybrid approach is proposed as a physiological solution for the muscle redundancy problem, the chosen objective function in Eq. 2.3 lacks a direct physiological basis for adjusting individual muscle forces estimated from EMG signals. Moreover, the necessity of EMG data as inputs restricts the ecological applicability of this method for workplaces, as considered in the current thesis. Therefore, all studies in the current thesis employ the optimization method to address the muscle redundancy problem. The following sections review spine modelling studies utilizing the optimization approach, discuss their limitations, and outline how the studies in the current thesis address these limitations.

## 2.7 Optimization-driven Spine Multibody Models

Various linear and nonlinear objective functions have been employed in the inverse dynamics simulation workflow to tackle the muscle redundancy problem and subsequently calculate intervertebral contact forces (Arjmand and Shirazi-Adl, 2006). Most optimization-driven models aim to minimize a polynomial objective function represented by $G$:

$$G = \sum_{i=1}^{N} \left(\frac{F_i}{S_i}\right)^p \quad \text{(Eq. 2.4)}$$

where $F_i$ denotes the muscle force in the $i^{\text{th}}$ muscle and $S_i$ represents a measure of muscle strength (e.g., the physiological cross-sectional area of the muscle) at each simulation instant (Damsgaard et al., 2006; De Zee et al., 2007; Rasmussen et al., 2001). Irrespective of the power ($p$) in the objective function or how different methods of modelling muscle dynamics impact both $F_i$ and $S_i$, this cost function inherently introduces bias against predicting antagonistic muscle activations. Assigning activations/forces to antagonistic muscles requires higher activations/forces in the agonistic muscles to maintain dynamic equilibrium, leading to an increase in the value of the cost function. Consequently, the inability of optimization-based models to predict antagonistic coactivity is acknowledged as a major shortcoming (Dreischarf et al., 2016; El Ouaaid et al., 2013).

The general limitation of optimization-driven models—their inability to predict antagonistic coactivity—has been underscored in spine models validated and used for lifting/lowering tasks. These models estimate nearly zero activities for antagonistic muscles during standing or flexed forward lifting tasks (Alemi et al., 2023; Beaucage-Gauvreau et al., 2019), which contradicts EMG experimental data. Predicted muscle forces directly impact estimated contact forces, the primary variables of interest in this thesis. Therefore, addressing the issue of predicting the co-activity of antagonistic muscles when using optimization-driven models in the inverse dynamics simulation workflow is a crucial step toward obtaining more accurate spinal loads from such models.

Several techniques have been introduced to tackle the challenge of estimating coactivity in antagonistic muscles within optimization-driven models. Hughes et al. (1995) demonstrated that estimating some degree of co-contraction is achievable in a single-level ($L_3L_4$) spine model when

minimizing intervertebral compression force, assuming non-zero lower bounds for muscle activations (Hughes et al., 1995). Raikova (1999) highlighted the necessity of assigning different signs to weight factors ($C_i$) for agonist and antagonist muscles to predict muscle co-activations when the objective function is of the form $\sum C_i \left|\vec{F}_i\right|^n$ ($\vec{F}_i$ is a module of the $i^{\text{th}}$ muscle force). The sign of $C_i$ depends on the joint net external moment (Raikova, 1999). For instance, El Ouaaid et al. (2013) used $G = \sum(\sigma^m_{back\ muscles} - \sigma^n_{abdominal\ muscles})$ as their objective function ($\sigma$ is denoting muscle stress) to simulate static lifting tasks where back and abdominal muscles were agonist and antagonist, respectively. However, these approaches are often perceived more as mathematical solutions than as physiologically-grounded strategies to address optimization-driven model limitations.

In reality, both biomechanical and non-biomechanical factors can influence the level of muscle co-activations. For example, sedentary tasks may necessitate increased muscle co-activations to promote blood flow and muscular substitution, mitigating myalgia or myofascial pain induced by prolonged loading (Le et al., 2017). Nevertheless, one crucial pathway used to illustrate trunk muscle co-activations involves providing neuromuscular stabilization to protect the spine (Granata and Orishimo, 2001; McGill and Cholewicki, 2001). Therefore, incorporating mechanical stability criteria, in addition to solving the equations of motion (Eq. 2.1), has been introduced as a method with a physiological basis to address the major shortcomings of common optimization problems (Eq. 2.4).

### *2.7.1 Mechanical Stability and Optimization-driven Spine Models*

Stability stands as a foundational concept in diverse scientific realms, particularly within the domain of musculoskeletal biomechanics; nevertheless, a universal definition of stability remains elusive (Reeves et al., 2007). The definition of stability can vary depending on the context,

such as in clinical vs. engineering settings. Moreover, diverse interpretations of the term mechanical stability emerge across applications in continuum mechanics, dynamics, or control within mechanical engineering. The exploration of stability, however, generally strives to "examine and improve the system performance under regular design inputs (e.g., loads) and sudden small external–internal perturbations to mitigate excessive outputs (e.g., motions), dysfunction, and failure" (Ghezelbash et al., 2023).

In this thesis, mechanical stability specifically refers to the static mechanical stability criterion designed to prevent Euler buckling, a concept commonly addressed in structural stability textbooks. The static mechanical stability entails the capacity of a mechanical structure to sustain static equilibrium in the face of disturbances around its equilibrium position. When subjected to a critical load, the shift from stability to instability takes place, leading to structural buckling (McGill et al., 2003). The derivation of stability equations in this context involves perturbing the equilibrium state with a small admissible displacement and forming equilibrium equations in this perturbed configuration. These equations are then linearized for small perturbations, and by leveraging non-trivial solutions, the critical load can be determined (Simitses and Hodges, 2006). An equivalent method to assess the stability of a mechanical system at equilibrium is the energy-criterion approach. In this approach, the equilibrium position is considered stable if the total potential energy of the system is locally minimal at that position. Consequently, the total potential energy is expressed in terms of the system's DOF in the energy-criterion approach. Stability is confirmed when the Hessian matrix (i.e., the second variation) of the total potential energy is positive definite; a loss of positive definiteness occurs at the critical load (Ghezelbash et al., 2023; Simitses and Hodges, 2006).

Cadaveric studies have revealed that the human ligamentous thoracolumbar spine shows instability (buckling) under very small compression loads, approximately 100 N, a stark contrast to the forces experienced during routine activities of daily living (Crisco et al., 1992; Shirazi-Adl and Parnianpour, 2000). These findings emphasize the crucial role of the motor control system, particularly muscles, in ensuring sufficient stiffness to prevent spinal instability (Ghezelbash et al., 2023). Co-activations of antagonist muscles have proven to be effective in stiffening and stabilizing the spine, particularly in standing lifting tasks where the spine is inherently less stable (Arjmand et al., 2008). Therefore, the incorporation of stability criteria (i.e., positive definiteness of the Hessian matrix) as constraints in optimization-driven models could potentially address their limitations in accurately predicting antagonist muscle activities.

Granata and Wilson (2001) developed an inverted double-pendulum model that represented the spine with six rotational DOF. This model was governed by 12 muscle equivalents, including three bilateral abdominal muscles and three bilateral back muscles. The researchers instructed ten participants to perform 12 static lifting tasks, holding an 11.3 kg mass at forward flexion angles of 0° (upright), 15°, 30°, and 45°, along with all combinations of these flexion angles at asymmetric postures of 10° and 20° of left twist. They concurrently measured EMG activities of the back and abdominal muscles. The model mirrored the flexion and rotation angles executed by the participants. The optimization problem to determine muscle forces aimed to minimize the sum of muscle stress, subject to three constraints: i) ensuring that muscle forces equilibrate the external moment at the joints, ii) maintaining a positive definite Hessian matrix of potential energy, and iii) ensuring that muscle forces did not exceed their physiological limits.

In Granata and Wilson's (2001) optimization-driven spine model, abdominal muscles, though antagonistic in their simulated tasks, were recruited in accordance with their measured

EMG data. This demonstrated the suitability of incorporating stability criteria as one of the constraints in the optimization algorithm (Granata and Wilson, 2001). Hajihosseinali et al. (2014) adopted a similar optimization approach but applied it to a more intricate spine model comprising seven segments (pelvis, thorax, and five lumbar vertebrae), six joints (18 rotational DOF), 76 trunk muscle fascicles, and considerations for the role of passive structures. Their study revealed that while this approach may not comprehensively explain the central nervous system's strategy in activating antagonistic muscles, the muscle activations predicted by this method were in better agreement than those estimated by the optimization-driven model that did not account for stability (Hajihosseinali et al., 2014).

The potential energy function ($V$) for an intervertebral joint *j* and about an axis *i* can be defined as (Howarth et al., 2004; Potvin and Brown, 2005) follows:

$$V_{ji} = U_{ji\ Muscles} + U_{ji\ Passive} - W_{ji\ External} \quad \text{(Eq. 2.5)}$$

Here, $U_{ji\ Muscles}$, $U_{ji\ Passive}$, and $W_{ji\ External}$ represent the energy stored in the muscles, passive tissues, and the work performed on each joint by inertial and external loads, respectively. The formulation for the total potential energy of the system depends on the number of joints and DOF, as well as how ligaments, discs, and other passive structures are represented in the model. For a spine model with $n$ generalized coordinates ($Q_1$, $Q_2$, …, $Q_n$), the Hessian matrix (**H**) of the potential energy ($V$) is an $n \times n$ matrix.

$$\mathbf{H} = \begin{bmatrix} \frac{\partial^2 V}{\partial Q_1^2} & \cdots & \frac{\partial^2 V}{\partial Q_1 \partial Q_n} \\ \vdots & \ddots & \vdots \\ \frac{\partial^2 V}{\partial Q_n \partial Q_1} & \cdots & \frac{\partial^2 V}{\partial Q_n^2} \end{bmatrix}_{n \times n} \quad \text{(Eq. 2.6)}$$

To maintain stability, both the determinant and principal minors of **H** must be positive (Cholewicki and McGill, 1996). Deriving and checking the positive definiteness of **H** is challenging, especially in inverse dynamics–based simulations. This complexity arises because the potential energy stored in muscles is a function of muscle activations/forces, which are the desired outputs of inverse dynamics simulations. Therefore, the Hessian matrix, its determinant, and its principal minors should be calculated and implemented implicitly in the optimization algorithm, posing a non-trivial task.

While the concept of mechanical stability of the spine and the role of muscles in providing stability are not new in spine biomechanics (Bergmark, 1989), widely-used spine models in well-known multibody modelling software packages (Lerchl et al., 2023) often employ the common optimization approach without stability constraints. Only a few spine models, developed using in-house codes, have considered stability constraints in simulating lifting tasks (Hajihosseinali et al., 2014). Therefore, the development of a framework capable of estimating muscle forces while considering joint stability criteria, and which is generalizable across various modelling studies, regardless of their model's features (e.g., number of joints and muscles), would be highly beneficial.

### *2.7.2 Modelling Software and Stability*

OpenSim (Delp et al., 2007; Seth et al., 2018, 2011) is an open-source, extensible, and collaborative platform that provides advanced computational tools for musculoskeletal multibody modelling and has been downloaded over 705,000 times. According to Google Scholar, the paper describing the first version of OpenSim (Delp et al., 2007) has been cited 4,891 times as of December 7, 2023. OpenSim was chosen as the musculoskeletal modelling platform in all studies within the current thesis because it is the most widely used open-source platform in biomechanics

worldwide, and it is well understood that the sharing of the model, simulation, and software directly affects the research's overall impact (Hicks et al., 2015).

The Static Optimization Tool in OpenSim is designed to calculate muscle forces using the common optimization approach in the inverse dynamics simulation workflow, as described in Section 2.7. Therefore, both the original spine models developed and validated in OpenSim (Bruno et al., 2015; Christophy et al., 2012; Favier et al., 2021), and their modified or extended versions (Beaucage-Gauvreau et al., 2021; Lerchl et al., 2023; Schmid et al., 2020), rely solely on the Static Optimization Tool and have not incorporated stability criteria in the calculation of muscle forces. The absence of stability criteria in muscle force calculations is not unique to OpenSim models. Muscle recruitment solvers in other well-known software packages, such as AnyBody, exclusively solve the equations of motion without considering stability criteria. Models developed in these software packages also lack such considerations (Bassani et al., 2017). Study 1 of the current thesis aims to address this gap by developing a framework that enhances the default Static Optimization solver in OpenSim. Importantly, this framework is designed to be generalizable across many OpenSim models, focusing on the broader consideration of stability in muscle recruitment algorithms rather than on the specific accuracy of intervertebral loads estimated by a particular spine model.

### 2.8. Sensitivity of Spine Musculoskeletal Models

The presented literature review on the modelling of bodies, joints, muscles, and the underlying assumptions in various motion-solving approaches underscores the inevitability of uncertainty and variability in nearly all aspects of musculoskeletal modelling. Consequently, it is important to assess the sensitivity of musculoskeletal models to unavoidable uncertainties in the input parameters (Anderson et al., 2007). This is particularly crucial for interpreting results and

elucidating which parameters are insignificant and can be eliminated from the model, reducing the complexity and computational cost of the problem (Antoniadis et al., 2021). It also aids in identifying inputs that significantly contribute to output variability, thereby requiring meticulous configuration in the model (Hicks et al., 2015).

Previous studies, employing different models, have explored the sensitivity of estimated intervertebral forces to various model components. Examples of these model components include the position of intervertebral joint centres (Ghezelbash et al., 2018; Senteler et al., 2018; Zander et al., 2016), intervertebral disc stiffness parameters (Bauer et al., 2016), anatomical parameters of vertebral bodies (Putzer et al., 2016), muscle geometry (Akhavanfar et al., 2018; Bayoglu et al., 2019), and personalized factors such as age and sex (Ghezelbash et al., 2016).

For lifting tasks, characteristics of the lifted mass, including its inertial properties and physical configuration (e.g., horizontal and vertical distances from the body and the asymmetry of the load handling posture), can significantly influence spinal stability, trunk muscle activations, and spinal loads predicted by spine musculoskeletal models (El-Rich and Shirazi-Adl, 2005; Madinei et al., 2018; Rohlmann et al., 2014e; Skals et al., 2021; Zander et al., 2015). The modelling method used for hand–mass interaction can affect the kinematics, external forces, and moments applied to a musculoskeletal model, thereby directly impacting the estimated muscle forces and joint loads. However, the extent to which different modelling decisions regarding external hand forces and moments could affect the estimated spinal joint loads remains unknown. This critical knowledge gap forms the basis of Study 2 in the present thesis.

### 2.9. Validation of Spine Musculoskeletal Models

In the past decade, various research groups have developed numerous multibody spine models, including those in OpenSim as well as other open-source and commercial software

packages (e.g., AnyBody, Simpack, ArtiSynth, and LifeMOD). One of the reasons for the existence of numerous spine models is the complexity of the human neuro-musculoskeletal system in general. Each newly developed model focuses on specific aspects of previously established models to address some of their limitations, and these limitations are diverse and numerous. Many of the spine models developed in the past decade have been used to simulate lifting tasks (Lerchl et al., 2023). These models exhibit significant improvements relative to earlier biomechanical models, all featuring detailed musculature, considering muscle dynamics to varying extents, and adhering to crucial equilibrium equations at all spinal levels. Therefore, reaching a consensus on which model is more appropriate for ergonomics and lifting applications is not a straightforward task, and appropriate validation studies are required to determine how well a model and simulation framework are able to represent a reality of interest (Viceconti et al., 2021); in the context of this thesis, the focus is on spinal joint loads.

As highlighted in Section 2.3, the measurement of intervertebral mechanical loads *in vivo* is a rare opportunity, constrained by ethical and safety considerations. Consequently, there are limited experimental datasets available, to which the intervertebral forces estimated by biomechanical models can be compared. To address this gap, many studies have sought alternative comparisons with variables that are more easily measurable experimentally. For instance, researchers have compared muscle activations or forces derived from a model with surface EMG data measurements (Alemi et al., 2023; Raabe and Chaudhari, 2016). While these indirect comparisons may offer some insights into a model's behaviour, they do not assure the model's ability to accurately predict the actual quantity of interest (Lund et al., 2012).

Table 2.1 presents recent validation studies in spine multibody modelling, detailing the total number of activities during which estimated intervertebral forces were validated against IDP

and implant data. The table also includes information on the total number of static and dynamic lifting tasks specifically analyzed. As depicted in Table 2.1, the majority of spine validation studies for intervertebral forces have focused on static lifting tasks. This trend may be attributed to the fact that existing IDP experimental studies (Andersson et al., 1977; Polga et al., 2004; Schultz et al., 1982; Wilke et al., 2001) measured IDP mostly during static lifting tasks. Additionally, it could be due to the challenges associated with estimating tissue loads for dynamic lifting tasks, which often involve intensive and time-consuming data collection and analysis (Banks et al., 2023). Nevertheless, it is crucial to recognize that in dynamic movements, trunk strength is diminished and external moments imposed on it are increased. Consequently, the risk of back injuries significantly rises during dynamic lifting tasks (Banks et al., 2023).

Table 2.1. Overview of recent spine multibody modelling validation studies. This table summarizes spine multibody modelling studies, detailing the total number of activities where estimated intervertebral forces were validated against intradiscal pressure (IDP) and implant data. It also indicates the number of static and dynamic lifting tasks, along with the primary software package used for each validation study. The table is organized in ascending order based on the publication year.

| Study | Total Activities | Static Lifting | Dynamic Lifting | Software |
|---|---|---|---|---|
| Huynh et al., (2013) | 1 | 1 | 0 | LifeMOD |
| Bruno et al., (2015) | 27 | 17 | 0 | OpenSim |
| Ignasiak et al., (2016) | 6 | 1 | 1 | AnyBody |
| Malakoutian et al., (2016) | 3 | 2 | 0 | ArtiSynth |
| Bassani et al., (2017) | 12 | 2 | 3 | AnyBody |
| Actis et al., (2018) | 5 | 0 | 0 | OpenSim |
| Beaucage-Gauvreau et al., (2019) | 9 | 3 | 2 | OpenSim |
| Favier et al., (2021) | 10 | 0 | 0 | OpenSim |
| Lerchl et al., (2022) | 12 | 6 | 0 | SIMPACK |

In addition to comparing computational and experimental results in validation studies, it is crucial to extrapolate model predictions to the intended usage conditions and assess whether the accuracy aligns with the intended application (Lund et al., 2012). The availability of both IDP and implant measurements is limited, with vertebral body implant data derived from older patients undergoing surgery. Consequently, validating a spine model for healthy individuals and extending beyond the anthropometric characteristics considered in experimental studies presents a considerable challenge. Therefore, Studies 3 and 4 aim to enhance the accuracy and reliability of musculoskeletal modelling in predicting spinal forces beyond the scope achieved in previous validation studies. Specifically, in Study 3, the advantages of previous spine modelling studies were integrated into a newly developed model. Study 3 served as a preliminary investigation for Study 4, where the appropriate mathematical approach to remove the effect of body weight from estimated spinal forces by the newly developed spine model was explored, given that body weight has been recognized as the most important anthropometric characteristic affecting predicted spinal loads (Ghezelbash et al., 2016). In Study 4, spinal forces estimated by this new model were validated for healthy individuals with body weights beyond the range of participants in the experimental datasets and for more dynamic lifting tasks than those for which previous models were validated.

## 2.10 Summary

The preceding discussion has highlighted several key factors:

1) Work-related back injuries are highly prevalent and incur significant costs.
2) High mechanical loads on intervertebral joints, particularly during lifting tasks, play a crucial role in the development of work-related back injuries.

3) Optimization-driven spine models are deemed appropriate computational tools for gaining comprehensive insights into spinal loading during lifting activities in work settings.
4) Despite the development of numerous biofidelic spine models over the past decade, there is a lack of adequate validation studies to confirm the accuracy and reliability of these models for dynamic lifting tasks.

In my PhD studies, the focus is on enhancing existing biofidelic spine models and providing researchers with more accurate methods and tools for estimating muscle forces and joint loads during lifting tasks. The specific objectives of the present thesis are threefold:

1) Development of a stability-based optimization framework for OpenSim (Study 1): This framework aims to improve the accuracy of estimated muscle activations in optimization-driven models during static lifting tasks.
2) Assessment of modelling decisions on external forces applied to the hands (Study 2): This study examines how different modelling decisions regarding external hand forces and moments impact estimated spinal loads during dynamic lifting tasks.
3) Development and validation of a new model for dynamic lifting tasks (Study 3 & 4): The goal is to create a model suitable for simulating dynamic lifting tasks and validate estimated intervertebral forces across a broader range of tasks compared to previous spine modelling studies.

The general hypotheses in this thesis are as follows:

1) The developed stability-based optimization framework can generate muscle activations aligning better with experimental EMG data than the default OpenSim muscle recruitment solver.

2) Various decisions for modelling external hand forces and moments greatly influence estimated spinal loads in dynamic lifting tasks, necessitating researchers to report uncertainties in their results due to these decisions.

3) The newly developed model can predict spinal forces accurately during dynamic lifting tasks.

## 2.11 References


Ackermann, M., Schiehlen, W., 2009. Physiological methods to solve the force-sharing problem in biomechanics. In: Bottasso, C. (Ed.), Multibody Dynamics: Computational Methods and Applications. Springer, Dordrecht, pp. 1–23.

Adams, M.A., Dolan, P., 2005. Spine biomechanics. J. Biomech. 38, 1972–1983.

Aiyangar, A.K., Zheng, L., Tashman, S., Anderst, W.J., Zhang, X., 2014. Capturing three-dimensional in vivo lumbar intervertebral joint kinematics using dynamic stereo-X-ray imaging. J. Biomech. Eng. 136, 11004.

Akhavanfar, M., Kazemi, H., Eskandari, A.H., Arjmand, N., 2018. Obesity and spinal loads; a combined MR imaging and subject-specific modelling investigation. J. Biomech. 70, 102–112.

Alemi, M.M., Banks, J.J., Lynch, A.C., Allaire, B.T., Bouxsein, M.L., Anderson, D.E., 2023. EMG validation of a subject-specific thoracolumbar spine musculoskeletal model during dynamic activities in older adults. Ann. Biomed. Eng. 1–10.

Alemi, M.M., Burkhart, K.A., Lynch, A.C., Allaire, B.T., Mousavi, S.J., Zhang, C., Bouxsein, M.L., Anderson, D.E., 2021. The influence of kinematic constraints on model performance during inverse kinematics analysis of the thoracolumbar spine. Front. Bioeng. Biotechnol. 9, 688041.

Anderson, A.E., Ellis, B.J., Weiss, J.A., 2007. Verification, validation and sensitivity studies in computational biomechanics. Comput. Methods Biomech. Biomed. Engin. 10, 171–184.

Andersson, G.B., Ortengren, R., Nachemson, A., 1977. Intradiskal pressure, intra-abdominal pressure and myoelectric back muscle activity related to posture and loading. Clin. Orthop. Relat. Res. 129, 156–164.

Antoniadis, A., Lambert-Lacroix, S., Poggi, J.-M., 2021. Random forests for global sensitivity analysis: A selective review. Reliab. Eng. Syst. Saf. 206, 107312.

Arjmand, N., Gagnon, D., Plamondon, A., Shirazi-Adl, A., Larivière, C., 2010. A comparative study of two trunk biomechanical models under symmetric and asymmetric loadings. J. Biomech. 43, 485–491.

Arjmand, N., Shirazi-Adl, A., 2006. Sensitivity of kinematics-based model predictions to optimization criteria in static lifting tasks. Med. Eng. Phys. 28, 504–514.

Arjmand, N., Shirazi-Adl, A., Bazrgari, B., 2006. Wrapping of trunk thoracic extensor muscles

influences muscle forces and spinal loads in lifting tasks. Clin. Biomech. 21, 668–675.

Arjmand, N., Shirazi-Adl, A., Parnianpour, M., 2008. Relative efficiency of abdominal muscles in spine stability. Comput. Methods Biomech. Biomed. Engin. 11, 291–299.

Arjmand, N., Shirazi-Adl, A., Parnianpour, M., 2007. Trunk biomechanical models based on equilibrium at a single-level violate equilibrium at other levels. Eur. Spine J. 16, 701–709.

Bahr, R., Krosshaug, T., 2005. Understanding injury mechanisms: a key component of preventing injuries in sport. Br. J. Sports Med. 39, 324–329.

Banks, J.J., Alemi, M.M., Allaire, B.T., Lynch, A.C., Bouxsein, M.L., Anderson, D.E., 2023. Using static postures to estimate spinal loading during dynamic lifts with participant-specific thoracolumbar musculoskeletal models. Appl. Ergon. 106, 103869.

Banks, J.J., Umberger, B.R., Caldwell, G.E., 2022. EMG optimization in OpenSim: A model for estimating lower back kinetics in gait. Med. Eng. Phys. 103, 103790.

Bassani, T., Stucovitz, E., Qian, Z., Briguglio, M., Galbusera, F., 2017. Validation of the AnyBody full body musculoskeletal model in computing lumbar spine loads at L4L5 level. J. Biomech. 58, 89–96.

Bauer, S., Keller, E., Paulus, D., 2016. Sensitivity analysis of intervertebral disc parameters: MBS model of the lumbar spine. Int. J. Eng. Appl. Sci. 3, 257659.

Bayoglu, R., Guldeniz, O., Verdonschot, N., Koopman, B., Homminga, J., 2019. Sensitivity of muscle and intervertebral disc force computations to variations in muscle attachment sites. Comput. Methods Biomech. Biomed. Engin. 22, 1135–1143.

Beaucage-Gauvreau, E., Brandon, S.C.E., Robertson, W.S.P., Fraser, R., Freeman, B.J.C., Graham, R.B., Thewlis, D., Jones, C.F., 2021. Lumbar spine loads are reduced for activities of daily living when using a braced arm-to-thigh technique. Eur. Spine J. 30, 1035–1042.

Beaucage-Gauvreau, E., Robertson, W.S.P., Brandon, S.C.E., Fraser, R., Freeman, B.J.C., Graham, R.B., Thewlis, D., Jones, C.F., 2019. Validation of an OpenSim full-body model with detailed lumbar spine for estimating lower lumbar spine loads during symmetric and asymmetric lifting tasks. Comput. Methods Biomech. Biomed. Engin. 22, 451–464.

Begon, M., Andersen, M.S., Dumas, R., 2018. Multibody kinematics optimization for the estimation of upper and lower limb human joint kinematics: a systematized methodological review. J. Biomech. Eng. 140, 30801.

Benos, L., Tsaopoulos, D., Bochtis, D., 2020. A review on ergonomics in agriculture. Part I: Manual operations. Appl. Sci. 10, 1905.

Bergmark, A., 1989. Stability of the lumbar spine: a study in mechanical engineering. Acta Orthop. Scand. 60, 1–54.

Bonfiglioli, R., Caraballo-Arias, Y., Salmen-Navarro, A., 2022. Epidemiology of work-related musculoskeletal disorders. Curr. Opin. Epidemiol. Public Heal. 1, 18–24.

Brekelmans, W.A.M., Poort, H.W., Slooff, T., 1972. A new method to analyse the mechanical behaviour of skeletal parts. Acta Orthop. Scand. 43, 301–317.

Bruno, A.G., Bouxsein, M.L., Anderson, D.E., 2015. Development and validation of a musculoskeletal model of the fully articulated thoracolumbar spine and rib cage. J. Biomech. Eng. 137, 081003.

Chaffin, D.B., 1969. A computerized biomechanical model—development of and use in studying gross body actions. J. Biomech. 2, 429–441.

Chen, C.S., Huang, C.H., Shih, S.L., 2015. Biomechanical evaluation of a new pedicle screw-based posterior dynamic stabilization device (Awesome Rod System) - a finite element analysis. BMC Musculoskelet. Disord. 16, 1–8.

Cholewicki, J., McGill, S.M., 1996. Mechanical stability of the in vivo lumbar spine: Implications for injury and chronic low back pain. Clin. Biomech. 11, 1–15.

Cholewicki, J., McGill, S.M., 1994. EMG assisted optimization: A hybrid approach for estimating muscle forces in an indeterminate biomechanical model. J. Biomech. 27, 1287–1289.

Cholewicki, J., McGill, S.M., Norman, R.W., 1995. Comparison of muscle forces and joint load from an optimization and EMG assisted lumbar spine model: towards development of a hybrid approach. J. Biomech. 28, 321–331.

Christophy, M., Curtin, M., Senan, N.A.F., Lotz, J.C., O'Reilly, O.M., 2013. On the modelling of the intervertebral joint in multibody models for the spine. Multibody Syst. Dyn. 30, 413–432.

Christophy, M., Faruk Senan, N.A., Lotz, J.C., O'Reilly, O.M., 2012. A musculoskeletal model for the lumbar spine. Biomech. Model. Mechanobiol. 11, 19–34.

Cieza, A., Causey, K., Kamenov, K., Hanson, S.W., Chatterji, S., Vos, T., 2020. Global estimates of the need for rehabilitation based on the Global Burden of Disease study 2019: a systematic analysis for the Global Burden of Disease Study 2019. Lancet 396, 2006–2017.

Clouet, J., Vinatier, C., Merceron, C., Pot-Vaucel, M., Hamel, O., Weiss, P., Grimandi, G., Guicheux, J., 2009. The intervertebral disc: from pathophysiology to tissue engineering. Jt. Bone Spine 76, 614–618.

Coenen, P., Gouttebarge, V., van der Burght, A.S.A.M., van Dieën, J.H., Frings-Dresen, M.H.W., van der Beek, A.J., Burdorf, A., 2014a. The effect of lifting during work on low back pain: a health impact assessment based on a meta-analysis. Occup. Environ. Med. 71, 871–877.

Coenen, P., Kingma, I., Boot, C.R.L., Bongers, P.M., Van Dieën, J.H., 2014b. Cumulative mechanical low-back load at work is a determinant of low-back pain. Occup. Environ. Med. 71, 332–337.

Crisco, J.J., Panjabi, M.M., Yamamoto, I., Oxland, T.R., 1992. Euler stability of the human ligamentous lumbar spine. Part II: Experiment. Clin. Biomech. 7, 27–32.

Damm, P., Reitmaier, S., Hahn, S., Waldheim, V., Firouzabadi, A., Schmidt, H., 2020. In vivo hip and lumbar spine implant loads during activities in forward bent postures. J. Biomech. 102, 109517.

Damsgaard, M., Rasmussen, J., Christensen, S.T., Surma, E., De Zee, M., 2006. Analysis of musculoskeletal systems in the AnyBody Modelling System. Simul. Model. Pract. Theory 14,

1100–1111.

De Zee, M., Hansen, L., Wong, C., Rasmussen, J., Simonsen, E.B., 2007. A generic detailed rigid-body lumbar spine model. J. Biomech. 40, 1219–1227.

Dehghan, P., Arjmand, N., 2022. The National Institute for Occupational Safety and Health (NIOSH) recommended weight generates different spine loads in load-handling activity performed using stoop, semi-squat and full-squat techniques; a full-body musculoskeletal model study. Hum. Factors 00187208221141652.

Delp, S.L., Anderson, F.C., Arnold, A.S., Loan, P., Habib, A., John, C.T., Guendelman, E., Thelen, D.G., 2007. OpenSim: Open-source software to create and analyze dynamic simulations of movement. IEEE Trans. Biomed. Eng. 54, 1940–1950.

Delp, S.L., Loan, J.P., 1995. A graphics-based software system to develop and analyze models of musculoskeletal structures. Comput. Biol. Med. 25, 21–34.

Desmoulin, G.T., Pradhan, V., Milner, T.E., 2020. Mechanical aspects of intervertebral disc injury and implications on biomechanics. Spine 45, 457–464.

Disselhorst-Klug, C., Schmitz-Rode, T., Rau, G., 2009. Surface electromyography and muscle force: Limits in sEMG-force relationship and new approaches for applications. Clin. Biomech. 24, 225–235.

Dreischarf, M., Rohlmann, A., Zhu, R., Schmidt, H., Zander, T., 2013. Is it possible to estimate the compressive force in the lumbar spine from intradiscal pressure measurements? A finite element evaluation. Med. Eng. Phys. 35, 1385–1390.

Dreischarf, M., Shirazi-Adl, A., Arjmand, N., Rohlmann, A., Schmidt, H., 2016. Estimation of loads on human lumbar spine: a review of in vivo and computational model studies. J. Biomech. 49, 833–845.

Duprey, S., Naaim, A., Moissenet, F., Begon, M., Chèze, L., 2017. Kinematic models of the upper limb joints for multibody kinematics optimisation: an overview. J. Biomech. 62, 87–94.

El-Rich, M., Shirazi-Adl, A., 2005. Effect of load position on muscle forces, internal loads and stability of the human spine in upright postures. Comput. Methods Biomech. Biomed. Engin. 8, 359–368.

El Ouaaid, Z., Shirazi-Adl, A., Arjmand, N., Plamondon, A., 2013. Coupled objective function to study the role of abdominal muscle forces in lifting using the kinematics-driven model. Comput. Methods Biomech. Biomed. Engin. 16, 54–65.

Erdemir, A., McLean, S., Herzog, W., van den Bogert, A.J., 2007. Model-based estimation of muscle forces exerted during movements. Clin. Biomech. 22, 131–154.

Farina, D., Merletti, R., Enoka, R.M., 2004. The extraction of neural strategies from the surface EMG. J. Appl. Physiol. 96, 1486–1495.

Favier, C.D., Finnegan, M.E., Quest, R.A., Honeyfield, L., McGregor, A.H., Phillips, A.T.M., 2021. An open-source musculoskeletal model of the lumbar spine and lower limbs: a validation for movements of the lumbar spine. Comput. Methods Biomech. Biomed. Engin.

24, 1310–1325.

Gagnon, D., Arjmand, N., Plamondon, A., Shirazi-Adl, A., Larivière, C., 2011. An improved multi-joint EMG-assisted optimization approach to estimate joint and muscle forces in a musculoskeletal model of the lumbar spine. J. Biomech. 44, 1521–1529.

Garner, B.A., Pandy, M.G., 2000. The obstacle-set method for representing muscle paths in musculoskeletal models. Comput. Methods Biomech. Biomed. Engin. 3, 1–30.

Ghezelbash, F., Eskandari, A.H., Shirazi-Adl, A., Arjmand, N., El-Ouaaid, Z., Plamondon, A., 2018. Effects of motion segment simulation and joint positioning on spinal loads in trunk musculoskeletal models. J. Biomech. 70, 149–156.

Ghezelbash, F., Shirazi-Adl, A., Arjmand, N., El-Ouaaid, Z., Plamondon, A., Meakin, J.R., 2016. Effects of sex, age, body height and body weight on spinal loads: sensitivity analyses in a subject-specific trunk musculoskeletal model. J. Biomech. 49, 3492–3501.

Ghezelbash, F., Shirazi-Adl, A., Sharifi, M., Arjmand, N., Bazrgari, B., 2023. Computational stability of human musculoskeletal systems. In: Paul, G., Doweidar, M.H. (Eds.), Digital Human Modelling and Medicine. Elsevier Inc., pp. 85–105.

Govaerts, R., Tassignon, B., Ghillebert, J., Serrien, B., De Bock, S., Ampe, T., El Makrini, I., Vanderborght, B., Meeusen, R., De Pauw, K., 2021. Prevalence and incidence of work-related musculoskeletal disorders in secondary industries of 21st century Europe: a systematic review and meta-analysis. BMC Musculoskelet. Disord. 22, 1–30.

Granata, K.P., Marras, W.S., 1993. An EMG-assisted model of loads on the lumbar spine during asymmetric trunk extensions. J. Biomech. 26, 1309–1317.

Granata, K.P., Orishimo, K.F., 2001. Response of trunk muscle coactivation to changes in spinal stability. J. Biomech. 34, 1117–1123.

Granata, K.P., Wilson, S.E., 2001. Trunk posture and spinal stability. Clin. Biomech. 16, 650–659.

Guo, L.-X., Wang, Q.-D., 2020. Biomechanical analysis of a new bilateral pedicle screw fixator system based on topological optimization. Int. J. Precis. Eng. Manuf. 21, 1363–1374.

Hajihosseinali, M., Arjmand, N., Shirazi-Adl, A., Farahmand, F., Ghiasi, M.S., 2014. A novel stability and kinematics-driven trunk biomechanical model to estimate muscle and spinal forces. Med. Eng. Phys. 36, 1296–1304.

Hicks, J.L., Uchida, T.K., Seth, A., Rajagopal, A., Delp, S.L., 2015. Is my model good enough? Best practices for verification and validation of musculoskeletal models and simulations of movement. J. Biomech. Eng. 137.

Howarth, S.J., Allison, A.E., Grenier, S.G., Cholewicki, J., McGill, S.M., 2004. On the implications of interpreting the stability index: A spine example. J. Biomech. 37, 1147–1154.

Howarth, S.J., Beach, T.A.C., Callaghan, J.P., 2010. Dynamic factors and force-weighting corrections influence estimates of cumulative vertebral joint compression. Theor. Issues Ergon. Sci. 11, 474–488.

Hughes, R.E., Bean, J.C., Chaffin, D.B., 1995. Evaluating the effect of co-contraction in

optimization models. J. Biomech. 28, 875–878.

Huynh, K.T., Gibson, I., Jagdish, B.N., Lu, W.F., 2015. Development and validation of a discretised multi-body spine model in LifeMOD for biodynamic behaviour simulation. Comput. Methods Biomech. Biomed. Engin. 18, 175–184.

Hwang, J., Knapik, G.G., Dufour, J.S., Marras, W.S., 2017. Curved muscles in biomechanical models of the spine: a systematic literature review. Ergonomics 60, 577–588.

Ignasiak, D., Dendorfer, S., Ferguson, S.J., 2016. Thoracolumbar spine model with articulated ribcage for the prediction of dynamic spinal loading. J. Biomech. 49, 959–966.

Jorgensen, M.J., Marras, W.S., Granata, K.P., Wiand, J.W., 2001. MRI-derived moment-arms of the female and male spine loading muscles. Clin. Biomech. 16, 182–193.

Jorgensen, M.J., Marras, W.S., Gupta, P., Waters, T.R., 2003. Effect of torso flexion on the lumbar torso extensor muscle sagittal plane moment arms. Spine J. 3, 363–369.

Kazemi, Z., Arjmand, N., Mazloumi, A., Karimi, Z., Keihani, A., Ghasemi, M.S., 2023. Effect of muscular fatigue on the cumulative lumbar damage during repetitive lifting task: a comparative study of damage calculation methods. Ergonomics 1–16.

Khoddam-Khorasani, P., Arjmand, N., Shirazi-Adl, A., 2018. Trunk hybrid passive–active musculoskeletal modelling to determine the detailed T12–S1 response under in vivo loads. Ann. Biomed. Eng. 46, 1830–1843.

Khurelbaatar, T., Kim, K., Kim, Y.H., 2015. A cervico-thoraco-lumbar multibody dynamic model for the estimation of joint loads and muscle forces. J. Biomech. Eng. 137, 111001.

Khuyagbaatar, B., Kim, K., Kim, Y.H., 2023. Recent developments in finite element analysis of the lumbar spine. Int. J. Precis. Eng. Manuf. 1–10.

Knapik, G.G., Mendel, E., Bourekas, E., Marras, W.S., 2022. Computational lumbar spine models: A literature review. Clin. Biomech. 100, 105816.

Kramer, P.A., Hammerberg, A.G., Sylvester, A.D., 2019. Modelling the spine using finite element models: considerations and cautions. Spinal Evol. Morphol. Funct. Pathol. spine hominoid Evol. 387–400.

Le, P., Best, T.M., Khan, S.N., Mendel, E., Marras, W.S., 2017. A review of methods to assess coactivation in the spine. J. Electromyogr. Kinesiol. 32, 51–60.

Lerchl, T., El Husseini, M., Bayat, A., Sekuboyina, A., Hermann, L., Nispel, K., Baum, T., Löffler, M.T., Senner, V., Kirschke, J.S., 2022. Validation of a patient-specific musculoskeletal model for lumbar load estimation generated by an automated pipeline from whole body CT. Front. Bioeng. Biotechnol. 10, 862804.

Lerchl, T., Nispel, K., Baum, T., Bodden, J., Senner, V., Kirschke, J.S., 2023. Multibody models of the thoracolumbar spine: A review on applications, limitations, and challenges. Bioengineering 10, 202.

Li, Guoan, Wang, S., Passias, P., Xia, Q., Li, Gang, Wood, K., 2009. Segmental in vivo vertebral motion during functional human lumbar spine activities. Eur. spine J. 18, 1013–1021.

Li, J.-Q., Kwong, W.-H., Chan, Y.-L., Kawabata, M., 2022. Comparison of in vivo intradiscal pressure between sitting and standing in human lumbar spine: a systematic review and meta-analysis. Life 12, 457.

Lund, M.E., de Zee, M., Andersen, M.S., Rasmussen, J., 2012. On validation of multibody musculoskeletal models. Proc. Inst. Mech. Eng. Part H J. Eng. Med. 226, 82–94.

Maas, E.T., Koehoorn, M., McLeod, C.B., 2020. Descriptive epidemiology of gradual return to work for workers with a work-acquired musculoskeletal disorder in British Columbia, Canada. J. Occup. Environ. Med. 62, 113–123.

Madinei, S., Motabar, H., Ning, X., 2018. The influence of external load configuration on trunk biomechanics and spinal loading during sudden loading. Ergonomics 61, 1364–1373.

Malakoutian, M., Street, J., Wilke, H.-J., Stavness, I., Fels, S., Oxland, T., 2018. A musculoskeletal model of the lumbar spine using ArtiSynth–development and validation. Comput. Methods Biomech. Biomed. Eng. Imaging Vis. 6, 483–490.

Marras, W.S., 2000. Occupational low back disorder causation and control. Ergonomics 43, 880–902.

McGill, S.M., 1997. The biomechanics of low back injury: Implications on current practice in industry and the clinic. J. Biomech. 30, 465–475.

McGill, S.M., Cholewicki, J., 2001. Biomechanical basis for stability: an explanation to enhance clinical utility. J. Orthop. Sports Phys. Ther. 31, 96–100.

McGill, S.M., Grenier, S., Kavcic, N., Cholewicki, J., 2003. Coordination of muscle activity to assure stability of the lumbar spine. J. Electromyogr. Kinesiol. 13, 353–359.

McGill, S.M., Norman, R.W., 1987. Effects of an anatomically detailed erector spinae model on L4L5 disc compression and shear. J. Biomech. 20, 591–600.

McGill, S.M., Norman, R.W., 1986. 1986 Volvo award in biomechanics: partitioning of the L4-L5 dynamic moment into disc, ligamentous, and muscular components during lifting. Spine 11, 666–678.

Merryweather, A.S., Loertscher, M.C., Bloswick, D.S., 2009. A revised back compressive force estimation model for ergonomic evaluation of lifting tasks. Work 34, 263–272.

Mohammadi, Y., Arjmand, N., Shirazi-Adl, A., 2015. Comparison of trunk muscle forces, spinal loads and stability estimated by one stability-and three EMG-assisted optimization approaches. Med. Eng. Phys. 37, 792–800.

Nispel, K., Lerchl, T., Senner, V., Kirschke, J.S., 2023. Recent advances in coupled MBS and FEM models of the spine—A review. Bioengineering 10, 315.

Nussbaum, M.A., Chaffin, D.B., Rechtien, C.J., 1995. Muscle lines-of-action affect predicted forces in optimization-based spine muscle modelling. J. Biomech. 28, 401–409.

Pandy, M.G., 2001. Computer modelling and simulation of human movement. Annu. Rev. Biomed. Eng. 3, 245–273.

Parreira, P., Maher, C.G., Steffens, D., Hancock, M.J., Ferreira, M.L., 2018. Risk factors for low back pain and sciatica: an umbrella review. Spine J. 18, 1715–1721.

Petit, A., Roquelaure, Y., 2015. Low back pain, intervertebral disc and occupational diseases. Int. J. Occup. Saf. Ergon. 21, 15–19.

Polga, D.J., Beaubien, B.P., Kallemeier, P.M., Schellhas, K.P., Lew, W.D., Buttermann, G.R., Wood, K.B., 2004. Measurement of in vivo intradiscal pressure in healthy thoracic intervertebral discs. Spine 29, 1320–1324.

Potvin, J.R., 2008. Occupational spine biomechanics: A journey to the spinal frontier. J. Electromyogr. Kinesiol. 18, 891–899.

Potvin, J.R., 1997. Use of NIOSH equation inputs to calculate lumbosacral compression forces. Ergonomics 40, 691–707.

Potvin, J. R., Brown, S. H., 2005. An equation to calculate individual muscle contributions to joint stability. J. Biomech. 38, 973–980.

Putzer, M., Ehrlich, I., Rasmussen, J., Gebbeken, N., Dendorfer, S., 2016. Sensitivity of lumbar spine loading to anatomical parameters. J. Biomech. 49, 953–958.

Raabe, M.E., Chaudhari, A.M.W., 2016. An investigation of jogging biomechanics using the full-body lumbar spine model: model development and validation. J. Biomech. 49, 1238–1243.

Raikova, R., 1999. About weight factors in the non-linear objective functions used for solving indeterminate problems in biomechanics. J. Biomech. 32, 689–694.

Rajaee, M.A., Arjmand, N., Shirazi-Adl, A., Plamondon, A., Schmidt, H., 2015. Comparative evaluation of six quantitative lifting tools to estimate spine loads during static activities. Appl. Ergon. 48, 22–32.

Rasmussen, J., Damsgaard, M., Voigt, M., 2001. Muscle recruitment by the min/max criterion—a comparative numerical study. J. Biomech. 34, 409–415.

Reeves, N.P., Narendra, K.S., Cholewicki, J., 2007. Spine stability: The six blind men and the elephant. Clin. Biomech. 22, 266–274.

Rohlmann, A., Arntz, U., Graichen, F., Bergmann, G., 2001. Loads on an internal spinal fixation device during sitting. J. Biomech. 34, 989–993.

Rohlmann, A, Dreischarf, M., Zander, T., Graichen, F., Bergmann, G., 2014a. Loads on a vertebral body replacement during locomotion measured in vivo. Gait Posture 39, 750–755.

Rohlmann, A., Dreischarf, M., Zander, T., Graichen, F., Strube, P., Schmidt, H., Bergmann, G., 2013. Monitoring the load on a telemeterised vertebral body replacement for a period of up to 65 months. Eur. Spine J. 22, 2575–2581.

Rohlmann, A., Graichen, F., Bergmann, G., 2002. Loads on an internal spinal fixation device during physical therapy. Phys. Ther. 82, 44–52.

Rohlmann, A., Graichen, F., Weber, U., Bergmann, G., 2000. Monitoring in vivo implant loads with a telemeterized internal spinal fixation device. Spine 25, 2981–2986.

Rohlmann, A., Pohl, D., Bender, A., Graichen, F., Dymke, J., Schmidt, H., Bergmann, G., 2014b. Activities of everyday life with high spinal loads. PLoS One 9, 3–11.

Rohlmann, A., Schmidt, H., Gast, U., Kutzner, I., Damm, P., Bergmann, G., 2014c. In vivo measurements of the effect of whole body vibration on spinal loads. Eur. Spine J. 23, 666–672.

Rohlmann, A., Zander, T., Graichen, F., Schmidt, H., Bergmann, G., 2014d. Spinal loads during cycling on an ergometer. PLoS One 9, 7–12.

Rohlmann, A, Zander, T., Graichen, F., Schmidt, H., Bergmann, G., 2014e. How does the way a weight is carried affect spinal loads? Ergonomics 57, 262–270.

Rosado, A.S., Baptista, J.S., Guilherme, M.N.H., Guedes, J.C., 2022. Economic impact of work-related musculoskeletal disorders—A systematic review. In: Arezes, P. M., Baptista, J. S., Melo, R. B., Castelo Branco, J., Carneiro, P., Colim, A., Costa, N., Costa, S., Duarte, J., Guedes, J.C. (Eds.), Occupational and Environmental Safety and Health IV. Springer International Publishing AG., Switzerland, pp. 599–613.

Schmid, S., Burkhart, K.A., Allaire, B.T., Grindle, D., Anderson, D.E., 2020. Musculoskeletal full-body models including a detailed thoracolumbar spine for children and adolescents aged 6–18 years. J. Biomech. 102, 109305.

Schmidt, H., Galbusera, F., Rohlmann, A., Shirazi-Adl, A., 2013. What have we learned from finite element model studies of lumbar intervertebral discs in the past four decades? J. Biomech. 46, 2342–2355.

Schultz, A., Andersson, G., Ortengren, R., Haderspeck, K., Nachemson, A., 1982. Loads on the lumbar spine. Validation of a biomechanical analysis by measurements of intradiscal pressures and myoelectric signals. J. Bone Joint Surg. Am. 64, 713–720.

Schultz, A.B., Andersson, G.B.J., 1981. Analysis of loads on the lumbar spine. Spine 6, 76–82.

Senteler, M., Aiyangar, A., Weisse, B., Farshad, M., Snedeker, J.G., 2018. Sensitivity of intervertebral joint forces to center of rotation location and trends along its migration path. J. Biomech. 70, 140–148.

Senteler, M., Weisse, B., Rothenfluh, D.A., Snedeker, J.G., 2016. Intervertebral reaction force prediction using an enhanced assembly of OpenSim models. Comput. Methods Biomech. Biomed. Engin. 19, 538–548.

Seth, A., Hicks, J.L., Uchida, T.K., Habib, A., Dembia, C.L., Dunne, J.J., Ong, C.F., DeMers, M.S., Rajagopal, A., Millard, M., 2018. OpenSim: Simulating musculoskeletal dynamics and neuromuscular control to study human and animal movement. PLoS Comput. Biol. 14, e1006223.

Seth, A., Sherman, M., Reinbolt, J.A., Delp, S.L., 2011. OpenSim: a musculoskeletal modelling and simulation framework for in silico investigations and exchange. Procedia IUTAM 2, 212–232.

Shirazi-Adl, A., Parnianpour, M., 2000. Load-bearing and stress analysis of the human spine under a novel wrapping compression loading. Clin. Biomech. 15, 718–725.

Shourijeh, M.S., McPhee, J., 2014a. Forward dynamic optimization of human gait simulations: a global parameterization approach. J. Comput. Nonlinear Dyn. 9, 31018.

Shourijeh, M.S., McPhee, J., 2014b. Optimal control and forward dynamics of human periodic motions using fourier series for muscle excitation patterns. J. Comput. Nonlinear Dyn. 9, 21005.

Shourijeh, M.S., Smale, K.B., Potvin, B.M., Benoit, D.L., 2016. A forward-muscular inverse-skeletal dynamics framework for human musculoskeletal simulations. J. Biomech. 49, 1718–1723.

Simitses, G., Hodges, D.H., 2006. Fundamentals of Structural Stability. Elsevier/Butterworth-Heinemann, Amsterdam.

Skals, S., Bláfoss, R., de Zee, M., Andersen, L.L., Andersen, M.S., 2021. Effects of load mass and position on the dynamic loading of the knees, shoulders and lumbar spine during lifting: a musculoskeletal modelling approach. Appl. Ergon. 96, 103491.

Soylar, P., Ozer, A., 2018. Evaluation of the prevalence of musculoskeletal disorders in nurses: a systematic review. Med Sci 7, 479–485.

Staudenmann, D., Kingma, I., Stegeman, D.F., van Dieën, J.H., 2005. Towards optimal multi-channel EMG electrode configurations in muscle force estimation: a high density EMG study. J. Electromyogr. Kinesiol. 15, 1–11.

Stokes, I.A.F., Henry, S.M., Single, R.M., 2003. Surface EMG electrodes do not accurately record from lumbar multifidus muscles. Clin. Biomech. 18, 9–13.

Suderman, B.L., Vasavada, A.N., 2012. Moving muscle points provide accurate curved muscle paths in a model of the cervical spine. J. Biomech. 45, 400–404.

Sultan-Taieb, H., Parent-Lamarche, A., Gaillard, A., Stock, S., Nicolakakis, N., Hong, Q.N., Vezina, M., Coulibaly, Y., Vezina, N., Berthelette, D., 2017. Economic evaluations of ergonomic interventions preventing work-related musculoskeletal disorders: a systematic review of organizational-level interventions. BMC Public Health 17, 1–13.

Takahashi, I., Kikuchi, S., Sato, K., Sato, N., 2006. Mechanical load of the lumbar spine during forward bending motion of the trunk–a biomechanical study. Spine 31, 18–23.

Thelen, D.G., Anderson, F.C., Delp, S.L., 2003. Generating dynamic simulations of movement using computed muscle control. J. Biomech. 36, 321–328.

Viceconti, M., Pappalardo, F., Rodriguez, B., Horner, M., Bischoff, J., Tshinanu, F.M., 2021. In silico trials: Verification, validation and uncertainty quantification of predictive models used in the regulatory evaluation of biomedical products. Methods 185, 120–127.

Vigouroux, L., Quaine, F., Labarre-Vila, A., Amarantini, D., Moutet, F., 2007. Using EMG data to constrain optimization procedure improves finger tendon tension estimations during static fingertip force production. J. Biomech. 40, 2846–2856.

Vos, T., Lim, S.S., Abbafati, C., Abbas, K.M., Abbasi, M., Abbasifard, M., Abbasi-Kangevari, M., Abbastabar, H., Abd-Allah, F., Abdelalim, A., 2020. Global burden of 369 diseases and

injuries in 204 countries and territories, 1990–2019: a systematic analysis for the Global Burden of Disease Study 2019. Lancet 396, 1204–1222.

Wang, D., Dai, F., Ning, X., 2015. Risk assessment of work-related musculoskeletal disorders in construction: State-of-the-art review. J. Constr. Eng. Manag. 141, 4015008.

Wang, Q.-D., Guo, L.-X., 2021. Prediction of complications and fusion outcomes of fused lumbar spine with or without fixation system under whole-body vibration. Med. Biol. Eng. Comput. 59, 1223–1233.

Waters, T., Yeung, S., Genaidy, A., Callaghan, J., Barriera-Viruet, H., & Deddens, J., 2006. Cumulative spinal loading exposure methods for manual material handling tasks. Part 1: is cumulative spinal loading associated with lower back disorders? Theor. Issues Ergon. Sci. 7, 113–130.

Welch-Phillips, A., Gibbons, D., Ahern, D.P., Butler, J.S., 2020. What is finite element analysis? Clin. Spine Surg. 33, 323–324.

Wilke, H.J., Neef, P., Caimi, M., Hoogland, T., Claes, L., 1999. New in vivo measurements of pressures in the intervertebral disc in daily life. Spine 24, 755–762.

Wilke, H.J., Neef, P., Hinz, B., Seidel, H., Claes, L., 2001. Intradiscal pressure together with anthropometric data–a data set for the validation of models. Clin. Biomech. 16, 111–126.

Xu, M., Yang, J., Lieberman, I., Haddas, R., 2019. Stress distribution in vertebral bone and pedicle screw and screw–bone load transfers among various fixation methods for lumbar spine surgical alignment: a finite element study. Med. Eng. Phys. 63, 26–32.

Zander, T., Dreischarf, M., Schmidt, H., 2016. Sensitivity analysis of the position of the intervertebral centres of reaction in upright standing–a musculoskeletal model investigation of the lumbar spine. Med. Eng. Phys. 38, 297–301.

Zander, T., Dreischarf, M., Schmidt, H., Bergmann, G., Rohlmann, A., 2015. Spinal loads as influenced by external loads: A combined in vivo and in silico investigation. J. Biomech. 48, 578–584.

# Chapter 3: Development of a Novel MATLAB-Based Framework for Implementing Mechanical Joint Stability Constraints within OpenSim Musculoskeletal Models

Published in Journal of Biomechanics 2019; 91: 61–68.
https://doi.org/10.1016/j.jbiomech.2019.05.007

## 3.1 Abstract

The Static Optimization (SO) solver in OpenSim estimates muscle activations and forces that only equilibrate applied moments. In this study, SO was enhanced through an open-access MATLAB interface, where calculated muscle activations can additionally satisfy crucial mechanical stability requirements. This stability-constrained SO (SCSO) is applicable to many OpenSim models and can potentially produce more biofidelic results than SO alone, especially when antagonistic muscle co-contraction is required to stabilize body joints. This hypothesis was tested using existing models and experimental data in the literature. Muscle activations were calculated by SO and SCSO for a spine model during two series of static trials (i.e. simulation 1 and 2), and also for a lower limb model (Appendix A–SI. 2). In simulation 1, symmetric and asymmetric flexion postures were compared, while in simulation 2, various external load heights were compared, where increases in load height did not change the external lumbar flexion moment, but necessitated higher EMG activations. During the tasks in simulation 1, the predicted muscle activations by SCSO demonstrated less average deviation from the EMG data (6.8% –7.5%) compared to those from SO (10.2%). In simulation 2, SO predicts constant muscle activations and forces, while SCSO predicts increases in the average activations of back and abdominal muscles that better match experimental data. Although the SCSO results are sensitive to some parameters (e.g., musculotendon stiffness), when considering the strategy of the central nervous system in distributing muscle forces and in activating antagonistic muscles, the assigned activations by SCSO are more biofidelic than SO.

## 3.2 Introduction

Comprehensive knowledge of internal loads acting on the human body, including muscle forces and joint loads, is essential for designing effective injury prevention (Bolsterlee et al., 2013), rehabilitation (Neptune and Kautz, 2000), and surgery programs (Gomes et al., 2013), to name a few applications. Musculoskeletal modelling is a widely used approach to estimate internal mechanical loads because the direct measurement of these loads requires invasive methods as well as complex and costly experiments (e.g., Rohlmann et al., 1994; Wilke et al., 2001).

Satisfying dynamic equilibrium equations is critical in all biomechanical models; however, within high-fidelity models, the equilibrium equations cannot be solved deterministically because the number of unknown muscle forces is greater than the number of equations (Dreischarf et al., 2016). Generally, optimization (OPT), electromyography (EMG), or hybrid approaches are used to resolve this redundancy (Dreischarf et al., 2016). Due to issues of using EMG such as recording activity from deep and wide muscles (Staudenmann et al., 2005; Stokes et al., 2003), cross-talk (Farina et al., 2004), and finding proper gains for muscles to satisfy equilibrium equations (Mohammadi et al., 2015), OPT methods remain the most common (Dreischarf et al., 2016).

In a common OPT problem, the solver minimizes or optimizes a cost function for muscle forces (e.g., minimize the sum of activation squared or cubed) subject to the equilibrium equations and minimum/maximum bounds for muscle forces. Failing to assign realistic activations to antagonistic muscles is introduced as the primary shortcoming of the common OPT problem (El Ouaaid et al., 2013). To address the primary limitation of the OPT-based models, some mathematics-based techniques, such as considering non-zero lower bounds for muscle activations (Hughes et al., 1995), or taking opposite signs for the weighting factors assigned to the agonist and antagonist muscles in the objective function (Raikova, 1999) have been proposed. However,

considering mechanical stability criteria as an additional constraint to the common OPT problem as a physiologic-based technique has been proposed in a few musculoskeletal modelling studies (Granata and Wilson, 2001; Brown and Potvin, 2005; Hajihosseinali et al., 2014; Samadi and Arjmand, 2018).

The common OPT methods are implemented within many musculoskeletal modelling platforms, including OpenSim, which is the most widely used open-source platform in biomechanics (Delp et al., 2007). To estimate muscle forces, for both inverse dynamic and forward dynamic procedures, there are analysis tools in OpenSim. The static optimization (SO) tool is designed in OpenSim to calculate muscle forces using an inverse dynamics approach and by solving the common OPT problem (Seth et al., 2011).

Previous OPT-based models that consider stability criteria are: (i) not accessible for all researchers, and/or (ii) designed only for the spine. Hence, incorporating mechanical stability constraints into the default SO solver in OpenSim would be extremely advantageous to many musculoskeletal biomechanics and biomedical engineering researchers. Therefore, the purpose of this study was to design a novel framework for OpenSim using MATLAB to calculate muscle forces that also satisfy given stability requirements. It was hypothesized that the stability-constrained static optimization (SCSO) framework would assign more accurate activations than SO to all muscles, and in particular to antagonistic muscles. To test the hypothesis, existing models and experimental data in the literature were used.

## 3.3 Methods

### *3.3.1 Framework Development*

The default OpenSim SO solver minimizes an objective function in the form of $\sum(a_m)^p$ (Crowninshield and Brand, 1981), subject to two constraints (outlined below), where $a_m$ is the

activation of the $m^{th}$ muscle and $p$ is a user-defined constant (default $p = 2$). Our novel MATLAB-based SCSO framework (The Mathworks, Natick, MA, USA) was developed to mirror this approach, while implementing one additional stability constraint. For the SCSO framework, the fmincon optimization solver in MATLAB (default settings) was employed to calculate muscle activations and forces subject to all three constraints, whereas the OpenSim Application Programming Interface (API, OpenSim 3.3) was used to gather all the required model information from OpenSim (Fig. 3.1).

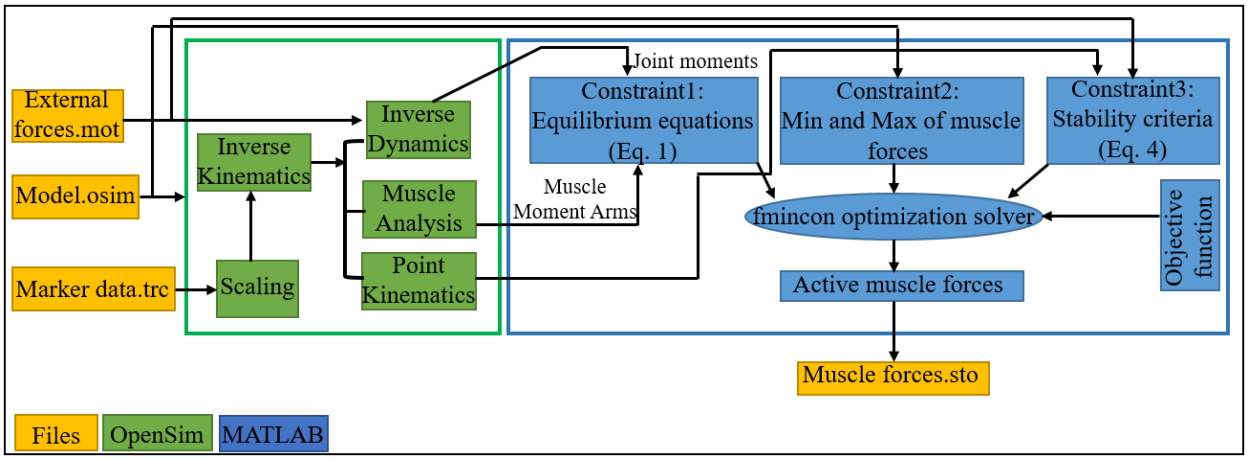


Fig. 3.1. Schematic of the designed framework. The green and blue boxes show the procedures that are accomplished by OpenSim and MATLAB, respectively. Using the fmincon solver in MATLAB, muscle activations and forces are calculated by solving an optimization (OPT) problem. This OPT problem has a user-defined objective function and three constraints. To form constraints 1, 2, and 3, the user-defined model and external force files, as well as Inverse Dynamics (ID), Muscle Analysis (MA), and Point Kinematics (PK) analysis outputs from OpenSim are required. In addtion to the model and external force files, Inverse Kinematics (IK) results are required in OpenSim to run ID, MA, and PK. IK results could be prepared by the user (e.g., the spine modelling in the present study), or by running the IK analysis tool in OpenSim using marker data (e.g., the lower limb model in Appendix A–SI. 2). Users can also scale their musculoskeletal models using the scaling feature provided by OpenSim before running IK. The arrows indicate that a file or outputs of an analysis are used by another part in the framework. MATLAB codes gather the required information from OpenSim either by reading the output files from OpenSim or using the OpenSim application programming interface (API). (For interpretation of the references to colour in this figure legend, the reader is referred to the web version of this article.)

The first constraint in both SO and SCSO maintains dynamic equilibrium between external and internal moments at each joint level for each instant in time such that:

$$\mathbf{r}_{nm} \times \mathbf{F}_{m1} = \mathbf{M}_{n1} \qquad \text{(Eq. 3.1)}$$

where $\mathbf{r}_{\mathrm{nm}}$ is the matrix of muscle moment arms about the model's coordinates, $\mathbf{F}_{\mathrm{m1}}$ represents unknown muscle forces, $\mathbf{M}_{\mathrm{n1}}$ is the matrix of net external moments about each coordinate due to gravity and external forces, n is the number of model coordinates, and m is the number of muscles in the model. To compose this constraint for a desired musculoskeletal model, we used the Inverse Dynamics (ID) tool in OpenSim to calculate $\mathbf{M}_{\mathrm{n1}}$ and Muscle Analysis (MA) tool to calculate $\mathbf{r}_{\mathrm{nm}}$ at each time step.

All constraints in an optimization problem should be written as a function of objective function variables (i.e. muscle activations in this framework). Although Eq. 3.1 is a function of muscle forces, in OpenSim, there are two ways to relate muscle activations to muscle forces:

$$f_i = a_i \mathrm{F}_{\mathrm{i}}^0 \qquad \text{(Eq. 3.2)}$$

$$f_i = a_i f(\mathrm{F}_{\mathrm{i}}^0, l_{\mathrm{i}}, v_{\mathrm{i}}) \qquad \text{(Eq. 3.3)}$$

where $f_i$ and $a_i$ are the force and activation level of muscle *i* at a discrete time step, respectively, $\mathrm{F}_{\mathrm{i}}^0$ is a muscle's maximum isometric force, $l_{\mathrm{i}}$ is the muscle length, $v_{\mathrm{i}}$ is the muscle's shortening/lengthening velocity, and $f(\mathrm{F}_{\mathrm{i}}^0, l_{\mathrm{i}}, v_{\mathrm{i}})$ is the muscle's force–length–velocity (FLV) manifold. In our SCSO framework, $\mathrm{F}_{\mathrm{i}}^0$ is determined from the model file, and $l_{\mathrm{i}}$ and $v_{\mathrm{i}}$ are determined from MA results during the movement. Similar to the native OpenSim solver, users can run SCSO with or without considering FLV by matching FLV characteristics to the muscle type used in their model (e.g., Thelen2003Muscle, Millard2012EquilibriumMuscle, etc.).

The second constraint for SO and SCSO states that muscle activations should be between minimum and maximum bounds (0 and 1 is the standard), and the framework pulls these bounds directly from the .osim model file.

The third constraint, found only in SCSO, is the mechanical stability constraint. A mechanical system can be regarded as stable in a static position when the total potential energy in all joints is at its relative minimum, which means the Hessian matrix of system potential energy with respect to its degrees of freedom should be positive semi-definite (Bergmark, 1989; Cholewicki and McGill, 1996). In the present framework, simplified quasi-static stability equations, describing a system's total stability (S) about individual rotational degrees of freedom in the system, were taken from Potvin and Brown (2005) to quantify the muscular and external work contributions to each joint's stability at each time step. The advantage of these equations is that they can be implemented into any 2D or 3D biomechanical model of a joint, or system of joints (Potvin and Brown, 2005).

The simplified stability (S) equation about each rotational coordinate of a system (Appendix A–SI. 1) is a function of three terms: (i) muscle forces (**F**), (ii) Geometric Stability (**GS**), which consists of parameters related to the muscles' geometry and the muscles' stiffness (q), and (iii) External Work (**EW**). For a user-defined model, movement, and external force set, the SCSO framework calculates **GS** and **EW** terms in all directions by performing Point Kinematics Analysis (PK) and Muscle Analysis (MA) via the OpenSim API. A detailed explanation about the calculation of **GS** and **EW** terms, as well as other important practical remarks about the SCSO framework, is provided in Appendix A–SI. 1. The general form of stability constraints composed at each time step is:

$$\begin{bmatrix} [\mathbf{GS}_x]_{jm} \\ [\mathbf{GS}_y]_{jm} \\ [\mathbf{GS}_z]_{jm} \end{bmatrix}_{3j\times m} \mathbf{F}_{m1} - \begin{bmatrix} [\mathbf{EW}_x]_{j1} \\ [\mathbf{EW}_y]_{j1} \\ [\mathbf{EW}_z]_{j1} \end{bmatrix}_{3j\times 1} \geq [\mathbf{Stability\ Level}]_{3j\times 1} \qquad \text{(Eq. 3.4)}$$

where *j* is the number of joints, *m* is the number of muscles, $\mathbf{F}_{m1}$ is the matrix of unknown muscle forces, and for each joint, both the **GS** and **EW** matrices are resolved about the joint-fixed x, y, and z-axes. Stability Level is a user-defined matrix with constant elements that should be equal to or greater than zero (Brown and Potvin, 2005).

In sum, for a given model and task, SCSO solves the traditional SO problem with one additional stability constraint and generates the outputs (i.e., muscle activations and forces) in the form of text (.sto) files. These files can then be used for further analysis (e.g., Joint Reaction analysis) in OpenSim.

### *3.3.2 Spine Model*

Granata and Wilson (2001) modelled the spine as a double inverted pendulum, where 12 springs were attached to their system as 12 equivalent trunk muscles. Their spine model possesses some limitations (e.g., the geometry of back muscles); however, it is a simple example of a musculoskeletal model with multiple joints and multi-articular muscles. Therefore, a similar spine musculoskeletal model was developed in OpenSim in the present study. The presented spine model in OpenSim had two custom joints (i.e., lumbar-pelvis and thorax-lumbar), 6 rotational degrees of freedom, and 12 Millard2012Equilibrium muscles (Millard et al., 2013). The six muscles included bilaterally (i.e., Left – L, and Right – R) were: Rectus Abdominis (RA), External Obliques (EO), Internal Obliques (IO), and three Erector Spinae (ES) muscles. Muscle geometry and maximum isometric forces were similar to those in Granata and Wilson (2001). Furthermore, to directly match their model, the allowable activation levels for the muscles were set between zero and one and FLV was not considered.

### *3.3.3 Experimental Data from Previous Research Studies*

#### *3.3.3.1 Experiment 1*

Granata and Wilson (2001) measured EMG of trunk muscles for five men and five women during a series of static trials to validate their model. The trials included four static symmetrical sagittal flexion tasks (i.e., 0º (upright), 15º, 30º, and 45º), and four asymmetrical flexion tasks (i.e., 10º left twist in combination with the aforementioned flexion angles). These published EMG data, normalized to maximum voluntary contraction (MVC), were used in the present study to test SO vs. SCSO performance during each trunk posture and are referred to as Experimental data 1.

#### *3.3.3.2 Experiment 2*

Granata and Orishimo (2001) measured EMG over four bilateral sets of trunk muscles in 10 males and 10 females during another series of static trials to show the role of muscles in joint stability. In this experiment the external moment ($M_{ext}$) was kept constant, once at 13.2 and once at 26.5 Nm, while the load height (H) was changed above the lumbo-sacral ($L_5S_1$) joint between 0 and 80 cm. These EMG data, referred to as Experimental data 2, were used in the present study to illustrate differences between default SO and the proposed SCSO framework in predicting changes in activation when the external moment is held constant, but load height is raised.

### *3.3.4 Study Simulations*

#### *3.3.4.1 Simulation 1*

The four static symmetrical sagittal flexion tasks, as well as the four asymmetric flexion tasks from Experiment 1 were simulated directly and both traditional SO and SCSO were applied.

*3.3.4.2 Simulation 2*

For simulation 2, the mass properties of the model were changed to match those in Granata and Orishimo (2001), where the trunk mass was 52 kg with zero sagittal moment arm and 20 cm elevation with respect to the lumbar-pelvic joint (Fig. 3.2). Then a 4.5 kg and 9 kg mass (M) were applied to the trunk at varying heights from the joint centre (i.e. 0≤H≤80 cm, at increments of 20 cm) with a constant sagittal moment arm of 30 cm (Fig. 3.2).

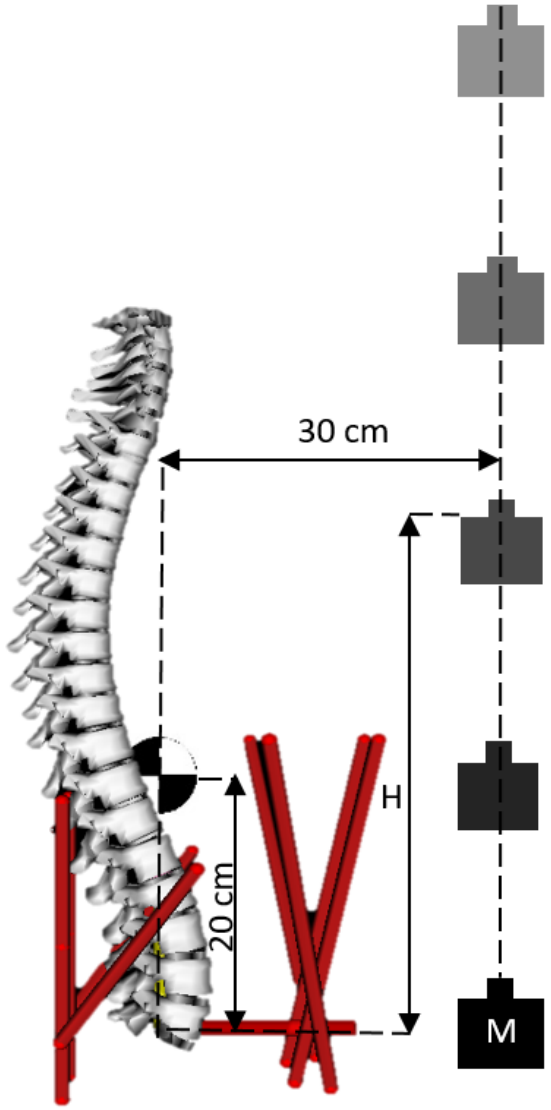


Fig. 3.2. The developed spine model in OpenSim and a schematic of the simulated tasks in simulation 2. A 4.5 kg and 9 kg mass (M) were applied to the trunk at varying heights (H) from the joint centre (i.e. 0≤H≤80 cm, at increments of 20 cm) with a constant sagittal moment arm of 30 cm.

### *3.3.5 Data Analysis*

#### *3.3.5.1 Simulation 1 vs. Experiment 1*

For simulation 1, the absolute differences between the estimated muscle activations (%MVC) and the mean normalized EMG activations in experiment 1 were computed. Calculated muscle activations by SO and SCSO solvers are not expected to exactly match the measured EMG data because of errors inherent in the musculoskeletal model as well as assumptions in the EMG-to-force transfer function to satisfy equilibrium requirements (Van Dieen and Kingma, 2005). Nevertheless, it was hypothesized that differences between experimental and simulation activations would be smaller for SCSO when compared to the traditional SO.

Due to the symmetric geometry of muscles in the model, both SO and SCSO assign equal activations to the right and left muscles during the symmetrical tasks in simulation 1, and therefore, for these tasks, only muscle activities from one side are reported.

#### *3.3.5.2 Simulation 2 vs. Experiment 2*

Granata and Orishimo (2001) reported average EMG activities (in mV) of back ($BCK_{EMG}$) and abdominal ($ABS_{EMG}$) muscles. Thus, in the present study, the calculated muscle activations (% MVC) by SO and SCSO were averaged across back (abdominal) muscles (i.e., $BCK_{SO}$ ($ABS_{SO}$) and $BCK_{SCSO}$ ($ABS_{SCSO}$) respectively). Since the EMG data in Granata and Orishimo (2001) were not normalized to MVC, Experimental data 2 were not comparable directly to the predicted muscle activities from SO and SCSO. Thus, both measured and estimated abdominal and back muscle activities at different heights were normalized to the corresponding values at H=0.

To assess the performance of SO and SCSO algorithms, we compared antagonist activity ratios (r_) between the abdominal and back muscles for EMG, SO, and SCSO results (Eqs. 3.5–

3.7). Additionally, we computed the root mean square errors (RMSE) of the predicted values (i.e., r_SO and r_SCSO) versus EMG (Eqs. 3.8 and 3.9).

$$\text{r\_EMG} = \text{ABS}_{\text{EMG}}/\text{BCK}_{\text{EMG}} \quad \text{(Eq. 3.5)}$$

$$\text{r\_SO} = \text{ABS}_{\text{SO}}/\text{BCK}_{\text{SO}} \quad \text{(Eq. 3.6)}$$

$$\text{r\_SCSO} = \text{ABS}_{\text{SCSO}}/\text{BCK}_{\text{SCSO}} \quad \text{(Eq. 3.7)}$$

$$SO_{RMSE} = \sqrt{\frac{\sum_H (r\_SO - r\_EMG)^2}{5}} \quad \text{(Eq. 3.8)}$$

$$SCSO_{RMSE} = \sqrt{\frac{\sum_H (r\_SCSO - r\_EMG)^2}{5}} \quad \text{(Eq. 3.9)}$$

*3.3.5.3 Sensitivity Analysis*

One of the parameters that affects the calculated muscle forces by SCSO is the linear muscle stiffness coefficient (q) (Appendix A–SI. 1). A wide range of values (0.5–42) for this user-defined coefficient (q) have been reported (Hajihosseinali et al., 2014). In the present study, for simulation 1 and 2, q was set to five for all muscles, consistent with that in Granata and Wilson (2001) and Granata and Orishimo (2001). However, in simulation 1, another q (i.e., three) in the reported range was also tested to shed light on how the users may adjust SCSO to obtain more biofidelic muscle activation estimates.

*3.3.5.4 Muscle Classification*

When in all coordinates, a muscle's moment arm's sign was the same as the external moment's sign, it was called an agonist. We called a muscle a complete antagonist when in all coordinates, the muscle's moment arm's sign was opposite to the external moment's sign. When a muscle was neither an agonist nor complete antagonist, it was called semi-antagonist. To better evaluate the predicted muscle activations, the signs of muscle moment arms' values and external

moments in the coordinates of the model that have a non-zero external moment were investigated (Table 3.1).

Table 3.1. Signs of external moments and muscle moment arm values. Presented values are for the flexion-extension coordinate and abduction-adduction coordinate of the lumbar-sacral joint, and the flexion-extension coordinate of thorax-lumbar joint in all tasks of simulation 2 and all symmetrical and asymmetrical tasks of simulation 1. When in all coordinates, a muscle's moment arm's sign is the same as the external moment's sign, it was called agonist. We called a muscle a complete antagonist when in all coordinates, the muscle's moment arms sign was opposite to the external moment's sign. When a muscle is neither an agonist or complete antagonist, it was called semi-antagonist.

| Simulation1 and 2-Symmetric tasks | ES-R | ES-L | RA-R | RA-L | EO-R | EO-L | IO-R | IO-L | External Moment |
|---|---|---|---|---|---|---|---|---|---|
| lumbar-pelvis joint, flexion-extension | + | + | - | - | - | - | + | + | + |
| thorax-lumbar joint, flexion-extension | + | + | - | - | - | - | - | - | + |
| Simulation2-Asymmetric tasks | ES-R | ES-L | RA-R | RA-L | EO-R | EO-L | IO-R | IO-L | External Moment |
| lumbar-pelvis joint, flexion-extension | + | + | - | - | - | - | + | + | + |
| lumbar-pelvis joint, abduction-adduction | + | - | + | - | + | - | + | - | + |
| thorax-lumbar joint, flexion-extension | + | + | - | - | - | - | - | - | + |

## 3.4 Results

### *3.4.1 Simulation 1 vs. Experiment 1 and Sensitivity Analysis*

Using traditional SO, neither RA nor EO (both are back extension antagonists) were activated in the symmetrical (Fig. 3.3) or asymmetrical (Fig. 3.4) tasks. These findings were contrary to the previously measured EMG activities of the trunk muscles in experiment 1. However, when considering q=5 in the proposed framework (SCSO-q5), a non-zero activity of EO in the symmetrical tasks and EO-R in the asymmetrical tasks was estimated. Still, RA was almost silent in all of the symmetrical tasks and in the asymmetric flexion task at 30º and 45º. Comparatively, when considering q=3 in the framework (SCSO-q3), the framework assigned a non-zero activity to RA and EO in the asymmetrical tasks and RA-R, RA-L, and EO-R in the

asymmetrical tasks. These findings were in much closer agreement with the EMG data presented in experiment 1.

In general, the average difference from measured EMG data was smallest for SCSO-q3 versus SCSO-q5 and SO simulation results (Table 3.2). Across all muscles, the average difference during all tasks was 10.2%, 7.5%, and 6.8%, for SO, SCSO-q5, and SCSO-q3 respectively, and thereby, SCSO-q3 produced results that were the most representative of the EMG data.

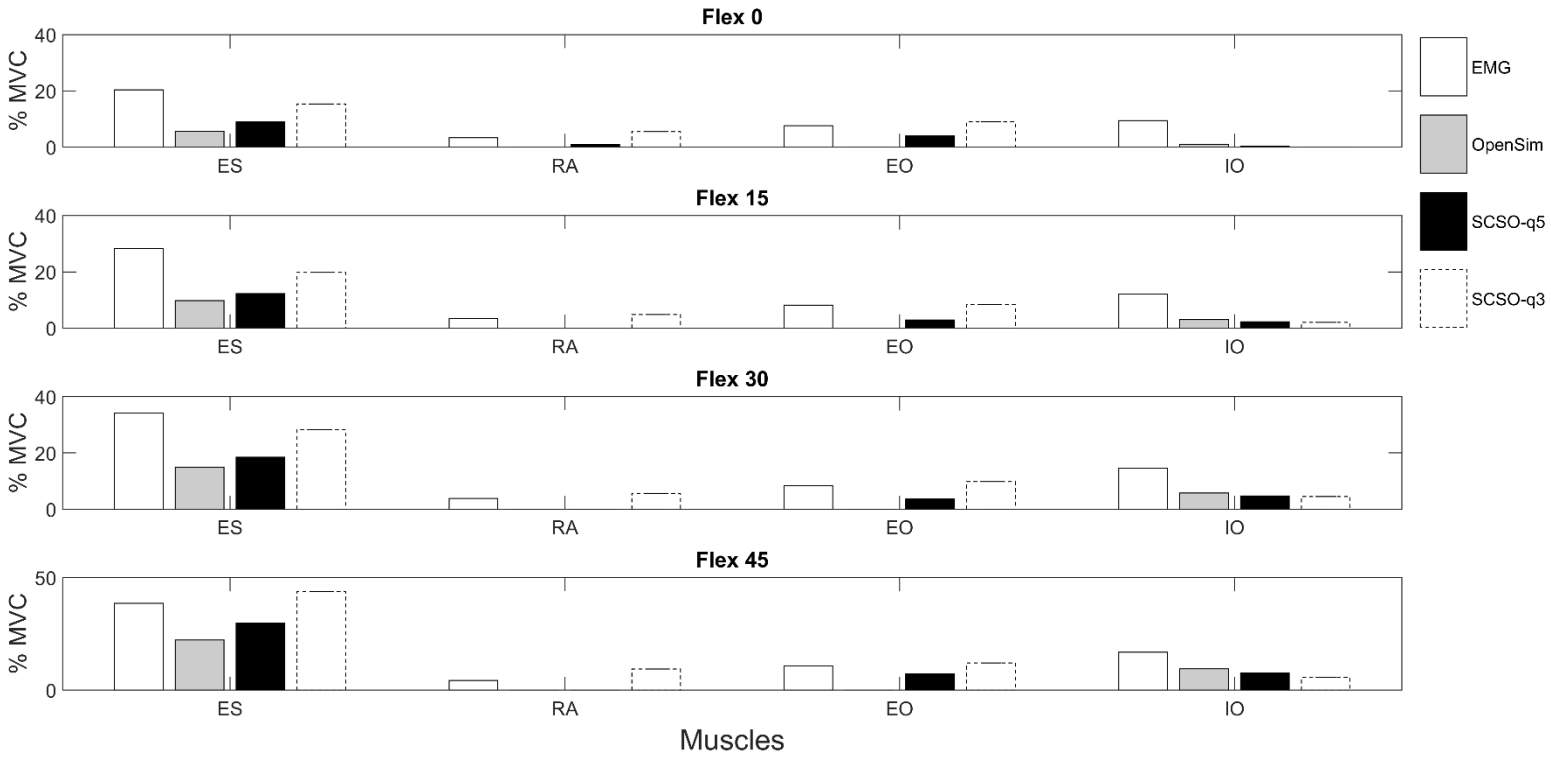


Fig. 3.3. Simulation 1 results. Muscle activations calculated by the Stability-Constrained Static Optimization (SCSO) framework and the default OpenSim Static Optimization (SO) solver were compared against the average EMG data for 5 men and 5 women reported in Granata and Wilson (2001) during four static symmetrical sagittal flexion tasks. In the framework, q was set to both 5 (SCSO-q5) and 3 (SCSO-q3). Since the estimated right and left muscle activities by SO, SCSO-q5, and SCSO-q3 were equal, the estimated muscle activations in one side were compared to the average of measured EMG activities between right and left muscles. The trunk muscles that were investigated in this study were Rectus Abdominis (RA), External Obliques (EO), Internal Obliques (IO), and Erector Spinae (ES).

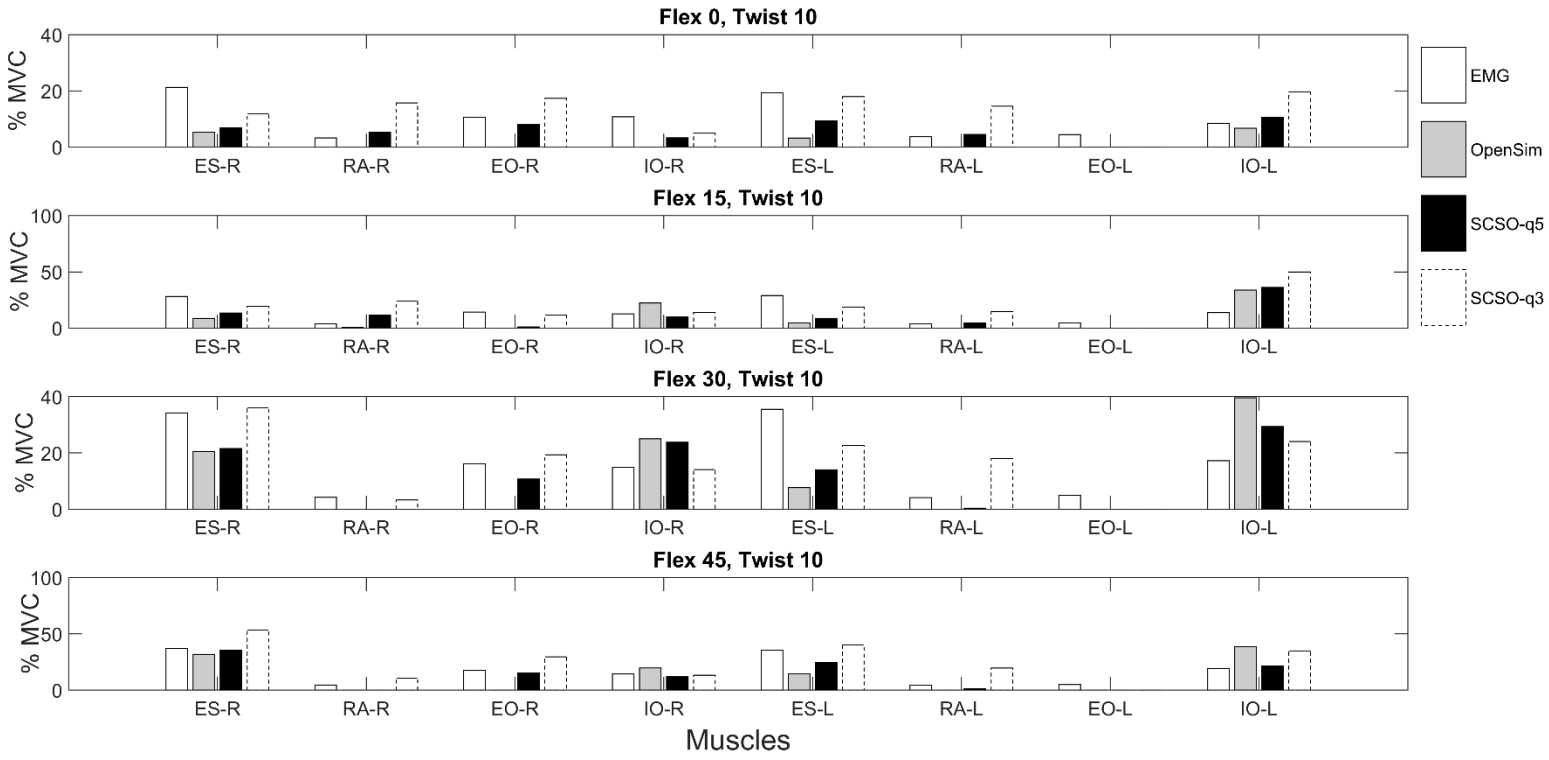


Fig. 3.4. Simulation 1 results. Muscle activations calculated by the Stability-Constrained Static Optimization (SCSO) framework and the default OpenSim Static Optimization (SO) solver were compared against the average EMG data for 5 men and 5 women reported in Granata and Wilson (2001) during four asymmetric flexion tasks. In the framework, q was set to both 5 (SCSO-q5) and 3 (SCSO-q3). The left (-L) and right (-R) trunk muscles that were investigated in this study were Rectus Abdominis (RA), External Obliques (EO), Internal Obliques (IO), and Erector Spinae (ES).

Table 3.2. Average percent activation differences between experimental and simulation results. Muscle activations were estimated by the default OpenSim Static Optimization (SO) solver, and the Stability-Constrained SO for both q=5 (SCSO-q5) and q=3 (SCSO-q3). The absolute value of the difference between the estimated muscle activations and the measured EMG data were calculated and reported during the symmetrical and asymmetrical tasks in simulation 1. The smallest errors were bolded and italicized in this table. In addition, muscles were categorized into the agonist, semi antagonist, and complete antagonist (Table 3.1) and the average values for these categories were reported. Furthermore, the average values of the absolute differences across all muscles for SO, SCSO-q5, and SCSO-q3 were calculated and reported.

| | | Muscles | SO | SCSO-q5 | SCSO-q3 |
|---|---|---|---|---|---|
| Symmetrical | Tasks | ES | 17.2% | 13.0% | ***6.1%*** |
| | | RA | 3.7% | 3.5% | ***2.6%*** |
| | | EO | 8.7% | 4.3% | ***1.1%*** |
| | | IO | ***8.4%*** | 9.5% | 10.2% |
| Asymmetrical | Tasks | ES-R | 13.6% | 10.9% | ***9.1%*** |
| | | RA-R | ***3.8%*** | 4.6% | 9.8% |
| | | EO-R | 14.6% | ***5.9%*** | 6.1% |
| | | IO-R | 9.0% | 5.4% | ***2.2%*** |
| | | ES-L | 22.3% | 15.7% | ***7.3%*** |
| | | RA-L | 3.9% | ***2.1%*** | 12.7% |
| | | EO-L | 4.8% | 4.8% | 4.8% |
| | | IO-L | 15.8% | ***9.7%*** | 17.4% |
| All Tasks | | Agonist | 16.0% | 12.3% | ***7.1%*** |
| | | Complete Antagonist | 5.6% | ***3.8%*** | 4.1% |
| | | Semi Antagonist | 11.8% | ***8.6%*** | 9% |
| Average | | All Muscles | 10.2% | 7.5% | ***6.8%*** |

### *3.4.2 Simulation 2 vs. Experiment 2*

When the load height was increased from 0 to 80 cm, the traditional SO predicted zero muscle activations of RA and EO, and constant muscle activations of all muscles, while the normalized $ABS_{SCSO}$ and $BCK_{SCSO}$ increased linearly (Fig. 3.5). Thus, the SCSO framework's results corroborate experiment 2 where $BCK_{EMG}$ and $ABS_{EMG}$ increased significantly ($p<0.05$)

when the load height increased (Granata and Orishimo, 2001). $SO_{RMSE}$ was 0.3 and 0.26 when holding 4.5 and 9 kg respectively, whereas SCSO was more accurate with $SCSO_{RMSE}$ of 0.03 for both loads (Fig. 3.6).

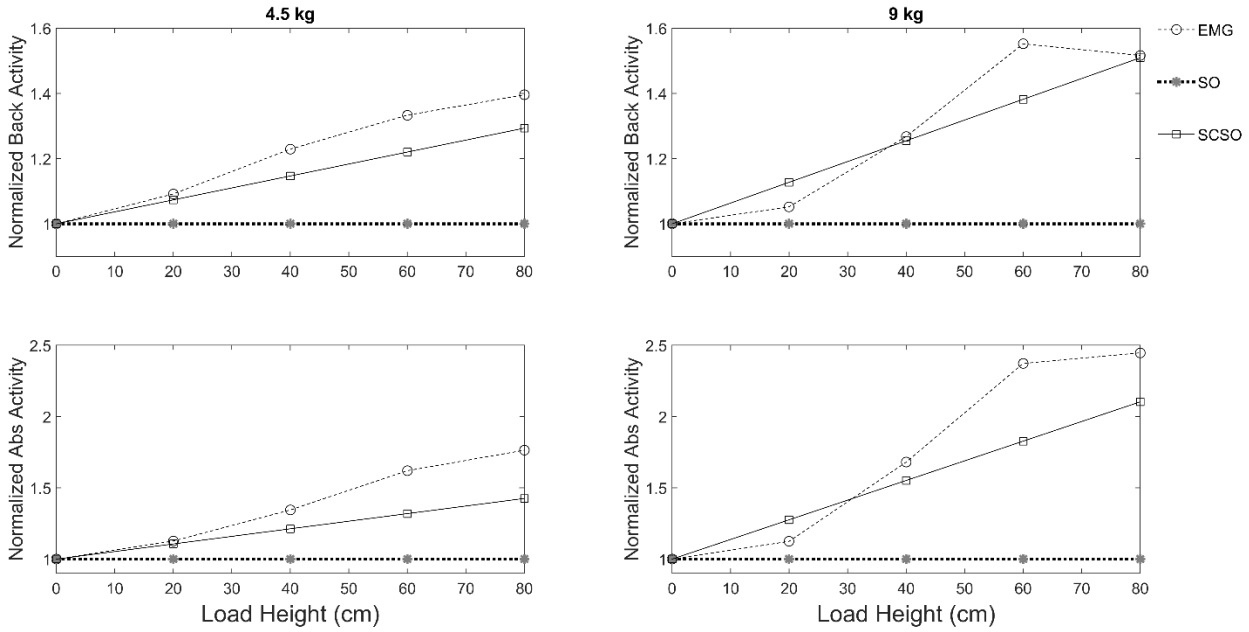


Fig. 3.5. Simulation 2 results. During the series of static trials in simulation 2 (Fig. 3.2), the measured and calculated average activities of back and abdominal muscles at each load height were normalized to the corresponding values at H=0.

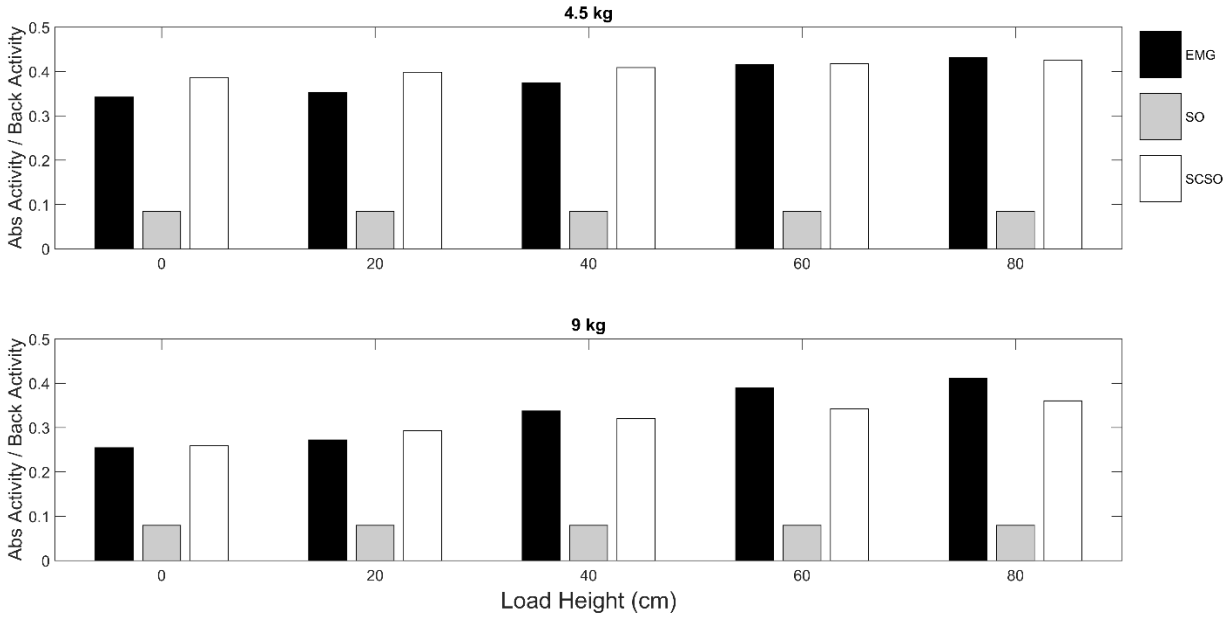


Fig. 3.6. Simulation 2 results. During the series of static trials in simulation 2 (Fig. 3.2), at each loading condition (i.e., 4.5 and 9 kg) and each load height, the ratios (Eqs. 3.5–3.7) between the average of abdominal and back muscles activations were compared.

## 3.5 Discussion

Muscle activations, in addition to maintaining dynamic equilibrium, play a significant role in joint stability, particularly within joints of the spine (Samadi and Arjmand, 2018), knee (Baratta et al., 1988), and shoulder (Labriola et al., 2005). The current SO solver in OpenSim considers limits on muscle forces and the equilibrium demands, yet does not consider stability requirements. Thus, this study aimed to develop a SCSO framework that is generalizable to many OpenSim models. As a proof of this concept, we tested the traditional SO and the new developed SCSO framework for a spine model in this main paper, as well as a lower limb model (Appendix A–SI. 2).

### *3.5.1 Analysis of Results*

By attempting to minimize the sum of muscle activations squared, the traditional SO assigns zero activations to complete antagonistic muscles in the present study. For instance, in

simulation 1, RA-L activation in all asymmetrical tasks, and in simulation 2, RA and EO activations were predicted zero by SO, which is contrary to the experimental data. However, the semi-antagonistic muscles may or may not be activated by SO, which depends on all parameters in the OPT problem, such as muscle moment arms (Herzog and Binding, 1992). For example, IO was activated in simulation 2 by SO, while EO-R in the asymmetrical tasks in simulation 1 was not activated, in disagreement with the experimental data.

The zero calculated activations of antagonistic muscles are not the only issue with traditional SO. In simulation 2, since none of the known input parameters (e.g., muscle moment arms or external moment) for the common OPT problem have changed, SO predicts constant muscle activations and forces at different load heights (Figs. 3.5 and 3.6), contrary to experimental data.

By considering the stability demands in addition to the equilibrium requirements, the calculated muscle activations by SCSO corroborated better with the experimental data. To maintain stability at each instant in time, SCSO requires that the muscles store a greater amount of potential (elastic) energy than the external work. In simulation 2, the external work (**EW**) term in Eq. 3.4 increases in proportion with the load height (Appendix A–SI. 1). Therefore, to achieve the stability and equilibrium simultaneously, the predicted activations for both back and abdominal muscles by SCSO should increase, in agreement with the experimental data.

### *3.5.2 SCSO Limitations*

Addition of stability constraints in the SCSO framework increases computational cost versus traditional SO. In the present implementation, SCSO was approximately 4-5x slower than SO (Appendix A–SI. 3). However, the majority of this cost comes from read-write operations where model states are gathered from text files (muscle moment arms, joint locations in the world

frame, etc.). In future implementations, it would be possible to access these variables directly from memory and significantly reduce computational time. Regardless, SCSO is still much faster than alternatives such as dynamic optimization (Anderson and Pandy, 2001) and simpler to implement than EMG-driven approaches (Lloyd and Besier, 2003).

The performance of the SCSO is highly dependent on the assumed linear muscle stiffness coefficient, q. The magnitude of q affects the amount of energy stored within a muscle during elongation (Appendix A–SI. 1). If q is large enough (e.g., $q > 13$ in simulations 1 and 2), muscles will always have the potential to store sufficient energy for stability; thus, SCSO will predict the same muscle forces as the traditional SO. This also explains why SCSO-q5 is similar to SO and in contrast with the experimental EMG data, assigning zero activation to RA in most of the tasks in simulation 1.

The current version of SCSO framework does not consider contributions of ligaments and other soft tissues to joint passive stiffness when composing of stability constraints. In addition, only static mechanical stability was incorporated into the default OpenSim solver, while dynamic stability, in which the role of kinetic energy and the role of time-dependent dynamic neural feedback for the control of stability are considered (Franklin and Granata, 2007; Graham et al., 2012) was neglected. These limitations will be addressed in future add-ons to the SCSO framework.

### *3.5.3 Conclusions*

In summary, the presented SCSO framework: (i) calculates muscle activations and forces that not only satisfy dynamic equilibrium in body joints but also satisfy crucial static stability requirements, (ii) can produce results (i.e., muscle activations and forces) that corroborate with

experimental data better than, or at least as well as, the default OpenSim SO solver, and (iii) could be used freely by many models that have been developed and will be developed through OpenSim.

### 3.6 References


Anderson, F.C., Pandy, M.G., 2001. Dynamic optimization of human walking. J. Biomech. Eng. 123, 381–390.

Baratta, R., Solomonow, M., Zhou, B.H., Letson, D., Chuinard, R., D'ambrosia, R., 1988. Muscular coactivation: the role of the antagonist musculature in maintaining knee stability. Am. J. Sports Med. 16, 113–122.

Bergmark, A., 1989. Stability of the lumbar spine: A study in mechanical engineering. Acta Orthopaedica Scandinavica 60, 1–54.

Bolsterlee, B., Veeger, D.H., Chadwick, E.K., 2013. Clinical applications of musculoskeletal modelling for the shoulder and upper limb. Med. Biol. Eng. Compu. 51, 953–963.

Brown, S.H., Potvin, J.R., 2005. Constraining spine stability levels in an optimization model leads to the prediction of trunk muscle cocontraction and improved spine compression force estimates. J. Biomech. 38, 745–754.

Cholewicki, J., McGill, S.M., 1996. Mechanical stability of the in vivo lumbar spine: implications for injury and chronic low back pain. Clin. Biomech. 11, 1–15.

Crowninshield, R.D., Brand, R.A., 1981. The prediction of forces in joint structures: distribution of intersegmental resultants. Exerc. Sport Sci. Rev. 9, 159–182.

Delp, S.L., Anderson, F.C., Arnold, A.S., Loan, P., Habib, A., John, C.T., Thelen, D.G., 2007. OpenSim: open-source software to create and analyze dynamic simulations of movement. IEEE Trans. Biomed. Eng. 54, 1940–1950.

Dreischarf, M., Shirazi-Adl, A., Arjmand, N., Rohlmann, A., Schmidt, H., 2016. Estimation of loads on human lumbar spine: a review of in vivo and computational model studies. J. Biomech. 49, 833–845.

El Ouaaid, Z., Shirazi-Adl, A., Arjmand, N., Plamondon, A., 2013. Coupled objective function to study the role of abdominal muscle forces in lifting using the kinematics-driven model. Comput. Methods Biomech. Biomed. Eng. 16, 54–65.

Farina, D., Merletti, R., Enoka, R.M., 2004. The extraction of neural strategies from the surface EMG. J. Appl. Physiol. 96, 1486–1495.

Franklin, T.C., Granata, K.P., 2007. Role of reflex gain and reflex delay in spinal stability—a dynamic simulation. J. Biomech. 40, 1762–1767.

Gomes, G.T., Van Cauter, S., De Beule, M., Vigneron, L., Pattyn, C., Audenaert, E.A., 2013. Patient-specific modelling in orthopedics: from image to surgery. In: Andreaus, U., Iacoviello, D. (Eds.), Biomedical Imaging and Computational Modelling in Biomechanics. Springer, Dordrecht, pp. 109–129.

Graham, R.B., Sheppard, P.S., Almosnino, S., Stevenson, J.M., 2012. Dynamic spinal stability and kinematic variability across automotive manufacturing work shifts and days. Int. J. Ind. Ergon. 42, 428–434.

Granata, K.P., Orishimo, K.F., 2001. Response of trunk muscle coactivation to changes in spinal stability. J. Biomech. 34, 1117–1123.

Granata, K.P., Wilson, S.E., 2001. Trunk posture and spinal stability. Clin. Biomech. 16, 650–659.

Hajihosseinali, M., Arjmand, N., Shirazi-Adl, A., Farahmand, F., Ghiasi, M.S., 2014. A novel stability and kinematics-driven trunk biomechanical model to estimate muscle and spinal forces. Med. Eng. Phys. 36, 1296–1304.

Herzog, W., Binding, P., 1992. Predictions of antagonistic muscular activity using nonlinear optimization. Math. Biosci. 111, 217–229.

Hughes, R.E., Bean, J.C., Chaffin, D.B., 1995. Evaluating the effect of co-contraction in optimization models. J. Biomech. 28, 875–878.

Labriola, J.E., Lee, T.Q., Debski, R.E., McMahon, P.J., 2005. Stability and instability of the glenohumeral joint: the role of shoulder muscles. J. Shoulder Elbow Surg. 14, 32–38.

Lloyd, D.G., Besier, T.F., 2003. An EMG-driven musculoskeletal model to estimate muscle forces and knee joint moments in vivo. J. Biomech. 36, 765–776.

Millard, M., Uchida, T., Seth, A., Delp, S.L., 2013. Flexing computational muscle: modelling and simulation of musculotendon dynamics. J. Biomech. Eng. 135, 021005.

Mohammadi, Y., Arjmand, N., Shirazi-Adl, A., 2015. Comparison of trunk muscle forces, spinal loads and stability estimated by one stability-and three EMG-assisted optimization approaches. Med. Eng. Phys. 37, 792–800.

Neptune, R.R., Kautz, S.A., 2000. Knee joint loading in forward versus backward pedaling: implications for rehabilitation strategies. Clin. Biomech. 15, 528–535.

Potvin, J.R., Brown, S.H., 2005. An equation to calculate individual muscle contributions to joint stability. J. Biomech. 38, 973–980.

Raikova, R., 1999. About weight factors in the non-linear objective functions used for solving indeterminate problems in biomechanics. J. Biomech. 32, 689–694.

Rohlmann, A., Bergmann, G., Graichen, F., 1994. A spinal fixation device for in vivo load measurement. J. Biomech. 27, 965–967.

Samadi, S., Arjmand, N., 2018. A novel stability-based EMG-assisted optimization method for the spine. Med. Eng. Phys. 58, 13–22.

Seth, A., Sherman, M., Reinbolt, J.A., Delp, S.L., 2011. OpenSim: a musculoskeletal modelling and simulation framework for in silico investigations and exchange. Procedia Iutam 2, 212–232.

Staudenmann, D., Kingma, I., Stegeman, D.F., van Dieën, J.H., 2005. Towards optimal multi-channel EMG electrode configurations in muscle force estimation: a high density EMG study. J. Electromyogr. Kinesiol. 15, 1–11.

Stokes, I.A., Henry, S.M., Single, R.M., 2003. Surface EMG electrodes do not accurately record from lumbar multifidus muscles. Clin. Biomech. 18, 9–13.

Van Dieen, J.H., Kingma, I., 2005. Effects of antagonistic co-contraction on differences between electromyography based and optimization based estimates of spinal forces. Ergonomics 48, 411–426.

Wilke, H.J., Neef, P., Hinz, B., Seidel, H., Claes, L., 2001. Intradiscal pressure together with anthropometric data–a data set for the validation of models. Clin. Biomech. 16, 111–126.

# Chapter 4: Sharing the Load: Modelling Loads in OpenSim to Simulate Two-Handed Lifting

Published in Multibody System Dynamics 2022; 54(2): 213–234.
https://doi.org/10.1007/s11044-021-09808-7

## 4.1 Abstract

Static Optimization (SO) procedures are commonly used to estimate muscle forces and joint loads from kinematics and external force data. The method of modelling hand–mass interaction during lifting tasks may affect the kinematics and/or external forces applied to the model, yet the extent to which different modelling decisions affect the estimated spinal joint loads is unknown. The present work compares five hand–mass interaction modelling approaches that differ in the complexity of implementation and runtime for the kinematic and SO analyses during two-handed lifting tasks. Intraclass correlation coefficients demonstrated strong agreement among the modelling approaches for the prediction of both maximum and average $L_5S_1$ resultant forces across all tasks. However, the five modelling approaches resulted in maximum relative differences in the $L_5S_1$ resultant force of up to 35% (2.6 kN). To compare the accuracy of each modelling approach, the resulting dynamic inconsistencies (i.e., residual forces and moments) were evaluated. The approach that resulted in the overall lowest residuals and incurred the least computational expense is recommended in the present study. The present work illustrates how different external-load modelling approaches can result in substantial differences in predicted spinal loads, especially as the movement speed increases, and how some models may perform better in terms of residual forces.

## 4.2 Introduction

Multibody dynamic simulation has been used extensively for various applications (Ren et al., 2014), including non-invasive estimation of the internal loads acting on the human body (e.g.,

muscle forces and joint loads). External contact loads affect the estimation of these internal forces (Robert et al., 2013; Shourijeh and McPhee, 2015); however, direct measurement of external loads using load cells, force plates, or pressure sensors may not be possible in many studies, especially where "out-of-the-lab" experiments are required (Skals et al., 2017). Therefore, different approaches have been developed to predict external contact loads.

Most external-contact-load prediction studies have been related to ground reaction force and moment (GRF&M) estimation during gait. Strategies to estimate GRF&M include empirical function methods (Koopman et al., 1995; Ren et al., 2008), machine learning methods (Choi et al., 2013; Johnson et al., 2018; Oh et al., 2013), kinematic constraint methods (Dorn et al., 2012; Hamner et al., 2013, 2010), and rigid and elastic contact models (Baraff, 1994; Gilchrist and Winter, 1996; Lopes, 2013; Sandhu and McPhee, 2010). Empirical function methods, such as the zero-moment-point technique, are limited to GRF&M prediction during gait. Machine learning methods require large sets of motions for the learning phase and can be reliably applied only to tasks that are sufficiently similar to the data used to train the models. Therefore, researchers often employ kinematic constraints and contact models to estimate GRF&M (Shourijeh and McPhee, 2015). In the latter case, tuning the contact parameters for a motion of interest can be very challenging; the least complex contact model that can capture the phenomena of interest with the greatest computational efficiency has been recommended (Hicks et al., 2015).

In spine biomechanics, the major role of manual material handling (and, more specifically, lifting) in the etiology of back disorders has been well established (Behjati and Arjmand, 2019; Genaidy et al., 1993; Graham et al., 2009; Waters et al., 1993). Inverse dynamics (ID)–based simulations are commonly used to assess net forces and torques at spinal joints, as well as to estimate muscle forces and joint loads using Static Optimization (SO) procedures with

musculoskeletal models (Akhavanfar et al., 2019). The external hand forces and moments (EHF&M) acting on the hands directly affect the results of SO during lifting tasks. Nevertheless, EHF&M are usually greatly simplified in spine modelling studies. The mass of the lifted object is often modelled by applying a gravity-oriented load to the hands (Bassani et al., 2017; Bruno et al., 2017) or by increasing the mass of the hands themselves (Beaucage-Gauvreau et al., 2019). The former does not consider the load accelerations, and neither method distinguishes between the two-handed lifting of one load and simultaneous lifting of one-half of the load by each hand.

EHF&M were estimated in some spine modelling studies using measured GRF&M (Faber et al., 2018; Koopman et al., 2018) and by using the methods proposed and validated in Faber et al., (2013), where EHF&M were calculated by subtracting the forces due to the weight and acceleration of each body segment from the measured GRF&M. However, only recently have EHF&M been estimated and validated using solely motion data (Muller et al., 2020a).

Muller et al., (2020a) used the optimization-based approach proposed by Fluit et al. (2014) to calculate EHF&M and GRF&M. In this optimization approach, artificial actuators were considered at contact points and the actuator forces were determined in the same way that muscle forces were calculated in their muscle recruitment algorithm. Hence, the artificial actuator forces were calculated by solving an optimization problem, in which a cost function for actuator forces was minimized subject to the equations of motion. The GRF&M and EHF&M were then considered as the estimated forces for the artificial muscle-like actuators. They defined 14 and 11 contact points under each foot and on each hand, respectively, to map the contact area, similar to Fluit et al., (2014) and Skals et al., (2017). GRF&M were always present in their simulations, where foot contact points were determined at each instant by identifying the points whose height and speed were below 0.02 m and 0.8 m/s, respectively (Muller et al., 2020a). However, during

some phases of their handling tasks, their participants did not hold the load, thus EHF&M were zero during those phases. Muller et al., (2020a) applied a trained neural network to the videos of the experiments to identify the load carriage phases (i.e., where the EHF&M were nonzero). After estimating EHF&M and GRF&M, $L_5S_1$ net joint moments were calculated using both predicted and measured GRF&M with a bottom-up recursive Newton–Euler ID algorithm (Featherstone, 2014). The results were compared during standardized lifting tasks with and without constrained foot motion (Muller et al., 2020a) and during tasks that were closer to workplace conditions (transferring boxes from a conveyor to a two-wheel hand trolley) (Muller et al., 2020b). In the latter study, however, the inertial parameters of the load were not fully considered: the load was modelled as a point mass located halfway between the two wrists. Furthermore, in both studies (Muller et al., 2020a, 2020b), the effect of EHF&M on muscle forces and joint loads was not assessed.

The effects of many parameters on muscle activations and spinal joint loads have been investigated. Some examples include muscle properties (Akhavanfar et al., 2018), personalized factors (e.g., sex, age, height, and body weight) (Ghezelbash et al., 2016), and speed of movement (Bazrgari et al., 2008). However, to the best of the authors' knowledge, the effect of different contact modelling approaches has been investigated only on lower-limb internal forces, and only during gait (Hamner et al., 2013). Therefore, it would be advantageous to evaluate the effect of various EHF&M modelling approaches on spinal loads during lifting tasks.

Hence, this study had three primary aims: i) to study five approaches to model EHF&M in OpenSim; ii) to evaluate the effect of these modelling approaches on the predicted spinal loads for one participant during two-handed lifting tasks; and iii) to compare the residual or "hand of god" forces produced by each EHF&M modelling approach at the pelvis–ground joint level, as these

forces quantify the dynamic inconsistencies in the model. Five modelling approaches were evaluated: Approaches 1 and 2 have been used in existing lifting studies and Approaches 3–5 were developed in the present study.

There are several rigid-body musculoskeletal modelling tools that could have been used in this study. The University of Michigan's 3D Static Strength Prediction Program™ (3DSSPP) software, the AnyBody Modelling System (AnyBody Technology, Aalborg, Denmark) (Damsgaard et al., 2006), and OpenSim (Delp et al., 2007) are popular analysis tools that have been used in many studies (Ghezelbash et al., 2020). The 3DSSPP software provides two user-friendly single-level spine models, yet it does not consider comprehensive muscle architecture and violates physical and physiological principles by not satisfying equilibrium equations at all spinal levels (Ghezelbash et al., 2020). In addition, neither 3DSSPP nor AnyBody are freely accessible, which may limit the scientific potential of studies that use these packages (Delp et al., 2007). OpenSim, on the other hand, offers advanced computational tools and is the most widely used open-source platform in biomechanics (Seth et al., 2018), and thus was chosen for the present study. The lifting full-body (LFB) model (Beaucage-Gauvreau et al., 2019) is a biofidelic and open-access spine model that has recently been developed and validated for lifting tasks in OpenSim, and thus was used as the base model for the present study. However, the methods that were developed in the present study are generalizable to different OpenSim lifting models and for studying other movements in which external loads are applied to the body.

## 4.3 Methods

### *4.3.1 Experiment*

One healthy male (94.5 kg, 178 cm, 27 years) provided informed written consent and participated in the experiment, which was approved by the University of Ottawa Research Ethics

Board (H-06-18-721). The lifting/lowering handling tasks in this study had three phases: i) the pre-handling phase, ii) the handling phase, and iii) the post-handling phase (Fig. 4.1). The second phase (i.e., the part of the motion during which the load was in the hands) was the motion of interest in the present study, which we refer to as the "motion cycle". The participant was instructed to perform symmetric lifting/lowering tasks with two lifting techniques (stoop and squat), three speeds of movement (slow, natural, and fast), and two loads (light and heavy).

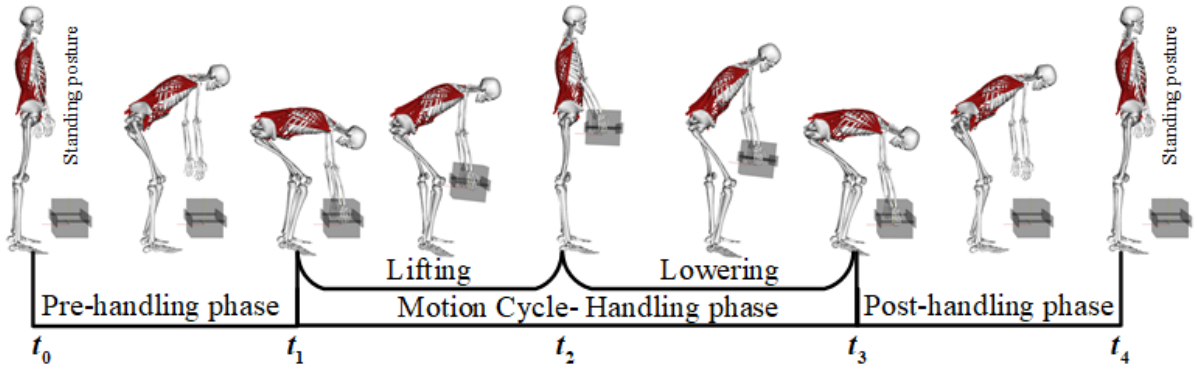


Fig. 4.1. The phases of movement during the lifting/lowering handling tasks in the present study.

In the experiments, the load being lifted was a box with two handles (Fig. 4.2(a)). For light and heavy lifting tasks, the box mass was set to 5 kg and 20 kg, respectively, by adjusting the amount of load inside the box. To isolate and evaluate the effect of inaccuracies in the mass distribution and geometry of the segments in the model, the participant was instructed to perform a "baseline task" (with a self-selected technique and speed) using a foam box (Fig. 4.2(b)) of identical dimensions but negligible mass. This scenario served as a datum for our modelling/simulation error. To study the relationship between the speed of movement and EHF&M modelling approaches, the participant was instructed to perform each heavy lifting task three times: at a natural speed, as slowly as possible, and as quickly as possible. Henceforth, the technique–load–speed format is used to identify each task. For instance, Stoop–20–Fast refers to the task in which the 20 kg box was lifted using the stoop technique as quickly as possible. If the

speed is not mentioned, the movement was performed at a natural speed. To provide a better understanding of the velocity differences among the tasks, the duration of the motion cycle (Fig. 4.1) for each task has been provided in the Supplementary Information (Appendix B–SI. 1).

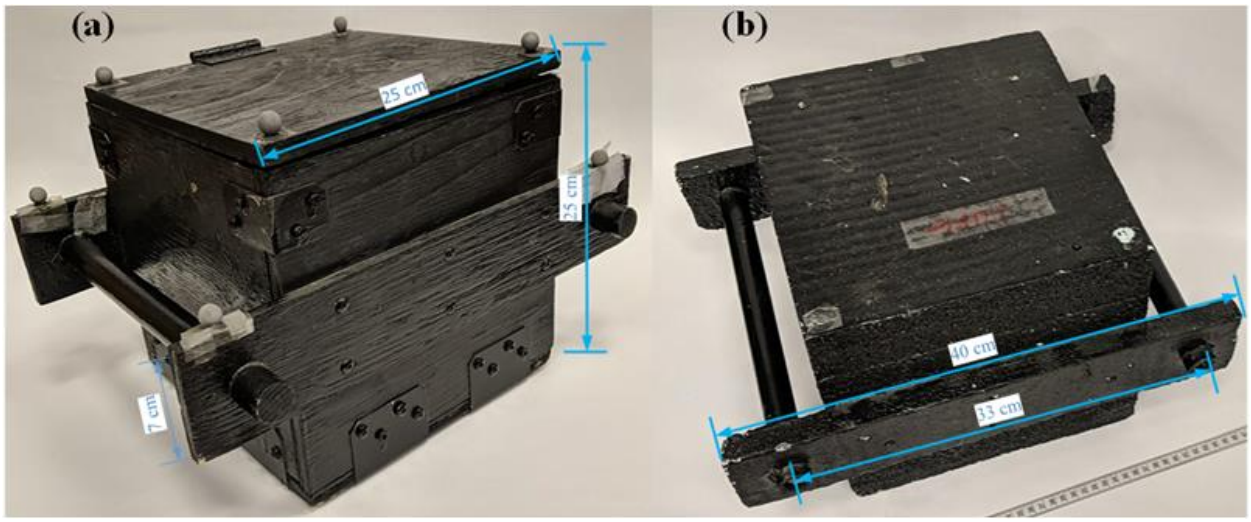


Fig. 4.2. The boxes that were used for the lifting tasks in the present study: (a) the main box (mass set to 5 kg or 20 kg) and (b) the foam box of identical dimensions which was used to perform a lifting task as a baseline for our modelling/simulation error.

The participant was outfitted with a full-body marker set (Beaucage-Gauvreau et al., 2019) and eight markers were placed on the box to measure the body and box kinematics, respectively. Marker data during lifting tasks were collected at 30 Hz using a 10-camera Vantage V5 motion capture system (Vicon, Oxford, UK) and force data were collected at 2160 Hz using FP4060 force plates (Bertec Corporation, Columbus, OH, USA).

### *4.3.2 Musculoskeletal Model*

By modifying a previously developed full-body lumbar spine model (Raabe and Chaudhari, 2016), Beaucage-Gauvreau and colleagues (2019) recently developed the LFB model, which consists of 30 segments, 29 degrees of freedom, and 238 Hill-type musculotendon actuators. The LFB model comprises upper and lower limb segments to better capture the body kinematics during lifting tasks. However, the upper and lower limbs do not include muscles and their

coordinates are actuated by ideal motors (Beaucage-Gauvreau et al., 2019). It is appropriate to use the LFB model for the ranges of motion in the present study because it is among the few biofidelic and publicly available spine models in the OpenSim database, it can be used with kinematic data collected in the laboratory, and it was validated for lifting tasks such as two-handed stoop and two-handed squat tasks.

In the LFB model, the pelvis is the floating base, where six generalized coordinates represent three translational and three rotational degrees of freedom between the model's pelvis and the ground. Modelling assumptions such as uncertainty in the segments' inertial properties, simplifications in hand-contact forces, and noise in the motion capture data will result in dynamic inconsistency. This means that the acceleration of the system's centre of mass (COM) and the net externally applied forces do not satisfy Newton's Second Law ($\mathbf{F} = m\mathbf{a}$), and the net externally applied moments to the COM are not equal to the time derivative of its angular momentum ($\mathbf{L}$). Therefore, six residual actuators between the pelvis and ground (3 forces and 3 moments) must be added to the equations of motion that account for the dynamic inconsistency:

$$\mathbf{F}_{\text{external}} + \mathbf{F}_{\text{residual}} = m\mathbf{a} \quad \text{(Eq. 4.1)}$$

$$\mathbf{M}_{\text{external}} + \mathbf{M}_{\text{residual}} = \frac{\mathrm{d}\mathbf{L}}{\mathrm{d}t} \quad \text{(Eq. 4.2)}$$

The above dynamic inconsistency nearly always exists in simulations that are generated from motion capture data; however, many studies have neither calculated nor reported the size of this error (Hicks et al., 2015). Residual forces and moments are compared among the five EHF&M modelling approaches in the present study. Because measured GRF&M were used in the present study and were the same for each approach, the magnitude of the residuals indicates the model's dynamic consistency for each approach, with lower values being preferable.

### *4.3.3 Simulation Workflow*

The simulation workflow in this study comprised seven steps (Fig. 4.3):

i) Using the Scale Tool, the generic LFB model (Model_Generic.osim) was scaled (Model_Scaled.osim) for the participant based on the marker data in the static pose (Static_Pose.trc).

ii) Using the Inverse Kinematics (IK) Tool, the joint angles for the baseline task (IKResultsBaselineTask.mot) were calculated using Model_Scaled.osim and the marker data collected during the baseline task (Baseline_Task.trc).

iii) The Residual Reduction Algorithm (RRA) Tool was employed to adjust the mass properties of the scaled model (Model_Scaled.osim) using the joint angles obtained from the baseline task (IKResultsBaselineTask.mot); the resulting model was Model_Scaled_Adjusted.osim.

iv) Using the methods developed in the present study to model EHF&M in OpenSim (EHF&M Approaches 1–5), Model_Scaled_Adjusted.osim was modified for the IK analysis (Model_IK.osim) and SO analysis (Model_SO.osim). Details about each EHF&M approach are provided in Section 4.3.4. Sample data for one task and all OpenSim model and setup files for the five EHF&M Approaches are freely available at https://simtk.org/projects/handloadinterac.

v) The IK Tool was used with Model_IK.osim and the marker data for each lifting task (Lifting_Task.trc) to calculate the joint angles during each task (IKResultsLiftingTask.mot).

vi) Muscle forces (Muscle_Force.sto) were estimated using a SO analysis, where Model_SO.osim, IKResultsLiftingTask.mot, and external forces (External_Forces.mot) were the main inputs. External_Forces.mot included the EHF&M data (which differed among the EHF&M approaches) as well as the measured GRF&M data (which were the same for all approaches).

vii) Finally, a Joint Reaction analysis was performed to estimate spinal joint loads (Joint_Loads.sto) using the input files for Step vi and Muscle_Force.sto.

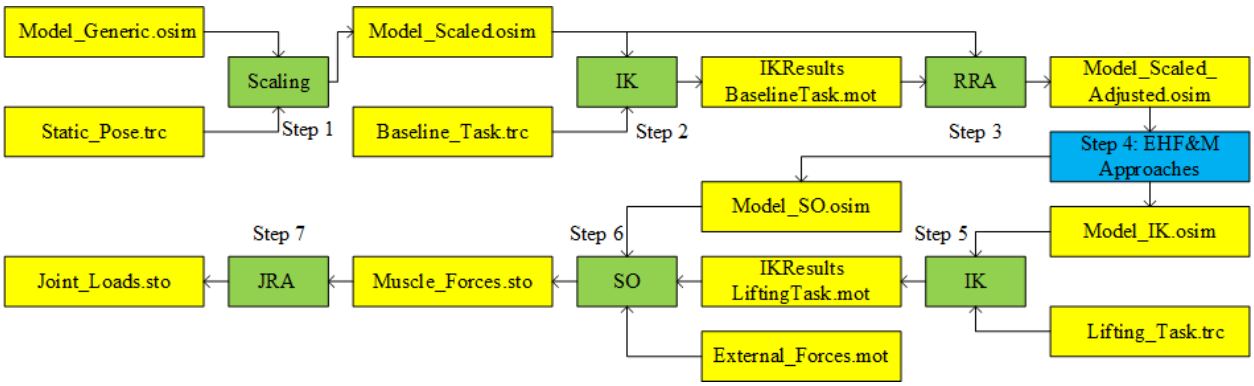


Fig. 4.3. Overview of the simulation workflow that was used in the present study. The green boxes show the OpenSim Tools that were used for each step (IK = Inverse Kinematics, RRA = Residual Reduction Algorithm, SO = Static Optimization, JRA = Joint Reaction Analysis), the yellow boxes show the main input and output files for each Tool, and the blue box represents the selected approach to model the external hand forces and moments (EHF&M) acting on the hands.

The second and third steps in the above workflow are not necessary to calculate muscle forces and joint loads; however, they generally improve simulation accuracy. The RRA Tool in OpenSim can be used to generate more dynamically consistent results with the GRF&M data by making small adjustments to the kinematics and mass centre location of a subject-specific model (Rajaee et al., 2015). As we intended to compare the residual forces induced by different EHF&M modelling approaches, RRA was run only for the baseline task (i.e., the lifting task using the foam box) to adjust the location of the pelvis centre of mass in the scaled model.

Although different files and procedures were used in Step vi above to set up the SO analysis for each EHF&M approach, the SO analysis in the present study always estimates muscle activations ($a_m$) and forces by solving the following optimization problem:

$$\text{minimize} \quad \sum_{m=1}^{n} a_m^2$$

$$\text{subject to} \quad \text{Equations of motion} \qquad \text{(Eq. 4.3)}$$

Muscle activation– to– force transformation constrained by muscle force– length– velocity properties

Using an iterative process at each time step, the SO solver attempts to determine the muscle forces that minimize the cost function (Eq. 4.3) and, when applied to the model, result in the desired joint accelerations, thus satisfying the equations of motion. Therefore, when constraint violations occur, it means that the solver cannot find a solution in which the coordinates' accelerations remain on the known acceleration manifold with errors less than $10^{-6}$ m/s$^2$ while solving for the internal forces in Eq. 4.3.

### *4.3.4 EHF&M Modelling Approaches*

#### *4.3.4.1 Modelling Approach 1: Apply a gravity-oriented half-load to each hand using an "external loads" setup file*

In this approach, the kinematics of the load are not considered so the eight markers attached to the box are not used in the IK analysis. One IK setup file is used for all phases of the trial (i.e., $t_0 \leq t \leq t_4$). Requiring only one IK setup file is simple and may be particularly beneficial for studies that involve repetitive lifting tasks. However, ignoring the markers on the box may cause kinematic errors in the body. For instance, the distance between the two hands may vary substantially during a simulation of a two-handed lifting task, while we know that it should be almost constant (i.e., equal to the distance between the handles). Therefore, to use Modelling Approach 1 for lifting tasks, we recommend that extra care be taken to verify that the distance between the hands is reasonable since it would not be inherently constrained by the definition of the model.

To set up SO, Approach 1 requires an "external loads" file. To configure an external load in OpenSim, one must specify the body to which the force is applied, the reference frame in which the force is expressed, and the reference frame in which the point of application is expressed; in this study, these parameters were the hand, ground, and ground bodies, respectively. External load setup is very convenient in Approach 1, and SO can be run once for the whole trial, similar to the IK analysis. In the present study, the force applied to each hand from $t_1$ to $t_3$ was half of the box weight and the hand markers (at the base of the third metacarpal bone) were used as the points of application of these forces. The limitation of this approach is that the interaction between the box and hands is modelled only indirectly. Nevertheless, this approach was used in previous lifting studies in OpenSim (Bruno et al., 2017, 2015) and other software (e.g., 3DSSPP (Rajaee et al., 2015), AnyBody (Bassani et al., 2017), and finite element models (Arjmand et al., 2011)) due to the ease of setup and application, and/or because the simulated tasks were static in nature.

*4.3.4.2 Modelling Approach 2: Increase the mass of each hand by half of the box mass*

The IK analysis for Approach 2 is the same as that for Approach 1. However, for the SO analysis, the original scaled model is modified for the second phase by adding half of the box mass to each hand. Therefore, although this approach does not require preparing an "external loads" setup file, as is required for Approach 1, SO cannot be run for the whole trial ($t_0$–$t_4$) with a single setup file. Contrary to Approach 1, Approach 2 considers the acceleration of the box, which is more reasonable and may be particularly important during fast movements. However, there may be unrealistic side effects of distributing the box mass equally between the two hands, especially if the lifting task is asymmetric or if the load tends more toward one side. The inertial properties of the hand-plus-box bodies may also be unrealistic. Moreover, this approach cannot be used in spine models that do not have hands. Although this approach was recently used by Beaucage-

Gauvreau et al. (2019) to validate several lifting tasks in OpenSim, the effect of the aforementioned simplifications on the simulation results has not yet been assessed.

*4.3.4.3 Modelling Approach 3: Create two half-box bodies, weld one to each hand, and connect them to each other with a Weld Constraint for both IK and SO analyses*

OpenSim uses the Simbody dynamics engine (Sherman et al., 2011), which uses an internal coordinate approach to formulate the equations of motion. In the OpenSim model file, each body must be connected to its parent body by exactly one joint (which specifies relative motions that are permitted) to create an open tree structure starting from the ground frame. Therefore, to form a closed kinematic chain, at least one constraint is required (to specify relative motions that are disallowed). In general, a unique system forming a closed kinematic chain can be composed in two ways: either one of the joints should be replaced by a constraint, or one of the bodies should be cut in half and a constraint should be added to enforce the relationship between the two halves of the "cut" body. During two-handed lifting, the system of interest contains a closed kinematic chain if a joint is used to connect each hand to the load. Therefore, for two-handed lifting, one of two strategies can be taken: i) model the box as a single rigid body, connect it to one of the hands by a joint, and then introduce a constraint between the box and the other hand; or ii) model the box in two halves with the same inertial properties (i.e., box_r and box_l), connect one half-box to each hand with a joint, and then introduce a weld constraint between the two half-boxes. The latter strategy (i.e., breaking the chain within the box) was used in the present work to treat the two box–hand joints uniformly (Sherman et al., 2011). In this study, box_r and box_l were connected to the right and left hands, respectively, with a Weld Joint because there was no substantial movement between the participant's hands and the handles. However, other joint types could also be used between each half-box and hand, in which case the following procedures would still be applicable.

In models with tree-like structures (e.g., Approaches 1 and 2 in this study), the IK analysis will always run but the quality of the results may vary. However, in closed-kinematic-chain systems, assembly errors (i.e., instances where the constraint equations are violated) might occur during the IK analysis if a system is not properly configured. The following steps demonstrate how Approach 3 was carried out to avoid assembly errors during the IK analysis for phase 2 (i.e., in the $t_1$–$t_3$ interval).

- Step 1) IK without box markers was run for $t_0$–$t_1$.
- Step 2) A new model file was created at $t_1$ by setting the default coordinate values of the original model to the IK results at $t_1$ using the OpenSim Application Programming Interface (API, OpenSim 3.3).
- Step 3) To connect box_r and box_l (child bodies) to the hands (parent bodies) with a Weld Joint, the position and orientation of the joint in both parent and child body reference frames were required. The 3×3 rotation matrix ${}_{\text{from}}\mathbf{R}_{\text{to}}$ represents the orientation of the "to" frame in the "from" frame and can be calculated using Euler angles (Schwab and Meijaard, 2006). A Body Kinematics (BK) analysis was run using the IK results from Step 1 to obtain the orientations (space-fixed X–Y–Z Euler angles) of the hands with respect to ground at $t_1$, and then ${}_{\text{GND}}\mathbf{R}_{\text{hand\_r}}$ and ${}_{\text{GND}}\mathbf{R}_{\text{hand\_l}}$ were calculated, where GND is the global (ground) reference frame. The following calculations were performed at time $t_1$:

$${}_{\text{box\_r}}\mathbf{R}_{\text{Weld\_r}}(t_1) = {}_{\text{GND}}\mathbf{R}_{\text{Weld\_r}}(t_1) = \mathbf{I} \quad \text{(Eq. 4.4)}$$

$${}_{\text{hand\_r}}\mathbf{R}_{\text{Weld\_r}}(t_1) = {}_{\text{hand\_r}}\mathbf{R}_{\text{GND}}(t_1) \times {}_{\text{GND}}\mathbf{R}_{\text{Weld\_r}}(t_1) =$$

$${}_{\text{GND}}\mathbf{R}^{\text{T}}_{\text{hand\_r}}(t_1) \times \mathbf{I} = {}_{\text{GND}}\mathbf{R}^{\text{T}}_{\text{hand\_r}}(t_1) \quad \text{(Eq. 4.5)}$$

where **I** is the identity matrix and $\mathbf{R}^T$ is the transpose of **R**.

The orientations of the Weld Joint in the parent- and child-body frames were then calculated from ${}_{\text{hand\_r}}\mathbf{R}_{\text{Weld\_r}}$ and ${}_{\text{box\_r}}\mathbf{R}_{\text{Weld\_r}}$, respectively. The above equations are presented for only the right hand; the same procedure was used for the left hand.

To find the location of the Weld Joint on the parent and child bodies, it was assumed that the joint was located at the centre of the cylindrical cross-section of the handle and was calculated accordingly for each trial using the box dimensions and its markers' positions at $t_1$. The box centre of mass (COM) was assumed to be in the centre of the box, and thus the box_r and box_l COMs were assumed to be halfway between the box centre and Weld Joints (Fig. 4.4).

- Step 4) A Weld Constraint between box_r and box_l was created at the box centre, with no orientation between the constraint and the two half-boxes it connected.
- Step 5) An IK analysis was run for the motion cycle (i.e., for $t_1$–$t_3$).

The IK setup process for Modelling Approach 3 takes much longer than that for Approaches 1 and 2, and despite the carefully configured steps listed above, assembly errors may still occur if marker weights are not set appropriately. When a kinematic loop is formed in a model, it affects the relative motions of all bodies in that loop. Therefore, although assigning a larger weight to specific markers means that the IK optimizer (which solves a weighted least squares problem) tries to better match those markers to the experimental data, assigning larger weights to the box and hand markers does not necessarily result in improved tracking of hand movements. In this case, the motion of the upper arm and forearm must satisfy the loop-closure constraints.

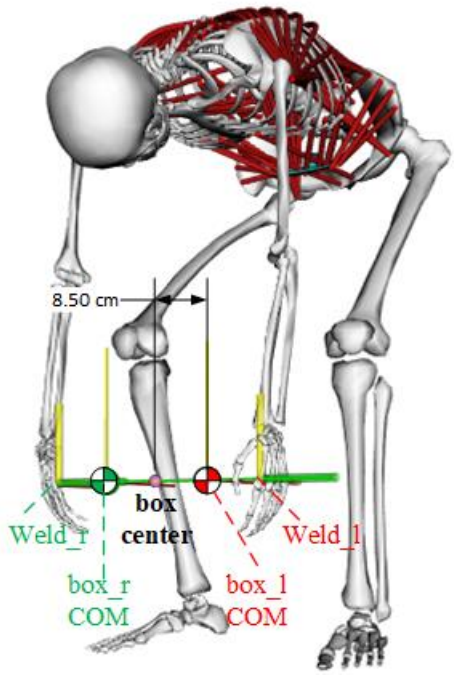


Fig. 4.4. The sample model file that was formed at $t_1$ in a lifting task for Modelling Approach 3, where two half-boxes with the same inertial properties (i.e., box_r and box_l) were created, each half was connected to one hand by a Weld Joint (i.e., Weld_r and Weld_l), and a Weld Constraint between the two halves was applied at the box centre.

In Approach 3, similar to other approaches proposed in the present study, SO (Eq. 4.3) was used to estimate muscle forces. However, solving dynamic equations in closed-kinematic-chain systems (e.g., Approach 3) is more challenging in general because nonlinear algebraic constraint equations are added to the ordinary differential equations of motion (Shabana, 2020). In unconstrained systems (e.g., Approaches 1, 2, 4, and 5), the equations of motion can be written as follows:

$$\mathbf{M}(\mathbf{q})\dot{\mathbf{u}} = \mathbf{f}_{\text{applied}}(t, \mathbf{q}, \mathbf{u}) - \mathbf{f}_{\text{inertial}}(\mathbf{q}, \mathbf{u}) \quad \text{(Eq. 4.6)}$$

where $\mathbf{q}$ and $\mathbf{u}$ are the generalized coordinates and speeds, respectively, $\mathbf{M}(\mathbf{q})$ is the mass matrix, $\mathbf{f}_{\text{applied}}$ is a column vector containing gravitational and all explicitly applied forces, and $\mathbf{f}_{\text{inertial}}$ is a column vector containing the Coriolis and gyroscopic forces. In this case, all generalized coordinates are independent and the equations of motion are simply ordinary differential equations. However, the topological loop in Approach 3 introduces additional unknown forces and moments

into the system to preserve the necessary relationships (constraints) among the generalized coordinates. The equations of motion for a constrained system can be written as follows:

$$\mathbf{M}(\mathbf{q})\dot{\mathbf{u}} + \mathbf{G}^{\mathrm{T}}\boldsymbol{\lambda} = \mathbf{f}_{\mathrm{applied}}(t, \mathbf{q}, \mathbf{u}) - \mathbf{f}_{\mathrm{inertial}}(\mathbf{q}, \mathbf{u}) \quad \text{(Eq. 4.7)}$$

where $\mathbf{G}$ is the Jacobian matrix of the constraint equations and $\boldsymbol{\lambda}$ is the vector of Lagrange multipliers representing the constraint forces.

In Approach 3, the SO Tool attempted to find both $\boldsymbol{\lambda}$ (Eq. 4.7) and the muscle forces in Eq. 4.3 at each time step. Hence, running SO using Approach 3 was computationally expensive, and acceleration-level constraint violations higher than the default value of $10^{-6}$ occurred for all coordinates. When using Approach 3, modellers should carefully track constraint violations at each time step to ensure they are acceptably small. It may be possible to decrease the computation time by decreasing the maximum number of iterations that the optimizer uses at each time step, provided the error remains acceptably low.

*4.3.4.4 Modelling Approach 4: Create two half-box bodies, weld one to each hand, and connect them to each other with a Weld Constraint only for IK analysis*

In Modelling Approach 3, the box was modelled in two halves, each half-box was connected to one hand with a Weld Joint, and then a Weld Constraint was defined between the two half-boxes. The IK Tool solves an optimization problem, in which it calculates the model's pose to make the model's markers "best match" the experimental markers. Therefore, if we do not enforce the relation between the half-boxes' movements, these half-boxes and the two arms would be able to move independently and, thus, the rigidity of the box would not be maintained (Appendix B–SI. 2), which is far from the physical reality. Therefore, to capture the box kinematics and the relative motions of the box, the upper arms, the forearms, and the hands, Modelling

Approach 4 is identical to Approach 3 in terms of the IK analysis. However, in Approach 4, the Weld Constraint between the two half-boxes was removed only for the SO analysis to remove the nonlinear algebraic constraint equations (Eq. 4.7) from the system, thus enabling SO to run much faster. If the results predicted by Approaches 3 and 4 are not significantly different from each other, Approach 4 may be the better alternative to reduce computation time.

*4.3.4.5 Modelling Approach 5: Create a box body, attach it to the ground with a Free Joint, and apply the estimated EHF&M to each hand using an "external loads" setup file*

As was discussed above, contact models can also be employed to predict contact forces during a dynamic simulation based only on material properties and geometry, but the parameters for contact models cannot be set arbitrarily and should be validated for each study. Estimated GRF&M can be compared against force plate data but measuring EHF&M using 6-axis force sensors is not common for musculoskeletal modelling studies. Another way to validate the estimated EHF&M is to apply the estimated EHF&M directly to the lifted external mass during a forward dynamic simulation, and then to compare the trajectories of the markers that were on the modelled mass against the measured marker data (Muller et al., 2020a).

In musculoskeletal dynamics, SO calculates muscle forces from the kinematics of the system at each instant of time (i.e., inverse dynamic analysis), but the estimated muscle forces will not necessarily reproduce the original model trajectory in a forward dynamic simulation. Thus, SO is usually used as part of forward simulation algorithms, such as the Computed Muscle Control algorithm in OpenSim (Thelen and Anderson, 2006). Therefore, if the estimated EHF&M from Approaches 1 or 2, or the predicted forces in the Weld Joint between the hands and box from Approaches 3 or 4, were applied to the box in a forward simulation, the measured box marker trajectories would not be reproduced (Appendix B–SI. 3). The purpose of Approach 5 was to

propose a new method for calculating EHF&M, and then to apply these forces and moments to the box handles in a forward dynamic simulation to validate the estimated box marker trajectories against experimental data. The required steps for the development of Approach 5 in OpenSim were as follows:

- Step 1) Three models were formed: i) ScaledModel.osim, which was the model that was used for Approaches 1 and 2 (the scaled generic model without a box); ii) JustBox.osim, which was a box segment connected to the ground by a Free Joint (6 degrees of freedom); and iii) ScaledModelWithBox.osim, which was the combination of ScaledModel.osim and JustBox.osim, but with a negligible box mass, where the model's pelvis and the box were both, separately, connected to the ground body.

- Step 2) For ScaledModel.osim and JustBox.osim, an IK analysis was run separately for the interval $t_1$–$t_3$. Then, the IK results for these models (i.e., ScaledModel.mot and JustBox.mot) were combined to generate ScaledModelWithBox.mot, a motion file that can be used with the ScaledModelWithBox.osim model. The combined motion file in the present study consisted of 66 columns (1 time column, which is the same between motion files, 6 box coordinates from JustBox.mot, and 59 human body coordinates from ScaledModel.mot).

- Step 3) First, for the JustBox.osim model, the box velocity with respect to ground ($\mathbf{v}_{\mathrm{box}}$) and its angular velocity ($\boldsymbol{\omega}_{\mathrm{box}}$) were obtained using the JustBox.mot file. Forces ($\mathbf{F}_{\mathrm{COM}}$) and moments ($\mathbf{M}_{\mathrm{COM}}$) were then calculated such that if, theoretically, we applied them to the box COM, the box would move along its experimental trajectory. Given the box mass

($m_{\text{box}}$), mass moment of inertia matrix ($\mathbf{I}_{\text{box}}$), and gravitational acceleration ($\mathbf{g}$), forces and moments were calculated as follows:

$$\mathbf{F}_{\text{COM}}(t) + m_{\text{box}} \cdot \mathbf{g} = m_{\text{box}} \cdot \frac{\mathrm{d}\mathbf{v}_{\text{box}}}{\mathrm{d}t} \quad \text{(Eq. 4.8)}$$

$$\mathbf{M}_{\text{COM}}(t) = \mathbf{I}_{\text{box}} \cdot \frac{\mathrm{d}\boldsymbol{\omega}_{\text{box}}}{\mathrm{d}t} \quad \text{(Eq. 4.9)}$$

- Step 4) The forces applied to the right and left handles ($\mathbf{F}_{\text{Rhandle}}(t)$ and $\mathbf{F}_{\text{Lhandle}}(t)$) and their corresponding points of application at the centre of pressure (COP) of each hand ($\mathbf{r}_{\text{RCOP}} = (x_{\text{Rhandle}}(t), y_{\text{Rhandle}}(t), z_{\text{Rhandle}}(t))$ and $\mathbf{r}_{\text{LCOP}} = (x_{\text{Lhandle}}(t), y_{\text{Lhandle}}(t), z_{\text{Lhandle}}(t))$) were estimated so as to produce $\mathbf{F}_{\text{COM}}(t)$ and $\mathbf{M}_{\text{COM}}(t)$ that were calculated in Step 3. The fmincon solver in MATLAB® was then employed to solve the following optimization problem at each time step between $t_1$ and $t_3$:

$$\begin{aligned}
\text{minimize} \quad & \|\mathbf{F}_{\text{Rhandle}}\|^2 + \|\mathbf{F}_{\text{Lhandle}}\|^2 \\
\text{subject to} \quad & \mathbf{F}_{\text{Rhandle}} + \mathbf{F}_{\text{Lhandle}} = \mathbf{F}_{\text{COM}} \\
& \mathbf{r}_{\text{RCOP}} \times \mathbf{F}_{\text{Rhandle}} + \mathbf{r}_{\text{LCOP}} \times \mathbf{F}_{\text{Lhandle}} = \mathbf{M}_{\text{COM}} \\
& -\Delta x \le x_{\text{Rhandle}} \le \Delta x \\
& -\Delta x \le x_{\text{Lhandle}} \le \Delta x \\
& -\Delta y \le y_{\text{Rhandle}} \le \Delta y \\
& -\Delta y \le y_{\text{Lhandle}} \le \Delta y \\
& -0.17 - \Delta z \le z_{\text{Rhandle}} \le -0.17 + \Delta z \\
& 0.17 - \Delta z \le z_{\text{Lhandle}} \le 0.17 + \Delta z
\end{aligned} \quad \text{(Eq. 4.10)}$$

Although the COP on each hand was unknown, an acceptable range for the COP locations can be determined from the dimensions of the box and hands. For instance, if the

participant's hand breadth is 9 cm and the participant holds the handles approximately in the middle (±3 cm), more than 7.5 cm (9/2 + 3 = 7.5) for the anterior–posterior distance of each COP and box centre might not be reasonable. In Eq. 4.10, $\Delta x$, $\Delta y$, and $\Delta z$ are half of the acceptable ranges for the COP. In this study, a maximum of 5 cm for $\Delta x$, $\Delta y$, and $\Delta z$ was considered to be acceptable based on the participant's hand breadth of 9 cm and hand length of 19 cm. 0.17 m in Eq. 4.10 is the medial–lateral distance between the box centre and the centre of the cylindrical cross-section of the handle.

- Step 5) The Forward Dynamics (FD) Tool was used to predict the positions of the eight markers on the box, where the predicted $\mathbf{F}_{\mathrm{Rhandle}}(t)$ and $\mathbf{F}_{\mathrm{Lhandle}}(t)$ were applied to the box at the $\mathbf{r}_{\mathrm{RCOP}}$ and $\mathbf{r}_{\mathrm{LCOP}}$ positions. It should be noted that the FD Tool was used to apply forces to the box body with no feedback or correction mechanism for tracking the kinematic data. Therefore, the experimental box markers can be used to validate the box marker trajectories estimated by the FD Tool. The predicted EHF&M were considered valid if the maximum distance between the predicted markers and the experimental markers was less than the values reported by Muller et al., (2020a). As an example, the distance between the predicted and measured box markers for the Stoop–20 task has been provided in the Supplementary Information (Appendix B–SI. 4).

- Step 6) SO was run for the ScaledModelWithBox.osim model using the ScaledModelWithBox.mot motion file and an external force file in which $-\mathbf{F}_{\mathrm{Rhandle}}(t)$ and $-\mathbf{F}_{\mathrm{Lhandle}}(t)$ were applied to the right and left COP positions, respectively. Note that the box is not connected to the human body model in Approach 5 for the SO analysis (in contrast to Approaches 3 and 4) because the box and pelvis are both, separately, connected to the ground body. ScaledModelWithBox was created because the box reference frame

was required to apply the forces and moments to the hands in ScaledModel. Since the box inertial properties were already considered in the forces applied to the hands, a negligible box mass was used in the ScaledModelWithBox model, thus avoiding the addition of pelvis–ground residual forces and enabling comparison of the obtained residuals against those obtained with other approaches.

As previously described, Approach 5 considers the inertial properties of the load better than Approach 1, while SO can be run as fast as in Approach 1 because the system does not contain a closed kinematic chain. However, estimating EHF&M in the SO setup phase of this approach takes much longer than with the other approaches.

## 4.4 Data Analysis

### *4.4.1 Spinal Loads*

After running a Joint Reaction analysis in OpenSim for each task with each EHF&M modelling approach, joint reaction force files (.sto) were analyzed using MATLAB®, where the $L_5S_1$ resultant forces (i.e., the Euclidean norm of reaction forces) were calculated at each instant and the data were normalized to 101 data points (i.e., 0–100% of the motion cycle at 1% increments) for each task. Indeed, one of the purposes of the present study was to evaluate the extent to which the proposed modelling decisions affect the absolute values of estimated spinal joint loads. However, solely reporting the absolute differences between the estimated results could have been misleading because the significance of the differences relates to the order of predicted spinal loads. Since there is no "correct" value by which to scale the difference between approaches, the relative differences in the predicted maximum $L_5S_1$ resultant forces with respect to Approach 1 were calculated for each task:

$$\text{Relative Difference}_{\text{Approach } i} = \frac{\max L_5S_{1\text{Approach } i} - \max L_5S_{1\text{Approach } 1}}{\max L_5S_{1\text{Approach } 1}} \times 100 \quad \text{(Eq. 4.11)}$$

The above relative difference for Approaches 2–5 was calculated for lifting and lowering separately, where the maxima of the first 50 and last 50 data points were considered to be the maximum spinal loads during lifting and lowering, respectively.

To assess how each EHF&M modelling approach predicts the differences in spinal loading between the tasks, first, the maximum and the average of $L_5S_1$ resultant forces predicted by each modelling approach were calculated for each task and across the motion cycle. Then, using a single-measurement, absolute-agreement, 2-way random-effects model with a 95% confidence interval, the intraclass correlation coefficients (ICCs) (McGraw and Wong, 1996) for the maximum and average $L_5S_1$ resultant forces were calculated across all tasks (n=8) in SPSS.

### *4.4.2 Residual Forces and Moments*

To analyze residual forces and moments, muscle-force files (.sto), which include residuals, were analyzed and plotted in MATLAB®. Similar to the spinal loads, residuals were normalized to 101 data points for the motion cycle; the root mean squares (RMS) of the residuals during the motion cycle were then calculated to compare the differences between the residuals resulting from the different EHF&M modelling approaches.

## 4.5 Results and Discussion

### *4.5.1 L5S1 Resultant Force Comparison*

The maximum difference in the maximum $L_5S_1$ resultant force was found during the Stoop–20–Fast task between Approaches 1 and 4 (2.6 kN; Fig. 4.5). To allow researchers to calculate the differences between the predictions of each EHF&M modelling approach at different

percentages of the motion cycle, all $L_5S_1$ resultant force figures have been provided in the Supplementary Information (Appendix B–SI. 5).

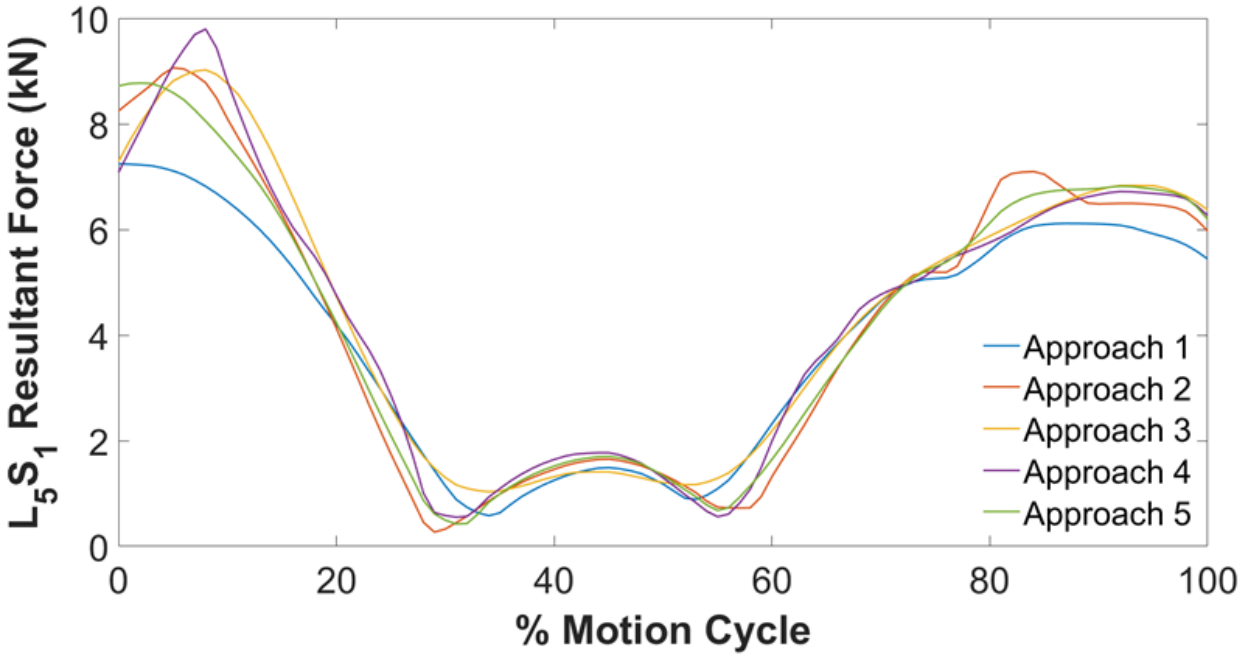


Fig. 4.5. The $L_5S_1$ resultant force predicted by each modelling approach during the Stoop–20–Fast task.

The relative differences in the predicted maximum $L_5S_1$ resultant forces with respect to Approach 1 are shown for each task in Table 4.1. When the differences in Table 4.1 are within the ranges of the modelling errors in a study, modellers may use the fastest approach (e.g., Approach 1 or 2). However, if the differences in Table 4.1 are higher than the uncertainties in their results that are due to other modelling assumptions, and if they choose an approach because it is faster, we recommend reporting the uncertainty in their results yielded only from the EHF&M modelling decision. To find the threshold for modelling errors due to other modelling assumptions, a sensitivity analysis (a factorial design experiment, sampling methods, etc.) for the input parameters can be conducted, which determines the effect of a change in particular parameters on the simulation outputs of interest. Best practices for sensitivity analysis of musculoskeletal models are reviewed by Hicks et al., (2015).

Table 4.1. The relative difference in predicted maximum $L_5S_1$ resultant forces by Modelling Approaches 2–5 with respect to Approach 1 when lifting and lowering the load.

| | **Relative difference of maximum $L_5S_1$ resultant force with respect to Approach 1 (%)** | | | | | | | |
|---|---|---|---|---|---|---|---|---|
| | Modelling Approach | | | | | | | |
| | 2 | | 3 | | 4 | | 5 | |
| | Lift | Lower | Lift | Lower | Lift | Lower | Lift | Lower |
| **Stoop–5** | 4.1 | 0.9 | 7.2 | 4.6 | 8.9 | 3.8 | 4.5 | 2.4 |
| **Stoop–20** | 4.8 | 3.4 | 7.7 | 4.3 | 4.8 | 4.2 | 3.7 | 3.9 |
| **Stoop–20–Slow** | 1.2 | 0.8 | 9.4 | 3.4 | 3.1 | 3.4 | 2.1 | 1.2 |
| **Stoop–20–Fast** | 25.1 | 16.1 | 24.6 | 11.7 | 35.2 | 9.9 | 21.1 | 11.5 |
| **Squat–5** | 2.9 | 3.8 | 2.0 | 1.7 | 1.2 | 0.4 | 1.3 | 2.0 |
| **Squat–20** | 7.1 | 2.8 | 5.1 | 3.4 | 6.9 | 3.6 | 8.9 | 5.0 |
| **Squat–20–Slow** | 3.5 | -0.6 | 4.2 | 3.7 | 5.4 | 2.0 | 4.5 | 0.7 |
| **Squat–20–Fast** | 17.7 | 13.7 | 21.7 | 10.9 | 20.7 | 15.4 | 20.2 | 22.8 |

When trends and maximum values of predicted spinal forces were compared between the modelling approaches, among the technique, speed, and lifted weight, the speed of movement had the most significant effect on the results. For instance, the maximum relative differences in the maximum $L_5S_1$ resultant force (Table 4.1) during the Stoop–5 and Stoop–20 tasks were 8.9% and 7.7%, respectively, whereas this relative difference reached up to 35.2% in the Stoop–20–Fast task. Evaluating load accelerations will shed light on these differences because each EHF&M approach considers the load accelerations differently.

To better illustrate the effect of load accelerations, the relative difference in vertical force applied to the box COM in Approach 5 with respect to Approach 1 was calculated for all stoop tasks (Fig. 4.6), as Approach 1 only captures the effect of the weight of the lifted load on spinal loads. As shown in Fig. 4.6, at 10% of the motion cycle, for instance, vertical forces applied to the body during the Stoop–5, Stoop–20, and Stoop–20–Fast tasks were, respectively, about 29%, 20%,

and 51% greater using Approach 5 compared to Approach 1. Therefore, due to the effect of load accelerations, the maximum difference in the predicted maximum spinal loads between the modelling approaches was higher during the Stoop–5 task than the Stoop–20 task, and the differences between the approaches in the predicted results were amplified when the movements were performed faster.

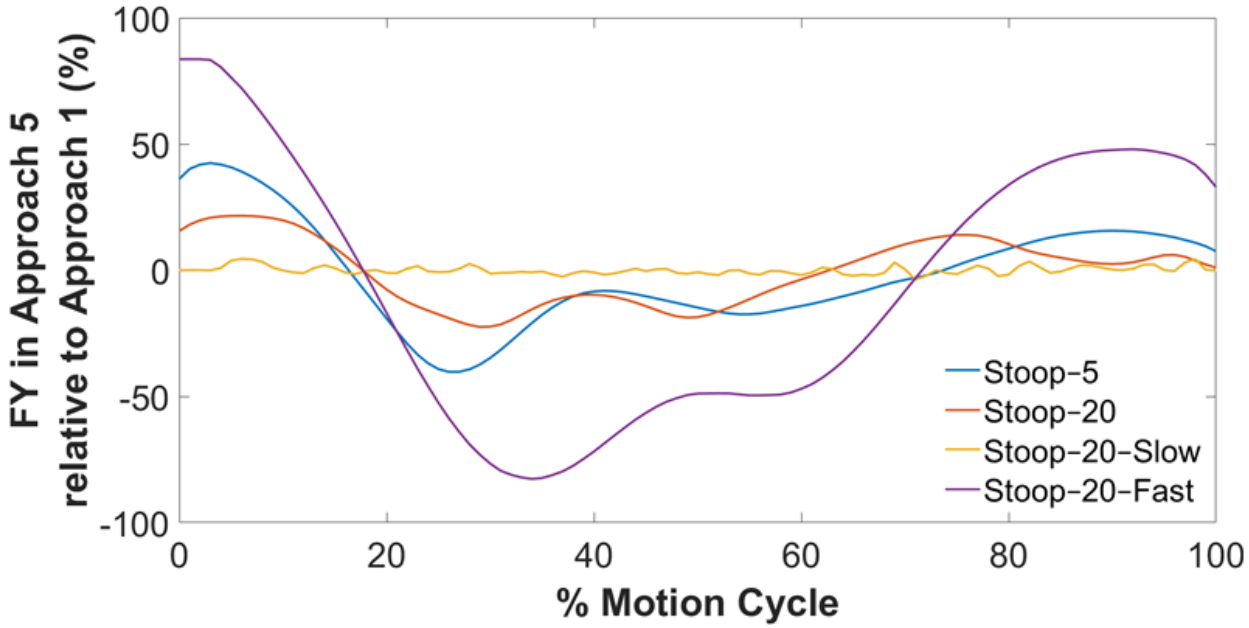


Fig. 4.6. The relative difference of vertical force (FY) applied to the box centre of mass in Approach 5 with respect to Approach 1 during the motion cycle for all stoop tasks.

ICC = 0.955 (0.881–0.989) and ICC = 0.933 (0.815–0.984) were obtained for the predicted maximum and average $L_5S_1$ resultant forces across all tasks, respectively, which indicate strong similarity among the modelling approaches. Previous spine modelling validation studies typically validated the predicted spinal loads by finding a strong correlation between the model estimates and previously reported intradiscal pressure measurements (Bassani et al., 2017; Beaucage-Gauvreau et al., 2019; Bruno et al., 2015). The ICC results in the present study suggest that, regardless of which external load modelling approach is used, similar trends and correlations across the lifting tasks and between spinal forces and intradiscal pressure data might be obtained.

However, we demonstrated that the actual peak values or the instants in the motion cycle at which the peaks occur could be substantially different, especially when the speed of movement is increased.

### *4.5.2 Pelvis–Ground Residual Forces*

In general, the largest residual forces and moments were found in the Y-direction (FY) and about the medial–lateral axis (MZ), respectively, because the largest change in the load acceleration was in the Y-direction and the most important moment for the simulated tasks was flexion–extension. Figure 4.7 shows an example of the FY residual force and MZ residual moment during the motion cycle for the Stoop–20 task. Previous studies have reported pelvis–ground residual forces during walking and running; however, to the best of the authors' knowledge, these residuals have not been reported for lifting tasks. Therefore, the baseline task can provide insight regarding the acceptable residuals for the ranges of motion in the present study.

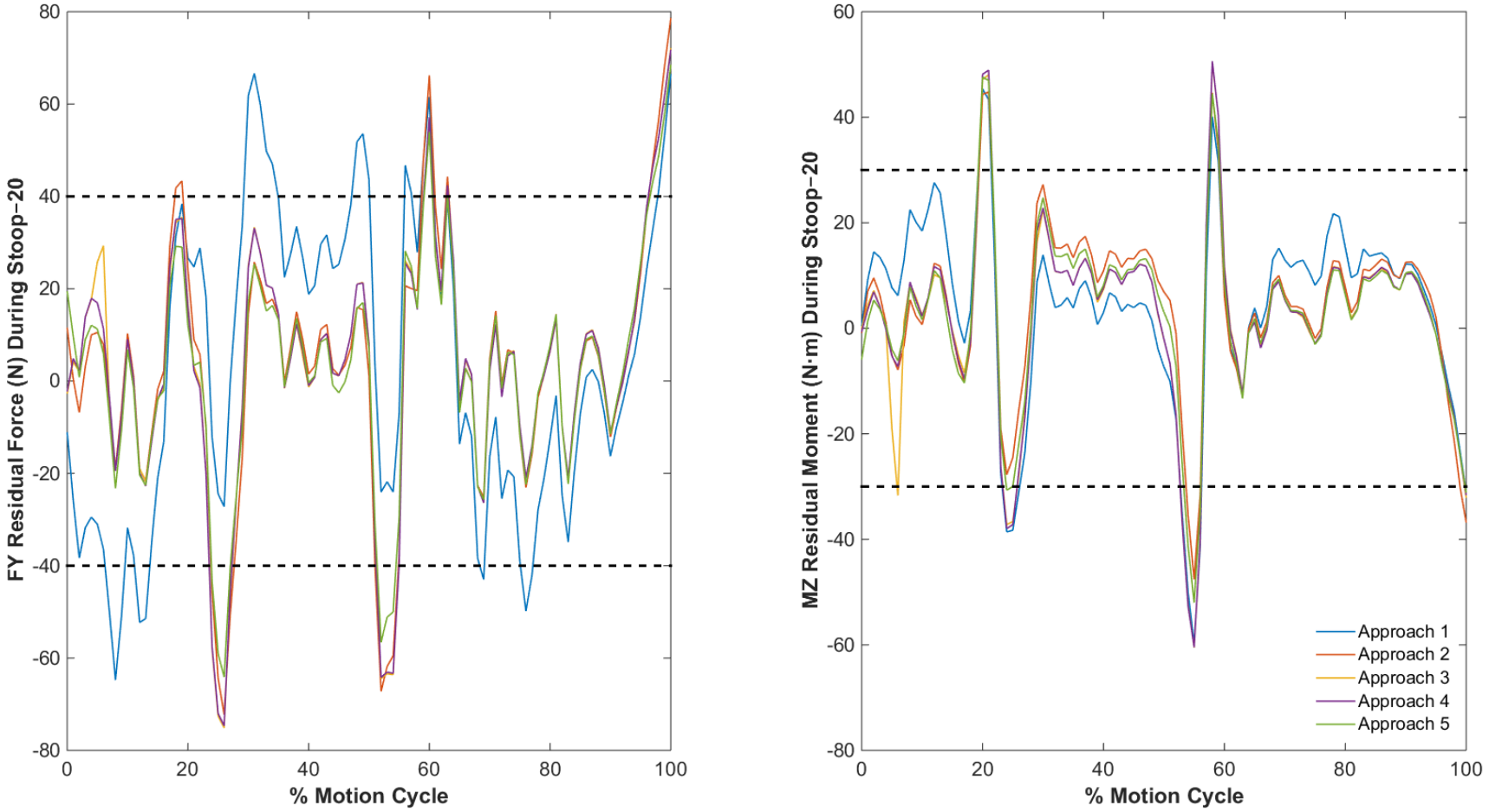


Fig. 4.7. FY residual force and MZ residual moment during the motion cycle for the Stoop–20 task. The dashed lines show the maximum absolute values of FY and MZ residuals during the baseline task.

In the baseline task, FY and MZ residuals reached absolute values of approximately 40 N and 30 N·m, respectively (the dashed lines in Fig. 4.7). If one were to choose these values as the acceptable thresholds for the residuals in the Stoop–20 task, FY residuals from Approaches 1 and 2 would be unacceptable in 23% and 17% of the motion cycle, respectively, and would be unacceptable in only 13% of the motion cycle for Approaches 3–5. Further, regarding MZ, all approaches would yield similar results and cause unacceptable residuals in approximately 10% of the motion cycle. Note, however, that higher residuals than those in the baseline task are expected in general when the lifted weight and the speed of movement are increased. In addition, if another threshold for residuals were considered, the above results would be different. For instance, as a rule of thumb, Hicks and colleagues (2015) recommended an acceptable threshold for residuals of no more than 5% of the magnitude of the experimentally measured net external force. Although this recommendation was for walking and running, where GRF&M are the only external forces and the body COM height does not change substantially during the motion, 5% of the magnitude of measured net GRF&M in the present study were approximately 65 N and 88 N for the Stoop–20 and Stoop–20–Fast tasks, respectively. By considering 65 N as the acceptable threshold for residual forces during the Stoop–20 task, one can conclude that Approach 1 performs better than Approach 2 because Approaches 1 and 2 result in unacceptable FY residuals in 2% and 5% of the motion cycle, respectively.

As discussed earlier (see Section 4.3.2), residual forces are induced in the model due to the modelling assumptions and measurement errors. For instance, in the LFB model that was used in this study, the thorax is modelled as a single body segment. There are many other inherent assumptions in the LFB model itself that may have contributed to the residuals observed in this study. Faber et al. (2018) reviewed the methods that can reduce residual forces and moments.

These methods are, in general, related to adjusting (time-invariant) anthropometric data, kinematics, and/or external forces. Therefore, regardless of the decision that researchers make on how to model EHF&M, residual forces can be reduced. Hence, in the present study, the difference between the resulting residuals is more important than the absolute values of residuals because, for any of the proposed EHF&M approaches, the absolute values of residuals may be reduced by modifying the LFB model and using the methods proposed in the literature (Faber et al., 2018).

Table 4.2 shows the RMS of residuals during the motion cycle for each task, as well as the average of RMS values across all tasks. It can be observed that Modelling Approach 1 generated considerably higher FY and MZ residuals than the other approaches because it did not consider the acceleration of the load. Similar to the spinal load results, the differences between RMS residuals of the five modelling approaches increase as the movement speed increases. Modelling Approach 4 generated lower FX, FY, FZ, MX, and MZ residuals overall (Table 4.2).

It is worth noting that the accuracy of the predicted spinal loads and the values of residuals are not necessarily correlated. For instance, Bruno and colleagues (2015) developed a spine model without lower extremities. In a model such as theirs, very high pelvis–ground residual forces are required to satisfy the model's dynamic equilibrium. For example, if the upper trunk mass is 40 kg, we expect a pelvis–ground FY residual force of approximately 400 N when this model is in a static standing posture. However, Bruno et al. (2015) validated their spinal loads against a variety of available intradiscal pressure data in the literature and their results are comparable to other spine modelling studies. Therefore, although models with fewer dynamic inconsistencies may appear to be more reliable, it cannot necessarily be inferred that more accurate spinal loads can be predicted if an EHF&M approach results in lower residual forces. Hence, in our future work, we aim to investigate which approach produces more accurate spinal loads.

Table 4.2. RMS of residual forces (FX (N), FY (N), FZ (N)) and moments (MX (N·m), MY (N·m), MZ (N·m)) during the motion cycle predicted by each modelling approach for all lifting tasks, as well as average RMS of residuals across all tasks.

| | FX (N) | | | | | FY (N) | | | | | FZ (N) | | | | |
|---|---|---|---|---|---|---|---|---|---|---|---|---|---|---|---|
| **Stoop–5** | 24 | 24 | 25 | 25 | 24 | 22 | 20 | 23 | 23 | 20 | 24 | 24 | 22 | 22 | 24 |
| **Stoop–20** | 21 | 18 | 18 | 18 | 19 | 33 | 27 | 27 | 27 | 24 | 25 | 26 | 23 | 23 | 25 |
| **Stoop–20–Slow** | 8 | 8 | 7 | 7 | 7 | 27 | 27 | 25 | 25 | 27 | 12 | 11 | 10 | 10 | 12 |
| **Stoop–20–Fast** | 118 | 106 | 60 | 58 | 115 | 139 | 104 | 86 | 81 | 94 | 109 | 113 | 89 | 89 | 110 |
| **Squat–5** | 29 | 27 | 22 | 22 | 29 | 40 | 39 | 29 | 29 | 38 | 41 | 41 | 34 | 34 | 41 |
| **Squat–20** | 17 | 16 | 15 | 15 | 16 | 84 | 83 | 83 | 83 | 81 | 24 | 24 | 20 | 20 | 24 |
| **Squat–20–Slow** | 8 | 8 | 8 | 7 | 7 | 13 | 12 | 11 | 11 | 11 | 10 | 10 | 8 | 8 | 10 |
| **Squat–20–Fast** | 45 | 44 | 47 | 44 | 41 | 126 | 66 | 67 | 63 | 62 | 39 | 38 | 48 | 48 | 38 |
| **Average** | 34 | 31 | 25 | 24 | 32 | 60 | 47 | 44 | 43 | 45 | 35 | 36 | 32 | 32 | 35 |

| | MX (N·m) | | | | | MY (N·m) | | | | | MZ (N·m) | | | | |
|---|---|---|---|---|---|---|---|---|---|---|---|---|---|---|---|
| **Stoop–5** | 11 | 10 | 10 | 10 | 11 | 6 | 6 | 9 | 9 | 6 | 21 | 21 | 21 | 21 | 20 |
| **Stoop–20** | 15 | 15 | 15 | 15 | 16 | 7 | 9 | 10 | 10 | 7 | 18 | 16 | 18 | 18 | 16 |
| **Stoop–20–Slow** | 12 | 13 | 11 | 11 | 13 | 7 | 8 | 7 | 7 | 7 | 14 | 14 | 13 | 13 | 14 |
| **Stoop–20–Fast** | 30 | 29 | 34 | 32 | 30 | 17 | 18 | 31 | 32 | 17 | 68 | 61 | 54 | 54 | 65 |
| **Squat–5** | 16 | 15 | 14 | 14 | 31 | 5 | 5 | 4 | 4 | 5 | 16 | 15 | 12 | 12 | 17 |
| **Squat–20** | 17 | 17 | 18 | 18 | 18 | 6 | 6 | 6 | 6 | 5 | 32 | 30 | 30 | 30 | 30 |
| **Squat–20–Slow** | 15 | 16 | 15 | 15 | 16 | 4 | 4 | 4 | 4 | 4 | 11 | 12 | 10 | 10 | 11 |
| **Squat–20–Fast** | 25 | 24 | 26 | 23 | 24 | 12 | 11 | 10 | 10 | 12 | 40 | 26 | 27 | 27 | 24 |
| **Average** | 18 | 18 | 18 | 17 | 20 | 8 | 8 | 10 | 10 | 8 | 28 | 25 | 23 | 23 | 25 |

**Legend**
- Approach 1
- Approach 2
- Approach 3
- Approach 4
- Approach 5

## 4.6 Conclusion

In the present study, we introduced and compared five approaches of varying complexity to model the interaction between the hands and the box while using an inverse dynamics–based approach (i.e., SO) to predict muscle forces and spinal joint loads. The modelling decisions that were made in the five approaches were inherently different, which affected the SO results. We compared the differences in the predicted $L_5S_1$ contact forces and residual forces among the proposed approaches in Section 4.5; the Supplementary Information (Appendix B–SI. 6 and B–SI. 7) provides additional examples comparing the differences among the five approaches in the calculated kinematics and the EHF&M acting between the hands and the lifted mass.

Some key features of these modelling approaches that were discussed in the Methods and Results sections are summarized in Table 4.3. In conclusion, if only residual forces are considered, Modelling Approach 4 appears to be the best option for lifting/lowering tasks. If it is not possible to collect data from markers attached to the load or if the computational expense of the IK analysis in Approach 4 is an issue, Modelling Approach 2 is a better option than Modelling Approach 1. To determine which approach predicts spinal loads more accurately, future studies should further validate the results of these modelling approaches for more participants and by using experimental data such as intradiscal pressure and *in vivo* implant data.

Table 4.3. Comparative evaluation of five EHF&M modelling approaches to model external loads acting on the hands in OpenSim. Approximate time required to configure the IK and SO Tools ("setup time") and the IK and SO runtimes for 100 frames are shown for each modelling approach. Roman numerals denote our subjective measure of performance, with III being the highest. ✓ means considered and × means not considered.

| | **Modelling Approach** | | | | |
|---|---|---|---|---|---|
| | 1 | 2 | 3 | 4 | 5 |
| **IK setup time, approx. (min)** | 5 | 5 | 15 | 15 | 5 |

| | | | | | |
|---|---|---|---|---|---|
| **IK runtime (s)** | 17 | 17 | 34 | 34 | 17 |
| **SO setup time, approx. (min)** | 5 | 5 | 15 | 15 | 20 |
| **SO runtime (min)** | 3 | 3 | 49 | 3 | 3 |
| **Load kinematics for IK analysis** | × | × | ✓ | ✓ | ✓ |
| **Load accelerations for SO analysis** | × | ✓ | ✓ | ✓ | ✓ |
| **RMS residuals (mean of all tasks)** | I | II | III | III | II |

### 4.7 References


Akhavanfar, M., Brandon, S.C.E., Brown, S.H.M., Graham, R.B., 2019. Development of a novel MATLAB-based framework for implementing mechanical joint stability constraints within OpenSim musculoskeletal models. J. Biomech. 91, 61–68.

Akhavanfar, M., Kazemi, H., Eskandari, A.H., Arjmand, N., 2018. Obesity and spinal loads; a combined MR imaging and subject-specific modelling investigation. J. Biomech. 70, 102–112.

Arjmand, N., Plamondon, A., Shirazi-Adl, A., Larivière, C., Parnianpour, M., 2011. Predictive equations to estimate spinal loads in symmetric lifting tasks. J. Biomech. 44, 84–91.

Baraff, D., 1994. Fast contact force computation for nonpenetrating rigid bodies. In: Proceedings of the 21st Annual Conference on Computer Graphics and Interactive Techniques. pp. 23–34.

Bassani, T., Stucovitz, E., Qian, Z., Briguglio, M., Galbusera, F., 2017. Validation of the AnyBody full body musculoskeletal model in computing lumbar spine loads at L4L5 level. J. Biomech. 58, 89–96.

Bazrgari, B., Shirazi-Adl, A., Trottier, M., Mathieu, P., 2008. Computation of trunk equilibrium and stability in free flexion–extension movements at different velocities. J. Biomech. 41, 412–421.

Beaucage-Gauvreau, E., Robertson, W.S.P., Brandon, S.C.E., Fraser, R., Freeman, B.J.C., Graham, R.B., Thewlis, D., Jones, C.F., 2019. Validation of an OpenSim full-body model with detailed lumbar spine for estimating lower lumbar spine loads during symmetric and asymmetric lifting tasks. Comput. Methods Biomech. Biomed. Engin. 22, 451–464.

Behjati, M., Arjmand, N., 2019. Biomechanical assessment of the NIOSH lifting equation in asymmetric load-handling activities using a detailed musculoskeletal model. Hum. Factors 61, 191–202.

Bruno, A.G., Bouxsein, M.L., Anderson, D.E., 2015. Development and validation of a musculoskeletal model of the fully articulated thoracolumbar spine and rib cage. J. Biomech. Eng. 137, 081003.

Bruno, A.G., Burkhart, K., Allaire, B., Anderson, D.E., Bouxsein, M.L., 2017. Spinal loading patterns from biomechanical modelling explain the high incidence of vertebral fractures in the thoracolumbar region. J. Bone Miner. Res. 32, 1282–1290.

Choi, A., Lee, J.-M., Mun, J.H., 2013. Ground reaction forces predicted by using artificial neural network during asymmetric movements. Int. J. Precis. Eng. Manuf. 14, 475–483.

Damsgaard, M., Rasmussen, J., Christensen, S.T., Surma, E., De Zee, M., 2006. Analysis of musculoskeletal systems in the AnyBody Modelling System. Simul. Model. Pract. Theory 14, 1100–1111.

Delp, S.L., Anderson, F.C., Arnold, A.S., Loan, P., Habib, A., John, C.T., Guendelman, E., Thelen, D.G., 2007. OpenSim: Open-source software to create and analyze dynamic simulations of movement. IEEE Trans. Biomed. Eng. 54, 1940–1950.

Dorn, T.W., Lin, Y.-C., Pandy, M.G., 2012. Estimates of muscle function in human gait depend on how foot-ground contact is modelled. Comput. Methods Biomech. Biomed. Engin. 15, 657–668.

Faber, G.S., Chang, C.-C., Kingma, I., Dennerlein, J.T., 2013. Estimating dynamic external hand forces during manual materials handling based on ground reaction forces and body segment accelerations. J. Biomech. 46, 2736–2740.

Faber, G.S., Koopman, A.S., Kingma, I., Chang, C.C., Dennerlein, J.T., van Dieën, J.H., 2018. Continuous ambulatory hand force monitoring during manual materials handling using instrumented force shoes and an inertial motion capture suit. J. Biomech. 70, 235–241.

Faber, H., Van Soest, A.J., Kistemaker, D.A., 2018. Inverse dynamics of mechanical multibody systems: An improved algorithm that ensures consistency between kinematics and external forces. PLoS One 13, e0204575.

Featherstone, R., 2014. Rigid body dynamics algorithms. Springer.

Fluit, R., Andersen, M.S., Kolk, S., Verdonschot, N., Koopman, H.F.J.M., 2014. Prediction of ground reaction forces and moments during various activities of daily living. J. Biomech. 47, 2321–2329.

Genaidy, A.M., Waly, S.M., Khalil, T.M., Hidalgo, J., 1993. Spinal compression tolerance limits for the design of manual material handling operations in the workplace. Ergonomics 36, 415–434.

Ghezelbash, F., Shirazi-Adl, A., Arjmand, N., El-Ouaaid, Z., Plamondon, A., Meakin, J.R., 2016. Effects of sex, age, body height and body weight on spinal loads: sensitivity analyses in a subject-specific trunk musculoskeletal model. J. Biomech. 49, 3492–3501.

Ghezelbash, F., Shirazi-Adl, A., Plamondon, A., Arjmand, N., 2020. Comparison of different lifting analysis tools in estimating lower spinal loads–Evaluation of NIOSH criterion. J. Biomech. 112, 110024.

Gilchrist, L.A., Winter, D.A., 1996. A two-part, viscoelastic foot model for use in gait simulations. J. Biomech. 29, 795–798.

Graham, R.B., Agnew, M.J., Stevenson, J.M., 2009. Effectiveness of an on-body lifting aid at reducing low back physical demands during an automotive assembly task: Assessment of EMG response and user acceptability. Appl. Ergon. 40, 936–942.

Hamner, S.R., Seth, A., Delp, S.L., 2010. Muscle contributions to propulsion and support during running. J. Biomech. 43, 2709–2716.

Hamner, S.R., Seth, A., Steele, K.M., Delp, S.L., 2013. A rolling constraint reproduces ground reaction forces and moments in dynamic simulations of walking, running, and crouch gait. J. Biomech. 46, 1772–1776.

Hicks, J.L., Uchida, T.K., Seth, A., Rajagopal, A., Delp, S.L., 2015. Is My Model Good Enough? Best Practices for Verification and Validation of Musculoskeletal Models and Simulations of Movement. J. Biomech. Eng. 137, 020905.

Johnson, W.R., Mian, A., Donnelly, C.J., Lloyd, D., Alderson, J., 2018. Predicting athlete ground reaction forces and moments from motion capture. Med. Biol. Eng. Comput. 56, 1781–1792.

Koopman, A.S., Kingma, I., Faber, G.S., Bornmann, J., van Dieën, J.H., 2018. Estimating the L5S1 flexion/extension moment in symmetrical lifting using a simplified ambulatory measurement system. J. Biomech. 70, 242–248.

Koopman, B., Grootenboer, H.J., De Jongh, H.J., 1995. An inverse dynamics model for the analysis, reconstruction and prediction of bipedal walking. J. Biomech. 28, 1369–1376.

Lopes, D.S., 2013. Smooth convex surfaces for modelling and simulating multibody systems with compliant contact elements. Ph. D. thesis, Instituto Superior Técnico, Universidade de Lisboa, Lisbon.

McGraw, K.O., Wong, S.P., 1996. Forming inferences about some intraclass correlation coefficients. Psychol. Methods 1, 30–46.

Muller, A., Pontonnier, C., Dumont, G., 2020a. Motion-based prediction of hands and feet contact efforts during asymmetric handling tasks. IEEE Trans. Biomed. Eng. 67, 344–352.

Muller, A., Pontonnier, C., Robert-Lachaine, X., Dumont, G., Plamondon, A., 2020b. Motion-based prediction of external forces and moments and back loading during manual material handling tasks. Appl. Ergon. 82, 102935.

Oh, S.E., Choi, A., Mun, J.H., 2013. Prediction of ground reaction forces during gait based on kinematics and a neural network model. J. Biomech. 46, 2372–2380.

Raabe, M.E., Chaudhari, A.M.W., 2016. An investigation of jogging biomechanics using the full-body lumbar spine model: model development and validation. J. Biomech. 49, 1238–1243.

Rajaee, M.A., Arjmand, N., Shirazi-Adl, A., Plamondon, A., Schmidt, H., 2015. Comparative evaluation of six quantitative lifting tools to estimate spine loads during static activities. Appl. Ergon. 48, 22–32.

Ren, L., Jones, R.K., Howard, D., 2008. Whole body inverse dynamics over a complete gait cycle based only on measured kinematics. J. Biomech. 41, 2750–2759.

Ren, Lei, Qian, Z., Ren, Luquan, 2014. Biomechanics of musculoskeletal system and its biomimetic implications: A review. J. Bionic Eng. 11, 159–175.

Robert, T., Causse, J., Monnier, G., 2013. Estimation of external contact loads using an inverse dynamics and optimization approach: general method and application to sit-to-stand maneuvers. J. Biomech. 46, 2220–2227.

Sandhu, S.S., McPhee, J., 2010. A two-dimensional nonlinear volumetric foot contact model. In Volume 2: Biomedical and Biotechnology Engineering. pp. 703–710.

Schwab, A.L., Meijaard, J.P., 2006. How to draw Euler angles and utilize Euler parameters. In: International Design Engineering Technical Conferences and Computers and Information in Engineering Conference. pp. 259–265.

Seth, A., Hicks, J.L., Uchida, T.K., Habib, A., Dembia, C.L., Dunne, J.J., Ong, C.F., DeMers, M.S., Rajagopal, A., Millard, M., 2018. OpenSim: Simulating musculoskeletal dynamics and neuromuscular control to study human and animal movement. PLoS Comput. Biol. 14, e1006223.

Shabana, A., 2020. Dynamics of multibody systems. Cambridge university press.

Sherman, M.A., Seth, A., Delp, S.L., 2011. Simbody: multibody dynamics for biomedical research. Procedia IUTAM 2, 241–261.

Shourijeh, M.S., McPhee, J., 2015. Foot–ground contact modelling within human gait simulations: from Kelvin–Voigt to hyper-volumetric models. Multibody Syst. Dyn. 35, 393–407.

Skals, S., Jung, M.K., Damsgaard, M., Andersen, M.S., 2017. Prediction of ground reaction forces and moments during sports-related movements. Multibody Syst. Dyn. 39, 175–195.

Thelen, D.G., Anderson, F.C., 2006. Using computed muscle control to generate forward dynamic simulations of human walking from experimental data. J. Biomech. 39, 1107–1115.

Waters, T.R., Putz-Anderson, V., Garg, A., Fine, L.J., 1993. Revised NIOSH equation for the design and evaluation of manual lifting tasks. Ergonomics 36, 749–776.

# Chapter 5: Evaluation of Spinal Force Normalization Techniques

Published in Journal of Biomechanics 2023; 147: 111441.
https://doi.org/10.1016/j.jbiomech.2023.111441

## 5.1 Abstract

Division normalization is commonly used in biomechanics studies to remove the effect of anthropometric differences (e.g., body weight) on kinetic variables, facilitating comparison across a population. In spine biomechanics, spinal forces are commonly divided by the body weight or the intervertebral load during a standing posture. However, it has been suggested that offset and power curve normalization are more appropriate than division normalization for normalizing kinetic variables such as ground reaction forces during walking and running. The present study investigated, for the first time, the effectiveness of four techniques for normalizing spinal forces to remove the effect of body weight. Spinal forces at all lumbar levels were estimated using a detailed OpenSim musculoskeletal model of the spine for 11 scaled models (50–100 kg) and during 13 upper-trunk flexion tasks. Pearson correlations of raw and normalized forces against body weight were used to assess the effectiveness of each normalization technique. Body weight and standing division normalization could only successfully normalize $L_4L_5$ spinal forces in three tasks, and $L_5S_1$ loads in five and three tasks, respectively; however, offset and power curve normalization techniques were successful across all lumbar spine levels and all tasks. Offset normalization successfully removed the effect of body weight and maintained the influence of flexion angle on spinal forces. Thus, we recommend offset normalization to account for anthropometric differences in studies of spinal forces.

## 5.2 Introduction

In biomechanics studies, anthropometrics greatly influence ground reaction forces (GRF), intersegmental forces, and other kinetic variables. Therefore, kinetic variables are often

normalized by anthropometric parameters such as body weight (BW) and height to remove the effects of anthropometric differences between participants as confounding factors (Derrick et al., 2020). For instance, non-dimensional normalization, in which each variable is divided by combinations of body mass, leg length, and gravitational acceleration, has been recommended for normalizing data in clinical gait analysis (Pinzone et al., 2016). Normalization is an ostensibly innocuous data analysis procedure, but it is critical to consider its effects as normalization can change the way results are interpreted. For instance, normalizing the knee abduction moment can significantly influence the interpretations of group comparisons in research on anterior cruciate ligament injury risk (Norcross et al., 2017). In addition, different techniques for normalization may have different effects on the results and the subsequent conclusions in a study; thus, it is important to determine the most appropriate technique for normalizing each biomechanical variable.

In spine biomechanics, spinal joint forces are of interest in many studies as these loads play a major role in the etiology of back disorders (Dreischarf et al., 2016). Among personalized factors (age, sex, BW, and height), BW has been found to have the greatest effect on spinal loads (Ghezelbash et al., 2016). Therefore, to remove the influence of anthropometric differences, previous studies have often simply divided the measured or estimated spinal forces by BW (Damm et al., 2020; Favier et al., 2021; Mavor et al., 2022) or divided spinal forces by the intervertebral load during a neutral, unloaded, standing posture (Actis et al., 2018; Beaucage-Gauvreau et al., 2019). These two division normalization techniques (sometimes called "ratio scaling" in the literature) will be referred to as *BW Division Normalization* (BWDN) and *Standing Division Normalization* (SDN) in the present study.

The effects of various normalization techniques have been investigated for GRF, primarily during walking (Wannop et al., 2012) and running (Stickley et al., 2018). The results of these

studies suggested that BWDN is not the best technique to normalize GRF because the normalized GRF values showed significant correlations with BW. In other words, when BWDN was used, a considerable portion of the variance in the normalized results was still attributable to BW. Offset and power curve normalization (also referred to as "allometric scaling" in the literature) have been shown to be more appropriate for normalizing GRF (Stickley et al., 2018; Wannop et al., 2012); however, to the best of the authors' knowledge, no studies have examined the effect of various normalization techniques on spinal forces. The present study explores the appropriateness of BWDN, SDN, *BW Offset Normalization* (BWON), and *BW Power Curve Normalization* (BWPCN) for normalizing spinal forces in upright and flexed postures.

Despite the similarity noted above with GRFs during gait, spinal forces can be more difficult to study due to a paucity of experimental data. Specifically, due to invasiveness and complexity, spinal force measurements are available for only a limited number of subjects (L1 level: four patients, 66 ± 4 kg; L3 level: one patient, 66 kg) using instrumented vertebral body implants (Rohlmann et al., 2014). Therefore, to compare the effectiveness of various normalization techniques over a broad range of BW, one may employ musculoskeletal modelling, which is widely used to estimate spinal joint forces (Akhavanfar et al., 2019).

## 5.3 Methods

### *5.3.1 Musculoskeletal Modelling*

Several detailed musculoskeletal models of the spine have been developed and validated in various modelling platforms (Actis et al., 2018; Akhavanfar et al., 2018; Bassani et al., 2017; Beaucage-Gauvreau et al., 2019; Bruno et al., 2015; Malakoutian et al., 2018). To estimate spinal loads in this study, we selected the fully articulated thoracolumbar spine (FATLS) model (Bruno et al., 2015) for several reasons. First, this model is an open-access model that has been developed

in OpenSim (Delp et al., 2007), which is the most widely used open-source platform in biomechanics (Seth et al., 2018). The FATLS model is an anatomically detailed model with 552 Hill-type muscle fascicles and is among the few models that allow researchers to estimate spinal forces for all lumbar and thoracic levels (Bruno et al., 2015). Finally, the muscle forces and joint loads estimated by this model have been extensively validated against the myoelectric activity of trunk muscles, *in vivo* measures of intradiscal pressure, and vertebral implant loads during a variety of static activities (Bruno et al., 2015).

Similar to a previous study (Schmid et al., 2020), we added the lower limbs of the Gait2354 model available in OpenSim to the FATLS model to make it a full-body model for scaling purposes. Thereafter, we scaled the mass properties of the model for 11 total body masses (50–100 kg in increments of 5 kg) using the Scale Tool in OpenSim. We enhanced the FATLS model by adding the role of passive structures at all spinal levels using bushing elements in OpenSim and the functions that have been derived and validated for the FATLS model (Wang et al., 2020). We simulated 13 static symmetric trunk flexion tasks (0–120° in increments of 10°) for each scaled model (11 BW × 13 tasks = 143 simulations in total). For each simulation, using the same strategy as was used by Bruno et al. (2015), we composed a motion file (.mot) where the total trunk flexion was divided between the pelvis and intersegmental segments using prior experimental studies (Tafazzol et al., 2014; Wong et al., 2006). The lower limbs were then removed and Static Optimization was used to estimate muscle forces. We recently demonstrated how the Static Optimization solver in OpenSim can be used to calculate muscle forces effectively (Akhavanfar et al., 2022). Using the calculated muscle forces, a Joint Reaction Analysis was performed to estimate spinal joint loads for each static task.

### *5.3.2 Normalization*

Normalization is a two-step process (O'Malley, 1996). In the first step, a mathematical model of the form $y = f(x)$ is derived to describe the dependent variable ($y$; in this case, spinal forces) as a function of the normalization parameter ($x$, BW). When BWDN is used, a linear relationship with a zero intercept ($y = ax$) between spinal forces and BW is assumed. SDN assumes that spinal forces during the studied task (e.g., static symmetric trunk flexion at 40°, referred to herein as "Flex 40°") is linearly related ($y = ax$) to the spinal forces while standing for each individual. The second step of normalization is to remove the correlation between $y$ and $x$; for BWDN and SDN, this is done through simple division ($y_n = y/x = a$). The analogous functions for BWON and BWPCN are $y = ax + b$ and $y = ax^b$, respectively. These functions were fit to the spinal forces for each trunk flexion angle using the fitting tool in MATLAB® and the significance of the regression was set at a 95% level of confidence. The normalized forces for BWON were calculated as $y_n = {(y - b)}/{x}$ and for BWPCN were calculated as $y_n = {y}/{x^b}$ (for more details about power curve normalization and its implications, see Appendix C–SI. 1). After normalization, Pearson correlation coefficients were determined between $y_n$ (normalized spinal forces) and $x$ (BW); if a significant correlation ($p < 0.05$) was found, the normalization procedure was deemed unsuccessful.

## 5.4 Results

Figure 5.1 compares the original resultant $L_1L_2$ spinal forces from our model with the spinal forces after normalization using each of the four techniques described above, for BW from 490 N to 980 N. Raw resultant forces at all lumbar spinal levels were significantly positively correlated with BW for all flexion tasks. Pearson correlation coefficients between BW and resultant forces (raw and normalized) at all lumbar spinal levels have been provided in the Supplementary

Information (Appendix C–SI. 2). When BWDN and SDN were used, significant correlations remained between spinal joint loads and BW for most tasks. BWDN and SDN successfully removed the significant correlations of $L_4L_5$ resultant force with BW for three tasks (Flex 70–90°), and they successfully normalized $L_5S_1$ loads in five and three tasks, respectively (Fig. 5.2).

BWON and BWPCN removed the effect of BW from all spinal forces ($p > 0.05$) during all tasks (Fig. 5.2). The derived coefficient ($b$) for the BWON and BWPCN functions is shown in Fig. 5.3 for each flexion task. When the BWON and BWPCN functions were fit to the spinal loads, the coefficient of determination ($R^2$) was always above 0.99, meaning that these functions effectively accounted for variation of spinal forces. For all BWPCN fitted curves, further regression diagnostic evaluations showed the normality of residuals using the Kolmogorov–Smirnov test and showed the homoscedasticity of the residuals (Batterham and George, 1997) as the absolute residual values resulting from the BWPCN functions had non-significant correlations with BW (i.e., the independent variable) during all tasks.

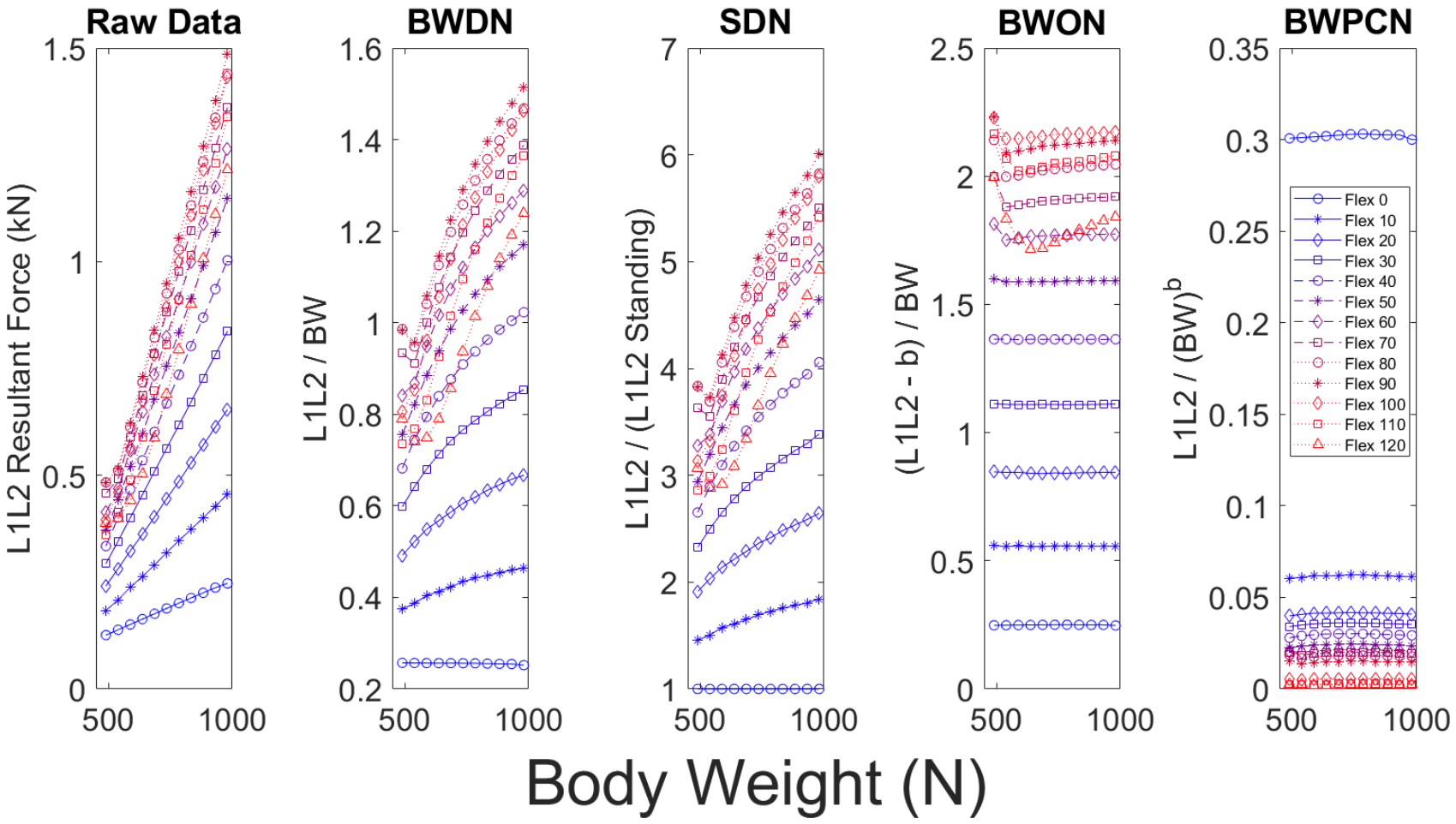


Fig. 5.1. Resultant $L_1L_2$ spinal forces from our model ("Raw Data") and normalized values using four normalization techniques, for 11 body weights (BW) during 13 static tasks. (BWDN: BW Division Normalization, SDN: Standing Division Normalization, BWON: BW Offset Normalization, BWPCN: BW Power Curve Normalization.)

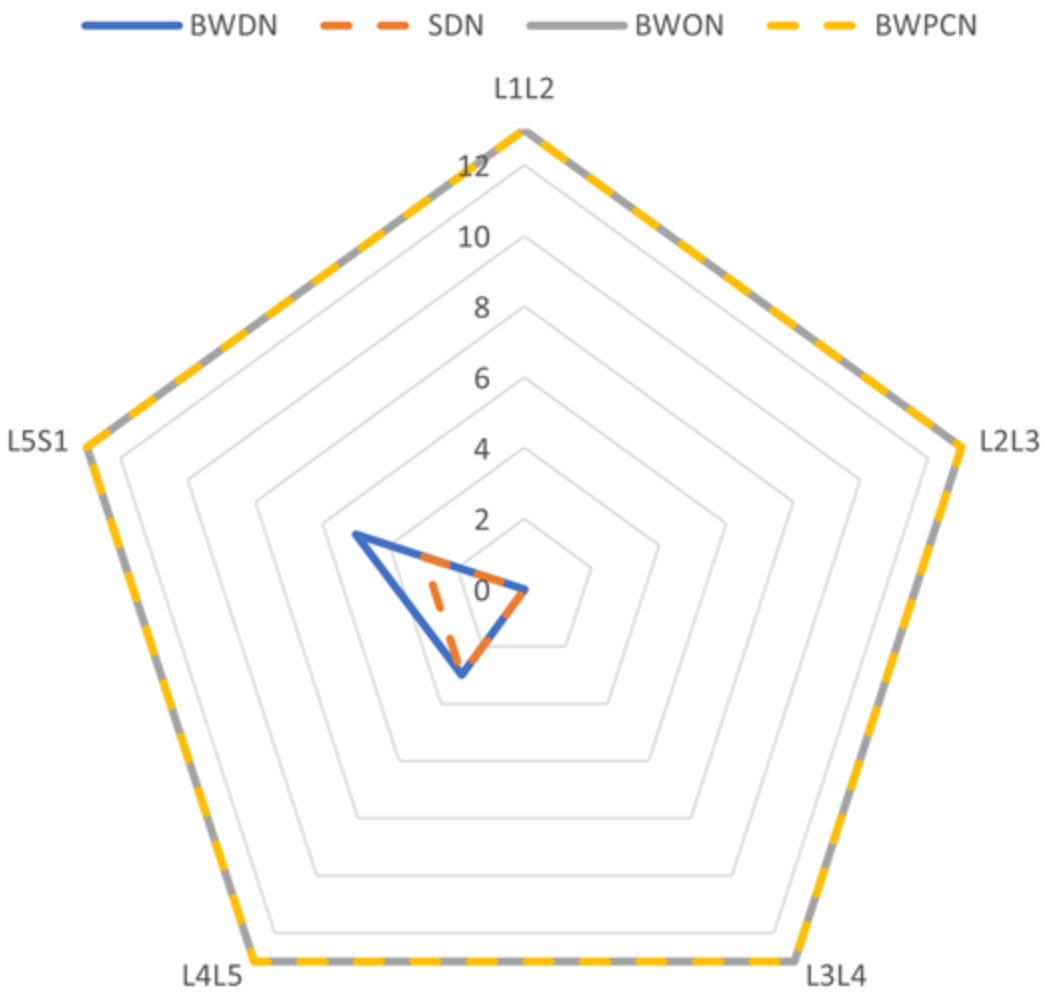


Fig. 5.2. Effectiveness of four techniques at normalizing lumbar spine forces ($L_1L_2$, $L_2L_3$, $L_3L_4$, $L_4L_5$, $L_5S_1$). BW Division Normalization (BWDN), Standing Division Normalization (SDN), BW Offset Normalization (BWON), and BW Power Curve Normalization (BWPCN) were used to normalize lumbar spine resultant forces during 13 flexion tasks. The radar chart shows the number of tasks for which each normalization technique successfully normalized each spinal force. The normalization technique was deemed successful if a significant correlation ($p < 0.05$) was not found between the normalized spine forces and BW.

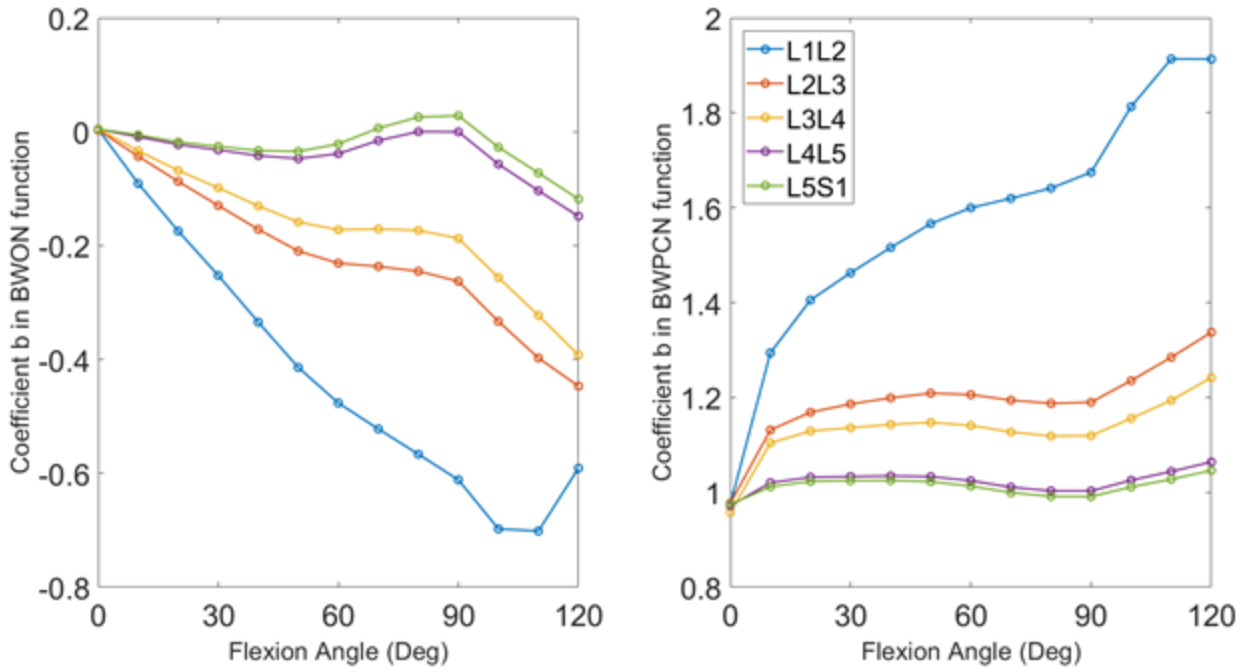


Fig. 5.3. Coefficient b in BWON and BWPCN functions at 5 spinal joints for 13 flexion tasks.

## 5.5 Discussion

Normalizing variables is crucial in biomechanics to reduce the variance between individuals (Derrick et al., 2020), thus revealing generalizable insights. Many studies in spine biomechanics are interested in spinal loads during tasks that involve trunk flexion (e.g., squat and stoop lifting tasks). Hence, we evaluated four techniques for normalizing spinal forces during static flexion tasks. Among personalized factors, BW is known to have the greatest effect on spinal forces (Akhavanfar et al., 2018).

The most important finding of the present study is that BWDN and SDN, which are commonly used in spine biomechanics to normalize spinal forces, do not adequately remove the effect of BW on spinal forces. This finding corroborates the results of previous studies that found limited effectiveness of BWDN for normalizing other kinetic variables such as GRF (Stickley et al., 2018; Wannop et al., 2012) due to the lack of a true linear relationship (with zero intercept)

between the kinetic variables and BW. Moreover, we found that BWDN resulted in negative correlations between the normalized spinal forces and BW in the standing posture (Appendix C–SI. 2). This over-correction has also been observed in previous studies for normalizing other biomechanical variables when BWDN was used (Hetzler et al., 2011; Stickley et al., 2013).

Although BWON and BWPCN of spinal forces were both effective at removing all residual errors across all flexion tasks (Fig. 5.2), the coefficient ($b$) in the BWON and BWPCN functions was found to be highly dependent on the flexion angle, especially in the upper intervertebral joints (Fig. 5.3). Consequently, calculating the proper coefficient may be difficult. Previous studies using BWON and BWPCN for normalizing other kinetic variables acknowledged the same limitation and reported task-specific (e.g., running at 4 m/s) coefficients for these normalization techniques (Stickley et al., 2018). However, in the present study we showed that BWON and BWPCN with any coefficient $b$ in the reported range are more successful than BWDN and SDN at eliminating the variability in results during tasks that involve trunk flexion. Therefore, researchers might calculate the average coefficient across all tasks and then use this value for any trunk flexion task (for instance, $b_{avg} = 1.1927$ for BWPCN at the $L_2L_3$ intervertebral joint). Dividing $L_2L_3$ forces by BW did not remove the correlation with BW for any tasks (Fig. 5.2), whereas dividing $L_2L_3$ forces by $BW^{1.1927}$ would remove the significant correlation with BW for the Flex 30°, 40°, and 60–90° tasks. Nevertheless, we recommend taking the following steps to calculate coefficient $b$ during a static task or at an instant during a dynamic task and then normalizing spinal forces using BWON or BWPCN. First, the total thorax flexion angle and the nearest range of static trunk flexion angle for which coefficient $b$ is known should be determined. For instance, if the flexion angle at an instant of a dynamic simulation was 68°, the nearest static trunk flexion range would be 60–

70°. Coefficient $b$ then can be calculated by assuming it varies linearly in the corresponding static trunk flexion range.

Resultant forces for all scaled models (50–100 kg) were significantly positively correlated ($r > 0.72, p < 0.05$) with the flexion angle at all lumbar spinal levels because the anterior moment arms of upper trunk gravity loads and their subsequent flexion moments increased as the flexion angle increased. The proper normalization technique must remove only the effect of the normalization parameter (i.e., BW in the present study). When BWON was used, the strong correlations of normalized forces with flexion angle remained at all lumbar spinal levels. However, BWPCN resulted in significant negative correlations ($r = -0.63$) between normalized forces and flexion angle at the $L_1L_2$ level, as well as non-significant ($p > 0.05$) positive correlations at the $L_2L_3$ level for all scaled models. Therefore, the results of the present study suggest that BWON is the most appropriate technique for normalizing spinal forces.

### 5.6 References


Actis, J.A., Honegger, J.D., Gates, D.H., Petrella, A.J., Nolasco, L.A., Silverman, A.K., 2018. Validation of lumbar spine loading from a musculoskeletal model including the lower limbs and lumbar spine. J. Biomech. 68, 107–114.

Akhavanfar, M., Brandon, S.C.E., Brown, S.H.M., Graham, R.B., 2019. Development of a novel MATLAB-based framework for implementing mechanical joint stability constraints within OpenSim musculoskeletal models. J. Biomech. 91, 61–68.

Akhavanfar, M., Kazemi, H., Eskandari, A.H., Arjmand, N., 2018. Obesity and spinal loads; a combined MR imaging and subject-specific modelling investigation. J. Biomech. 70, 102–112.

Akhavanfar, M., Uchida, T.K., Clouthier, A.L., Graham, R.B., 2022. Sharing the load: modelling loads in OpenSim to simulate two-handed lifting. Multibody Syst. Dyn. 54, 213–234.

Bassani, T., Stucovitz, E., Qian, Z., Briguglio, M., Galbusera, F., 2017. Validation of the AnyBody full body musculoskeletal model in computing lumbar spine loads at L4L5 level. J. Biomech. 58, 89–96.

Batterham, A.M., George, K.P., 1997. Allometric modelling does not determine a dimensionless power function ratio for maximal muscular function. J. Appl. Physiol. 83, 2158–2166.

Beaucage-Gauvreau, E., Robertson, W.S.P., Brandon, S.C.E., Fraser, R., Freeman, B.J.C., Graham, R.B., Thewlis, D., Jones, C.F., 2019. Validation of an OpenSim full-body model with detailed lumbar spine for estimating lower lumbar spine loads during symmetric and asymmetric lifting tasks. Comput. Methods Biomech. Biomed. Engin. 22, 451–464.

Bruno, A.G., Bouxsein, M.L., Anderson, D.E., 2015. Development and validation of a musculoskeletal model of the fully articulated thoracolumbar spine and rib cage. J. Biomech. Eng. 137, 081003.

Damm, P., Reitmaier, S., Hahn, S., Waldheim, V., Firouzabadi, A., Schmidt, H., 2020. In vivo hip and lumbar spine implant loads during activities in forward bent postures. J. Biomech. 102, 109517.

Delp, S.L., Anderson, F.C., Arnold, A.S., Loan, P., Habib, A., John, C.T., Guendelman, E., Thelen, D.G., 2007. OpenSim: Open-source software to create and analyze dynamic simulations of movement. IEEE Trans. Biomed. Eng. 54, 1940–1950.

Derrick, T.R., van den Bogert, A.J., Cereatti, A., Dumas, R., Fantozzi, S., Leardini, A., 2020. ISB recommendations on the reporting of intersegmental forces and moments during human motion analysis. J. Biomech. 99, 109533.

Dreischarf, M., Shirazi-Adl, A., Arjmand, N., Rohlmann, A., Schmidt, H., 2016. Estimation of loads on human lumbar spine: a review of in vivo and computational model studies. J. Biomech. 49, 833–845.

Favier, C.D., Finnegan, M.E., Quest, R.A., Honeyfield, L., McGregor, A.H., Phillips, A.T.M., 2021. An open-source musculoskeletal model of the lumbar spine and lower limbs: a validation for movements of the lumbar spine. Comput. Methods Biomech. Biomed. Engin. 24, 1310–1325.

Ghezelbash, F., Shirazi-Adl, A., Arjmand, N., El-Ouaaid, Z., Plamondon, A., Meakin, J.R., 2016. Effects of sex, age, body height and body weight on spinal loads: sensitivity analyses in a subject-specific trunk musculoskeletal model. J. Biomech. 49, 3492–3501.

Hetzler, R.K., Stickley, C.D., Kimura, I.F., 2011. Allometric scaling of Wingate anaerobic power test scores in women. Res. Q. Exerc. Sport 82, 70–78.

Malakoutian, M., Street, J., Wilke, H.-J., Stavness, I., Fels, S., Oxland, T., 2018. A musculoskeletal model of the lumbar spine using ArtiSynth–development and validation. Comput. Methods Biomech. Biomed. Eng. Imaging Vis. 6, 483–490.

Mavor, M.P., Gruevski, K.M., Ross, G.B., Akhavanfar, M., Clouthier, A.L., Bossi, L.L.M., Karakolis, T., Graham, R.B., 2022. A data-driven framework for assessing soldier performance, health, and survivability. Appl. Ergon. 104, 103809.

Norcross, M.F., Johnson, S.T., Pollard, C.D., Chang, E.W., Hoffman, M.A., 2017. Normalization influences knee abduction moment results: Could it influence ACL-injury research, too? J. Sci. Med. Sport 20, 318–321.

O'Malley, M.J., 1996. Normalization of temporal-distance parameters in pediatric gait. J. Biomech. 29, 619–625.

Pinzone, O., Schwartz, M.H., Baker, R., 2016. Comprehensive non-dimensional normalization of gait data. Gait Posture 44, 68–73.

Rohlmann, A., Pohl, D., Bender, A., Graichen, F., Dymke, J., Schmidt, H., Bergmann, G., 2014. Activities of everyday life with high spinal loads. PLoS One 9, e98510.

Schmid, S., Burkhart, K.A., Allaire, B.T., Grindle, D., Anderson, D.E., 2020. Musculoskeletal full-body models including a detailed thoracolumbar spine for children and adolescents aged 6–18 years. J. Biomech. 102, 109305.

Seth, A., Hicks, J.L., Uchida, T.K., Habib, A., Dembia, C.L., Dunne, J.J., Ong, C.F., DeMers, M.S., Rajagopal, A., Millard, M., 2018. OpenSim: Simulating musculoskeletal dynamics and neuromuscular control to study human and animal movement. PLoS Comput. Biol. 14, e1006223.

Stickley, C.D., Andrews, S.N., Parke, E.A., Hetzler, R.K., 2018. The effectiveness of scaling procedures for comparing ground reaction forces. J. Biomech. 77, 55–61.

Stickley, C.D., Hetzler, R.K., Wages, J.J., Freemyer, B.G., Kimura, I.F., 2013. Allometric scaling of Wingate anaerobic power test scores in men. J. Strength Cond. Res. 27, 2603–2611.

Tafazzol, A., Arjmand, N., Shirazi-Adl, A., Parnianpour, M., 2014. Lumbopelvic rhythm during forward and backward sagittal trunk rotations: combined in vivo measurement with inertial tracking device and biomechanical modelling. Clin. Biomech. 29, 7–13.

Wang, W., Wang, D., De Groote, F., Scheys, L., Jonkers, I., 2020. Implementation of physiological functional spinal units in a rigid-body model of the thoracolumbar spine. J. Biomech. 98, 109437.

Wannop, J.W., Worobets, J.T., Stefanyshyn, D.J., 2012. Normalization of ground reaction forces, joint moments, and free moments in human locomotion. J. Appl. Biomech. 28, 665–676.

Wong, K.W.N., Luk, K.D.K., Leong, J.C.Y., Wong, S.F., Wong, K.K.Y., 2006. Continuous dynamic spinal motion analysis. Spine. 31, 414–419.

# Chapter 6: An Enhanced Spine Model Validated for Simulating Dynamic Lifting Tasks in OpenSim

Published in Annals of Biomedical Engineering 2024; 52(2): 259–269.
https://doi.org/10.1007/s10439-023-03368-x

## 6.1 Abstract

A fully articulated thoracolumbar spine model had been previously developed in OpenSim and had been extensively validated against experimental data during various static tasks. In the present study, we enhanced this detailed musculoskeletal model by adding the role of passive structures and adding kinematic constraints to make it suitable for dynamic tasks. We validated the spinal forces estimated by this enhanced model during nine dynamic lifting/lowering tasks. Moreover, we recently developed and evaluated five approaches in OpenSim to model the external loads applied to the hands during lifting/lowering tasks, and in the present study, we assessed which approach results in more accurate spinal forces. Regardless of the external load modelling approach, the maximum forces predicted by our enhanced spine model across all tasks, as well as the pattern of estimated spinal forces within each task, showed strong correlations (r-values and cross-correlation coefficients > 0.9) with experimental data. Given the biofidelity of our enhanced model, its accessibility via the open-source OpenSim software, and the extent to which this model has been validated, we recommend it for applications requiring estimation of spinal forces during lifting/lowering tasks using multibody-based models and inverse dynamic analyses.

## 6.2 Introduction

Knowledge of internal joint forces is essential for implant design, surgical and rehabilitation planning, development of injury prevention programs, and many other applications (Akhavanfar et al., 2019; Dreischarf et al., 2016b; Malakoutian et al., 2018). Various computational tools have been used for musculoskeletal (MSK) modelling and assessment of

internal joint forces, including multibody dynamics (Halloran et al., 2010), finite element methods (Schmidt et al., 2013), and flexi-multibody methods (Nazer et al., 2008). Although the selection of an appropriate MSK model ultimately depends on the research question, the existence of numerous MSK models all developed for the same application can lead to a lack of consensus and confusion among users, potentially diminishing the impact of MSK modelling. To improve the impact of MSK models in various applications (e.g., clinical, ergonomics, and sports biomechanics), appropriate validation studies must be performed to assess the accuracy and reliability of these models, and ultimately to advise both modellers and non-modellers on which MSK model is best for a given application.

In spine biomechanics, multibody dynamics–based models along with inverse dynamic analyses are commonly used to estimate muscle forces and intervertebral joint loads during various tasks (Akhavanfar et al., 2019). These models have descriptive rather than predictive applications (Erdemir et al., 2007), meaning that kinematic measurements are used as the inputs to the simulation pipeline to estimate internal forces. These models can provide insight into experimental observations, such as the maximum spinal force during a certain task and whether this force is likely to cause an injury. In spine biomechanics, lifting/lowering tasks are of interest in many MSK modelling studies because of the well-known association between these tasks and the high risk of spine injury (Dreischarf et al., 2016a). Therefore, we will first briefly review the multibody dynamics–based MSK models that have been developed, validated, and applied to understand lifting/lowering tasks.

OpenSim (Delp et al., 2007; Seth et al., 2018) and AnyBody (De Zee et al., 2007) are, respectively, open-source and commercial multibody dynamics–based software packages that are widely used for MSK modelling (Ghezelbash et al., 2020; Seth et al., 2018). These software

packages incorporate muscle physiology into the governing dynamic equations and use formulations that satisfy moment equilibrium at all joints (Malakoutian et al., 2018). In recent years, several detailed MSK models of the spine have been developed and validated for lifting tasks in these software packages. Bassani et al. (2017) validated the $L_4L_5$ spinal forces estimated by the full-body MSK model in AnyBody (AMMR, v.1.6.3) for one participant. This validation was performed for 12 activities from the intradiscal pressure (IDP) dataset of one subject (Wilke et al., 2001); four of these activities were static lifting tasks. In OpenSim, the lifting full-body (LFB) model (Beaucage-Gauvreau et al., 2019) and the fully articulated thoracolumbar spine (FATLS) model (Bruno et al., 2015) are two biofidelic and open-access spine models, which have been widely used for various applications (Banks et al., 2022; Lerchl et al., 2023), including lifting/lowering (Beaucage-Gauvreau et al., 2020; von Arx et al., 2021).

The LFB and FATLS models differ in their construction. In the LFB model (Beaucage-Gauvreau et al., 2019), the spine comprises six segments (five lumbar and one rigid thorax) with 15 dependent and three independent degrees of freedom and 238 Hill-type muscles, whereas the FATLS model (Bruno et al., 2015) includes all thoracic and lumbar segments and 552 Hill-type muscle fascicles. Passive stiffness was not considered in either model, yet passive intervertebral structures play a critical role in spinal loading (Han et al., 2012). The LFB model (Beaucage-Gauvreau et al., 2019) possesses lower limbs and was validated using participant-specific kinematic data (reflective markers) collected in the laboratory, contrary to the original FATLS model (Bruno et al., 2015). Nevertheless, the research group that developed the original FATLS model has recently enhanced this model to a full-body model (Burkhart et al., 2020) and added kinematic constraints to run this model using marker data for several applications (Banks et al., 2023).

The FATLS and LFB models have undergone different amounts of validation. Estimates from the FATLS model have been extensively validated at all spinal levels (T1–L5), for which IDP and vertebral implant loads are available. The FATLS model has been validated for a total of 27 static activities, 17 of which were lifting tasks, and it was reported to be at least as accurate as other models (Bruno et al., 2015). To the best of the authors' knowledge, no other existing spine MSK model has been validated to this extent for static activities. Although muscle activations predicted by the FATLS model were recently validated against electromyography measurements for elderly participants during five dynamic tasks (Alemi et al., 2023), the intervertebral forces estimated by this model have not been validated for dynamic lifting tasks. The LFB model has been validated for fewer static tasks than the FATLS model; however, the intervertebral forces estimated by the LFB model have been validated against implant data for two dynamic lifting tasks (stoop and squat lifting of a 10 kg mass). As stated above, the FATLS and LFB models were both developed and validated in OpenSim, a widely used open-source software platform in biomechanics (Seth et al., 2018), and these models have contributed significantly to advancements in spine biomechanics. We selected the FATLS model to build upon in the present study for two specific reasons. First, the FATLS model is more anatomically detailed than the LFB model and allows researchers to predict both lumbar and thoracic vertebral loading. Second, decomposing spinal forces into compression and shear forces are of interest in many studies, and it is reasonable to assume that the reaction forces estimated by the FATLS model are representative of the intervertebral compression and shear forces, while due to the definition of joint orientations in the LFB model, extra care is required to obtain these forces from the LFB model estimations (see Appendix D–SI. 1).

Modelling decisions can dramatically affect the results of simulations. We recently conducted a study in which we introduced and compared five approaches for modelling external hand forces and moments (EHF&M) during dynamic stoop and squat lifting tasks (Akhavanfar et al., 2022). We described these EHF&M approaches in detail in our previous work (Akhavanfar et al., 2022) and briefly outline them in this paper (see Section 6.3.3, below). The findings of our previous study revealed substantial differences in the spinal loads predicted by the LFB model based on the chosen EHF&M approach, particularly at higher movement speeds. Furthermore, we assessed the accuracy of each EHF&M modelling approach by examining the resulting dynamic inconsistencies (i.e., residual forces) in the LFB model. Among these approaches, EHF&M Approach 4, in which the lifted mass was explicitly modelled and attached to the hands, exhibited lower residual forces overall. However, lower residuals do not necessarily imply more accurate spinal load predictions. Therefore, determining which EHF&M modelling approach yields the most accurate spinal loads remains an important question that warrants further investigation. Comparing the accuracy of the estimated spinal forces when using different EHF&M modelling approaches can provide insight into the reliability of the predicted joint loads.

In the present study, we enhanced the original FATLS model, including consideration of the passive stiffness of intervertebral structures, and we aim to validate this new model for more dynamic lifting/lowering tasks than those used to validate previous spine MSK models. We aim to investigate which EHF&M modelling approach produces the most accurate spinal load estimates using our new OpenSim FATLS model. Given the accuracy of prior validation of the original FATLS model during static tasks and considering the enhancements made in the present study, we hypothesize that the maximum and the time-varying characteristics of the spinal forces predicted by our new model will strongly correlate with the measured spinal forces. Moreover, we

hypothesize that spinal forces predicted by EHF&M Approach 4, which has been shown to yield lower residuals during two-handed dynamic stoop and squat lifting/lowering tasks (Akhavanfar et al., 2022), will be more accurate than those predicted by other EHF&M modelling approaches during the dynamic lifting/lowering tasks assessed in this study.

## 6.3 Materials and Methods

### *6.3.1 Validation Dataset*

In the present validation study, we used a freely available vertebral implant dataset (Rohlmann et al., 2014) and extracted intervertebral load data during nine symmetric dynamic lifting/lowering tasks obtained from three male patients (66.7 ± 7.0 kg, 169 ± 1 cm, 65 ± 5 years old at the time of surgery) who underwent vertebral body replacement at the L1 level. We refer to the individuals who had received vertebral body replacement as "patients" (similar to previous studies (Rohlmann et al., 2014)), although all implant data that we used were collected at least four months after the surgery. The nine dynamic tasks that were selected consisted of five stoop and squat lifting/lowering movements, as well as four lifting/lowering movements in the standing posture, where the patients elevated a dumbbell from the shoulder-neutral position to the shoulder-flexed position in front of them at eye level. We selected these particular dynamic tasks from the implant dataset for two reasons. First, we required that the spinal forces must have been measured for more than one patient to allow us to average the data across multiple patients, which we believe will increase the reliability of generalizing the comparison of spinal forces between activities from the experimental data. Second, we aimed to include in our validation study several high-demanding dynamic lifting tasks that were performed by the patients in the implant dataset, and the largest mass that was lifted by the patients was 10 kg.

### *6.3.2 Experiments*

Three healthy male volunteers (mass 91.3 ± 9.4 kg, height 179 ± 5 cm, age 25 ± 4 years) provided informed written consent and participated in the experiment, which was approved by the University of Ottawa Research Ethics Board (H-06-21-7034). Our aim was to investigate the accuracy of our model for a healthy population, beyond the mass and height ranges of the patients from the implant dataset. Therefore, we did not constrain our participant recruitment to resemble the mass, height, or age of the patients.

To evaluate the performance of our model, our participants replicated the nine symmetric dynamic lifting/lowering tasks (Fig. 6.1) that were performed by the patients. For the stoop and squat tasks, the participants lifted a box whose mass was set according to the trial. In the standing-posture lifting tasks (Tasks 6–9), the participants lifted dumbbells with the same mass as those used by the patients. We refer to the lifting technique used in Tasks 6–9 as "Elev1Hand" and "Elev2Hands" when performed with one hand or two hands, respectively. Tasks 2 and 8 were performed as quickly as possible; all other tasks were performed at a self-selected speed. Henceforth, the technique–load–speed format is used to identify each task; if the speed is not mentioned, the movement was performed at a self-selected speed. For instance, "Elev2Hands–5" refers to the task in which the 5 kg dumbbell was lifted at a self-selected speed with two hands while in a standing posture, and "Squat–7–Fast" refers to the task in which the 7 kg box was lifted as quickly as possible using a squatting technique.

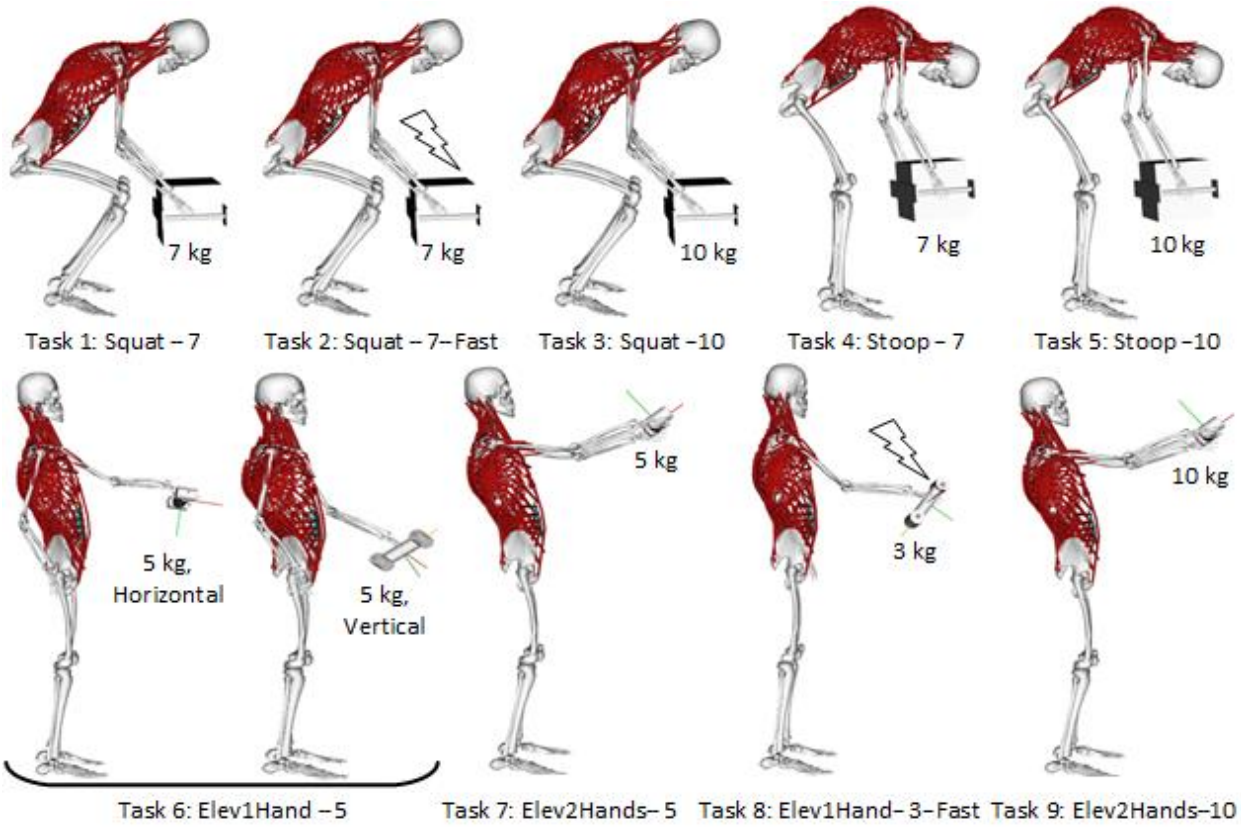


Fig. 6.1. The nine symmetric dynamic lifting/lowering tasks performed by three male participants in the present study, replicating the tasks that were performed by three male patients who had previously received vertebral body replacement at the L1 level. The lightning bolt symbols indicate tasks that were performed as quickly as possible.

To measure the kinematics of the body and the lifted mass, the participants were outfitted with a full-body marker set (Beaucage-Gauvreau et al., 2019) and eight and four markers were placed on the box and dumbbells, respectively (a photograph of the box and dumbbells used in the present study is provided in Appendix D–SI. 2). Marker data during the dynamic lifting tasks were collected at 120 Hz using an 11-camera motion capture system (Vantage V5, Vicon, Oxford, UK). The marker data were cleaned and gap-filled in the Vicon software (Nexus 2.12.1, Vicon, Oxford, UK).

### *6.3.3 Modelling*

The spine in the original FATLS model (Bruno et al., 2015) has 54 independent rotational degrees of freedom, which is considerably greater than the extent to which the intervertebral motions can be reliably calculated using only the trajectories of skin-mounted markers affixed on bony landmarks (Alemi et al., 2021). We added 51 coupler constraints to the spine in the FATLS model based on the results of prior experimental studies (Fujii et al., 2007; Fujimori et al., 2012; Fujimori et al., 2014; Rozumalski et al., 2008; Wong et al., 2006) to reduce the spinal motion to three independent $L_5S_1$ degrees of freedom for scaling and kinematic analysis. The motions of the abdomen were also coupled to the $L_5S_1$ motions using linear and piecewise-linear functions (see Appendix D–SI. 3). Later in the simulation workflow, all constraints were removed for dynamic analysis to exclude the additional moments generated by these constraints as these moments do not exist in reality. We also replaced the Custom Joints defined for the ribs and sternum in the original FATLS model with Weld Joints to remove the three rotational degrees of freedom of these segments. Moreover, to better scale the model's mass properties for each participant using the Scale Tool in OpenSim and to better capture the joint kinematics, the lower limbs of the Gait2354 model available in OpenSim were added to the original FATLS model (Bruno et al., 2015) to make it a full-body model; however, the lower limb muscles were removed, as was done in the LFB model (Beaucage-Gauvreau et al., 2019).

Wang et al. (2020) recently derived exponential functions from *in vitro* moment–displacement experimental data to describe passive moments at all spinal levels. These functions were validated for the FATLS model using forward dynamic simulations, showing good agreement with the literature in terms of spine segmental motions. However, these exponential functions were developed based on in vitro ranges of motion; extrapolating these functions to the greater *in vivo*

ranges of motion in the present study could result in unrealistically high moments in the model. For instance, 2.5° flexion of $L_5S_1$, which results in 5.75° flexion of $T_{12}L_1$ due to our kinematic constraints, would generate a 668 N m passive extension moment at the $T_{12}L_1$ level according to the exponential functions of Wang and colleagues, whereas the maximum flexion–extension bending moment tested for these functions was 10 N m. Therefore, to ensure the passive moments generated in the present model remain below the maximum values reported in the literature (Miller et al., 1986), we linearized the exponential functions derived by Wang and colleagues (2020). For each direction and intervertebral level, we identified the intervertebral angle $\theta$ at which the exponential functions generate a passive moment of 10 N m. Subsequently, we derived linear or piecewise-linear functions to relate passive moments to intervertebral angles below $\theta$ and we assumed the same linear function for intervertebral angles above $\theta$. In OpenSim, we enhanced the FATLS model by adding bushing elements that use these linear functions to represent the dynamic effect of the passive structures. The bushing elements apply passive moments for *in vivo* ranges of motion during our dynamic tasks.

The general simulation workflow in this study was the common inverse dynamics–based MSK modelling procedure used in OpenSim: model calibration using the Scale Tool, Inverse Kinematics, Static Optimization to estimate muscle forces, and Joint Reaction Analysis (Beaucage-Gauvreau et al., 2019). Five EHF&M modelling approaches were tested within this simulation workflow to determine their effect on estimates of intervertebral forces during each trial (Akhavanfar et al., 2022). We recently reported how each of these EHF&M modelling strategies can be implemented and how the differences between these approaches may affect the results of kinematic and dynamic analyses (Akhavanfar et al., 2022).

In brief, in EHF&M Approaches 1 and 2, the load kinematics were not considered. In Approach 1, the external load was modelled during each trial as constant gravity-oriented loads applied to each hand using an "external loads" setup file in OpenSim. In Approach 2, the mass of one hand was increased by the lifted mass or the mass of each hand was increased by half of the lifted mass, depending on the nature of the task (one-handed vs. two-handed lifting tasks). Approaches 1 and 2 are simple to implement within the above-mentioned simulation workflow, thus they have often been used in previous spine MSK modelling studies (Akhavanfar et al., 2022).

EHF&M Approaches 3 and 4 were identical for one-handed lifting tasks, where the lifted mass was modelled as a body that was "welded" (rigidly attached) to the lifting hand. However, these approaches differed for two-handed lifting tasks. In both approaches, the lifted mass was modelled as two half-bodies, with one welded to each hand. During two-handed lifting tasks, a closed kinematic chain was formed for the kinematic analysis when Approaches 3 and 4 were used because a Weld Constraint was added to enforce the relationship between the two halves of the lifted mass (to maintain the rigidity of the box during the tasks). However, the Weld Constraint between the two halves was removed in Approach 4 when running Static Optimization and the Joint Reaction Analysis, which removed the nonlinear algebraic constraint equations from the system thereby allowing the dynamic simulations to run much faster.

To use EHF&M Approach 5, the kinematics of the lifted mass were calculated separately from the body kinematics. Afterward, based on the kinematics of the lifted mass, the external forces applied to the hands and the locations at which these forces should be applied were estimated as functions of time for each trial. Similar to Approach 1, these forces were applied to each hand using an "external loads" setup file. However, when we conducted a forward dynamic simulation for the lifted mass, our results demonstrated that the external hand forces calculated in Approach

5, when applied to the lifted mass, accurately reproduced the trajectories of the markers on it. In contrast, the constant load used in Approach 1 cannot move the lifted mass in a forward dynamic simulation and, therefore, cannot replicate its marker trajectories during dynamic movements. Additional details can be found in Akhavanfar et al. (2022)

It should be noted that properly configuring the system for each trial using Approaches 3–5 (e.g., finding the orientations of the lifted mass with respect to the hands in Approaches 3 and 4) is a complex and time-consuming procedure (Akhavanfar et al., 2022) that limits the use of these approaches for practical and high-throughput applications. In the present study, we developed MATLAB® scripts that automatically generate the models required for the kinematic and dynamic analysis of Approaches 3–5 from the model and motion files required for Approaches 1 and 2, as Approaches 1 and 2 are the easiest to set up. These MATLAB® scripts and our new model are freely available at https://simtk.org/projects/handloadinterac to help others use these EHF&M modelling approaches in their studies.

In total, 39 motion trials were collected for each participant: 21 two-handed trials (7 tasks × 3 reps), 12 Elev1Hand–5 trials (1 task × 2 hands × 2 load orientations × 3 reps), and 6 Elev1Hand–3–Fast trials (1 task × 2 hands × 3 reps). Subsequently, 315 dynamic simulations for two-handed lifting tasks (3 participants × 21 trials × 5 EHF&M Approaches) and 216 dynamic simulations for one-handed lifting tasks (3 participants × 18 trials × 4 EHF&M Approaches) were generated and analyzed in the present study.

### *6.3.4 Data Analysis*

#### *6.3.4.1 Motion Cycles*

For the lifting/lowering motion cycles, the instants at which the load started and stopped moving substantially were defined as 0% and 100% of the motion cycle, respectively. The load motion during the implant data trials was evaluated subjectively from the videos of the movements (50 videos in total) performed by the patients (https://orthoload.com/). For the simulated results, the instants of 0% and 100% of the lifting/lowering motion cycles were determined using the hand accelerations: the load was deemed to be starting and stopping when the hand accelerations crossed a threshold of 0.6 m $s^{-2}$. For each simulation trial, we verified that the selected threshold (0.6 m $s^{-2}$) was appropriate by plotting and evaluating the marker data of the hands and the load between the instants that were identified as 0% and 100% of the lifting/lowering motion cycles.

We obtained the estimated forces in the child body reference frame in OpenSim. However, the choice of frame does not impact our validation results because the implant and estimated $L_1L_2$ resultant forces (i.e., the Euclidean norm of measured and reaction forces) were calculated at each instant. The data were then normalized to 601 data points (0–100%) for each lifting and lowering motion cycle.

#### *6.3.4.2 Model Validation*

The implant and estimated $L_1L_2$ resultant forces were both normalized using body weight offset normalization (Akhavanfar et al., 2023) (details provided in Appendix D–SI. 4) to adequately remove the effect of body weight on spinal forces. Afterward, the average of normalized peak forces for each task during the lifting and lowering motion cycles was calculated by, first, averaging normalized peak forces for each individual across all trials within a task, and then averaging across the patients/participants. Subsequently, the correlation between the average

values estimated using each EHF&M modelling approach and average measured values was calculated across all tasks using MATLAB®.

We also calculated the average curves for each task (one curve for lifting and one curve for lowering) using dynamic time warping (Bender et al., 2012) and the same averaging sequence as that described above for peak forces (i.e., first averaging across the trials for each individual and then averaging across the patients/participants). For each motion cycle, the estimated average curve using each EHF&M approach was then compared against the average implant curve using a cross-correlation analysis (the "xcorr" function in MATLAB®) to assess the accuracy of increment/decrement patterns of estimated spinal forces over time.

### 6.4 Results

Strong significant correlations ($r > 0.90$, $p < 0.05$) were found between the measured and estimated maximum forces across all tasks during lifting (Fig. 6.2) and lowering (Fig. 6.3). Figures 6.4 and 6.5 show the estimated and measured average curves during all tasks (the raw normalized forces for all trials of each task are provided in Appendix D–SI. 5). During all tasks, the cross-correlation coefficient for all EHF&M approaches was greater than 0.90 (Figs. 4 and 5).

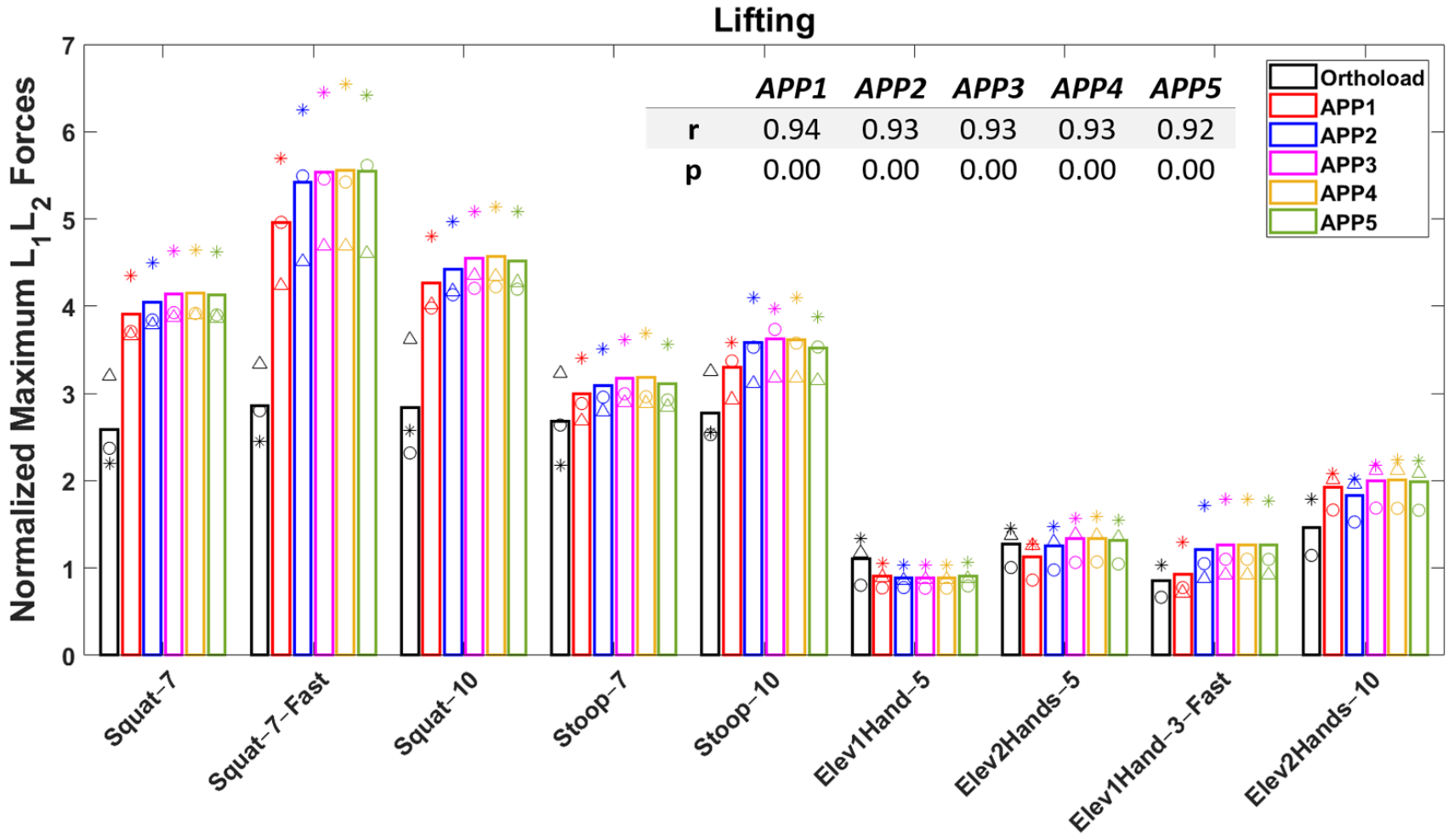


Fig. 6.2. Average of estimated and measured normalized maximum $L_1L_2$ forces during the lifting cycle of all tasks, as well as the correlation coefficients and p-values between the average values estimated using each external hand forces and moments (EHF&M) modelling approach ("APP") and average measured values across all tasks. The circles, asterisks, and triangles indicate, respectively, the average values for participants/patients 1, 2, and 3. Patients 1–3 who had L1 vertebral replacement surgery were named WP1, WP2, and WP4 in previous studies (Rohlmann et al., 2014). For the Elev1Hand–3–Fast and Elev2Hands–10 tasks, we did not find any available data for WP4.

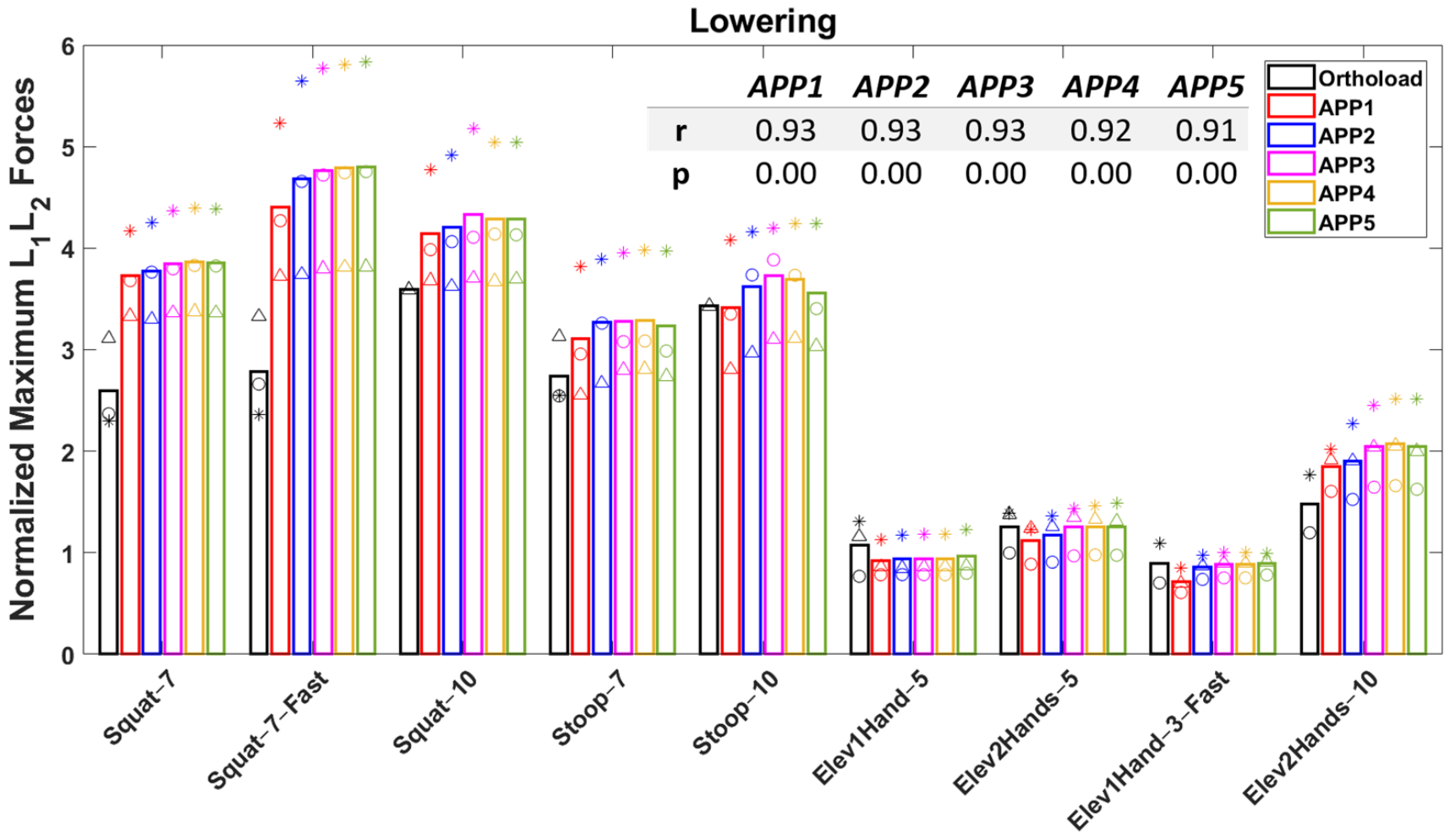


Fig. 6.3. Average of estimated and measured normalized maximum $L_1L_2$ forces during the lowering cycle of all tasks, as well as the correlation coefficients and p-values between the average values estimated using each external hand forces and moments (EHF&M) modelling approach ("APP") and average measured values across all tasks. The circles, asterisks, and triangles indicate, respectively, the average values for participants/patients 1, 2, and 3. Patients 1–3 who had L1 vertebral replacement surgery were named WP1, WP2, and WP4 in previous studies (Rohlmann et al., 2014). For the Squat–10 and Stoop–10 tasks, we did not find any available data for WP1 or WP2. For the Elev1Hand–3–Fast and Elev2Hands–10 tasks, we did not find any available data for WP4.

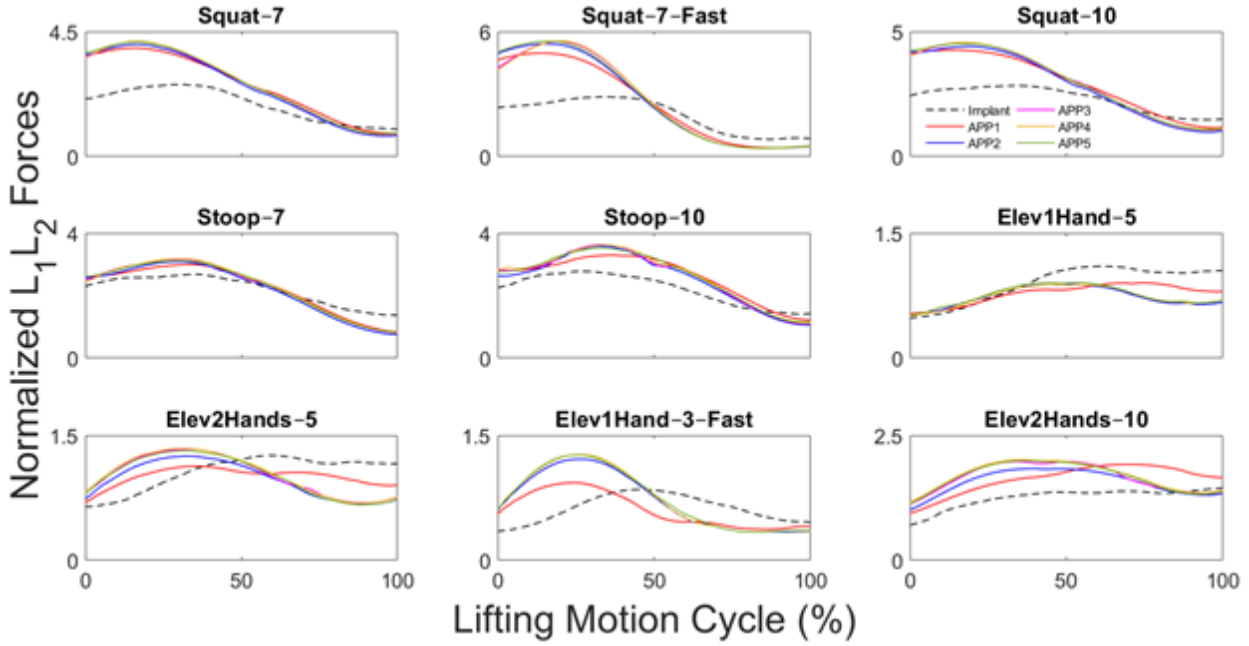


Fig. 6.4. Measured (black dashed lines) and estimated (solid lines) average curves during the lifting motion cycle of all tasks. The normalized measured and estimated forces using each external hand forces and moments (EHF&M) approach were first averaged across all trials for each individual and then across all patients/participants.

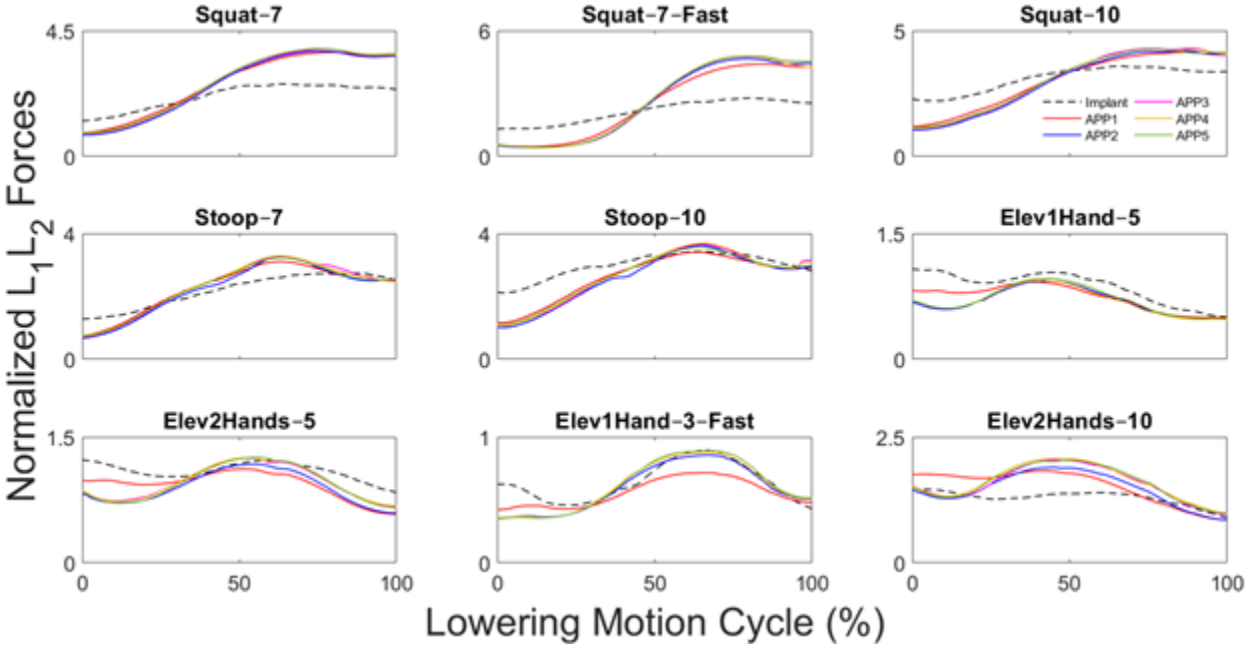


Fig. 6.5. Measured (black dashed lines) and estimated (solid lines) average curves during the lowering motion cycle of all tasks. The normalized measured and estimated forces using each external hand forces and moments (EHF&M) approach were first averaged across all trials for each individual and then across all patients/participants.

For the stoop and squat lifting/lowering tasks (Tasks 1–5), linear trend lines (y = ax) effectively (with $R^2$ > 0.96 for Tasks 1–4 and $R^2$ > 0.86 for Task 5) related the estimated $L_1L_2$ spinal forces to each other (see Appendix D–SI. 6 for an example of the fitted trend lines). However, for Tasks 6–9, the linear trends between the predicted $L_1L_2$ forces were found only for EHF&M Approaches 2–5 (with $R^2$ > 0.96). Figure 6.6 shows coefficient a in the linear trend lines, where x was the estimated $L_1L_2$ spinal forces using EHF&M Approach 2 (arbitrarily selected) and y was the estimated $L_1L_2$ spinal forces using the other approaches. Among Tasks 1–5, the maximum relative difference in the predicted $L_1L_2$ forces was found for the Squat–7–Fast task between Approaches 1 and 5 (Fig. 6.6).

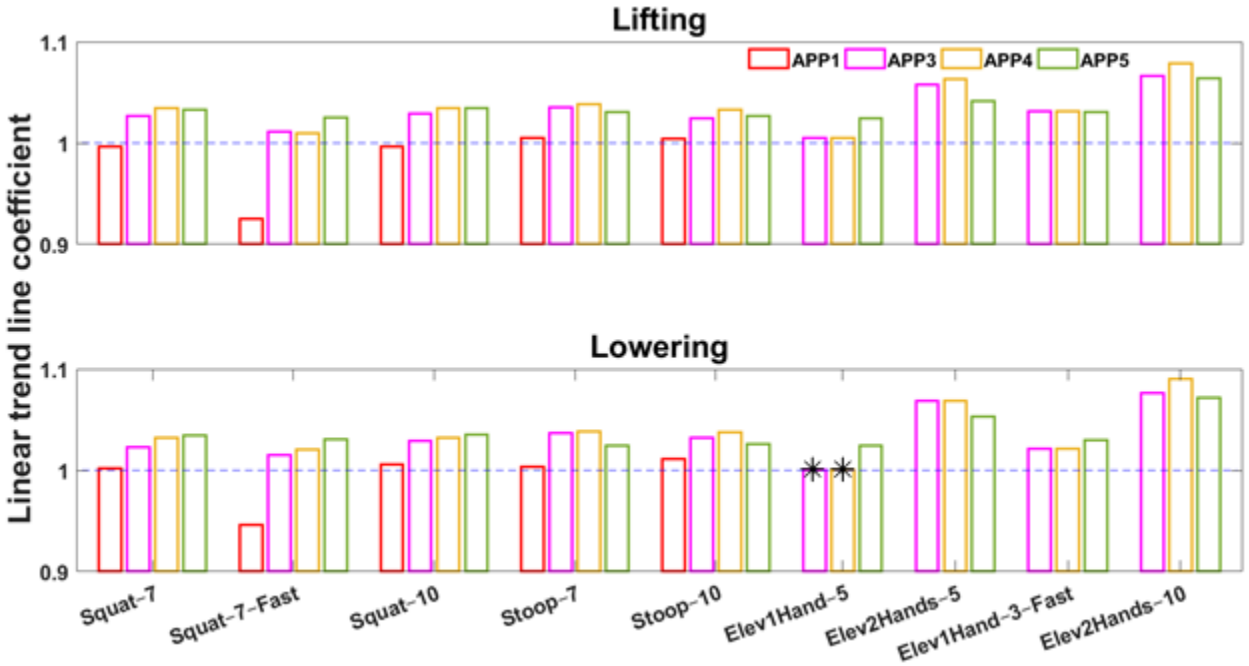


Fig. 6.6. Coefficient *a* in the linear trend lines (*y*=*ax*) that were fit between the estimated $L_1L_2$ spinal forces using external hand forces and moments (EHF&M) Approach 2 (*x*) and the estimated $L_1L_2$ spinal forces using other approaches (*y*). For Tasks 6–9, the linear trend lines did not effectively relate the obtained results using EHF&M Approach 1 to those obtained using other EHF&M approaches, thus EHF&M Approach 1 was not included in the figure for these tasks. Asterisks in the Elev1Hand–5 task indicate that the slope of the linear trend (*a*) was not significantly different from 1.00 (the blue dashed line) with a 95% level of confidence.

## 6.5 Discussion

In the present study, we developed a new spine model in OpenSim by enhancing the existing FATLS model (Bruno et al., 2015). The main objective of our study was to validate the intervertebral spinal forces estimated by our model during a variety of dynamic lifting/lowering tasks using various EHF&M modelling approaches (Akhavanfar et al., 2022). Due to the paucity of experimental data, validation of model-estimated intervertebral spinal forces is challenging. The nature of our validation can be considered both direct and indirect: direct (Lund et al., 2012) because we compared our model's output of interest (i.e., intervertebral forces) with experimental measurements of the same quantity; indirect (Jones and Wilcox, 2008) because we used experimental data from another study (i.e., implant data) to validate our model.

We did not use available IDP datasets in the present study to validate our model, for several reasons. First, the few existing IDP experimental studies (Andersson et al., 1977; Polga et al., 2004; Schultz et al., 1982; Wilke et al., 2001) either measured IDP during static lifting tasks or reported only the maximum pressure during dynamic lifting tasks. In addition to investigating the maximum forces, the present study aims to validate the time series of spinal forces against experimental data to assess the extent to which the biomechanics community can rely on this new model for practical lifting applications. Furthermore, to validate model-estimated intervertebral forces against measured IDP data, various assumptions (Bassani et al., 2017; Beaucage-Gauvreau et al., 2019) can be employed to convert the estimated forces to IDP, which may introduce bias into the analysis thus diminishing the impact of the model. Finally, the original FATLS model had previously been validated against various IDP datasets to a considerably greater extent than other existing models, so we did not consider it to be critical to validate against additional IDP data in the present study.

The normalized estimated peak forces were greater than the corresponding measurements for the stoop and squat tasks (Figs. 6.2 and 6.3), likely for several reasons. First, the real *in vivo* loads at the L1 level were greater than those measured by the implant because part of the actual *in vivo* loads was transferred via the internal spinal fixation device used to stabilize the patients' spines (Damm et al., 2020). Moreover, when performing the same stoop and squat lifting tasks, the healthy participants generally experienced greater external flexion/extension moments than the patients because the healthy participants performed these tasks with greater flexion angles and speeds. More specifically, healthy participants consistently exhibited a greater trunk flexion range of motion, averaging 124° for stoops and 83° for squats, in contrast to patients' values of 85° for stoops and 62° for squats. Across all stoop and squat tasks, our healthy volunteers exhibited average lifting cycle times of 1.19 s compared to 1.25 s for patients and average lowering cycle times of 1.38 s compared to 1.58 s for patients, indicating that the healthy individuals tended to perform stoop and squat tasks more swiftly than the patients. Previous modelling studies have also reported greater normalized estimated forces than the vertebral implant data. For instance, Damm and colleagues (2020) employed a full-body AnyBody model and reported estimated normalized forces (normalized by body weight) that were 1.2 times greater than the normalized implant forces during the Stoop–10 task. Similarly, the peak normalized forces (normalized by standing force) predicted by the LFB model (Beaucage-Gauvreau et al, 2019) in OpenSim were 2.7 and 3 times greater than those measured by the implants during the Stoop–10 and Squat–10 tasks, respectively (Beaucage-Gauvreau et al., 2019).

Thorough calibration and validation of MSK models against implant data require detailed information from patients, such as surface marker trajectories, ground reaction forces, and medical imaging data. Given the limited data available to precisely calibrate MSK models for patients with

vertebral implants, a good match between the magnitude of estimated and measured forces could be obtained for the wrong reasons and may lead to incorrect conclusions. Consequently, when comparing the forces estimated for healthy individuals against the implant data, metrics quantifying the increase or decrease of estimated spinal forces (e.g., correlation and cross-correlation coefficients) are more appropriate than metrics such as root mean square errors, which would compare the absolute errors between model predictions and implant data.

The strong correlations and cross-correlations (r-values $> 0.90$) in the present study demonstrated that, regardless of the approach used to model the interaction between the external load and the hands during the lifting/lowering tasks, our new FATLS model accurately captured the change in maximum forces across various lifting/lowering tasks, as well as the time-varying spinal forces during the lifting/lowering motion cycles within each task. Damm and colleagues (2020) recently analyzed the implant data as a percentage of body weight, and based on median curves, presented the following important spinal load patterns for the Squat–10 and Stoop–10 tasks: (i) the measured peak forces during the Squat–10 task were slightly greater than those measured in the Stoop–10 task; (ii) the peak forces for these lifting tasks did not occur when the upper body was maximally flexed as might typically be expected; and (iii) for the Stoop–10 task, the peak normalized forces during lifting were less than those during lowering, whereas for Squat–10 this trend was the opposite. Our average, normalized curves (both model estimates and analyzed implant data) revealed the same conclusions with respect to the spinal load patterns for the Squat–10 and Stoop–10 tasks as those reported by Damm and colleagues (2020), suggesting that the derived load patterns for the Squat–10 and Stoop–10 tasks are robust to the analytical methods employed (e.g., the normalization technique) and providing evidence that the FATLS model is reliable for analyzing these tasks.

Our model effectively captured the effect of increasing external load on spinal forces, as evidenced by both estimated and measured forces during Squat–7, Stoop–7, and Elev2Hands–5 being less than those during Squat–10, Stoop–10, and Elev2Hands–10, respectively (Figs. 6.2, 6.3, 6.4, 6.5). Regarding the effect of movement speed on spinal forces during stoop and squat tasks, our simulation results aligned with the measured data, indicating higher intervertebral forces during the lifting phase of Squat–7–Fast compared to Squat–10. However, discrepancies were observed during the lowering phase, which we attribute to the lack of available measured data for the Squat–10 task. The intersession variability of measured forces also may have influenced the results. For instance, the Squat–7 and Squat–7–Fast data were collected in the same session for each patient, and the measured intervertebral forces showed higher values for Squat–7–Fast, which aligns with our simulation results. However, the Squat–10 data collection occurred at different time intervals after surgery than the Squat–7–Fast data collection, so comparisons between these tasks may not be valid.

In agreement with our previous findings (Akhavanfar et al., 2022), when the movement speed increased, the differences between the EHF&M approaches in the predicted results were amplified (Fig. 6.6). Our current findings challenge our initial expectations that EHF&M Approach 4 would yield the most accurate spinal forces. Instead, all proposed EHF&M approaches resulted in equally valid spinal loads. Therefore, modellers may use EHF&M Approaches 1 and 2 for dynamic lifting tasks due to the relative ease of setup and application. However, they should note that the uncertainty in the spinal forces estimated using a particular EHF&M modelling approach could change the interpretation of their results (see Appendix D–SI. 7). In general, we advocate for considering Approach 4 in studies where it is feasible to collect data from markers attached to the external load and where the computational expense of the inverse kinematic analysis is

manageable. Approach 4 better represents the physical reality, especially during two-handed lifting tasks, as it can distinguish between the two-handed lifting of one load and the simultaneous lifting of one-half of the load by each hand—which is not possible with Approaches 1 and 2. Additionally, Approach 4 yielded similar results to Approach 3 while effectively addressing its limitations. Finally, Approach 4 is less complicated than Approach 5 and, as demonstrated in our previous study (Akhavanfar et al., 2022), Approach 4 resulted in lower residual forces than the other approaches.

Future studies should focus on validating this model with a larger number of participants and during a wider range of dynamic tasks to enhance its reliability and generalizability. Additionally, conducting comprehensive sensitivity analyses is essential to investigate the influence of various modelling assumptions on the predicted spinal forces. Several critical modelling assumptions related to our model calibration require attention, such as uncertainties in body segment and muscle parameters (Myers et al., 2015), kinematic constraints (Alemi et al., 2021), and passive elements (Meszaros-Beller et al., 2023). We employed simple and common modelling choices to define the intervertebral joints, scale the musculoskeletal geometry, and incorporate the effect of passive structures. However, more intricate modelling options are available. For example, one may include translational degrees of freedom between vertebral bodies, scale the musculoskeletal geometry using medical images, and model passive elements (such as ligaments, facet bony articulations, and intervertebral discs) explicitly rather than considering only their net moments. Future studies should investigate the effect of these modelling decisions on the accuracy of spinal forces estimated during dynamic lifting tasks. Given that our MSK model's primary enhancement was the incorporation of passive structures, we have provided

further discussion on the effect of the added passive torque elements on the predicted intervertebral forces in Supplementary Information (Appendix D–SI. 8).

For future applications and research studies, we believe that our new FATLS model is the most appropriate choice among the existing multibody-based models that use the common inverse dynamics–based simulation workflow in OpenSim to estimate intervertebral spinal forces during lifting/lowering tasks. The advantages of our new FATLS model can be summarized as follows. (1) The new FATLS model is a detailed spine model possessing all thoracic and lumbar segments, can satisfy moment equilibrium at all joints, and can be run using kinematics data collected in the laboratory during static and dynamic tasks. (2) The spinal forces estimated by the FATLS model at various spinal levels had been previously validated against experimental data (both IDP and implant) for many static lifting tasks in addition to the tasks for which other models have been validated. (3) We extensively validated the spinal forces estimated by this model during various dynamic lifting/lowering tasks and our results demonstrated the high accuracy of this model's predictions. (4) Finally, using this model will improve the impact of future research studies because it is freely available in OpenSim (see https://simtk.org/projects/handloadinterac).

### 6.6 References


Akhavanfar, M., Brandon, S.C.E., Brown, S.H.M., Graham, R.B., 2019. Development of a novel MATLAB-based framework for implementing mechanical joint stability constraints within OpenSim musculoskeletal models. J. Biomech. 91, 61–68.

Akhavanfar, M., Uchida, T.K., Clouthier, A.L., Graham, R.B., 2022. Sharing the load: modelling loads in OpenSim to simulate two-handed lifting. Multibody Syst. Dyn. 54, 213–234.

Akhavanfar, M., Uchida, T.K., Graham, R.B., 2023. Evaluation of spinal force normalization techniques. J. Biomech. 147, 111441.

Alemi, M.M., Banks, J.J., Lynch, A.C., Allaire, B.T., Bouxsein, M.L., Anderson, D.E., 2023. EMG validation of a subject-specific thoracolumbar spine musculoskeletal model during dynamic activities in older adults. Ann. Biomed. Eng. 1–10.

Alemi, M.M., Burkhart, K.A., Lynch, A.C., Allaire, B.T., Mousavi, S.J., Zhang, C., Bouxsein, M.L., Anderson, D.E., 2021. The influence of kinematic constraints on model performance during inverse kinematics analysis of the thoracolumbar spine. Front. Bioeng. Biotechnol. 9, 688041.

Andersson, G.B., Ortengren, R., Nachemson, A., 1977. Intradiskal pressure, intra-abdominal pressure and myoelectric back muscle activity related to posture and loading. Clin. Orthop. Relat. Res. 129, 156–164.

Banks, J.J., Alemi, M.M., Allaire, B.T., Lynch, A.C., Bouxsein, M.L., Anderson, D.E., 2023. Using static postures to estimate spinal loading during dynamic lifts with participant-specific thoracolumbar musculoskeletal models. Appl. Ergon. 106, 103869.

Banks, J.J., Umberger, B.R., Caldwell, G.E., 2022. EMG optimization in OpenSim: a model for estimating lower back kinetics in gait. Med. Eng. Phys. 103, 103790.

Bassani, T., Stucovitz, E., Qian, Z., Briguglio, M., Galbusera, F., 2017. Validation of the AnyBody full body musculoskeletal model in computing lumbar spine loads at L4L5 level. J. Biomech. 58, 89–96.

Beaucage-Gauvreau, E., Brandon, S.C.E., Robertson, W.S.P., Fraser, R., Freeman, B.J.C., Graham, R.B., Thewlis, D., Jones, C.F., 2020. A braced arm-to-thigh (BATT) lifting technique reduces lumbar spine loads in healthy and low back pain participants. J. Biomech. 100, 109584.

Beaucage-Gauvreau, E., Robertson, W.S.P., Brandon, S.C.E., Fraser, R., Freeman, B.J.C., Graham, R.B., Thewlis, D., Jones, C.F., 2019. Validation of an OpenSim full-body model with detailed lumbar spine for estimating lower lumbar spine loads during symmetric and asymmetric lifting tasks. Comput. Methods Biomech. Biomed. Engin. 22, 451–464.

Bender, A., Bergmann, G., 2012. Determination of typical patterns from strongly varying signals. Comput. Methods Biomech. Biomed. Engin. 15, 761–769.

Bruno, A.G., Bouxsein, M.L., Anderson, D.E., 2015. Development and validation of a musculoskeletal model of the fully articulated thoracolumbar spine and rib cage. J. Biomech. Eng. 137, 081003.

Burkhart, K., Grindle, D., Bouxsein, M.L., Anderson, D.E., 2020. Between-session reliability of subject-specific musculoskeletal models of the spine derived from optoelectronic motion capture data. J. Biomech. 112, 110044.

Damm, P., Reitmaier, S., Hahn, S., Waldheim, V., Firouzabadi, A., Schmidt, H., 2020. In vivo hip and lumbar spine implant loads during activities in forward bent postures. J. Biomech. 102, 109517.

De Zee, M., Hansen, L., Wong, C., Rasmussen, J., Simonsen, E.B., 2007. A generic detailed rigid-body lumbar spine model. J. Biomech. 40, 1219–1227.

Delp, S.L., Anderson, F.C., Arnold, A.S., Loan, P., Habib, A., John, C.T., Guendelman, E., Thelen, D.G., 2007. OpenSim: Open-source software to create and analyze dynamic simulations of movement. IEEE Trans. Biomed. Eng. 54, 1940–1950.

Dreischarf, M., Rohlmann, A., Graichen, F., Bergmann, G., Schmidt, H., 2016a. In vivo loads on a vertebral body replacement during different lifting techniques. J. Biomech. 49, 890–895.

Dreischarf, M., Shirazi-Adl, A., Arjmand, N., Rohlmann, A., Schmidt, H., 2016b. Estimation of loads on human lumbar spine: A review of in vivo and computational model studies. J. Biomech. 49, 833–845.

Erdemir, A., McLean, S., Herzog, W., van den Bogert, A.J., 2007. Model-based estimation of muscle forces exerted during movements. Clin. Biomech. 22, 131–154.

Fujii, R., Sakaura, H., Mukai, Y., Hosono, N., Ishii, T., Iwasaki, M., Yoshikawa, H., Sugamoto, K., 2007. Kinematics of the lumbar spine in trunk rotation: in vivo three-dimensional analysis using magnetic resonance imaging. Eur. spine J. 16, 1867–1874.

Fujimori, T., Iwasaki, M., Nagamoto, Y., Ishii, T., Kashii, M., Murase, T., Sugiura, T., Matsuo, Y., Sugamoto, K., Yoshikawa, H., 2012. Kinematics of the thoracic spine in trunk rotation: in vivo 3-dimensional analysis. Spine 37, 1318–1328.

Fujimori, T., Iwasaki, M., Nagamoto, Y., Matsuo, Y., Ishii, T., Sugiura, T., Kashii, M., Murase, T., Sugamoto, K., Yoshikawa, H., 2014. Kinematics of the thoracic spine in trunk lateral bending: in vivo three-dimensional analysis. Spine J. 14, 1991–1999.

Ghezelbash, F., Shirazi-Adl, A., Plamondon, A., Arjmand, N., 2020. Comparison of different lifting analysis tools in estimating lower spinal loads – evaluation of NIOSH criterion. J. Biomech. 112, 110024.

Halloran, J.P., Ackermann, M., Erdemir, A., Bogert, A.J. Van Den, 2010. Concurrent musculoskeletal dynamics and finite element analysis predicts altered gait patterns to reduce foot tissue loading. J. Biomech. 43, 2810–2815.

Han, K.S., Zander, T., Taylor, W.R., Rohlmann, A., 2012. An enhanced and validated generic thoraco-lumbar spine model for prediction of muscle forces. Med. Eng. Phys. 34, 709–716.

Jones, A.C., Wilcox, R.K., 2008. Finite element analysis of the spine: towards a framework of verification, validation and sensitivity analysis. Med. Eng. Phys. 30, 1287–1304.

Lerchl, T., Nispel, K., Baum, T., Bodden, J., Senner, V., Kirschke, J.S., 2023. Multibody models of the thoracolumbar spine: a review on applications, limitations, and challenges. Bioengineering 10, 202.

Lund, M.E., de Zee, M., Andersen, M.S., Rasmussen, J., 2012. On validation of multibody musculoskeletal models. Proc. Inst. Mech. Eng. Part H J. Eng. Med. 226, 82–94.

Malakoutian, M., Street, J., Wilke, H.-J., Stavness, I., Fels, S., Oxland, T., 2018. A musculoskeletal model of the lumbar spine using ArtiSynth–development and validation. Comput. Methods Biomech. Biomed. Eng. Imaging Vis. 6, 483–490.

Meszaros-Beller, L., Hammer, M., Schmitt, S., Pivonka, P., 2023. Effect of neglecting passive spinal structures: a quantitative investigation using the forward-dynamics and inverse-dynamics musculoskeletal approach. Front. Physiol. 14, 1135531.

Miller, J.A.A., Schultz, A.B., Warwick, D.N., Spencer, D.L., 1986. Mechanical properties of lumbar spine motion segments under large loads. J. Biomech. 19, 79–84.

Myers, C.A., Laz, P.J., Shelburne, K.B., Davidson, B.S., 2015. A probabilistic approach to quantify the impact of uncertainty propagation in musculoskeletal simulations. Ann. Biomed. Eng. 43, 1098–1111.

Nazer, R. Al, Rantalainen, T., Heinonen, A., Sieva, H., Mikkola, A., 2008. Flexible multibody simulation approach in the analysis of tibial strain during walking. J. Biomech. 41, 1036–1043.

Polga, D.J., Beaubien, B.P., Kallemeier, P.M., Schellhas, K.P., Lew, W.D., Buttermann, G.R., Wood, K.B., 2004. Measurement of in vivo intradiscal pressure in healthy thoracic intervertebral discs. Spine 29, 1320–1324.

Rohlmann, A., Pohl, D., Bender, A., Graichen, F., Dymke, J., Schmidt, H., Bergmann, G., 2014. Activities of everyday life with high spinal loads. PLoS One 9, 3–11.

Rozumalski, A., Schwartz, M.H., Wervey, R., Swanson, A., Dykes, D.C., Novacheck, T., 2008. The in vivo three-dimensional motion of the human lumbar spine during gait. Gait Posture 28, 378–384.

Schmidt, H., Galbusera, F., Rohlmann, A., Shirazi-adl, A., 2013. What have we learned from finite element model studies of lumbar intervertebral discs in the past four decades? J. Biomech. 46, 2342–2355.

Schultz, A., Andersson, G., Ortengren, R., Haderspeck, K., Nachemson, A., 1982. Loads on the lumbar spine. Validation of a biomechanical analysis by measurements of intradiscal pressures and myoelectric signals. J. Bone Joint Surg. Am. 64, 713–720.

Seth, A., Hicks, J.L., Uchida, T.K., Habib, A., Dembia, C.L., Dunne, J.J., Ong, C.F., DeMers, M.S., Rajagopal, A., Millard, M., 2018. OpenSim: Simulating musculoskeletal dynamics and neuromuscular control to study human and animal movement. PLoS Comput. Biol. 14, e1006223.

von Arx, M., Liechti, M., Connolly, L., Bangerter, C., Meier, M.L., Schmid, S., 2021. From stoop to squat: a comprehensive analysis of lumbar loading among different lifting styles. Front. Bioeng. Biotechnol. 9, 1070.

Wang, W., Wang, D., De Groote, F., Scheys, L., Jonkers, I., 2020. Implementation of physiological functional spinal units in a rigid-body model of the thoracolumbar spine. J. Biomech. 98, 109437.

Wilke, H.J., Neef, P., Hinz, B., Seidel, H., Claes, L., 2001. Intradiscal pressure together with anthropometric data–a data set for the validation of models. Clin. Biomech. 16, 111–126.

Wong, K.W.N., Luk, K.D.K., Leong, J.C.Y., Wong, S.F., Wong, K.K.Y., 2006. Continuous dynamic spinal motion analysis. Spine 31, 414–419.

# Chapter 7: General Discussion

## 7.1 Introduction

Musculoskeletal disorders, particularly those affecting the back, pose a global health challenge (Cieza et al., 2020). In Canada, musculoskeletal disorders incur an annual cost of approximately $15 billion and are the most prevalent among chronic conditions (Maas et al., 2020). Work-related musculoskeletal disorders (WMSDs) contribute significantly to the public health and economic burden. European industries, for instance, experienced substantial absenteeism due to WMSDs, with associated costs reaching 240 billion euros annually (Govaerts et al., 2021).

Back disorders stand out as a primary global cause of disability, and the spine is the most common site for WMSDs (Govaerts et al., 2021). Extensive research into the multifactorial causation of WMSDs has identified biomechanical, psychosocial, and personal risk factors (Afsharian et al., 2023). Notably, occupational tasks involving lifting and lowering are strongly associated with back injuries (Coenen et al., 2014). From a biomechanical perspective, excessive mechanical loads on spinal joints during lifting and lowering tasks emerge as crucial physical risk factors for work-related back injuries (Coenen et al., 2014; Parreira et al., 2018).

In the absence of non-invasive measurements, using multibody-based musculoskeletal models along with the inverse dynamic motion-solving approach and optimization algorithms to solve for muscle forces is a widely-used simulation workflow for estimating spinal joint loads during various tasks, including lifting (Dreischarf et al., 2016; Lerchl et al., 2023). The suitability of this simulation workflow for estimating intervertebral joint loads and comprehending biomechanical risk factors associated with lifting tasks in diverse workplaces is underpinned by several advantages: i) a multibody model can be swiftly developed and scaled for large populations in this framework, as opposed to the time-intensive nature of finite element models (Nispel et al.,

2023), ii) inverse dynamic analyses are less computationally expensive compared to forward dynamic motion-solving approaches (Erdemir et al., 2007), and iii) optimization-driven models are more ecologically applicable when compared to EMG-based models.

Although numerous biofidelic spine models have been developed, validated, and utilized within the aforementioned simulation workflow (i.e., inverse dynamics–based multibody modelling with optimization-based muscle recruitments) to advance our knowledge of the mechanical loads acting on the human spine (Lerchl et al., 2023), several key limitations exist in the literature that the current thesis aimed to address:

1) Optimization-based models commonly cannot predict the co-activations of antagonist muscles, which disagrees with measured EMG activities. Some spine models have attempted to overcome this limitation by incorporating stability criteria within the optimization algorithm (Hajihosseinali et al., 2014). However, these models have been developed using in-house codes, are not open-access, and the mathematical formulation of stability in these studies is limited to their specific model and cannot be extended to other spine models.
2) In modelling studies where dynamic lifting tasks were simulated, the external load applied to the hands was represented in the simulation workflow as a constant gravity-oriented load (similar to static lifting conditions) or by increasing the hand mass. However, the effects of these simplifications on predicted spinal forces were not investigated.
3) The accuracy of intervertebral loads estimated by existing models has primarily been evaluated during static lifting tasks (Actis et al., 2018; Bassani et al., 2017; Bruno et al., 2015). Therefore, it is unknown to what extent we can trust these models for simulating dynamic lifting tasks.

The major limitations listed above are related, one way or another, to the accuracy, reliability, and accessibility of existing musculoskeletal modelling studies. Therefore, the

overarching purpose of this thesis was to estimate intervertebral forces during lifting/lowering tasks with improved accuracy, reliability, and accessibility compared to previous efforts. To achieve this overarching goal, four musculoskeletal multibody modelling studies were conducted using OpenSim, and the findings of each study are summarized in Section 7.2 below. The outcomes of these studies have the potential to enhance our understanding of spinal joint loads. By using these outcomes in future studies, improvements in back health in various settings, including workplaces, can be facilitated.

### 7.2 Summary of Findings

In the first study (Chapter 3), entitled *"Development of a novel MATLAB-based framework for implementing mechanical joint stability constraints within OpenSim musculoskeletal models"*, the Stability-Constrained Static Optimization (SCSO) framework was developed to calculate muscle forces that satisfy crucial mechanical stability requirements in addition to the constraints considered by the default Static Optimization (SO) solver in OpenSim. Experimental data from the literature, referred to as Experimental data 1 and 2, were used to evaluate the accuracy of estimated muscle activations using the framework and the default SO solver for a spine model. Experimental data 1 involved static symmetrical and asymmetrical flexion tasks, while Experimental data 2 included tasks with different masses held at various heights above the lumbo-sacral ($L_5S_1$) joint. The default SO solver did not assign any activations to antagonistic muscles during Experimental data 1 trials, and it assigned constant muscle activations and forces at different load heights during Experimental data 2 trials, contrary to the measured EMG data. The muscle activations predicted by SCSO showed less average deviation from the EMG data (6.8%−7.5%) compared to SO (10.2%) during Experimental data 1 tasks. Additionally, for the ratios of agonist to antagonist muscle activities during Experimental data 2 tasks, the root mean

square errors of the results obtained by SO were approximately 10 times higher than those estimated by SCSO. These findings indicate that the new SCSO framework provides muscle activations in closer agreement with EMG data in terms of both absolute values and activation patterns of agonist and antagonist muscles compared to the default optimization solver in OpenSim. Therefore, the newly developed SCSO framework is considered more suitable for estimating muscle forces during static tasks.

In the second study (Chapter 4), entitled *"Sharing the load: modelling loads in OpenSim to simulate two-handed lifting"*, five approaches were introduced to model the hand–mass interaction. The investigation explored the extent to which these modelling decisions affect the estimated spinal joint loads during eight two-handed dynamic lifting tasks, and evaluated the accuracy of these approaches in terms of resulting dynamic inconsistencies in a spine model. Modelling Approach 1 involved applying external hand forces and moments (EHF&M) as a gravity-oriented half-load to each hand. Approach 1 does not consider the effect of load inertial properties on estimated spinal forces, yet it offers a convenient modelling procedure. In Approach 2, the mass of each hand was increased by half the mass of the lifted box for the SO analysis, thus taking into account the acceleration of the box. To model the lifted box as a rigid body, it should be noted that in OpenSim each rigid body must be connected to another body (its 'parent') with a joint. Therefore, Approach 3 involved modelling the box in two halves with the same inertial properties, connecting one half-box to each hand with a joint, and introducing a Weld Constraint between the two half-boxes. Modelling Approach 3 formed a closed-kinematic-chain system, which necessitated a more complex procedure for preparing the model for the kinematic and SO analyses compared to Approaches 1 and 2, as well as resulted in considerably higher runtime. Modelling Approach 4, identical to Approach 3 in terms of kinematic analysis, removed the Weld

Constraint between the two half-boxes only for the SO analysis, thereby eliminating the closed kinematic chain and its resultant nonlinear algebraic constraint equations, enabling SO to run much faster. In Modelling Approach 5, a box body was created and attached to the ground with a Free Joint, and the kinematics of the box were calculated separately from those of the human body. Subsequently, a new method was developed to calculate EHF&M and their corresponding points of application at the centre of pressure of each hand, ensuring that applying the negative of EHF&M to the box handles would result in the box moving along its experimental trajectory. Approach 5 considers the inertial properties of the load better than Approaches 1 and 2, while allowing SO to run as fast as these approaches due to the absence of a closed kinematic chain. The results of Study 2 demonstrated that the EHF&M modelling approaches can lead to substantial differences in the predicted spinal loads (e.g., 2.6 kN in a fast stoop lifting task), especially as the movement speed increases. Modelling Approach 4 resulted in fewer overall dynamic inconsistencies in the model, making it considered more reliable than other approaches. However, it was discussed that EHF&M Modelling Approach 4 does not necessarily result in estimating more accurate spinal loads. Therefore, the fourth study in this thesis addressed the question of which approach produces more accurate spinal loads.

By enhancing an existing model in the literature, I developed a new fully articulated thoracolumbar spine (FATLS) model, which was used in Studies 3 and 4. The new FATLS model developed for Studies 3 and 4 is an anatomically detailed full-body model which considers the role of spine passive structures and is suitable to be used for both static and dynamic tasks, where the kinematics of the model could be determined by trajectories of skin-mounted markers affixed on bony landmarks.

The third study (Chapter 5), entitled *"Evaluation of spinal force normalization techniques"*, aimed to assess the effectiveness of four techniques in normalizing spinal forces estimated by the new FATLS model during 13 static symmetric trunk flexion tasks, with the goal of removing the effect of body weight (BW) variations between participants on the estimated spinal forces. The four techniques examined were BW Division Normalization (BWDN), Standing Division Normalization (SDN), BW Offset Normalization (BWON), and BW Power Curve Normalization (BWPCN). In BWDN and SDN, the estimated spinal forces were divided by BW and the intervertebral loads during a standing posture, respectively. The BWON and BWPCN techniques assumed a linear relationship (with a non-zero intercept) and a curvilinear relationship between the dependent variable (spinal forces) and BW, respectively. Following normalization, the relationship between normalized spinal forces and BW was assessed using Pearson correlation coefficients. If a significant correlation was detected, the normalization procedure was considered ineffective. BWDN and SDN achieved successful normalization of $L_4L_5$ spinal forces in three tasks and $L_5S_1$ loads in five and three tasks, respectively. In contrast, the BWON and BWPCN techniques demonstrated consistent success across all lumbar spine levels and tasks. BWON successfully removed the confounding effect of body weight while maintaining the influence of flexion angle on spinal forces. Consequently, the results of this study suggest that when using the new FATLS model for static or dynamic tasks, the coefficient required for BWON should be determined from this study, and then spinal forces can be normalized using BWON to account for differences in BW.

The purpose of the final study (Chapter 6), entitled *"An Enhanced Spine Model Validated for Simulating Dynamic Lifting Tasks in OpenSim"*, was twofold: to validate the spinal forces estimated by the new FATLS model against available implant data, and to compare the accuracy

of different EHF&M approaches, as demonstrated in Study 2, in predicting spinal forces during various dynamic lifting/lowering tasks. Three male participants replicated nine symmetric dynamic lifting/lowering tasks that were performed by three male patients who had vertebral body replacement at the L1 level. In total, 39 motion trials were collected for each participant, and 315 dynamic simulations for two-handed lifting tasks and 216 dynamic simulations for one-handed lifting tasks were generated and analyzed in Study 4. The results of this study showed that regardless of the EHF&M approach used for the simulation, the new FATLS model accurately captured the change in maximum forces, where strong significant correlations ($r > 0.9$, $p < 0.05$) were found between the measured and estimated maximum forces across all tasks. Moreover, during the lifting/lowering motion cycles within each task, the cross-correlation coefficients between the estimated and measured spinal forces were greater than 0.90, which demonstrate that the time-varying feature of spinal forces can also be well-predicted by the new FATLS model.

In conclusion, this dissertation provides valuable insights and recommendations for the biomechanics community regarding spinal load analysis during lifting/lowering tasks using multibody-based modelling and inverse dynamics simulation. Based on the findings and discussions presented, three key recommendations can be made. Firstly, researchers are advised to use the newly developed FATLS model due to its high level of biofidelity, accessibility, and validation across a broader range of tasks compared to previous models. Secondly, it is recommended to use the SCSO framework to estimate muscle activation patterns during static lifting tasks, as it has demonstrated better accuracy compared to the common SO. Lastly, in the simulation workflow, it is suggested to employ EHF&M Approach 2 for its ease of setup and accuracy. However, it is important to report the uncertainty associated with spinal force estimates

using other EHF&M Approaches, as this uncertainty could potentially impact the interpretation of research findings.

## 7.3 Limitations

While the findings of the four studies presented in this thesis contribute to advancing our comprehension of spinal joint loads during lifting tasks, it is crucial to acknowledge various limitations inherent in the employed methods within these studies. Additionally, as Studies 1–3 primarily centred on establishing proof-of-principle concepts, it is important to discuss the limitations linked to the interpretation of results obtained from these studies.

### *7.3.1 Study 1 Limitations*

In Study 1, the SCSO framework for OpenSim was developed in MATLAB, which is a widely-used commercial programming platform. While the MATLAB codes developed in Study 1 are open-access for the biomechanics community, the use of a commercial software platform may pose accessibility challenges. Furthermore, the MATLAB framework was developed with the OpenSim 3.3 API, thus it would face compatibility issues with recent OpenSim versions, limiting its usability. Additionally, Study 1 revealed that the current framework is approximately 4–5 times slower than the default SO solver due to read-write operations from text files of the model's states. To address these issues, it is recommended to update the framework for the latest OpenSim version using Python, an open-source programming language, and implement direct access to the model's states in memory to improve computation time.

The developed SCSO framework was evaluated as a proof of concept for a simple spine model with 2 joints and 12 muscles, without considering joint passive stiffness. By testing the SCSO framework for a more detailed model (i.e., a lower limb model with 12 joints, 23 DOF, and 92 muscles), Study 1 demonstrated the potential applicability of the framework to various

OpenSim models with different levels of complexity. However, this framework was not tested for a biofidelic spine model. Therefore, I recommend evaluating the performance of the SCSO framework in estimating muscle forces during static tasks using our new FATLS model in future studies.

It was also demonstrated in Study 1 that the performance of the SCSO framework in predicting antagonist muscle co-contractions is considerably influenced by the assumed linear muscle stiffness coefficient ($q$). A broad range of values for $q$ has been reported. If $q$ is chosen to be sufficiently large in a model, agonist muscle forces alone would be adequate to maintain stability, resulting in muscle force estimates that are not different from those calculated by the traditional optimization solver. To mitigate potential bias in selecting $q$ for the intended static tasks, I propose conducting a priori EMG-based experiment. In this preliminary experiment, researchers can instruct each participant to perform a task similar to Simulation 2 in Study 1 (e.g., holding a load with a constant sagittal moment arm from the body at varying heights) and measure EMG activities of the trunk muscles. Subsequently, researchers can determine, for each participant, the $q$ value that best aligns with their model and produces optimal agreement with EMG data. Once the appropriate value for $q$ is determined and the model is accordingly calibrated, the muscle activations predicted by the SCSO framework can be validated against the measured EMG data for the actual lifting tasks.

### *7.3.2 Study 2 Limitations*

Study 2 focused on introducing various EHF&M approaches and delving into the complexity of implementing each approach within a simulation workflow for estimating spinal joint loads. For one participant, this study highlighted considerable differences in predicted spinal loads resulting from the use of various EHF&M modelling approaches, especially during fast

dynamic stoop and squat lifting tasks. Future studies should expand this assessment to include more participants and dynamic lifting tasks. Additionally, the participant was instructed to perform the fast stoop and squat lifting tasks as quickly as possible, leading to substantial differences (up to 35%) between approaches. However, lifting with the maximum effort is not a common scenario in real-life occupational settings. Subsequent studies should evaluate the differences in spinal loads estimated by various EHF&M approaches within a time frame that better represents the fast lifting pace in industrial settings (Harari et al., 2018).

The accuracy of the presented EHF&M modelling approaches in Study 2 was indirectly assessed by evaluating the resulting dynamic inconsistency (i.e., residual forces) in the model when each approach was employed. However, the residual forces in the model could be influenced by many assumptions inherent in musculoskeletal modelling, and not just the modelling decision for hand–load interaction (Faber et al., 2018). Nevertheless, we discussed in Study 2 that we interpreted the difference between the resulting residuals rather than focusing on the absolute values of residuals. Future studies can measure forces between hands and the lifted mass using, for example, a box instrumented with load cells or pressure sensors (Faber et al., 2013), and then directly assess the accuracy of forces and moments applied to the hands when each EHF&M modelling approach is used.

### *7.3.3 Study 3 Limitations*

The assumptions related to body mass distribution and body kinematics can significantly impact the joint loads predicted by a model (Akhavanfar et al., 2018; Myers et al., 2015). In Study 3, both kinematics and model scaling were not based on laboratory-measured data for various individuals. Instead, our new generic FATLS model's body mass was scaled linearly by adjusting the input target mass while preserving the mass distribution of the generic model, representing 11

body masses ranging from 50 to 100 kg. Additionally, joint angles were prescribed for the 13 static symmetric trunk flexion tasks simulated in this study. Consequently, future research should evaluate the appropriateness of different normalization techniques by performing more accurate model scaling, such as utilizing medical imaging data, and obtaining kinematic data through optical markers or inertial measurement sensors.

While this study discussed the superiority of BWON over other introduced approaches for normalizing spinal forces, it is important to note that this technique requires a coefficient that is highly dependent on the flexion angle. Although Study 3 provided this coefficient for various flexion angles, it is likely that the coefficient would differ if another spine musculoskeletal model were used to estimate spinal forces. This implies that BWON, with the current coefficients, is not a robust technique for normalizing intervertebral forces. Consequently, modelling studies that do not employ our new FATLS model should determine, if necessary, the optimal way to normalize spinal forces estimated by their model. Furthermore, this study did not assess the effect of dynamic movements. Hence, future studies should strive to identify an appropriate and robust approach for normalizing spinal forces during dynamic lifting tasks.

Finally, Study 3 did not delve into a comprehensive discussion of the broader implications of normalization. Within the scope of my research, the noticeable disparity in body weight between our recruited participants and patients with implants in Study 4 had the potential to obscure result interpretation and introduce bias in the comparison of different EHF&M modelling approaches for accuracy assessment. Therefore, adhering to the recommendations of the International Society of Biomechanics (Derrick et al., 2020), BWON enhanced the data analysis in Study 4 by mitigating the confounding effect of body weight. However, in general, the transformation of raw data during normalization may introduce other confounding factors as well as lose information (Hughes and

Bartlet, 2002). This aspect was briefly touched upon in Study 3, where it was discussed how BWPCN could influence the relationship between spinal load variations and change in the trunk flexion angle. However, it warrants further investigation to comprehensively understand the artifacts of the introduced normalization procedures especially when comparing spinal forces across different populations.

### *7.3.4 Study 4 Limitations*

In this study, estimated spinal forces were validated to a greater extent than those validated in previous studies: more dynamic lifting tasks were assessed and both maximum forces and time series of spinal forces were validated. Due to the lack of comprehensive datasets (e.g., surface marker trajectories, ground reaction forces, and imaging data) for patients with vertebral implants, whose data were utilized in this study, Study 4 focused on validating the trend of estimated forces within and across dynamic tasks. This trend validation is particularly important to assess how the underlying variables of the model interact and, thereby, the extent to which the model can be trusted (Lund et al., 2012). However, Study 4 suffered from a limited number of participants (three male individuals); thus, future studies should extend such trend validations to include more participants and greater diversity (e.g., female individuals).

There are numerous assumptions made when building a musculoskeletal model and when defining the simulation workflow (e.g., the objective function in the muscle recruitment solver). A validation study of estimated spinal forces, in fact, assesses the accuracy of the overall package of these assumptions. Therefore, the more one can explain how well these assumptions work, the more reliable the model will be. Future studies should, therefore, validate spinal forces for a broader range of tasks involving lifting. However, joint loads were commonly measured in a conservative manner— with a few repetitions, relatively small lifted weight, and not in awkward

postures— to reduce the risk of injury for participants. However, to design injury prevention programs, it is necessary to extrapolate the model predictions to more demanding conditions. Therefore, I suggest including the highest demanding tasks for which measured data are available. For instance, implant data for load-carrying tasks up to 20 kg are accessible, providing a valuable addition to assessing the performance of the new FATLS model in spinal load estimation for dynamic tasks involving lifting.

In certain lifting tasks, especially in the stoop and squat lifting tasks explored in this study, the movement involves an intricate interplay between the spine, lower limbs, and upper limbs. In Study 4, the model consisted of both arm and leg segments to better capture the interactions of different segments in the kinematic analysis. However, the role of lower limb and upper limb muscles was not incorporated into the dynamic analysis of the simulations (i.e., estimating intervertebral joint loads). Integrating these muscles into a spine modelling study adds complexity, and determining whether this complexity is necessary requires further investigation. Subsequent studies should explore the extent to which modelling lower and upper limb muscles influences the accuracy of estimated spinal loads. Moreover, I propose a significant enhancement to spine validation studies by determining lower or upper limb joint loads alongside spinal joint loads during lifting tasks where internal loads are measured for various body joints. If the model accurately reflects the ratios between the joint loads, its reliability is strengthened. For instance, Damm et al. (2020) compared hip and spine implant data during 10 kg stoop and squat lifting activities, a comparison not yet explored in spine modelling validation studies. This avenue could contribute valuable insights to the field.

## 7.4 Future Directions

In this thesis, an accessible framework was developed to enhance the prediction of antagonist muscle co-contractions in static lifting tasks for various models (Study 1). Additionally, a novel spine model was developed and its suitability for simulating both static and dynamic lifting tasks was demonstrated (Studies 3 and 4). Furthermore, the requisite level of complexity in our new spine model to accurately capture the hand–load interaction during dynamic lifting tasks was investigated (Studies 2 and 4). In Section 7.3, the major limitations within each study of this thesis were discussed and several suggestions on how future studies could overcome these limitations were provided. In this section, I propose several recommendations for leveraging the findings of the studies presented in this thesis to mitigate the risk of back injuries associated with lifting and lowering tasks across diverse workplaces. These suggestions aim to contribute to the enhancement of back health in various occupational settings.

Due to the established credibility of the newly developed FATLS model in this thesis, it can now be effectively applied to address practical questions in ergonomics, particularly in situations where assessing spinal joint loads informs decision-making. For instance, various spine modelling studies have explored spinal forces during stoop and squat lifting tasks to advocate specific techniques for preventing work-related back disorders (Bazrgari et al., 2007; von Arx et al., 2021). Nevertheless, the existing literature on safer lifting techniques often presents conflicting viewpoints. To leverage the FATLS model in addressing such practical inquiries, it is crucial to assess the sensitivity of the estimated forces to the critical modelling assumptions made in our study before relying on the model predictions for decision-making. For example, altering the kinematic constraints used in our model to link the motions of all vertebrae to $L_5S_1$ motions in different directions, as well as the functions employed to represent net passive moments in relation

to intervertebral rotations, could potentially change the pattern of forces estimated by the model and, consequently, influence the interpretation of results.

The sensitivity of spinal forces estimated by different spine models to certain model parameters, such as maximum muscle stress, has been investigated in prior spine studies (Bruno et al., 2015). However, a comprehensive sensitivity analysis, evaluating how various uncertainties in the model calibration, scaling, and kinematic analysis propagate through different stages of the inverse dynamic simulation workflow and impact joint load predictions, has only been employed in a limited number of lower limb studies and during gait (Langenderfer et al., 2008; Myers et al., 2015; Nguyen and Reynolds, 2014). Therefore, future researchers could adopt a similar workflow to the one used by Myers et al. (2015) to thoroughly assess how uncertainties in body segment parameters (e.g., the segments' mass and centre of mass locations), kinematic-associated parameters (e.g., coupler constraint functions), and muscle parameters (e.g., muscle moment arms) collectively influence the spinal forces estimated by the new FATLS model during lifting tasks. Such sensitivity analysis studies are complementary to the validation study presented in this thesis, providing a holistic understanding of the model's performance. This comprehensive evaluation will contribute to the refinement and robustness of the model, ensuring its applicability in diverse scenarios and enhancing its utility for ergonomic decision-making.

In Study 4, relative to spine computational modelling studies, we opted for simple and common modelling choices to scale the model for participants, capture kinematics during lifting tasks, and subsequently estimate spinal joint loads. However, advanced biofidelic musculoskeletal models designed for accurate joint load estimation, such as our new FATLS model, pose challenges for broader adoption. These models are intricate, demanding many inputs, time-intensive to run, and, consequently, primarily confined to laboratory settings, with limited

application in ergonomics practice. Recognizing the impediment posed by the complexity of these biomechanical models for practitioners who may lack expertise in the musculoskeletal modelling domain, and aiming to alleviate the computational burden associated with musculoskeletal models across various biomechanical applications, surrogate models have emerged as an effective solution (Eskinazi and Fregly, 2015). These surrogate models (e.g., regression equations) map specific inputs to the outcomes of intricate biomechanical models. The inputs chosen for these surrogate models should be easily measurable by practitioners who may not possess specialized knowledge in musculoskeletal modelling.

Based on previous computational spine modelling studies, several surrogate models have been developed to facilitate the easy estimation of spinal loads (Arjmand et al., 2012, 2011; Calder and Potvin, 2012; Fathallah et al., 1999; Ghezelbash et al., 2020). It is essential to note that even if a surrogate model accurately and reliably links input parameters to desired outputs (in this case, intervertebral forces) from a biomechanical model, the limitations and accuracy level of the original biomechanical model directly influence their corresponding surrogate models. Moreover, the domain in which surrogate models can reliably be applied is determined by where the original model was validated. As a result, existing surrogate models developed based on biofidelic spine models exhibit one or more of the following major limitations: i) an inability to estimate spinal loads at all intervertebral joints, ii) applicability limited to static lifting tasks, iii) reporting only the maximum spinal forces without detailing the time history of spinal forces, and v) neglecting anthropometric differences among individuals. The outcomes of the present thesis offer a valuable foundation for the development of new surrogate models to overcome these limitations. These new surrogate models based on our new FATLS model aim to empower ergonomics professionals with

user-friendly, robust, and accurate tools, facilitating the estimation of spinal loads in diverse workplaces.

### 7.5 References


Actis, J.A., Honegger, J.D., Gates, D.H., Petrella, A.J., Nolasco, L.A., Silverman, A.K., 2018. Validation of lumbar spine loading from a musculoskeletal model including the lower limbs and lumbar spine. J. Biomech. 68, 107–114.

Afsharian, A., Dollard, M.F., Glozier, N., Morris, R.W., Bailey, T.S., Nguyen, H., Crispin, C., 2023. Work-related psychosocial and physical paths to future musculoskeletal disorders (MSDs). Saf. Sci. 164, 106177.

Akhavanfar, M., Kazemi, H., Eskandari, A.H., Arjmand, N., 2018. Obesity and spinal loads; a combined MR imaging and subject-specific modelling investigation. J. Biomech. 70, 102–112.

Arjmand, N., Plamondon, A., Shirazi-Adl, A., Larivière, C., Parnianpour, M., 2011. Predictive equations to estimate spinal loads in symmetric lifting tasks. J. Biomech. 44, 84–91.

Arjmand, N., Plamondon, A., Shirazi-Adl, A., Parnianpour, M., Larivière, C., 2012. Predictive equations for lumbar spine loads in load-dependent asymmetric one-and two-handed lifting activities. Clin. Biomech. 27, 537–544.

Bassani, T., Stucovitz, E., Qian, Z., Briguglio, M., Galbusera, F., 2017. Validation of the AnyBody full body musculoskeletal model in computing lumbar spine loads at L4L5 level. J. Biomech. 58, 89–96.

Bazrgari, B., Shirazi-Adl, A., Arjmand, N., 2007. Analysis of squat and stoop dynamic liftings: Muscle forces and internal spinal loads. Eur. Spine J. 16, 687–699.

Bruno, A.G., Bouxsein, M.L., Anderson, D.E., 2015. Development and validation of a musculoskeletal model of the fully articulated thoracolumbar spine and rib cage. J. Biomech. Eng. 137, 081003.

Calder, I.C., Potvin, J.R., 2012. A polynomial equation to predict low back compression force: Accounting for the effects of load height on instability. Work 41, 388–393.

Cieza, A., Causey, K., Kamenov, K., Hanson, S.W., Chatterji, S., Vos, T., 2020. Global estimates of the need for rehabilitation based on the Global Burden of Disease study 2019: a systematic analysis for the Global Burden of Disease Study 2019. Lancet 396, 2006–2017.

Coenen, P., Gouttebarge, V., Van Der Burght, A.S.A.M., Van Dieën, J.H., Frings-Dresen, M.H.W., Van Der Beek, A.J., Burdorf, A., 2014. The effect of lifting during work on low back pain: a health impact assessment based on a meta-analysis. Occup. Environ. Med. 71, 871–877.

Damm, P., Reitmaier, S., Hahn, S., Waldheim, V., Firouzabadi, A., Schmidt, H., 2020. In vivo hip and lumbar spine implant loads during activities in forward bent postures. J. Biomech. 102, 109517.

Derrick, T.R., van den Bogert, A.J., Cereatti, A., Dumas, R., Fantozzi, S., Leardini, A., 2020. ISB recommendations on the reporting of intersegmental forces and moments during human motion analysis. J. Biomech. 99, 109533.

Dreischarf, M., Shirazi-Adl, A., Arjmand, N., Rohlmann, A., Schmidt, H., 2016. Estimation of loads on human lumbar spine: A review of in vivo and computational model studies. J. Biomech. 49, 833–845.

Erdemir, A., McLean, S., Herzog, W., van den Bogert, A.J., 2007. Model-based estimation of muscle forces exerted during movements. Clin. Biomech. 22, 131–154.

Eskinazi, I., Fregly, B.J., 2015. Surrogate modelling of deformable joint contact using artificial neural networks. Med. Eng. Phys. 37, 885–891.

Faber, G.S., Chang, C.-C., Kingma, I., Dennerlein, J.T., 2013. Estimating dynamic external hand forces during manual materials handling based on ground reaction forces and body segment accelerations. J. Biomech. 46, 2736–2740.

Faber, H., Van Soest, A.J., Kistemaker, D.A., 2018. Inverse dynamics of mechanical multibody systems: An improved algorithm that ensures consistency between kinematics and external forces. PLoS One 13, e0204575.

Fathallah, F.A., Marras, W.S., Parnianpour, M., 1999. Regression models for predicting peak and continuous three-dimensional spinal loads during symmetric and asymmetric lifting tasks. Hum. Factors 41, 373–388.

Ghezelbash, F., Shirazi-Adl, A., El Ouaaid, Z., Plamondon, A., Arjmand, N., 2020. Subject-specific regression equations to estimate lower spinal loads during symmetric and asymmetric static lifting. J. Biomech. 102, 109550.

Govaerts, R., Tassignon, B., Ghillebert, J., Serrien, B., De Bock, S., Ampe, T., El Makrini, I., Vanderborght, B., Meeusen, R., De Pauw, K., 2021. Prevalence and incidence of work-related musculoskeletal disorders in secondary industries of 21st century Europe: a systematic review and meta-analysis. BMC Musculoskelet. Disord. 22, 1–30.

Hajihosseinali, M., Arjmand, N., Shirazi-Adl, A., Farahmand, F., Ghiasi, M.S., 2014. A novel stability and kinematics-driven trunk biomechanical model to estimate muscle and spinal forces. Med. Eng. Phys. 36, 1296–1304.

Harari, Y., Riemer, R., Bechar, A., 2018. Factors determining workers' pace while conducting continuous sequential lifting, carrying, and lowering tasks. Appl. Ergon. 67, 61–70.

Hughes, M.D., Bartlett, R.M., 2002. The use of performance indicators in performance analysis. J. Sports Sci. 20, 739–754.

Langenderfer, J.E., Laz, P.J., Petrella, A.J., Rullkoetter, P.J., 2008. An efficient probabilistic methodology for incorporating uncertainty in body segment parameters and anatomical landmarks in joint loadings estimated from inverse dynamics. J. Biomech. Eng. 130, 14502.

Lerchl, T., Nispel, K., Baum, T., Bodden, J., Senner, V., Kirschke, J.S., 2023. Multibody models of the thoracolumbar spine: a review on applications, limitations, and challenges. Bioengineering 10, 202.

Lund, M.E., de Zee, M., Andersen, M.S., Rasmussen, J., 2012. On validation of multibody musculoskeletal models. Proc. Inst. Mech. Eng. Part H J. Eng. Med. 226, 82–94.

Maas, E.T., Koehoorn, M., McLeod, C.B., 2020. Descriptive epidemiology of gradual return to work for workers with a work-acquired musculoskeletal disorder in British Columbia, Canada. J. Occup. Environ. Med. 62, 113–123.

Myers, C.A., Laz, P.J., Shelburne, K.B., Davidson, B.S., 2015. A probabilistic approach to quantify the impact of uncertainty propagation in musculoskeletal simulations. Ann. Biomed. Eng. 43, 1098–1111.

Nguyen, T.C., Reynolds, K.J., 2014. The effect of variability in body segment parameters on joint moment using Monte Carlo simulations. Gait Posture 39, 346–353.

Nispel, K., Lerchl, T., Senner, V., Kirschke, J.S., 2023. Recent advances in coupled MBS and FEM models of the spine—A review. Bioengineering 10, 315.

Parreira, P., Maher, C.G., Steffens, D., Hancock, M.J., Ferreira, M.L., 2018. Risk factors for low back pain and sciatica: an umbrella review. Spine J. 18, 1715–1721.

von Arx, M., Liechti, M., Connolly, L., Bangerter, C., Meier, M.L., Schmid, S., 2021. From stoop to squat: a comprehensive analysis of lumbar loading among different lifting styles. Front. Bioeng. Biotechnol. 9, 1070.

# Appendix A: Study 1 Supplementary Information

## A–SI. 1

### *A–SI. 1.1 Introduction*

This supplementary material contains additional explanations about the Stability-Constrained Static Optimization (SCSO) framework, including how the framework specifically composes the stability constraints as well as some important assumptions and practical remarks.

### *A–SI. 1.2 Framework Development: Stability Constraint*

The third constraint that the framework composes in the optimization (OPT) problem to calculate muscle activations and forces is the stability constraint. To generalize the applicability of the framework, the simplified stability equations by Potvin & Brown (2005) were employed because the parameters in these equations can be elicited for any musculoskeletal model during any movement in OpenSim.

Potvin & Brown (2005) discussed the simplified equations for a static system, when an external load P is applied at height h with respect to a joint centre. They discussed the simplified equations for all directions and provided a detailed explanation of the parameters in each equation. However, to elaborate on how the framework works, parameters of the stability equation in the z-direction (i.e., one of the joint-fixed rotational axes) will be explained here. If for the sake of simplicity, we ignore the contribution of passive structures, we have:

$$S_z = \sum_{m=1}^{N}\left[\frac{F(A_x B_x + A_y B_y - r_z^2)}{l} + \frac{q r_z^2}{L}\right] - Ph \qquad \text{(Eq. A.1)}$$

where $S_z$ is the stability of the joint about the Z axis as a function of three terms: i) muscle forces (F), ii) Geometric Stability (GS), which consists of parameters related to the muscles' geometry (i.e., $A_x$, $B_x$, $r_z$, $l$, $L$) and the muscles' stiffness (i.e., $q$), and iii) External Work (EW) parameters

(i.e., $P$, $h$). Stability equations in other directions are similar to this equation (Potvin & Brown, 2005). For a user-defined model, movement, and external force set, all parameters in Eq. A.1 are known parameters except for muscle forces. Therefore, the third constraint in the optimization problem is that $S_z$ should be greater than zero (i.e., the necessary condition of stability) or greater than any other user-defined positive number (i.e., sufficient condition of stability).

To calculate the GS term, points $\mathbf{A}(A_x, A_y, A_z)$ and $\mathbf{B}(B_x, B_y, B_z)$ in Eq. A.1 are muscle insertion node coordinates with respect to the joint of interest and $r_z$ is the functional moment arm of the muscle in relation to the points **A** and **B**. Therefore, this framework computes global coordinates of joints and muscle attachments at each time step by using the Point Kinematics (PK) analysis in OpenSim and then calculates the GS term in Eq. A.1. $q$ is a user-defined constant which relates muscle force and length to stiffness. Some muscles may act on more than one joint, or they might be defined by more than 2 nodes. In Eq. A.1, to calculate stability at a given joint, $l$ for each muscle represents the length of that muscle that acts on that joint, while $L$ is the total length of the muscle. If a muscle has been defined by only 2 nodes, then $l$ is equal to $L$. Considering this fact, the framework first uses a search method in the Muscle Analysis (MA) results to determine which muscles have moment arms (i.e., are active) about each coordinate of a model. In addition, the framework identifies which muscles have moment arms about more than one coordinate (e.g., in the gait2392 model, Rectus Femoris has moment arms about both the hip and knee joints). Then, to calculate the GS term about a certain coordinate, using the .osim file, the framework determines the number of muscle nodes that act on that coordinate and which muscle nodes should be considered for calculation of $l$. Using PK analysis for those nodes, $l$ is calculated about each coordinate. For the calculation of $L$, however, the framework easily elicits it from MA results.

The external work (EW) term in Eq. A.1 could be due to gravity and/or an external load. To calculate this term, since the presented framework was designed to be as general as possible, users should be aware of the model they are using and might need to modify the required files for running the framework or slightly change the framework's default code. In a model file in OpenSim, users define bodies (i.e., black boxes in Fig. A.1) and every two bodies (i.e., parent and child) are connected together by a joint and each joint may have one or more coordinate(s), which are that joint's degrees of freedom.

Equation A.1 was extracted from an inverted pendulum model (Potvin & Brown, 2005). Based on this model, bodies that are located higher than the joint of interest should be considered in the calculation of the EW term. However, when the joint of interest is a lower limb joint (e.g., left knee in Fig. A.1(b)), some bodies (i.e., right tibia, talus, calcaneus, toes) that have even lower height than the joint of interest should be considered in the calculation of EW because right and left legs are connected to each other through the pelvis. For example, when we flex our right hip and stand on our left leg, the body centre of mass goes up and thereby makes the system less stable because the EW term in Eq. A.1 increases. Therefore, the framework uses an inclusion algorithm (IA) to determine which bodies should be considered in the calculation of the EW term at each joint.

The IA (Fig. A.1): i) examines parent and child bodies at each joint and chooses the body with higher y coordinate (vertical height), ii) ignores the lower parent/child bodies and all children in that chain (e.g., red chain in Fig. A.1(b)), iii) for the chosen body in the first step of the IA, all children should be included in EW calculation (i.e., the green box in Fig. A.1(b)), and also, parent bodies are included only if their height is greater than the child, and any time a parent body is

included, all of its children are included. By using the IA and PK analysis for the model's joints and bodies during a movement, the framework calculates the EW term due to gravity.

The same concept is applied for the calculation of the EW term due to an external load. To define an external load in OpenSim, an XML file and a .mot file are required. In the XML file users define: i) a body to which to apply the force, ii) the bodies to express the force and its location in, and iii) the identifiers that show names of a force and its exertion point in the .mot file. The .mot file contains all measured forces, or desired forces, and their location to which users want to apply them. Since there are many potential ways to define the XML file, the framework has not yet been generalized for all external load conditions. Currently, to apply an external load to any segment in a model, users should express their force and its location based on the global coordinate system. In this way, by examining the XML file, the framework recognizes to which body the force should be applied and thereby can calculate EW due to external load similar to gravity.

In the original article, the general form of stability constraints (i.e., the inequality equation), composed by the framework at each time step, was illustrated as:

$$\begin{bmatrix} [GS_x]_{jm} \\ [GS_y]_{jm} \\ [GS_z]_{jm} \end{bmatrix}_{3j*m} [F]_{m1} - \begin{bmatrix} [EW_x]_{j1} \\ [EW_y]_{j1} \\ [EW_z]_{j1} \end{bmatrix}_{3j*1} \geq [\text{Stability level}]_{3j*1} \qquad \text{(Eq. A.2)}$$

It should be noted in Eq. A.1, the *Ph* term is due to a load in the y-direction, but in fact, in the stability equations, it represents the EW term in the z-direction (i.e., the $EW_z$ matrix in Eq. A.2). This is because the *Ph* term was obtained (Potvin & Brown, 2005) by calculating the second derivative of the work done (W) by load *P* during an infinitesimal rotation about the Z-axis ($\theta_z$)

with respect to Z coordinate (i.e. $EW_z = \frac{d^2W}{d\theta_z^2} = Ph$). Using the same procedure as what Potvin & Brown (2005) used, the EW term due to the load *P* about other coordinates are:

$$EW_y = \frac{d^2W}{d\theta_y^2} = 0 \quad \text{(Eq. A.3)}$$

$$EW_x = \frac{d^2W}{d\theta_x^2} = Ph \quad \text{(Eq. A.4)}$$

In many studies, there only exist gravity loads or sometimes an external force in the gravity direction (i.e., y), and thus, usually $EW_y$=0. If the Stability level matrix in the inequality equation (Eq. A.2) was set to zero, any activation of muscles would satisfy stability in the y-direction. Hence, users of the framework usually can omit the second row of GS and EW matrices in the inequality equation (Eq. A.2) to reduce the runtime.

It is obvious that the central nervous system activates muscles in a way that they can provide stability in all body joints. However, there are some assumptions and limitations within all musculoskeletal models such as modelling a joint with a few number of muscles, or estimation of maximum allowable force for each muscle. Therefore, considering stability constraints at all joints may cause the framework's solver to assign very high activations to some muscles that may not corroborate with experimental (e.g., EMG) data. Hence, some users might be interested to consider stability constraints only for specific joints or specific directions. If users did not intend the SCSO solver to increase the muscle activations to maintain the stability condition at a specific joint and in a specific direction, they would be expected to know the joint number to slightly change the MATLAB code. In OpenSim, joint numbers are based on their chronological order in the osim file. Therefore, for example, if users do not want to consider the stability of the $k^{th}$ joint in a direction (e.g., x-direction), they should put: $[EW_x]_{k1} = [\text{Stability level}]_{k1} = 0$ because in

this way, we cancel the effect of external work; thus, the required muscle activations to maintain the dynamic equilibrium are sufficient to satisfy the inequality equation (Eq. A.2).

### *A–SI. 1.3 Important Considerations with the Framework*

Since the first and second constraints for the optimization problem in the current framework are the same as the default OpenSim Static Optimization solver, as a verification process, it was ensured that without considering the third constraint (i.e., stability constraints), the framework would produce the same results as the default OpenSim solver. However, there is another assumption in the framework's design. OpenSim allows users to define actuators other than muscles for any coordinate because sometimes muscles are not powerful enough to satisfy equilibrium equations by themselves. Since muscles are the only real actuators in the human body, the framework was designed for models that do not require any additional actuators, unless they need actuators for coordinates about which no muscles have moment arms. For instance, in the Gait2392 model, the pelvis-ground joint has 6 coordinates (i.e., pelvis list, tilt, rot, tx, ty, tz), which are required for gait movement simulation, but no muscles have moment arms about these coordinates. Therefore, the default SO solver would not be able to find a solution for muscle forces unless reserve actuators have been defined for these coordinates. These actuators produce exactly the force required for maintaining dynamic equilibrium (i.e., equal to inverse dynamics results). Therefore, users of the presented framework should be aware of their own model, and for models similar to Gait2392, if about coordinate k, no muscles have a moment arm, they should put $[\mathrm{M}]_{c1} = 0$ in Eq. 3.1.

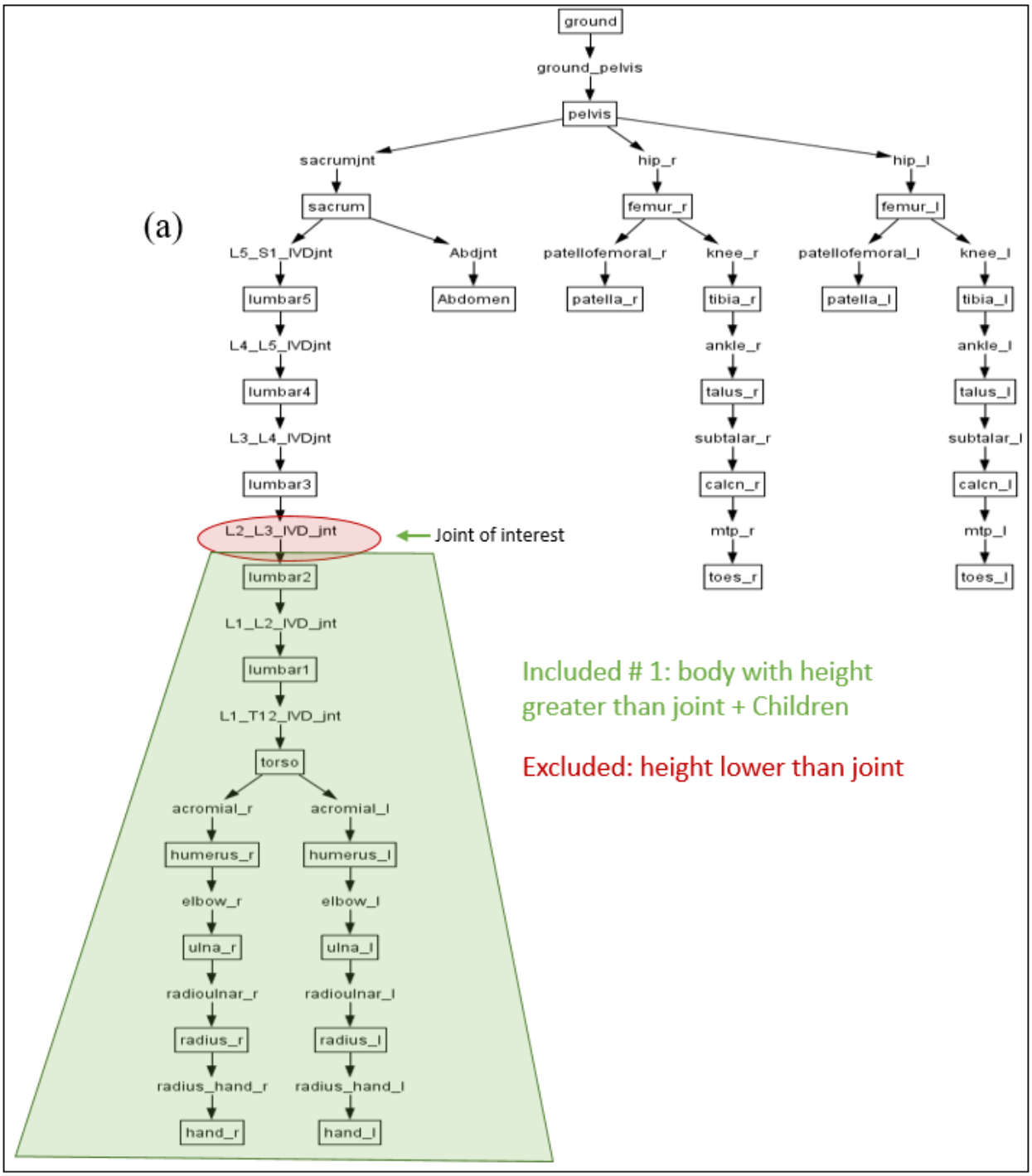
(a)
ground
ground_pelvis
pelvis
sacrumjnt
hip_r
hip_l
sacrum
femur_r
femur_l
L5_S1_IVDjnt
Abdjnt
patellofemoral_r
knee_r
patellofemoral_l
knee_l
lumbar5
Abdomen
patella_r
tibia_r
patella_l
tibia_l
L4_L5_IVDjnt
ankle_r
ankle_l
lumbar4
talus_r
talus_l
L3_L4_IVDjnt
subtalar_r
subtalar_l
lumbar3
calcn_r
calcn_l
L2_L3_IVD_jnt
Joint of interest
mtp_r
mtp_l
lumbar2
toes_r
toes_l
L1_L2_IVD_jnt
lumbar1
L1_T12_IVD_jnt
torso
acromial_r
acromial_l
humerus_r
humerus_l
elbow_r
elbow_l
ulna_r
ulna_l
radioulnar_r
radioulnar_l
radius_r
radius_l
radius_hand_r
radius_hand_l
hand_r
hand_l
Included # 1: body with height greater than joint + Children
Excluded: height lower than joint

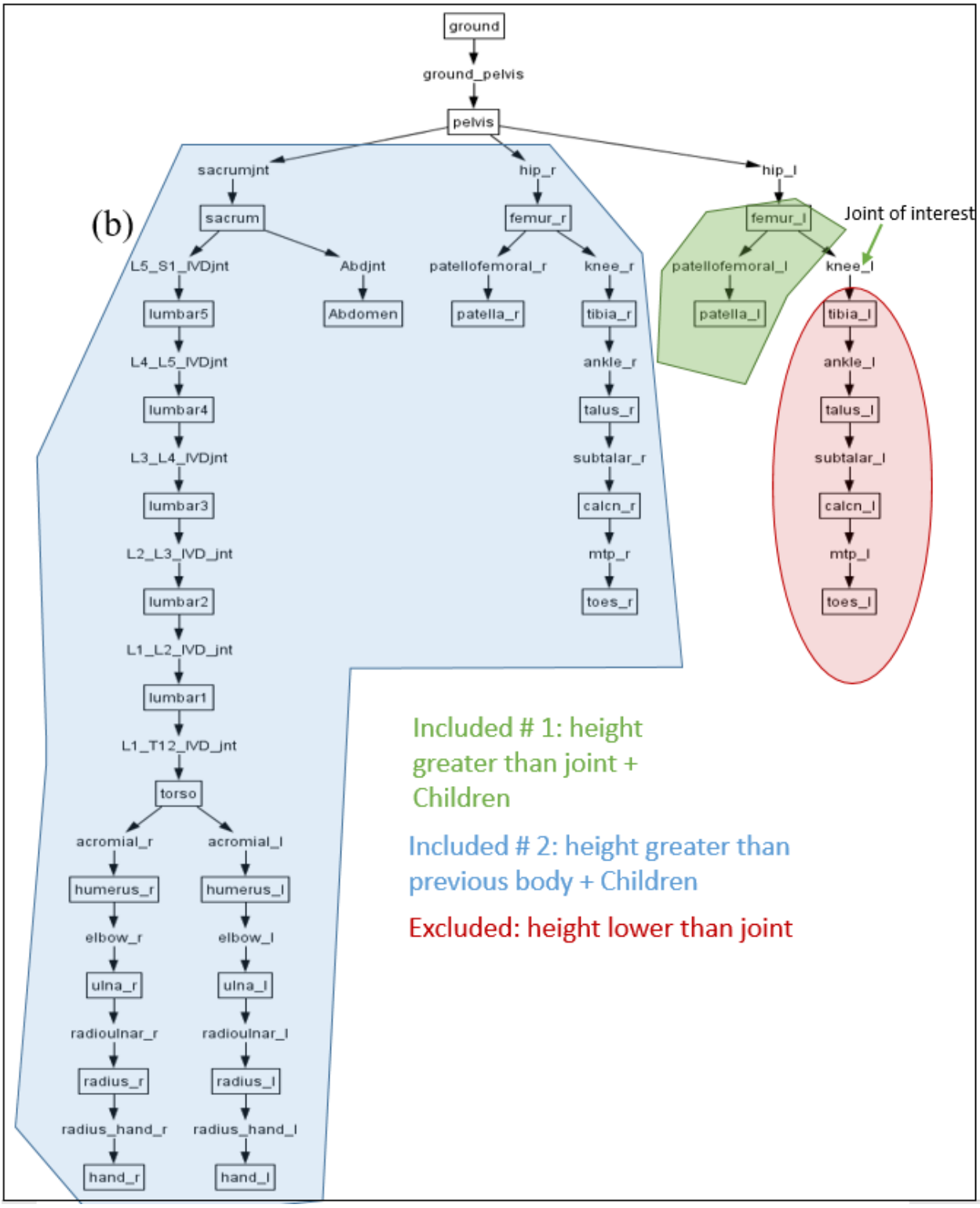


Fig. A.1. Schematic of the inclusion algorithm. (a) shows how the inclusion algorithm works for a desired upper limb joint, and (b) shows how it works for a desired lower limb joint.

### *A–SI. 1.4 references*

Potvin, J.R., Brown, S.H.M., 2005. An equation to calculate individual muscle contributions to joint stability. J. Biomech. 38, 973–980.

## A–SI. 2

### *A–SI. 2.1 Introduction*

This supplementary material consists of methods, results, and discussion about the lower limb study (i.e., gait2392 model).

### *A–SI. 2.2 Methods*

To show the Stability-Constrained Static Optimization (SCSO) framework could be used within previously developed models in OpenSim, the gait2392 model from OpenSim was chosen to assess the SCSO framework's performance versus the default Static Optimization (SO) solver in the estimation of muscle activations. The gait2392 model has 12 joints, 23 degrees of freedom (DOF), and 92 muscles. As a verification process, it was assured that during a gait movement (motion data exist in the OpenSim example files), without considering stability constraints, SCSO produces the same muscle forces as the default SO solver while considering muscles' force-length-velocity (FLV) manifold. Thus, hypothetically, the framework can be used within any model, with any number of DOF and muscles.

In the present study, SO and SCSO solvers were compared against experimental EMG data during a normal standing task and a hip flexion task. Three healthy males voluntarily participated in the experiment. Mean (SD) participant mass, height, and age were 79 (9) kg, 175 (6) cm, and 25 (1) years, respectively. The study was approved by the University of Ottawa's Research Ethics Board (H-06-18-721) and written informed consent was obtained from the participants. The participants were asked to stand normally for five seconds. Then, they were asked to flex their right hip as much as they could and maintain a static single-leg stance for five seconds while their

arms were relaxed at their sides (Fig. A.2), and this hip flex trial was repeated three times for each participant. The experiment was conducted in the Human Movement Biomechanics Laboratory at the University of Ottawa. 39 markers were placed on participants according to an example OpenSim model for the study of gait (i.e., subject01_simbody.osim). Marker data during standing and hip flexion tasks were collected at 30 Hz using a 10 camera Vicon Vantage V5 (Vicon Motion Systems, Oxford, UK) motion capture system and force data were collected at 2000 Hz using FP4060 force plates (Bertec Corporation, Columbus, OH, USA). Six wireless surface EMG electrodes (Trigno, Delsys Inc., Natick, MA, USA) were placed on the left leg (i.e., the contralateral leg in the hip flexion task), and EMG data from six muscles, namely Rectus Femoris (RecFem), Vastus Medialis (VastMed), Vastus Lateralis (VastLat), Biceps Femoris (BiFem), Tibialis Anterior (TibAnt), and Gastrocnemius Medialis (GasMed) were collected at 2000 Hz.

Fig. A.2. The simulated hip flexion task in OpenSim.

EMG was measured during the static trials and a maximum isometric voluntary contraction (MVC) task for each muscle. All EMG data were filtered in MATLAB using a common procedure (Ross et al., 2015). First, the DC bias was removed and then the raw EMG data were bandpass filtered between 20 and 450 Hz using a $4^{th}$ order Butterworth filter. Afterwards, to produce a linear envelope, the bandpass filtered data were rectified and a low pass filter with a 2.5 Hz cutoff frequency was applied using a $2^{nd}$ order Butterworth filter. After filtering of the EMG signals, for each muscle, the mean activity of that muscle during each static trial was calculated and normalized to the maximum value of the MVC signal (% mean activity). Then, for each participant, the % mean activity of each muscle were averaged across all static trials, and this average value for each muscle was used for analyzing the data.

The gait2392 model was scaled for each participant using the Scale tool in OpenSim, where the dimensions of body segments for each participant were determined using the markers that were placed on the anatomical landmarks. Then, using the marker data, Inverse Kinematics (IK) analysis was accomplished in OpenSim. Muscle activations and forces were calculated by the default SO solver using the IK data, force plate data, and the 6 necessary reserve coordinate actuators (i.e., actuators for the pelvis list, tilt, rot, tx, ty, tz coordinates) for the gait2392 model.

As was already explained (Appendix A–SI. 1), there are some assumptions and simplifications within both the SCSO framework (e.g., value of $q$) and musculoskeletal models. For the gait2392 model, if we wanted to satisfy the stability constraint about all coordinates, even with $q$=150, SCSO would not work properly (e.g., muscles reach their maximum allowable force). Thus, to keep the $q$ in the reported range without changing the muscle features in the model file, only hip stability in x (i.e., anterior-posterior) and z (i.e., medial-lateral) directions were considered. Satisfying stability requirements only at the hip joint is an improvement by itself

because the predicted muscle forces by the default SO solver do not satisfy these requirements at the hip nor other joints.

In this study, $q$ was set to 15 for all muscles (SCSO-q15) as well as a varying q to show how different values of q affect the SCSO framework's results. In this case, q was set 25 for BiFem, 5 for RecFem, and 15 for other muscles (SCSO-qDiff).

To evaluate the performance of the traditional SO and SCSO, first, the average of measured EMG data (%MVC) during the standing and 3 hip flexion trials, as well as the average of estimated muscle activations by SO, SCSO-q15, and SCSO-qDiff, were calculated. Then, we defined the term index number, which for each muscle means the difference of the measured or estimated activity between the hip flexion task and standing. For example, a positive index number for a muscle means the measured or the estimated muscle activity in the hip flexion task is more than the standing posture. Comparing the signs of the index numbers for the different models (i.e., SO, SCSO-q15, and SCSO-qDiff) against the measured EMG index numbers, demonstrates whether the strategy of the models in activating muscles corroborate with the trend of the experimental data. To elaborate on how the estimated muscle activations are quantitatively in agreement with the experimental data, for each muscle, the absolute value of the difference between the prediction methods index number and the measured EMG index number was calculated as an error indicator (eTrend).

***A–SI. 2.2 Results***

For each participant, the average of measured EMG data (%MVC) and estimated muscle activations by SO, SCSO-q15, and SCSO-qDiff across the three trials were shown (Fig. A.3). The calculated index numbers show that out of a total of 18 possible modes (6 muscles × 3 participants), traditional SO, SCSO-q15, and SCSO-qDiff, in 10, 6, and 6 cases respectively, predicts an opposite

trend to the experimental (EMG) data. Furthermore, the eTrend analysis shows for all muscles, except for the GasMed, the SCSO framework, especially SCSO-qDiff, generally predicts muscle activations that are more representative of EMG data (Fig. A.3, average results).

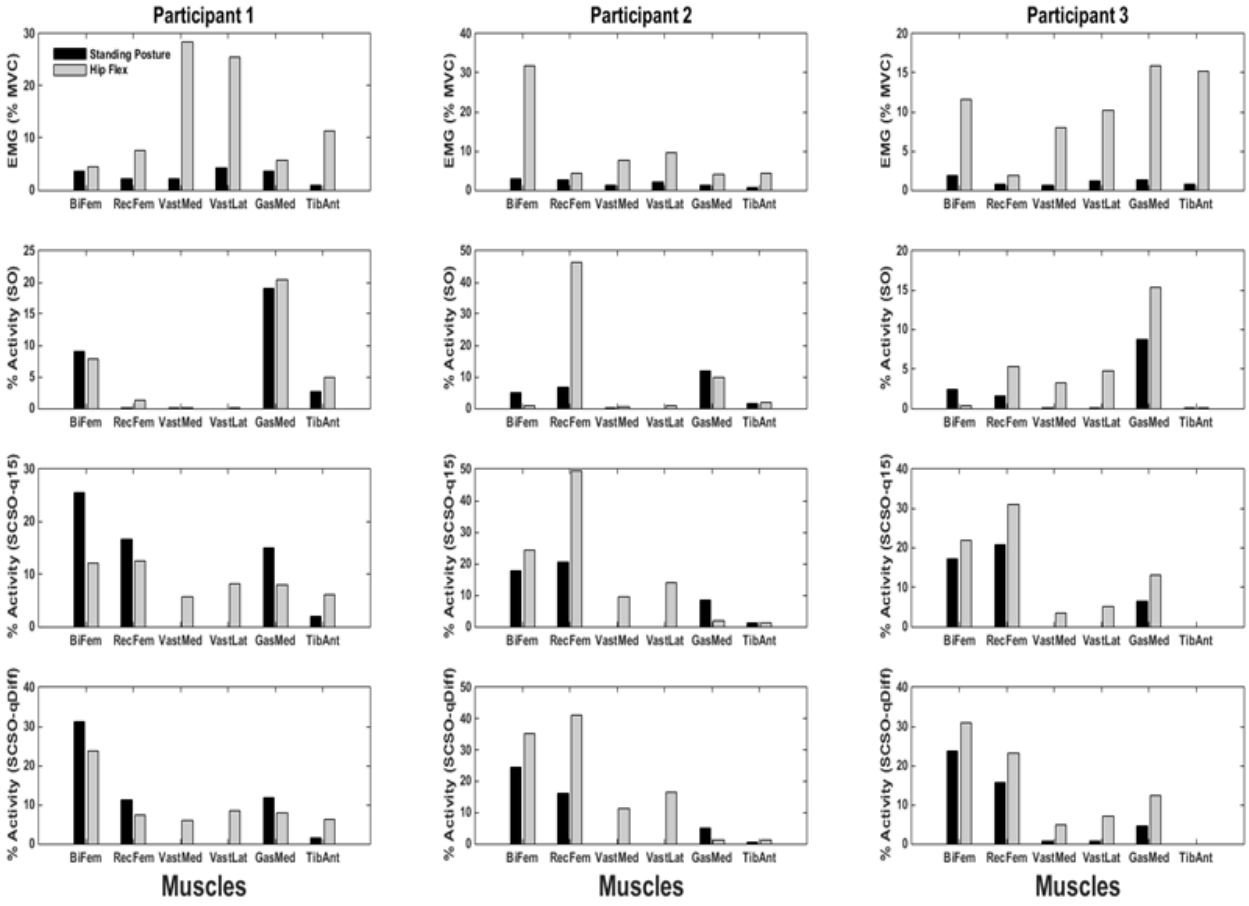


Fig. A.3. Muscle activation results. Average of measured EMG activities of muscles (%MVC), including BiFem, RecFem, VastMed, VastMed, VastLat, GasMed, and TibAnt, from the left leg, during the standing and right hip flexion tasks, were compared to the estimated activities of these muscles by the traditional SO, SCSO-q15, SCSO-qDiff for the three participants in the present study.

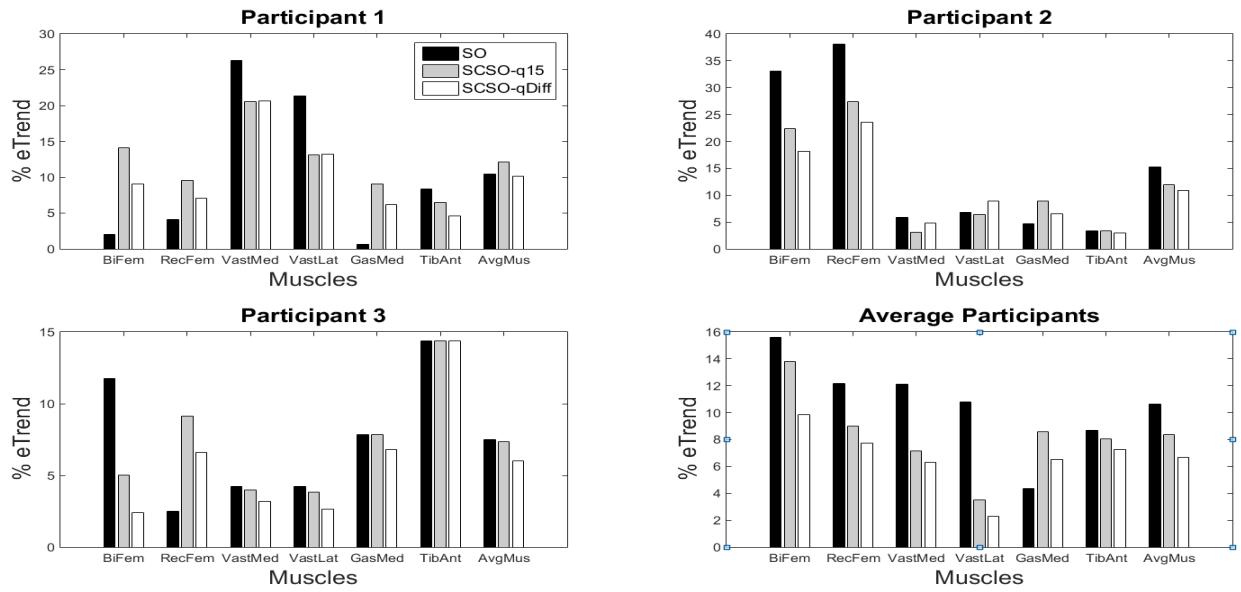


Fig. A.4. Percentage of eTrend values. The % eTrend value for each muscle and each individual were computed and shown. In addition, the average of eTrend values for all participants was shown.

### *A–SI. 2.4 Discussion*

In this lower limb study, there are many coordinates and muscles, and many muscles are multi-articular, thus, many muscles might be semi-antagonist (i.e., agonist relative to one coordinate and antagonist with respect to another coordinate). As it was explained in Chapter 3, the assigned muscle activations to the semi-antagonist muscles depend on many factors and cannot simply be analyzed. In addition, in the present lower limb study, sometimes the sign and value of the external moment about a same coordinate were different between different participants. For example, in the standing posture, there is a flexor moment in the hip joint for participant 1, while for participant 2 and 3 there is an extensor moment in this joint. Therefore, to compare the estimated muscle activations to the experimental data, a separate explanation for each individual and muscle is required.

VastMed and VastLat only have moment arms about the knee joint (one coordinate), thus analyzing the external moment at the knee could elaborate on how the prediction methods assign

activations to these muscles. In the standing posture, for all participants VastMed and VastLat are antagonistic muscles, and thereby, the traditional SO assigns zero activations to these muscles. Similarly, attempting to minimize the same objective function for muscle activations as the default SO solver, the SCSO framework in most cases assigns zero activations to the VastMed and VastLat in the standing posture. Although the measured EMG shows that VastMed and VastLat are active in the standing posture contrary to the models, the measured activities are very small (i.e., an average of ~1.3% and 2.5% for VastMed and VastLat respectively).

When changing from the standing to the hip flexion task, the measured EMG data clearly show the activities of VastMed and VastLat increase for all participants. In the hip flexion task, for participant 1, VastMed and VastLat are antagonist, and thus, with the same reasoning as the standing posture, SO does not activate these muscles contrary to the experimental data. However, due to the existence of external knee extension moment for both participant 2 and 3 in the hip flex task, VastMed, VastLat, and RecFem are agonist with respect to the knee joint and could be activated by the default SO solver. Since RecFem also articulates the hip joint, its assigned activation by the default SO solver also depends on the three hip coordinate (i.e. hip-flex, hip-add, and hip-rot coordinates) moments. During the hip flexion task, the hip-flexion coordinate moment is different between participants 2 and 3 (i.e., extension (+) for participant 2 and flexion (-) for participant 3). This difference means that for participant 2, the default SO solver only activates RecFem, in disagreement with the experimental data; however, for participant 3, it distributes muscle activations between VasMed, VasLat, and RecFem. To mathematically explain this phenomenon, consider these sets of the OPT problem:

Problem Set 1:
Minimize $x^2 + y^2 + z^2 + t^2 + u^2$

Subject to:

$$x + y + z = 5$$

$$x + t = 10$$

$$x + u = 10$$

$$x, y, z, t, u \geq 0$$

Answer: x=5, y=0, z=0, t=5, u=5

Problem Set 2:

Minimize $x^2 + y^2 + z^2 + t^2 + u^2$

Subject to:

$$x + y + z = 5$$

$$x + t = 10$$

$$-x + u = 10$$

$$x, y, z, t, u \geq 0$$

Answer: x=0.7, y=2.15, z=2.15, t=9.3, u=10.7

Problem set 1 and 2 are mathematical models for participants 2 and 3 respectively during the hip flexion task, assuming that everything for participants 2 and 3 is the same, except that RecFem for participant 3 is antagonistic with respect to the hip-flexion coordinate. In both problem sets, x, y, z, t, u are respectively a model of RecFem, VastMed, VastLat, all agonist muscles that have moment arms about the hip-adduction coordinate, and all agonist muscles that have moment arms about the hip-flexion coordinate in the gait2392 model. The OPT problems' equality constraints are models of the equilibrium equations in the knee, hip-adduction, and hip-flexion coordinates. The answers of these problem sets show how it is possible that for participant 2 (problem set 1), during the hip flexion task, the default SO solver only activates RecFem (x), but for participant 3 (problem set 2) distributes muscle activations between RecFem (x), VastMed (y),

and VastLat (z), although all of these muscles are agonist with respect to the knee joint (i.e. equality constraint 1 in problem set 1 & 2 is same).

Similar to RecFem, BiFem also has moment arms about both hip and knee joints. Therefore, to explain the assigned BiFem activation by the models, the external moment at both knee and hip coordinates should be considered. For all participants, the hip-adduction coordinate moment changes from a small positive or negative number (absolute average value of all participants ~2 N.m) at the standing posture to a large negative number (~ –55, ~ –50, and ~ –40 Nm for participant 1, 2, and 3 respectively) at the hip flexion posture. Therefore, in the hip flexion task, BiFem is considered an antagonist muscle by the models with respect to the hip-adduction coordinate. Thus, the default SO solver assigns less activation to BiFem in the hip-flexion task than in the standing posture, which is clearly opposite of the EMG data, especially for participant 2 and 3.

Explanation of the framework's results in this study should be based on the dynamic equilibrium requirements in all coordinates and stability requirements at the hip coordinates simultaneously. Attempting to stabilize the hip joint, in both standing and the hip flexion task, the SCSO framework assigns higher activation to BiFem than SO. To compensate the generated moment by the BiFem at the knee joint, the framework either assigns a higher activation to only RecFem (e.g., standing posture for all participants), or distributes the activations between RecFem, VastMed, and VastLat (e.g., in the hip-flexion task for all participants). Part of the increment in the calculated RecFem activation by the framework may also be due to its role in stabilizing the hip joint.

The calculated TibAnt activations by the default SO solver are due to its agonist role about the subtalar coordinate in this study, and since the external moment at the subtalar coordinate was

very small during all tasks, predicted muscle activations by the default SO solver are very small (average of ~1.4% and ~3.3% during the standing and hip flexion postures respectively). However, the higher measured EMG activity of TibAnt in the hip flexion posture than in the standing posture suggests the CNS might activate TibAnt in the hip flexion task to stabilize the ankle. Since ankle stability was not considered in this study, the calculated TibAnt activations by SCSO do not match well the experiment, similar to the default SO solver.

GasMed has moment arms about the knee and the ankle. Similar to TibAnt, since the stability of knee joint was not considered, patterns of estimated muscle activations by the default SO solver and the SCSO framework are similar.

In sum, in this lower limb study, it was shown that the predicted muscle activations by the default SO solver, which solely considers equilibrium constraints, do not match the experimental data. By considering only hip stability, the SCSO framework better estimates trends of activation of BiFem, RecFem, VastMed, and VastLat than the traditional SO, and by changing the $q$ value, it was also improved (Fig. A.4). Nevertheless, it cannot be concluded that the strategy of the SCSO framework to activate these muscles in this study is the same strategy as the CNS because of two main reasons. First, in some cases (e.g., BiFem and RecFem for participant 1), the predicted muscle activation trends do not match the experiment. Second, the strategy of the CNS can be predicted better if we utilize a model that can satisfy the equilibrium and stability constraints at all coordinates. For example, the higher activation of VastMed calculated by the SCSO framework in the hip flexion task versus the standing posture corroborates with experimental data, but it was achieved because of BiFem and RecFem roles in the hip joint's stability, while the CNS might in actuality activate VastMed to stabilize the knee.

This study showed that due to the existence of many muscles and coordinates in the gait2392 model, interpretation of results obtained by the traditional SO solver is complicated. Clearly, the interpretation of the SCSO framework's results is more complex because the parameters of stability are also included in the OPT problem. Nevertheless, based on the spine study in the original article and this lower limb study, there are general rules that can be concluded for a desired model and series of tasks that users intend to simulate:

1) If the estimated results by the traditional SO solver fully corroborate with experimental data, it means that the behaviour of the system can be explained by the role of muscles only by balancing external moments (i.e., all respected previous OpenSim studies that validated their models' results). In this situation, by assigning a proper stiffness to muscles, the SCSO framework could produce the same results as the default SO solver.

2) If the estimated results by the default SO solver do not match well to experimental data, by considering the role of muscles in stability, the framework could produce more promising results than the default SO solver (the spine study in Chapter 3).

3) If the framework produces results that are similar to the default SO solver's results and both do not match well with experimental data (the lower limb study in the present supplementary material) there might exist several possible reasons:

    a) Issues that also affect the common OPT problem (i.e., without stability criteria) such as muscles' geometry and features. In this case, attempting to build subject-specific models by assigning more accurate values to the parameters used in the common OPT problem might improve the calculated results by the framework.

b) Issues related to the stability constraints. For example, the predicted muscle forces by the default SO solver are also satisfied the defined stability constraints. In this case, by lowering $q$, or increasing the required stability level, the SCSO framework's results might match better with the experimental results.

### *A–SI. 2.5 References*

Ross, G.B., Mavor, M.P., Brown, S.H.M., Graham, R.B., 2015. The effects of experimentally induced low back pain on spine rotational stiffness and local dynamic stability. Ann. Biomed. Eng. 43, 2120–2130.

## A–SI. 3

### *A–SI. 3.1 Introduction*

The results in the original article and A–SI.2 indicated that the calculated muscle activations and forces by the new SCSO framework can better-replicate experimental EMG, versus predictions from traditional SO. However, the computational time of SCSO is also required to be compared against that of SO.

### *A–SI. 3.2 Methods*

All simulations in the original article and A–SI. 2 were run on a computer with a 3.41 GHz Intel(R) Core (TM) i5-7500 CPU and 16 GB of RAM. The reported runtime for SCSO includes the runtime for Inverse Dynamics, Muscle Analysis, and Point Kinematics Analysis for bodies, joints, and muscles. Scaling and Inverse Kinematics runtimes were not included because both SO and SCSO require these steps to calculate muscle forces. Eleven and 150 frames were analyzed, respectively, for all simulations of the spine model (Chapter 3) and the lower limb model (A–SI. 2).

### *A–SI. 3.3 Results*

For both models, the details of read/write times for different operations (e.g., Muscle Analysis) in the framework were reported (Table A.1). The average SO and SCSO runtimes for the spine model were 0.2 and 1.08 s respectively (i.e., SCSO was ~ 5 times slower than SO). For the lower limb model with 13 bodies, 12 joints, and 92 muscles (A–SI. 2), the average SO and SCSO runtimes were 21.4 and 79.6 s respectively (i.e., SCSO runtime was ~ 4 times more than SO).

Table A.1. Details of read/write runtimes for different operations in the framework. Each step in the new developed SCSO framework was run separately for both spine (original article) and Gait2392 (supplementary material 2) models during different tasks, and the average runtime for each operation was reported in this table.

| Operation Name | Runtime for Spine Model (s) | Runtime for Gait2392 Model (s) |
|---|---|---|
| Point Kinematics for bodies | 0.08 | 4.67 |
| Point Kinematics for joints | 0.06 | 0.73 |
| Point Kinematics for muscles | 0.47 | 38.62 |
| Muscle Analysis | 0.11 | 24.75 |
| Inverse Dynamics | 0.04 | 1.27 |
| External work calculation | 0.09 | 0.09 |
| Internal work calculation | 0.04 | 0.22 |
| Optimization and calculating muscle forces | 0.19 | 9.25 |
| Total time | 1.08 | 79.6 |

### *A–SI. 3.4 Discussion*

The newly developed SCSO framework runtime depends on the number of bodies, joints, and more importantly on the number of time steps and muscles. For example, for the very simple spine model, which only has 12 muscles and each muscle has been defined by only two insertion points, 24 nodes should have been read and analyzed. However, for the lower limb model with 92

muscles, in which some muscles have been defined with more than two insertion points, many more nodes should have been analyzed.

Point Kinematics analysis for joints took significantly longer than the same analysis for bodies in the gait2392 model because we considered stability only in the right and left hip joints (A–SI. 2), and thus, only global positions for these two joints were obtained. However, regardless of the number of joints, all bodies' centre of masses were required for the inclusion algorithm (A–SI. 1). Even if all joints were considered in the simulation for gait2392 model, the Point Kinematics analysis runtime for joints would not be longer than 4.67 s because the number of bodies was more than joints.

Although the total runtime was more in SCSO, the optimization speed for calculating muscle forces was the same (spine model), or even faster (gait2392 model) in SCSO (Table A. 1). The main part of the SCSO runtime is allocated to the processing of the data before the optimization procedure (mainly Muscle Analysis and Point Kinematics for muscles).

There is a trade-off between the accuracy of SCSO and the performance speed of SO. In the present study, we developed this novel SCSO framework in MATLAB due to its widespread use in the biomechanics community (Lee and Umberger, 2016). However, by interfacing the present framework directly with the OpenSim C++ libraries and hence accessing the state variables (muscle moment arms, joint locations in the world frame, etc.) directly from memory, it would be possible to reduce the total runtime for the new developed SCSO framework in future implementations. Nevertheless, regarding the time cost, the aforementioned runtime results suggest that using the new developed SCSO framework is feasible and still much faster than other alternative methods (e.g., forward dynamic approach) that have been suggested to address the limitations of static optimization (Anderson and Pandy, 2001).

### *A–SI. 3.5 References*

Anderson, F.C., Pandy, M.G., 2001. Dynamic optimization of human walking. J. Biomech. Eng. 123, 381–390.

Lee, L.-F., Umberger, B.R., 2016. Generating optimal control simulations of musculoskeletal movement using OpenSim and MATLAB. PeerJ 4, e1638.

# Appendix B: Study 2 Supplementary Information

## B–SI. 1

This supplementary table provides the duration of the motion cycle for each task to allow a better understanding of the velocity differences among the tasks.

Table B.1. Duration of the motion cycle for each task.

| Task | Motion Cycle Duration (s) |
|---|---|
| **Stoop–5** | 2.2667 |
| **Stoop–20** | 2.9667 |
| **Stoop–20–Slow** | 11.1000 |
| **Stoop–20–Fast** | 1.2667 |
| **Squat–5** | 2.4667 |
| **Squat–20** | 3.4667 |
| **Squat–20–Slow** | 8.2000 |
| **Squat–20–Fast** | 1.3667 |

**B–SI. 2**

We provide this example to show that the two half-boxes will move substantially if they are not fused with a Weld Constraint in Approaches 3 and 4 for the IK analysis. We removed the Weld Constraint between the half-boxes in Approach 3 and ran an IK analysis for the Stoop–20 task. The marker errors were in the same range as those obtained when there was a Weld Constraint between the two half-boxes; therefore, the relative movement of the half-boxes is not due to marker tracking error. Afterwards, to calculate the relative location and orientation of the Box_R and Box_L bodies, we ran a Body Kinematics (BK) analysis for Box_R and Box_L in two conditions: i) the Weld Constraint was present, and ii) the Weld Constraint was removed. We plotted the distance between the Box_R and Box_L centres of mass, as well as the differences in the orientations (space-fixed X–Y–Z Euler angles) of Box_R and Box_L for both conditions (Fig. B.1). During the motion cycle, the COM distance change (*max – min*) was 2.4 cm, and the X, Y, and Z orientation change between Box_R and Box_L were 11.1°, 6.9°, and 1.5°, respectively, when there was no Weld Constraint between the half-boxes. Therefore, the rigidity of the box would not be maintained if the half-boxes were not connected with a Weld Constraint during the IK analysis.

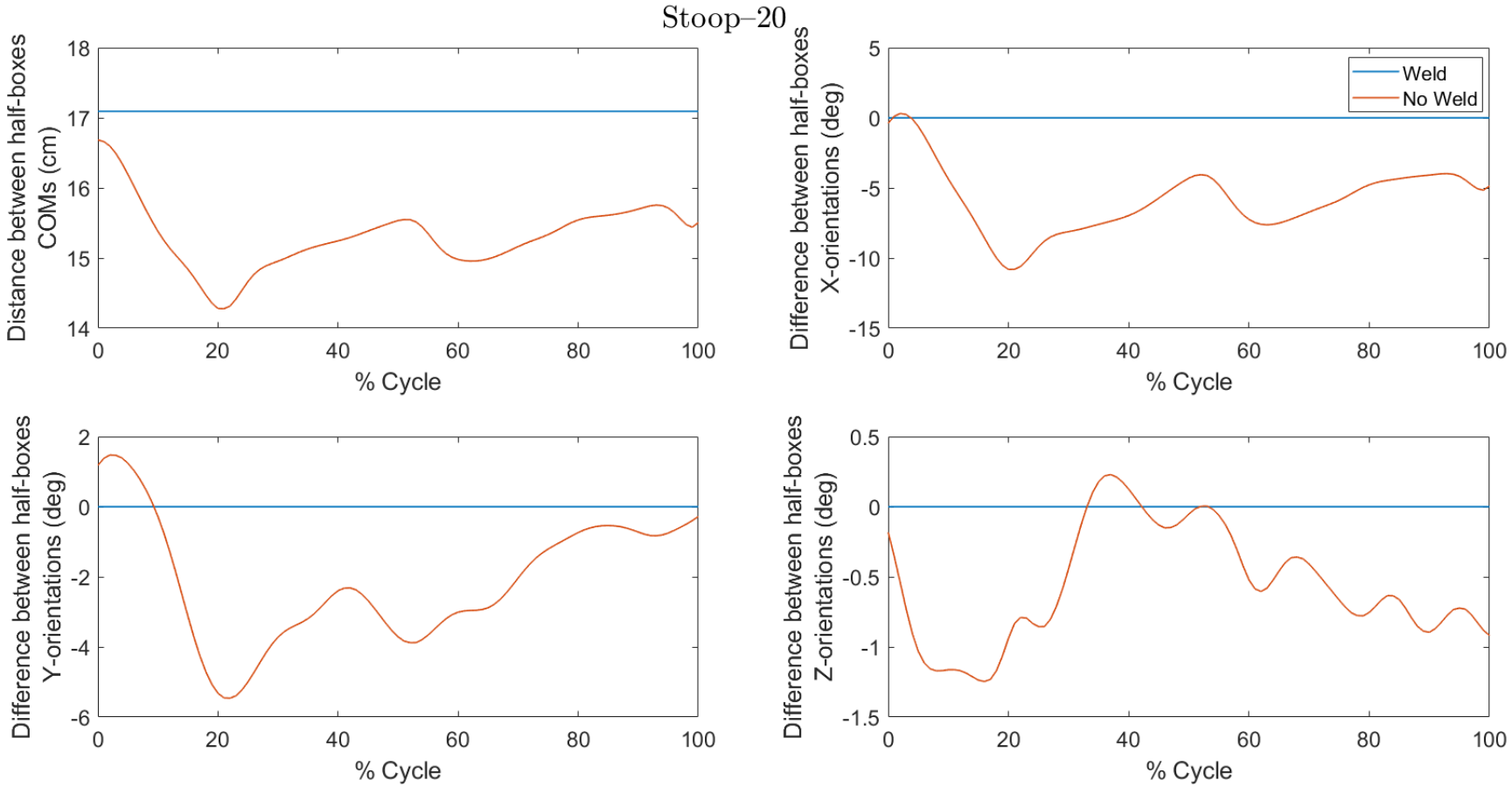


Fig. B.1. The distance between the Box_R and Box_L centres of mass, as well as the differences in the orientations (space-fixed X–Y–Z Euler angles) of Box_R and Box_L for two conditions: with the Weld Constraint (blue), and without the Weld Constraint (orange) between the two half-boxes.

**B–SI. 3**

In general, if we apply the internal forces obtained by an inverse approach (e.g., SO) to the model with no feedback or correction mechanism, the predicted coordinates will diverge from the original trajectory over time. This is true for any chaotic system. Therefore, for instance, in the Computed Muscle Control (CMC) algorithm in OpenSim, proportional–integral–derivative controllers are used along with SO to ensure the target trajectories are tracked (see the methods for Approach 5 in the manuscript). Here, we provide an illustrative example. For the Stoop–20 task, the forces predicted in the Weld Joint between the hands and box from Approaches 3 and 4 were applied to the box in a forward simulation. The distance (cm) between the predicted and measured box top-front-right (TFR) marker was compared to that obtained when Approach 5 was used to calculate the external hand forces and moments (EHF&M). We observe the expected increases in error.

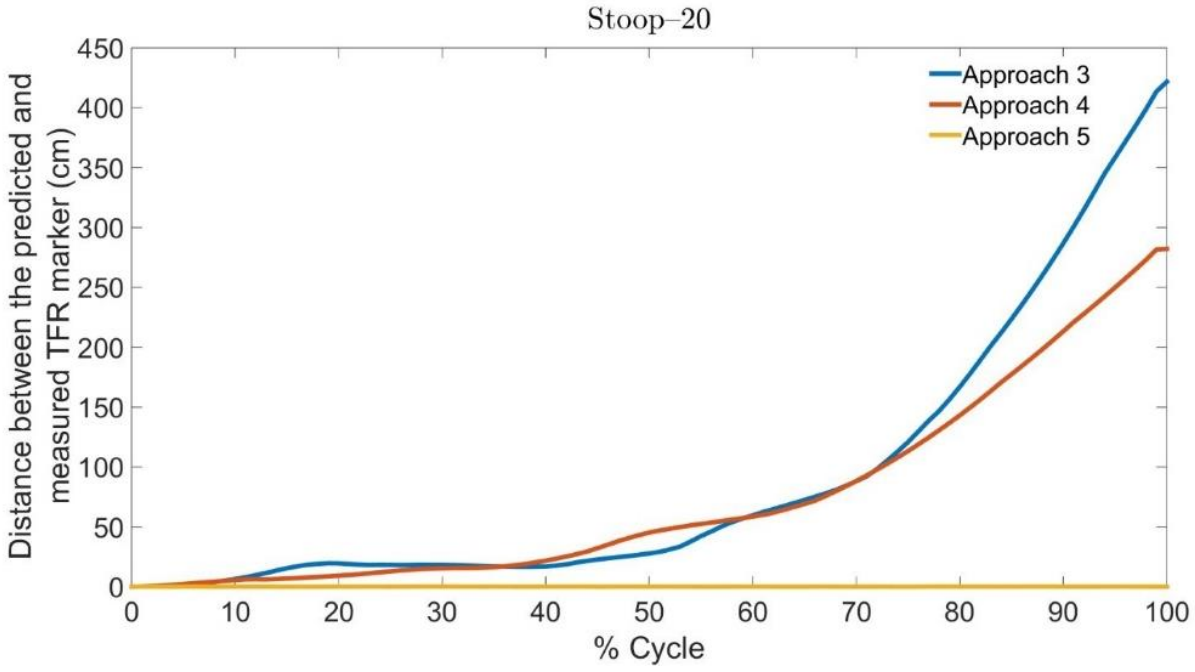


Fig. B.2. The distance (cm) between the predicted and measured box markers during the motion cycle for the Stoop–20 task, where the Forward Dynamics Tool was used to predict the positions of the box top-front-right (TFR) marker using the external forces and moments obtained by Approaches 3 and 4 versus those obtained by Approach 5.

**B–SI. 4**

To assess the validity of predicted EHF&M in Approach 5, the Forward Dynamics Tool was used to predict the positions of the eight markers on the box, where the predicted $\mathbf{F}_{\text{Rhandle}}$ and $\mathbf{F}_{\text{Lhandle}}$ in Approach 5 were applied to the box at the predicted $\mathbf{r}_{\text{RCOP}}$ and $\mathbf{r}_{\text{LCOP}}$ positions. As an example, the distance between the predicted and measured box markers for the Stoop–20 task is shown in Fig. B.3.

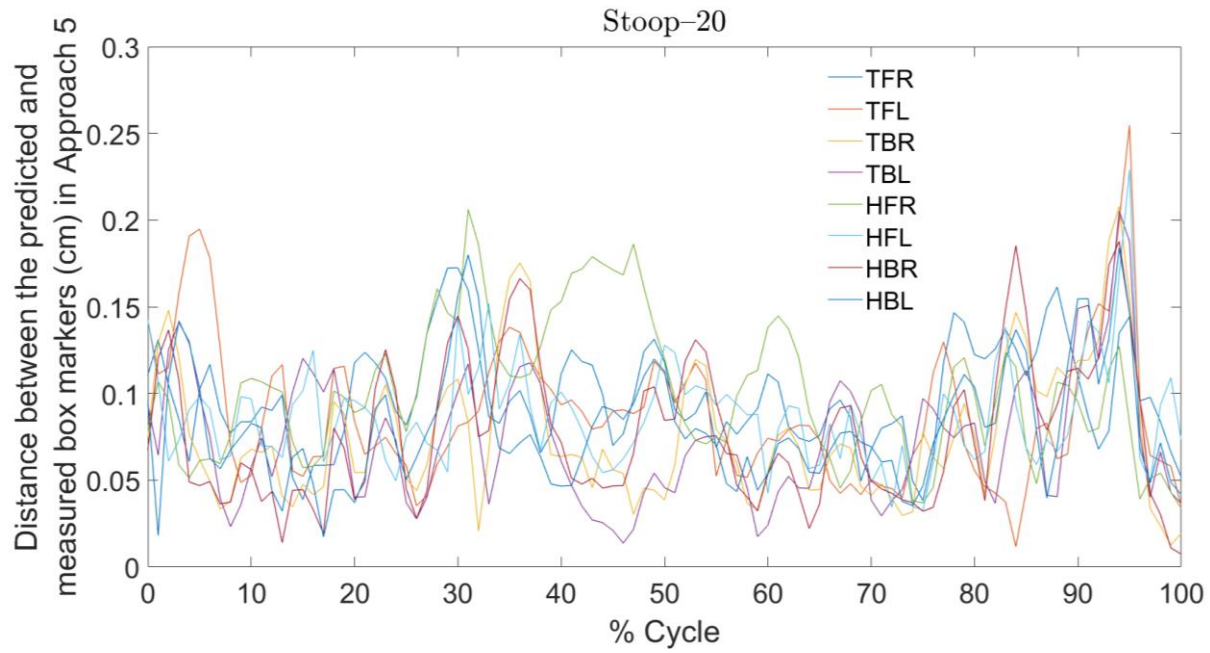


Fig. B.3. The distance (cm) between the predicted and measured box markers during the motion cycle for the Stoop–20 task, where the Forward Dynamics Tool was used to predict the positions of the eight markers on the box using the external forces and moments obtained by Approach 5. Labels are composed of the letters T, H, F, B, R, and L to denote markers on the top, handle, front, back, right side, and left side of the box, respectively.

**B–SI. 5**

Figures B.4–B.11 allow researchers to calculate the differences between the predictions of each EHF&M modelling approach at different percentages of the motion cycle during each task.

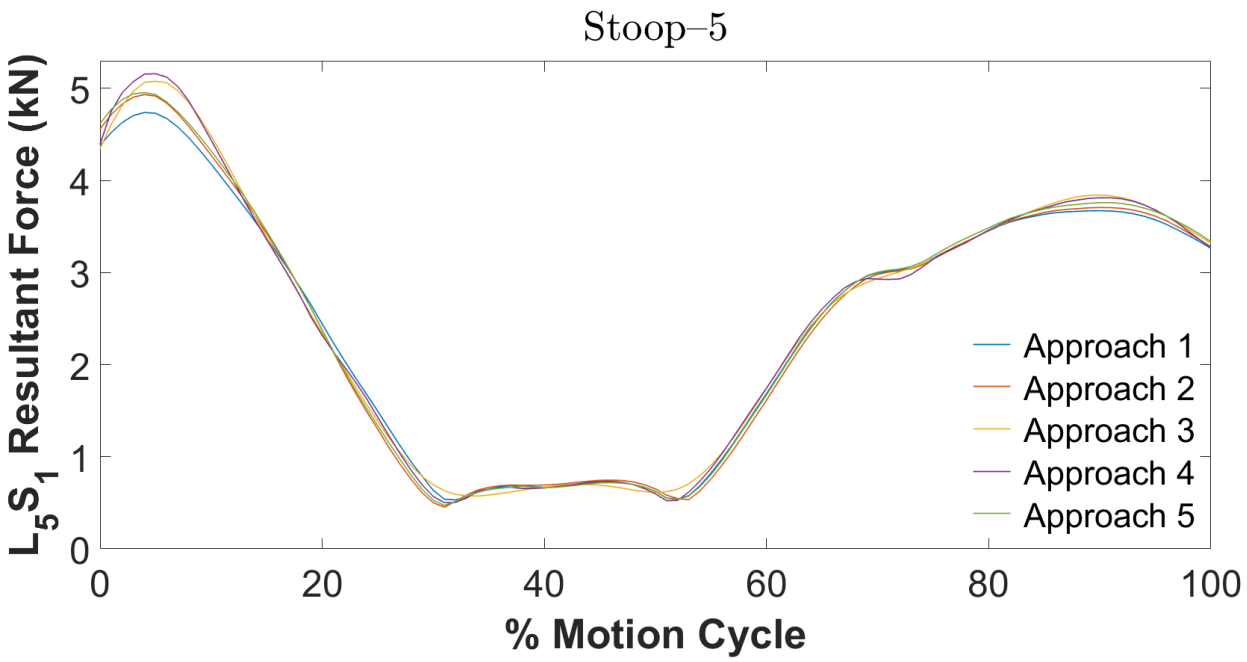


Fig. B.4. The $L_5S_1$ resultant force predicted by each modelling approach during the Stoop–5 task.

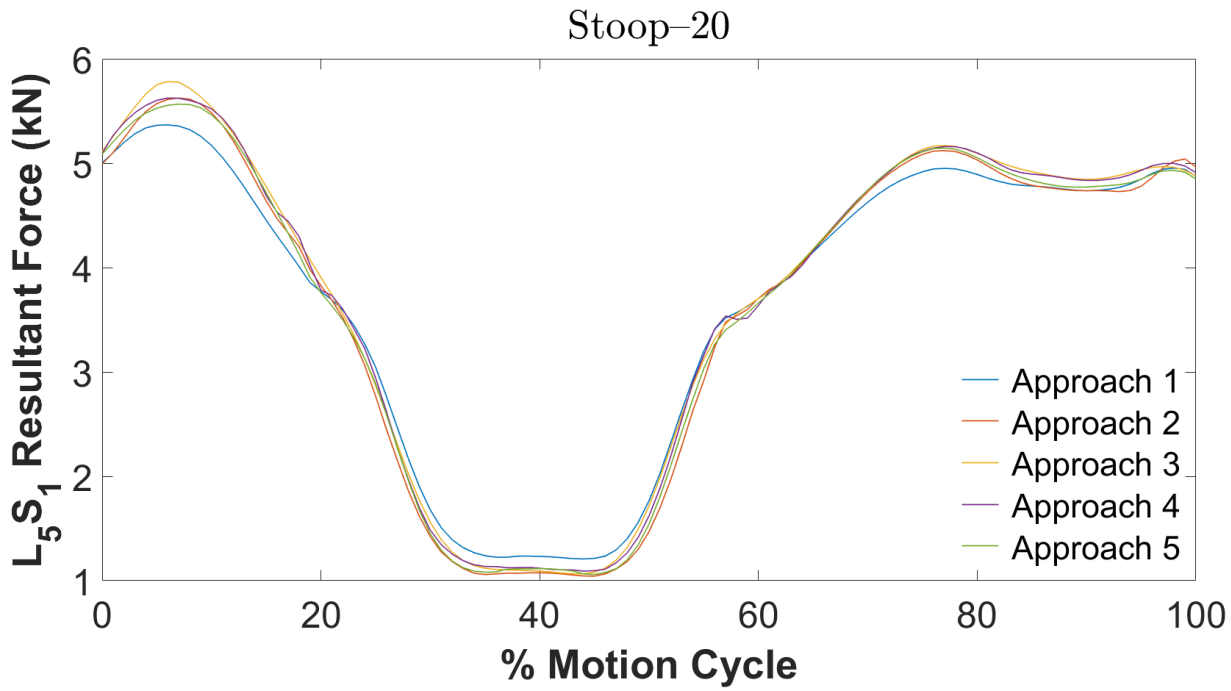


Fig. B.5. The $L_5S_1$ resultant force predicted by each modelling approach during the Stoop–20 task.

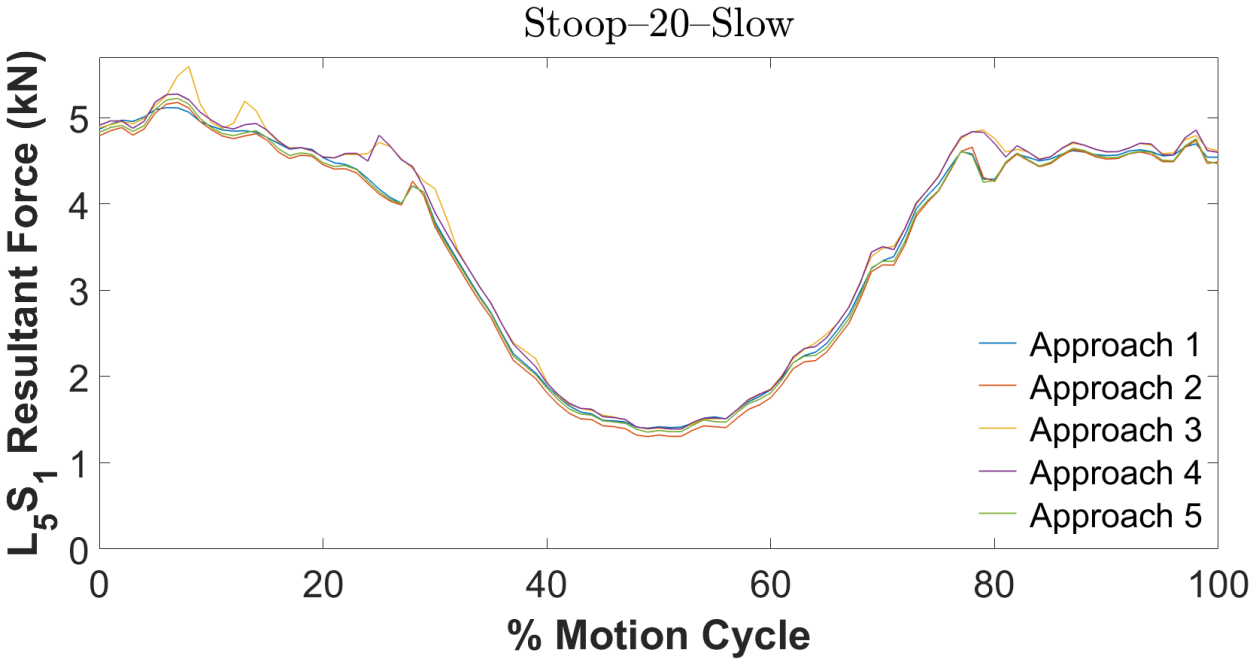


Fig. B.6. The $L_5S_1$ resultant force predicted by each modelling approach during the Stoop–20–Slow task.

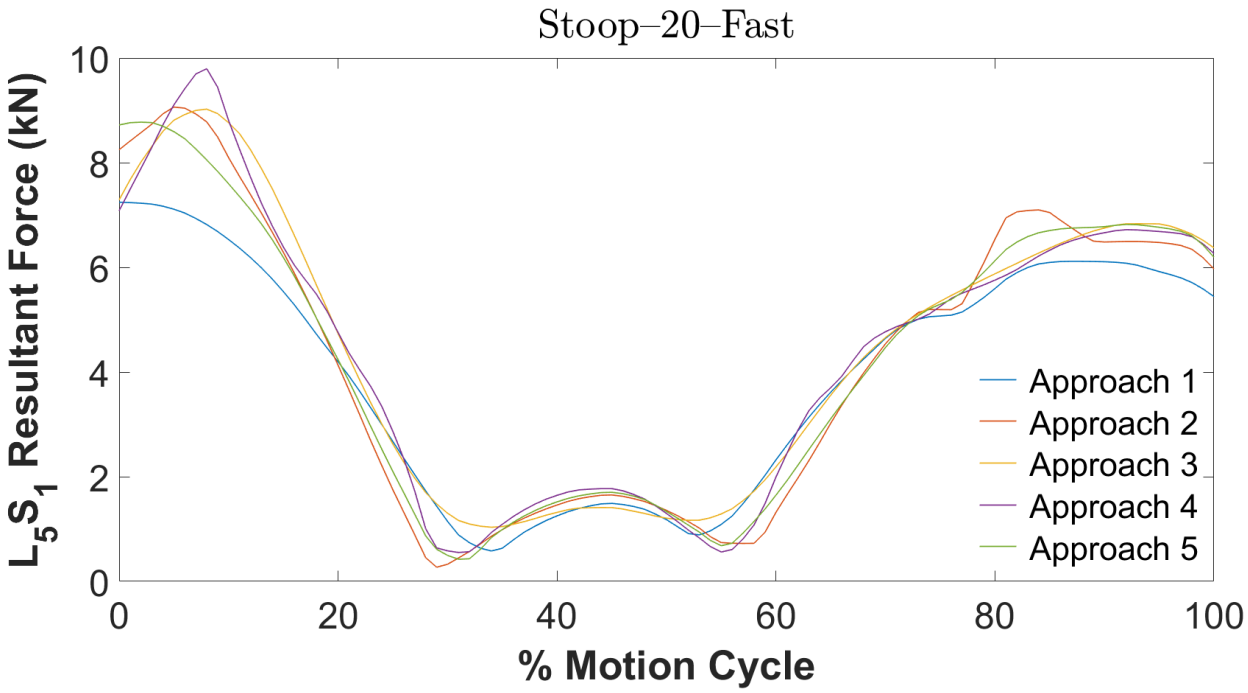


Fig. B.7. The $L_5S_1$ resultant force predicted by each modelling approach during the Stoop–20–Fast task.

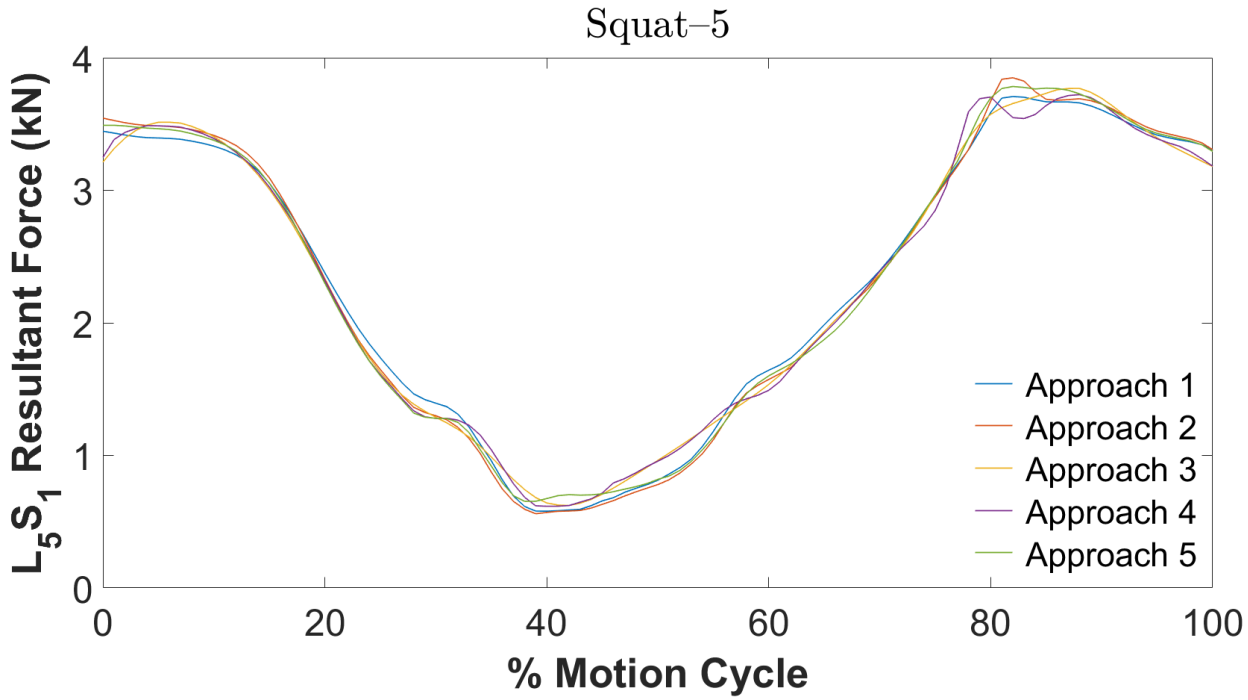


Fig. B.8. The $L_5S_1$ resultant force predicted by each modelling approach during the Squat–5 task.

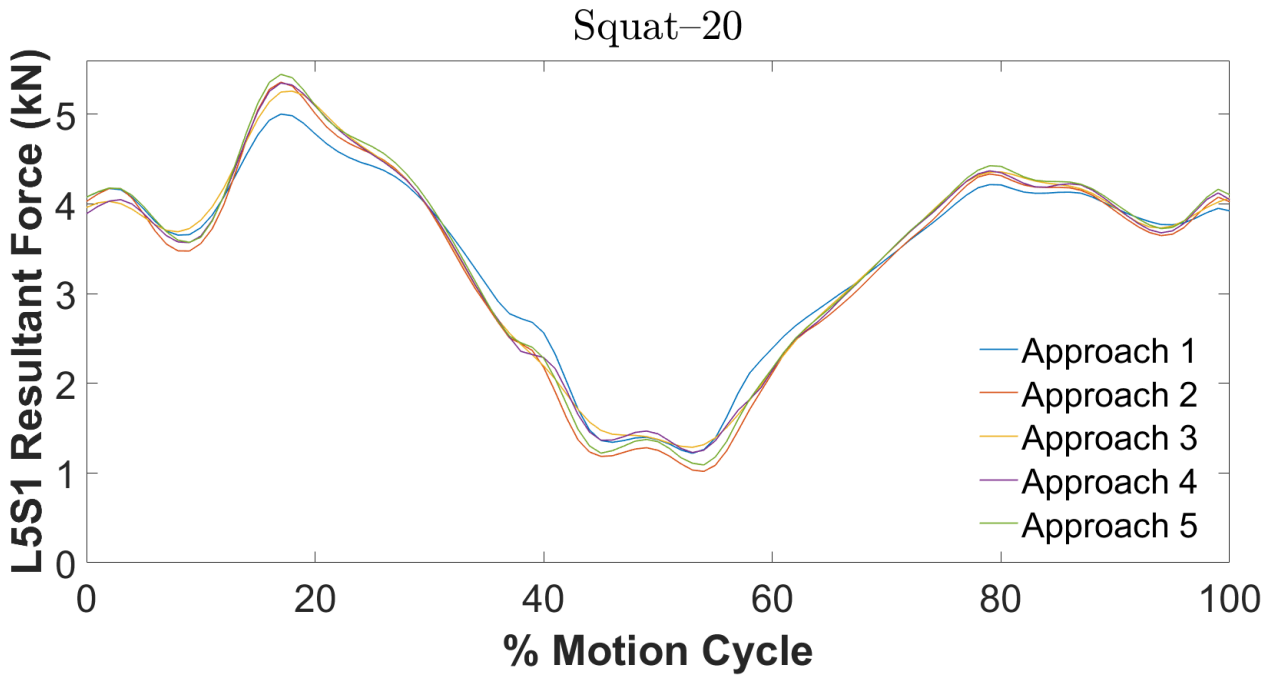


Fig. B.9. The $L_5S_1$ resultant force predicted by each modelling approach during the Squat–20 task.

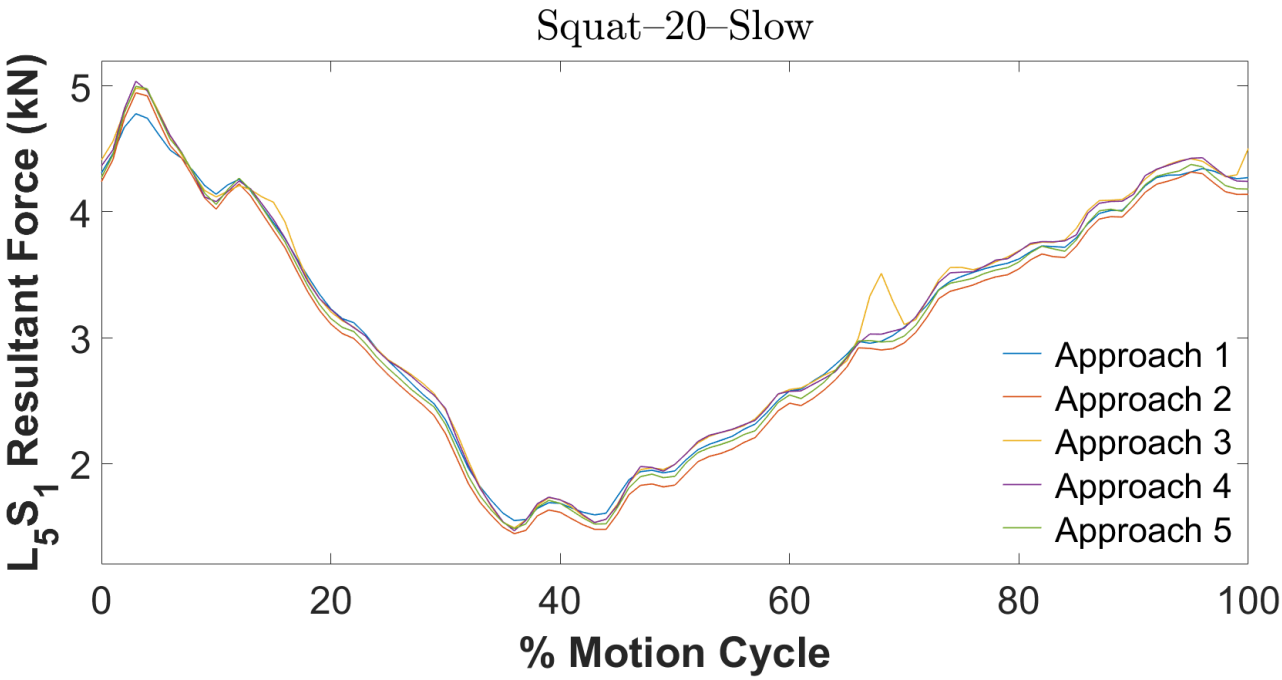


Fig. B.10. The $L_5S_1$ resultant force predicted by each modelling approach during the Squat–20–Slow task.

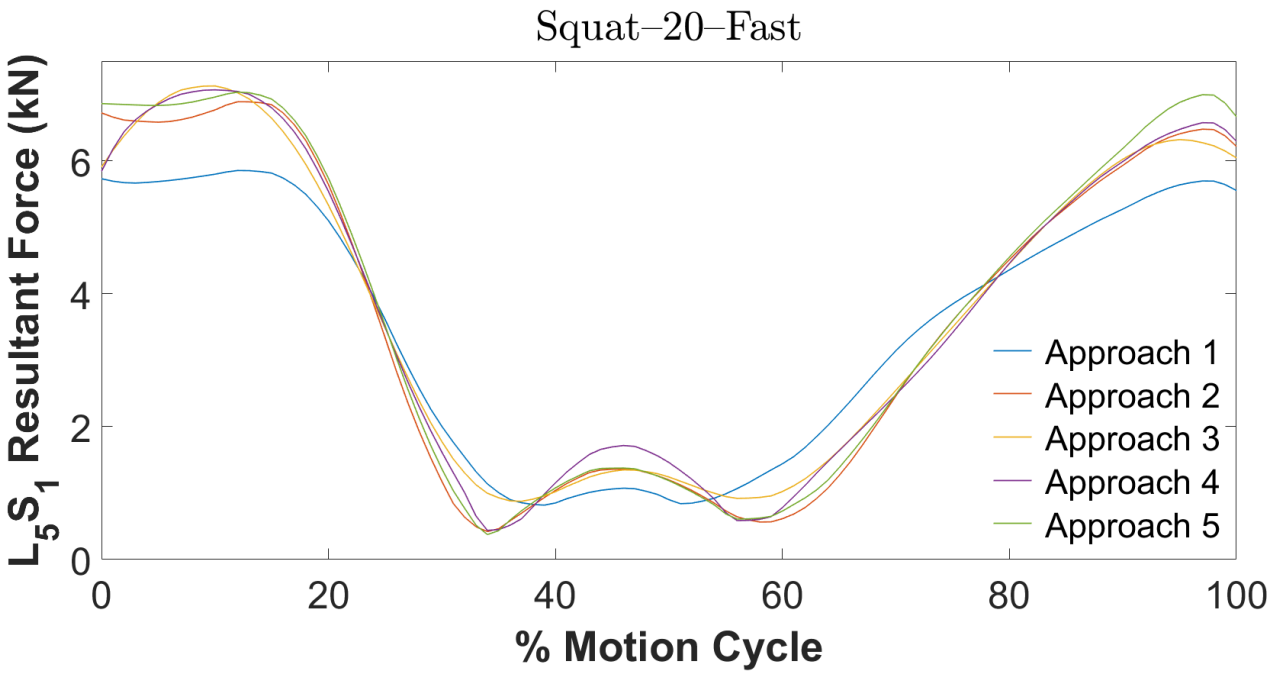


Fig. B.11. The $L_5S_1$ resultant force predicted by each modelling approach during the Squat–20–Fast task.

**B–SI. 6**

The model that was used in Approaches 3 and 4 possessed two more segments (i.e., the half-box segments) and more constraints (i.e., the Weld Constraint and its loop closure effect) than the model used in Approaches 1, 2, and 5 for the IK analysis. Therefore, the joint angles calculated by these approaches are not expected to be the same. The comparisons in B–SI. 6 show that the kinematics are only slightly different among the EHF&M approaches. Therefore, the observed differences in the $L_5S_1$ and residual forces are mostly due to the fact that the five approaches consider the dynamics of the problem differently.

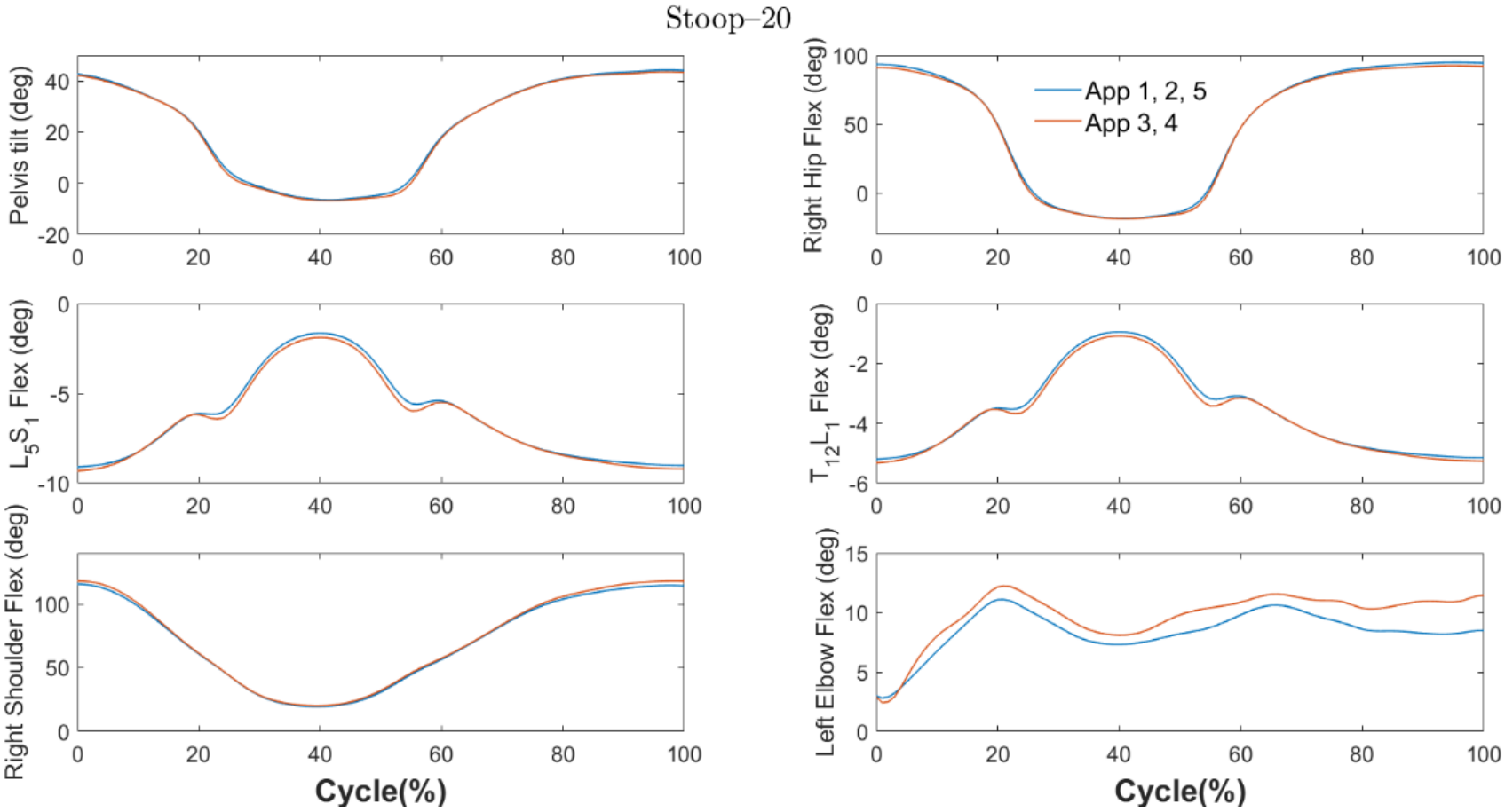


Fig. B.12. Various joint angles predicted by each modelling approach during the Stoop–20 task.

**B–SI. 7**

EHF&M are modelled differently in the proposed modelling approaches, which affects the dynamics of the SO problem. Approaches 2–4 do not explicitly model EHF&M as an "external load" applied to the hands, which means that additional steps are required to calculate EHF&M in these approaches if we intend to compare EHF&M among approaches. In Approach 2, we increased the mass of each hand by half of the box mass for the SO analysis. Therefore, in Approach 2, external hand forces can be calculated as $-\frac{m_{box}}{2} \cdot (\mathbf{a}_{\text{hand}} - \mathbf{g})$. To calculate the acceleration of each hand ($\mathbf{a}_{\text{hand}}$), further steps are required. Specifically, we run a Body Kinematics analysis for each task to extract the acceleration of each hand. In Approaches 3 and 4, an additional Joint Reaction analysis is required to extract the contact forces between the half-boxes and hands expressed in the ground frame to be comparable to the other approaches. As an example, for the Stoop–20, Stoop–20–Fast, and Stoop–20–Slow tasks, we extracted the external hand forces calculated by each approach. Figure B.13 shows the external forces applied to the right hand by each approach. Figure B.13 highlights the fact that the observed differences in the $L_5S_1$ and residual forces are mostly due to the dynamics of the problem rather than the kinematics.

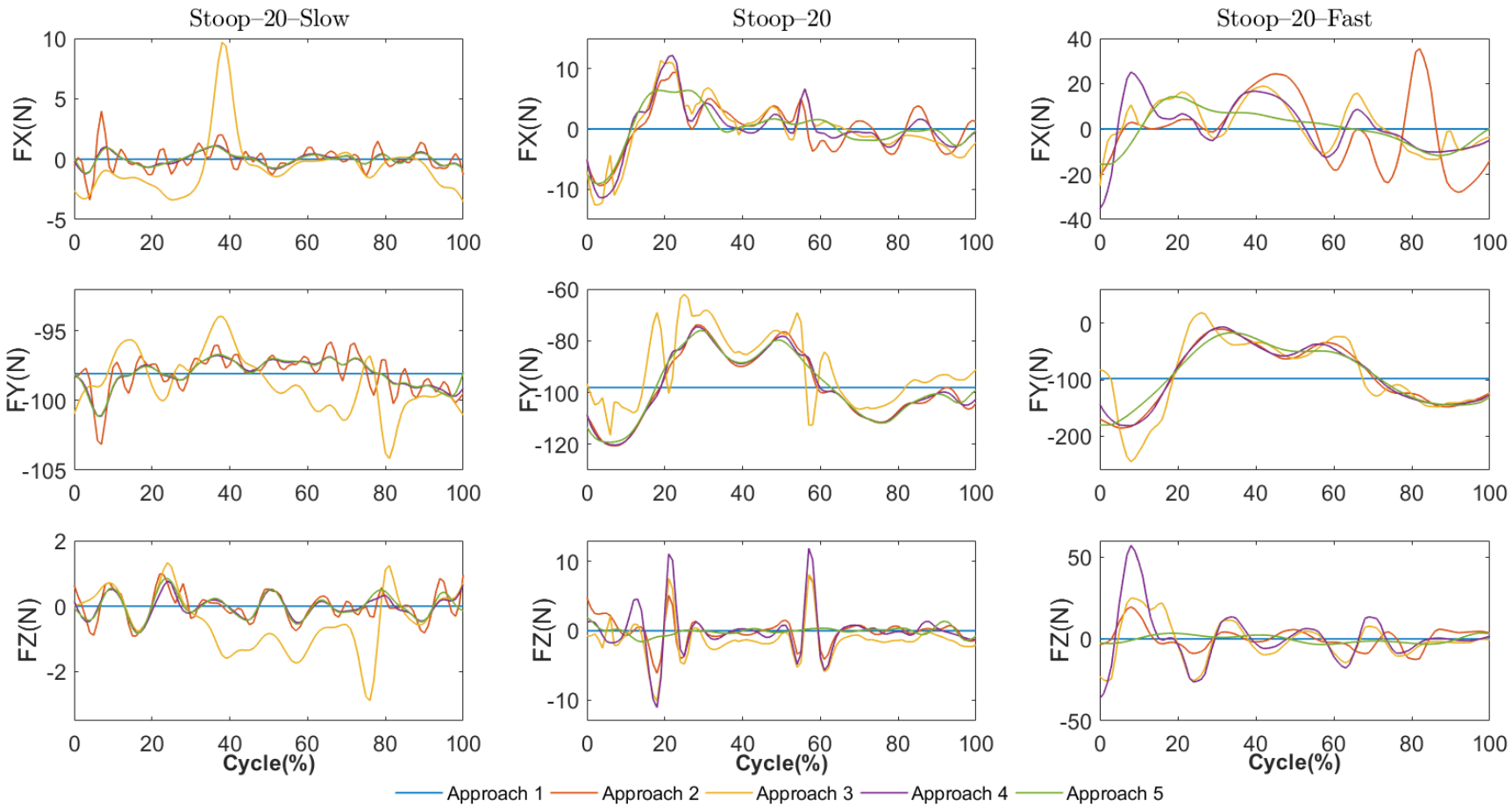


Fig. B.13. Comparison of the predicted external forces acting between the box and the right hand among different EHF&M modelling approaches during the Stoop–20–Slow, Stoop–20, and Stoop–20–Fast tasks.

# Appendix C: Study 3 Supplementary Information

## C–SI. 1

### *C–SI. 1.1 Power Curve Normalization*

In removing the effects of a covariate (body weight (BW) in this study, $x$) from the dependent variable (intervertebral forces in this study, $y$), a theoretical relationship between the covariate and the dependent variable should first be explained (Mullineaux et al., 2006). Intervertebral forces are directly related to muscle forces through the equilibrium equations (Akhavanfar et al., 2019). Muscle forces are usually estimated using a biomechanical model; within high-fidelity models, such as that used in the present study, the equilibrium equations cannot be solved deterministically (Akhavanfar et al., 2019). In this study, we estimated muscle forces using Static Optimization in OpenSim and by minimizing an objective function of the form $\sum a_m^2$, where $a_m$ is the activation of the m$^{th}$ muscle (see Akhavanfar et al., 2022 and the references cited therein for more details about how Static Optimization works in OpenSim). The objective function used for estimating muscle forces is curvilinear, and thus assuming a nonlinear function to describe the change in estimated intervertebral forces when BW increases is reasonable. A nonlinear increase in spinal loads with an increase in BW has also been reported in other musculoskeletal modelling studies (Ghezelbash et al., 2016). Therefore, the power curve normalization (allometric scaling) used in the present study is based on the assumption that the relationship between the estimated spinal forces ($y$) and BW ($x$) is curvilinear:

$$y = ax^b \quad \text{(Eq. C.1)}$$

where $a$ and $b$ are constants. Equation C.1 passes through the origin, meaning that the intervertebral forces are zero when BW is zero ($x = 0$).

As we explained in Chapter 5, to theoretically make $y$ free of the influence of the scaling/normalization variable ($x$) using the power curve normalization technique, $y/x^b$ should be calculated as the scaled/normalized variable. To calculate coefficient $b$ for *Body Weight Power Curve Normalization* (BWPCN), we fit a curvilinear function between the raw estimated intervertebral forces ($y$) and BW ($x$) during different static tasks and demonstrated the results in the main text. However, in some studies, coefficient $b$ has been calculated using the log–log transformation method (Stickley et al., 2018; Vanderburgh et al., 1995), which will be described here for more information.

In the log–log transformation method, the natural logarithms of the dependent and independent variables are determined first, and then a linear regression model is fit to calculate coefficient $b$ for BWPCN. Mathematically, this strategy can be derived by taking the natural logarithm on both sides of Eq. C.1:

$$\ln(y) = \ln(a) + b\ln(x) \qquad \text{(Eq. C.2)}$$

In Eq. C.2, coefficient $b$ is the slope of the linear function that relates the natural logarithms of estimated spinal forces ($\ln(y)$) to the natural logarithms of BW ($\ln(x)$).

In the present study, we also evaluated BWPCN using the log–log transformation method. The figure shown below is an example of results when the log–log transformation method was used to determine coefficient $b$ in BWPCN. The left panel (Fig. C.1(a)) compares coefficient $b$ in BWPCN derived from the raw $L_1L_2$ resultant forces data and from the log–log transformation data during all tasks. The right panel (Fig. C.1(b)) shows the normalized $L_1L_2$ spinal forces for 11 BW values during the Flex 50° and Flex 60° tasks. It can be observed that the log–log transformation method resulted in a different coefficient $b$ and consequently different normalized spinal forces compared to the condition in which the raw spinal forces were used for BWPCN. However, the

pattern of normalized spinal forces and the discussions presented about BWPCN in Chapter 5 are unaffected. The key conclusions in the main text for BWPCN using the raw estimated spinal forces were as follows: i) BWPCN was successful at removing all residual errors across all flexion tasks, meaning that normalized spinal forces ($y/x^b$) at all spinal levels were not correlated to BW ($x$), and ii) BWPCN resulted in significant negative correlations between normalized forces and flexion angle at the $L_1L_2$ level, as well as non-significant positive correlations at the $L_2L_3$ level for all scaled models. The same conclusions can be drawn when the log–log transformation method was used to calculate coefficient $b$ in BWPCN.

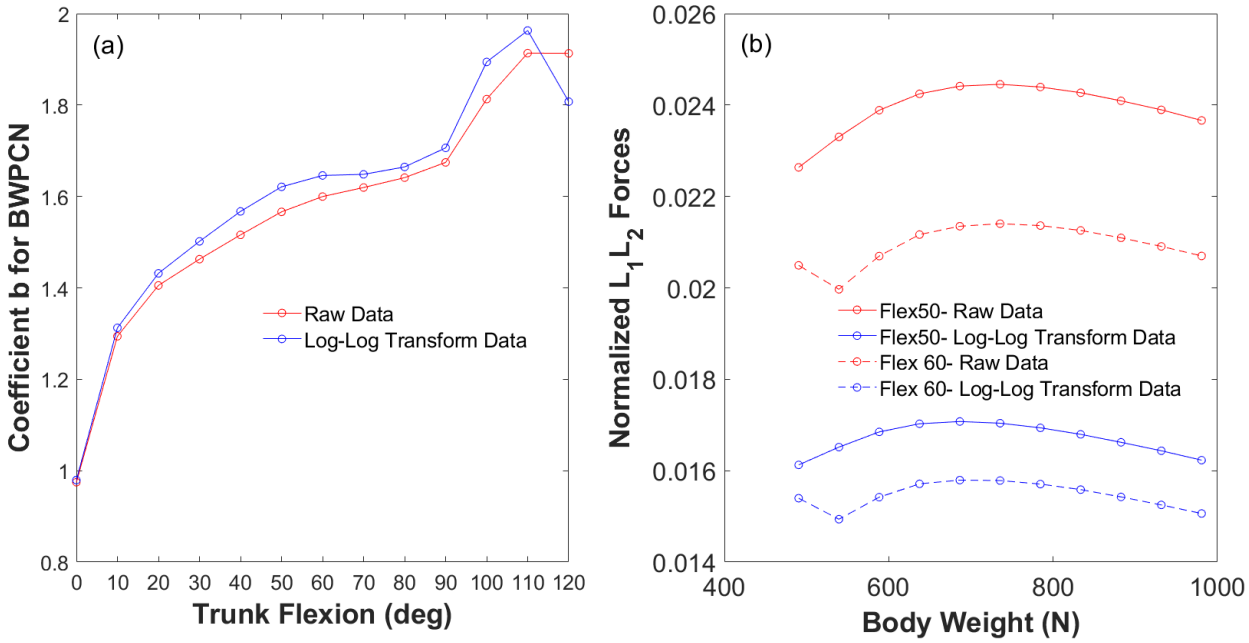


Fig. C.1. Example of results using the log–log transformation method. (a) Comparison of coefficient *b* in *Body Weight Power Curve Normalization* (BWPCN) derived from raw $L_1L_2$ resultant forces data and log–log transformation data across all tasks. (b) Normalized $L_1L_2$ spinal forces for 11 body weight values during the Flex 50° and Flex 60° tasks.

### *C–SI. 1.2 References*


Akhavanfar, M., Brandon, S.C.E., Brown, S.H.M., Graham, R.B., 2019. Development of a novel MATLAB-based framework for implementing mechanical joint stability constraints within OpenSim musculoskeletal models. J. Biomech. 91, 61–68.

Akhavanfar, M., Uchida, T.K., Clouthier, A.L., Graham, R.B., 2022. Sharing the load: modelling loads in OpenSim to simulate two-handed lifting. Multibody Syst. Dyn. 54, 213–234.

Ghezelbash, F., Shirazi-Adl, A., Arjmand, N., El-Ouaaid, Z., Plamondon, A., Meakin, J.R., 2016. Effects of sex, age, body height and body weight on spinal loads: sensitivity analyses in a subject-specific trunk musculoskeletal model. J. Biomech. 49, 3492–3501.

Mullineaux, D.R., Milner, C.E., Davis, I.S., Hamill, J., 2006. Normalization of ground reaction forces. J. Appl. Biomech. 22, 230–233.

Stickley, C.D., Andrews, S.N., Parke, E.A., Hetzler, R.K., 2018. The effectiveness of scaling procedures for comparing ground reaction forces. J. Biomech. 77, 55–61.

Vanderburgh, P.M., Mahar, M.T., Chou, C.H., 1995. Allometric scaling of grip strength by body mass in college-age men and women. Res. Q. Exerc. Sport 66, 80–84.

## C–SI. 2

Table C.1. Correlations between $L_1L_2$ resultant forces (raw and normalized) and body weight (BW). $L_1L_2$ resultant forces were estimated during various flexion tasks for the scaled models (50–100 kg). Four techniques were used to normalize the resultant forces, namely *BW Division Normalization* (BWDN), *Standing Division Normalization* (SDN), *BW Offset Normalization* (BWON), and *BW Power Curve Normalization* (BWPCN). Pearson correlation coefficients (r) were determined for each task between the raw or normalized resultant forces and BW. In SDN, resultant forces for each scaled model were normalized to the corresponding values at Flex 0, thus correlation analysis for SDN was not applicable (N/A) during this task. Bold values represent significant correlations between the normalized forces and BW (unsuccessful normalization).

| | **Raw Data** | | **BWDN** | | **SDN** | | **BWON** | | **BWPCN** | |
|---|---|---|---|---|---|---|---|---|---|---|
| | r | p | r | p | r | p | r | p | r | p |
| **Flex 0** | 1.00 | 0.000 | -0.87 | **0.001** | N/A | N/A | 0.17 | 0.610 | 0.24 | 0.473 |
| **Flex 10** | 1.00 | 0.000 | 0.98 | **0.000** | 0.99 | **0.000** | -0.05 | 0.888 | 0.36 | 0.281 |
| **Flex 20** | 1.00 | 0.000 | 0.99 | **0.000** | 0.99 | **0.000** | -0.16 | 0.640 | 0.39 | 0.241 |
| **Flex 30** | 1.00 | 0.000 | 0.98 | **0.000** | 0.99 | **0.000** | -0.17 | 0.626 | 0.40 | 0.219 |
| **Flex 40** | 1.00 | 0.000 | 0.98 | **0.000** | 0.99 | **0.000** | -0.04 | 0.910 | 0.42 | 0.201 |
| **Flex 50** | 1.00 | 0.000 | 0.98 | **0.000** | 0.99 | **0.000** | -0.12 | 0.724 | 0.44 | 0.175 |
| **Flex 60** | 1.00 | 0.000 | 0.99 | **0.000** | 0.99 | **0.000** | -0.09 | 0.785 | 0.42 | 0.202 |
| **Flex 70** | 1.00 | 0.000 | 0.99 | **0.000** | 0.99 | **0.000** | -0.10 | 0.767 | 0.23 | 0.492 |
| **Flex 80** | 1.00 | 0.000 | 0.99 | **0.000** | 0.99 | **0.000** | -0.11 | 0.756 | 0.17 | 0.617 |
| **Flex 90** | 1.00 | 0.000 | 0.99 | **0.000** | 0.99 | **0.000** | -0.11 | 0.755 | 0.24 | 0.486 |
| **Flex 100** | 1.00 | 0.000 | 0.99 | **0.000** | 0.99 | **0.000** | -0.11 | 0.743 | 0.49 | 0.125 |
| **Flex 110** | 1.00 | 0.000 | 0.99 | **0.000** | 1.00 | **0.000** | -0.14 | 0.675 | 0.40 | 0.222 |
| **Flex 120** | 0.99 | 0.000 | 0.97 | **0.000** | 0.97 | **0.000** | -0.16 | 0.630 | -0.33 | 0.317 |

Table C.2. Correlations between $L_2L_3$ resultant forces (raw and normalized) and body weight (BW). $L_2L_3$ resultant forces were estimated during various flexion tasks for the scaled models (50–100 kg). Four techniques were used to normalize the resultant forces, namely *BW Division Normalization* (BWDN), *Standing Division Normalization* (SDN), *BW Offset Normalization* (BWON), and *BW Power Curve Normalization* (BWPCN). Pearson correlation coefficients (r) were determined for each task between the raw or normalized resultant forces and BW. In SDN, resultant forces for each scaled model were normalized to the corresponding values at Flex 0, thus correlation analysis for SDN was not applicable (N/A) during this task. Bold values represent significant correlations between the normalized forces and BW (unsuccessful normalization).

| | **Raw Data** | | **BWDN** | | **SDN** | | **BWON** | | **BWPCN** | |
|---|---|---|---|---|---|---|---|---|---|---|
| | r | p | r | p | r | p | r | p | r | p |
| **Flex 0** | 1.00 | 0.000 | -0.85 | **0.001** | N/A | N/A | 0.17 | 0.612 | 0.24 | 0.473 |
| **Flex 10** | 1.00 | 0.000 | 0.98 | **0.000** | 0.99 | **0.000** | -0.03 | 0.941 | 0.30 | 0.366 |
| **Flex 20** | 1.00 | 0.000 | 0.98 | **0.000** | 0.99 | **0.000** | 0.01 | 0.978 | 0.32 | 0.333 |
| **Flex 30** | 1.00 | 0.000 | 0.98 | **0.000** | 0.99 | **0.000** | 0.02 | 0.954 | 0.33 | 0.316 |
| **Flex 40** | 1.00 | 0.000 | 0.98 | **0.000** | 0.99 | **0.000** | 0.13 | 0.698 | 0.33 | 0.319 |
| **Flex 50** | 1.00 | 0.000 | 0.99 | **0.000** | 0.99 | **0.000** | -0.12 | 0.725 | 0.35 | 0.298 |
| **Flex 60** | 1.00 | 0.000 | 0.99 | **0.000** | 0.99 | **0.000** | -0.10 | 0.766 | 0.05 | 0.891 |
| **Flex 70** | 1.00 | 0.000 | 0.95 | **0.000** | 0.96 | **0.000** | -0.11 | 0.754 | -0.10 | 0.769 |
| **Flex 80** | 1.00 | 0.000 | 0.93 | **0.000** | 0.94 | **0.000** | -0.11 | 0.751 | -0.12 | 0.722 |
| **Flex 90** | 1.00 | 0.000 | 0.94 | **0.000** | 0.95 | **0.000** | -0.11 | 0.756 | -0.11 | 0.747 |
| **Flex 100** | 1.00 | 0.000 | 0.99 | **0.000** | 0.99 | **0.000** | -0.08 | 0.813 | 0.23 | 0.489 |
| **Flex 110** | 1.00 | 0.000 | 0.98 | **0.000** | 0.99 | **0.000** | 0.14 | 0.690 | 0.36 | 0.272 |
| **Flex 120** | 1.00 | 0.000 | 0.99 | **0.000** | 0.99 | **0.000** | -0.14 | 0.690 | 0.39 | 0.238 |

Table C.3. Correlations between $L_3L_4$ resultant forces (raw and normalized) and body weight (BW). $L_3L_4$ resultant forces were estimated during various flexion tasks for the scaled models (50–100 kg). Four techniques were used to normalize the resultant forces, namely *BW Division Normalization* (BWDN), *Standing Division Normalization* (SDN), *BW Offset Normalization* (BWON), and *BW Power Curve Normalization* (BWPCN). Pearson correlation coefficients (r) were determined for each task between the raw or normalized resultant forces and BW. In SDN, resultant forces for each scaled model were normalized to the corresponding values at Flex 0, thus correlation analysis for SDN was not applicable (N/A) during this task. Bold values represent significant correlations between the normalized forces and BW (unsuccessful normalization).

| | **Raw Data** | | **BWDN** | | **SDN** | | **BWON** | | **BWPCN** | |
|---|---|---|---|---|---|---|---|---|---|---|
| | r | p | r | p | r | p | r | p | r | p |
| **Flex 0** | 1.00 | 0.000 | -0.87 | **0.001** | N/A | N/A | 0.17 | 0.607 | 0.24 | 0.480 |
| **Flex 10** | 1.00 | 0.000 | 0.98 | **0.000** | 0.99 | **0.000** | -0.04 | 0.908 | 0.22 | 0.523 |
| **Flex 20** | 1.00 | 0.000 | 0.98 | **0.000** | 1.00 | **0.000** | -0.10 | 0.764 | 0.30 | 0.371 |
| **Flex 30** | 1.00 | 0.000 | 0.98 | **0.000** | 1.00 | **0.000** | -0.12 | 0.723 | 0.32 | 0.339 |
| **Flex 40** | 1.00 | 0.000 | 0.98 | **0.000** | 0.99 | **0.000** | -0.04 | 0.899 | 0.32 | 0.344 |
| **Flex 50** | 1.00 | 0.000 | 0.99 | **0.000** | 1.00 | **0.000** | -0.14 | 0.676 | 0.32 | 0.330 |
| **Flex 60** | 1.00 | 0.000 | 0.98 | **0.000** | 0.99 | **0.000** | -0.10 | 0.764 | -0.01 | 0.982 |
| **Flex 70** | 1.00 | 0.000 | 0.92 | **0.000** | 0.95 | **0.000** | -0.10 | 0.760 | -0.12 | 0.736 |
| **Flex 80** | 1.00 | 0.000 | 0.86 | **0.001** | 0.91 | **0.000** | -0.10 | 0.763 | -0.13 | 0.711 |
| **Flex 90** | 1.00 | 0.000 | 0.88 | **0.000** | 0.92 | **0.000** | -0.10 | 0.770 | -0.12 | 0.732 |
| **Flex 100** | 1.00 | 0.000 | 0.98 | **0.000** | 0.99 | **0.000** | -0.07 | 0.844 | 0.15 | 0.660 |
| **Flex 110** | 1.00 | 0.000 | 0.97 | **0.000** | 0.99 | **0.000** | 0.18 | 0.596 | 0.33 | 0.321 |
| **Flex 120** | 1.00 | 0.000 | 0.98 | **0.000** | 0.99 | **0.000** | 0.13 | 0.703 | 0.36 | 0.281 |

Table C.4. Correlations between $L_4L_5$ resultant forces (raw and normalized) and body weight (BW). $L_4L_5$ resultant forces were estimated during various flexion tasks for the scaled models (50–100 kg). Four techniques were used to normalize the resultant forces, namely *BW Division Normalization* (BWDN), *Standing Division Normalization* (SDN), *BW Offset Normalization* (BWON), and *BW Power Curve Normalization* (BWPCN). Pearson correlation coefficients (r) were determined for each task between the raw or normalized resultant forces and BW. In SDN, resultant forces for each scaled model were normalized to the corresponding values at Flex 0, thus correlation analysis for SDN was not applicable (N/A) during this task. Bold values represent significant correlations between the normalized forces and BW (unsuccessful normalization).

| | **Raw Data** | | **BWDN** | | **SDN** | | **BWON** | | **BWPCN** | |
|---|---|---|---|---|---|---|---|---|---|---|
| | r | p | r | p | r | p | r | p | r | p |
| **Flex 0** | 1.00 | 0.000 | -0.84 | **0.001** | N/A | N/A | 0.17 | 0.611 | 0.24 | 0.475 |
| **Flex 10** | 1.00 | 0.000 | 0.92 | **0.000** | 0.94 | **0.000** | -0.04 | 0.902 | 0.01 | 0.983 |
| **Flex 20** | 1.00 | 0.000 | 0.98 | **0.000** | 0.98 | **0.000** | -0.03 | 0.927 | 0.20 | 0.563 |
| **Flex 30** | 1.00 | 0.000 | 0.99 | **0.000** | 0.98 | **0.000** | -0.12 | 0.727 | 0.17 | 0.624 |
| **Flex 40** | 1.00 | 0.000 | 0.99 | **0.000** | 0.98 | **0.000** | -0.15 | 0.666 | 0.24 | 0.472 |
| **Flex 50** | 1.00 | 0.000 | 0.99 | **0.000** | 0.97 | **0.000** | -0.15 | 0.651 | -0.17 | 0.620 |
| **Flex 60** | 1.00 | 0.000 | 0.68 | **0.020** | 0.85 | **0.001** | -0.11 | 0.754 | -0.14 | 0.680 |
| **Flex 70** | 1.00 | 0.000 | 0.06 | 0.870 | 0.44 | 0.178 | -0.11 | 0.755 | -0.15 | 0.654 |
| **Flex 80** | 1.00 | 0.000 | -0.11 | 0.756 | 0.24 | 0.470 | -0.10 | 0.759 | -0.15 | 0.656 |
| **Flex 90** | 1.00 | 0.000 | -0.10 | 0.773 | 0.26 | 0.439 | -0.10 | 0.771 | -0.14 | 0.672 |
| **Flex 100** | 1.00 | 0.000 | 0.73 | **0.010** | 0.89 | **0.000** | -0.06 | 0.864 | -0.05 | 0.874 |
| **Flex 110** | 1.00 | 0.000 | 0.95 | **0.000** | 0.99 | **0.000** | 0.15 | 0.652 | 0.28 | 0.401 |
| **Flex 120** | 1.00 | 0.000 | 0.98 | **0.000** | 0.99 | **0.000** | -0.06 | 0.866 | 0.27 | 0.419 |

Table C.5. Correlations between $L_5S_1$ resultant forces (raw and normalized) and body weight (BW). $L_5S_1$ resultant forces were estimated during various flexion tasks for the scaled models (50–100 kg). Four techniques were used to normalize the resultant forces, namely *BW Division Normalization* (BWDN), *Standing Division Normalization* (SDN), *BW Offset Normalization* (BWON), and *BW Power Curve Normalization* (BWPCN). Pearson correlation coefficients (r) were determined for each task between the raw or normalized resultant forces and BW. In SDN, resultant forces for each scaled model were normalized to the corresponding values at Flex 0, thus correlation analysis for SDN was not applicable (N/A) during this task. Bold values represent significant correlations between the normalized forces and BW (unsuccessful normalization).

| | **Raw Data** | | **BWDN** | | **SDN** | | **BWON** | | **BWPCN** | |
|---|---|---|---|---|---|---|---|---|---|---|
| | r | p | r | p | r | p | r | p | r | p |
| **Flex 0** | 1.00 | 0.000 | -0.83 | **0.001** | N/A | N/A | 0.17 | 0.612 | 0.24 | 0.475 |
| **Flex 10** | 1.00 | 0.000 | 0.83 | **0.002** | 0.91 | **0.000** | -0.04 | 0.898 | -0.02 | 0.951 |
| **Flex 20** | 1.00 | 0.000 | 0.98 | **0.000** | 0.97 | **0.000** | 0.00 | 0.998 | 0.19 | 0.566 |
| **Flex 30** | 1.00 | 0.000 | 0.99 | **0.000** | 0.97 | **0.000** | -0.12 | 0.726 | 0.06 | 0.858 |
| **Flex 40** | 1.00 | 0.000 | 0.99 | **0.000** | 0.97 | **0.000** | -0.16 | 0.646 | 0.11 | 0.741 |
| **Flex 50** | 1.00 | 0.000 | 0.98 | **0.000** | 0.94 | **0.000** | -0.16 | 0.644 | -0.21 | 0.545 |
| **Flex 60** | 1.00 | 0.000 | 0.39 | 0.231 | 0.74 | **0.009** | -0.11 | 0.750 | -0.15 | 0.658 |
| **Flex 70** | 1.00 | 0.000 | -0.17 | 0.620 | 0.23 | 0.487 | -0.11 | 0.755 | -0.16 | 0.648 |
| **Flex 80** | 1.00 | 0.000 | -0.28 | 0.407 | 0.05 | 0.884 | -0.10 | 0.760 | -0.15 | 0.653 |
| **Flex 90** | 1.00 | 0.000 | -0.28 | 0.403 | 0.06 | 0.869 | -0.10 | 0.772 | -0.15 | 0.670 |
| **Flex 100** | 1.00 | 0.000 | 0.42 | 0.198 | 0.79 | **0.004** | -0.05 | 0.876 | -0.06 | 0.857 |
| **Flex 110** | 1.00 | 0.000 | 0.92 | **0.000** | 0.98 | **0.000** | 0.17 | 0.622 | 0.28 | 0.410 |
| **Flex 120** | 1.00 | 0.000 | 0.98 | **0.000** | 0.99 | **0.000** | 0.04 | 0.913 | 0.27 | 0.416 |

# Appendix D: Study 4 Supplementary Information

**D–SI. 1**

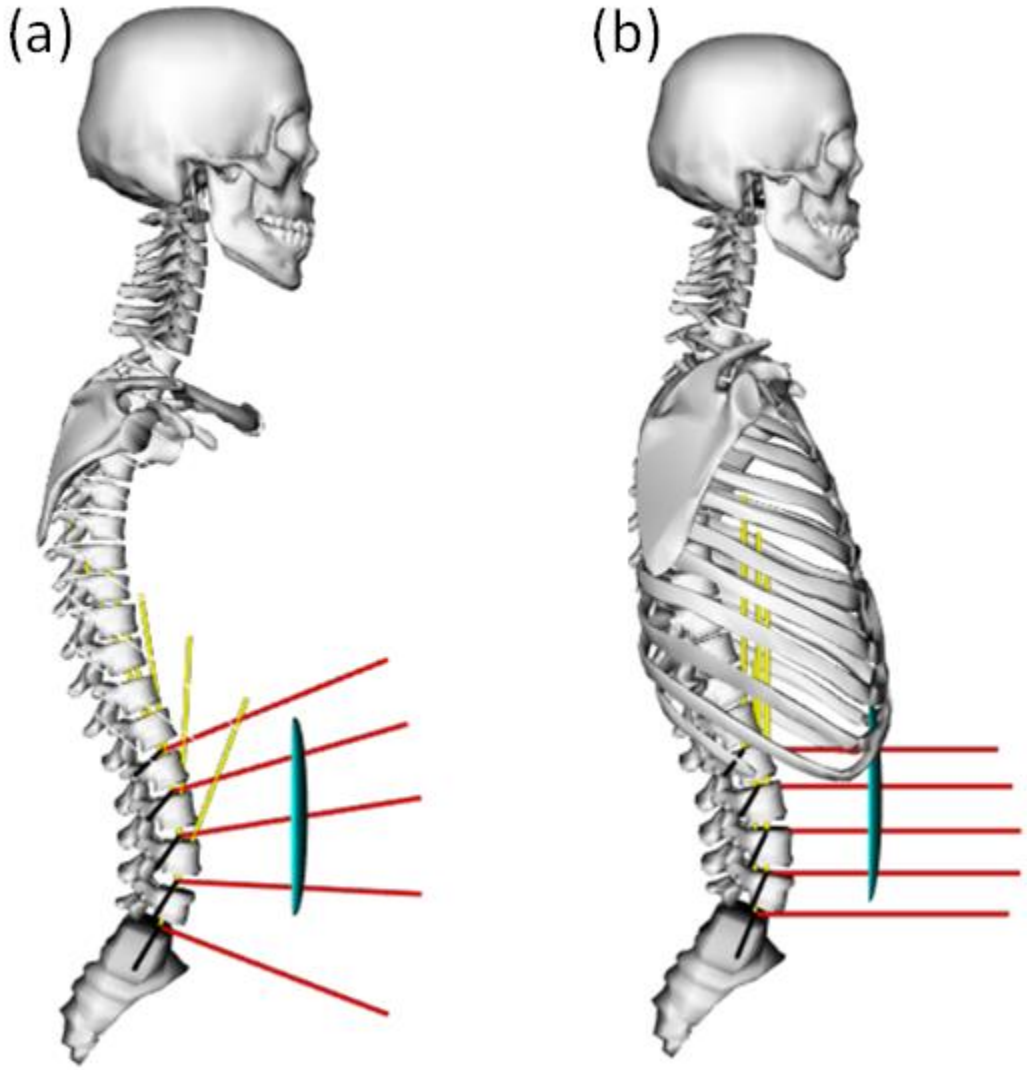


Fig. D.1. Reference frames fixed to the L1–L5 segments of the spine in the standing posture for (a) the fully articulated thoracolumbar spine (FATLS) model and (b) the lifting full-body (LFB) model. When a Joint Reaction Analysis is run in OpenSim, the reaction forces are expressed with respect to these reference frames. It is more realistic to consider the y-components (i.e., along the yellow axes) of the estimated reaction forces in the FATLS model as compression forces because the y-components are perpendicular to the intervertebral discs; this is not the case for the LFB model. A similar argument applies to the estimated fore–aft shear forces (the x-components, along the red axes). Therefore, when using the LFB model, reporting the raw Joint Reaction Analysis results as shear and compression forces might not be reasonable. To report compression and shear forces in the LFB model at each intervertebral level, modellers should consider the orientation of the corresponding vertebrae with respect to the ground reference frame.

**D–SI. 2**


Fig. D.2. The box and dumbbells that were used for the lifting tasks in the present study.

## D–SI. 3

### *D–SI. 3.1 Abdomen Kinematic Constraints*

In our model, the abdomen is represented as a body with negligible mass, connected to the sacrum using a Custom Joint. The abdomen is used to define the paths of the abdominal muscles. Similar to the intervertebral coordinates, we established coupler constraints between the coordinates of the abdomen and the $L_5S_1$ coordinates to improve tracking of their movements during dynamic tasks. Previous modelling studies (Alemi et al., 2021; Raabe et al., 2016) have used similar coupler constraints, but they did not provide detailed information on how the function for coupling the abdomen coordinates was derived.

Our goal was to avoid non-physiological configurations, such as muscles passing through bones, within the ranges of motion studied. For the lateral bending and axial rotation degrees of freedom, we found that defining a linear function, ensuring the abdomen's total rotation is equal to the total lumbar rotation, results in plausible muscle configurations. However, since the primary motion in this study was flexion–extension, we encountered an issue when defining a similar linear function for this degree of freedom, especially for lumbar flexion greater than 30°. This problem arose due to the varying contributions of the pelvis, lumbar, and thorax bodies to the total upper trunk flexion movement. Consequently, establishing a simple linear function between the abdomen and the $L_5S_1$ flexion–extension coordinates became problematic, particularly for the long abdominal fascicles that originate on the pelvis, pass through the abdomen, and insert onto the ribs.

In the original FATLS model developed and validated by Bruno and colleagues (Bruno et al., 2015), the lumbopelvic ratio was calculated as a function of total trunk flexion, ranging from approximately 2.5 at 12° of trunk flexion to 1.0 at 121° of trunk flexion. In our model, we

independently tracked the pelvis and $L_5S_1$ coordinates using reflective markers. However, to account for the lumbopelvic rhythm and establish a function between the abdomen and $L_5S_1$ coordinates, we incorporated the lumbopelvic ratios provided by Bruno et al. (2015) and assumed that abdomen flexion is equal to the difference between lumbar flexion and pelvic flexion. The figure below illustrates the data points we used to define the piecewise-linear function for coupling $L_5S_1$ and abdomen coordinates. As depicted, when the total lumbar flexion varies between 0 and 41.3° (total trunk flexion between 0 and 121°), the proportion of pelvic contribution to the total trunk flexion increases; consequently, based on our assumed function, the abdomen flexion decreases. Our findings indicate that this assumption yields reasonable muscle geometry in our model, particularly for the trunk flexion range of motion in this study.

### *D–SI. 3.2 References*


Alemi, M.M., Burkhart, K.A., Lynch, A.C., Allaire, B.T., Mousavi, S.J., Zhang, C., Bouxsein, M.L., Anderson, D.E., 2021. The influence of kinematic constraints on model performance during inverse kinematics analysis of the thoracolumbar spine. Front. Bioeng. Biotechnol. 9, 688041.

Bruno, A.G., Bouxsein, M.L., Anderson, D.E., 2015. Development and validation of a musculoskeletal model of the fully articulated thoracolumbar spine and rib cage. J. Biomech. Eng. 137, 081003.

Raabe, M.E., Chaudhari, A.M.W., 2016. An investigation of jogging biomechanics using the full-body lumbar spine model: model development and validation. J. Biomech. 49, 1238–1243.

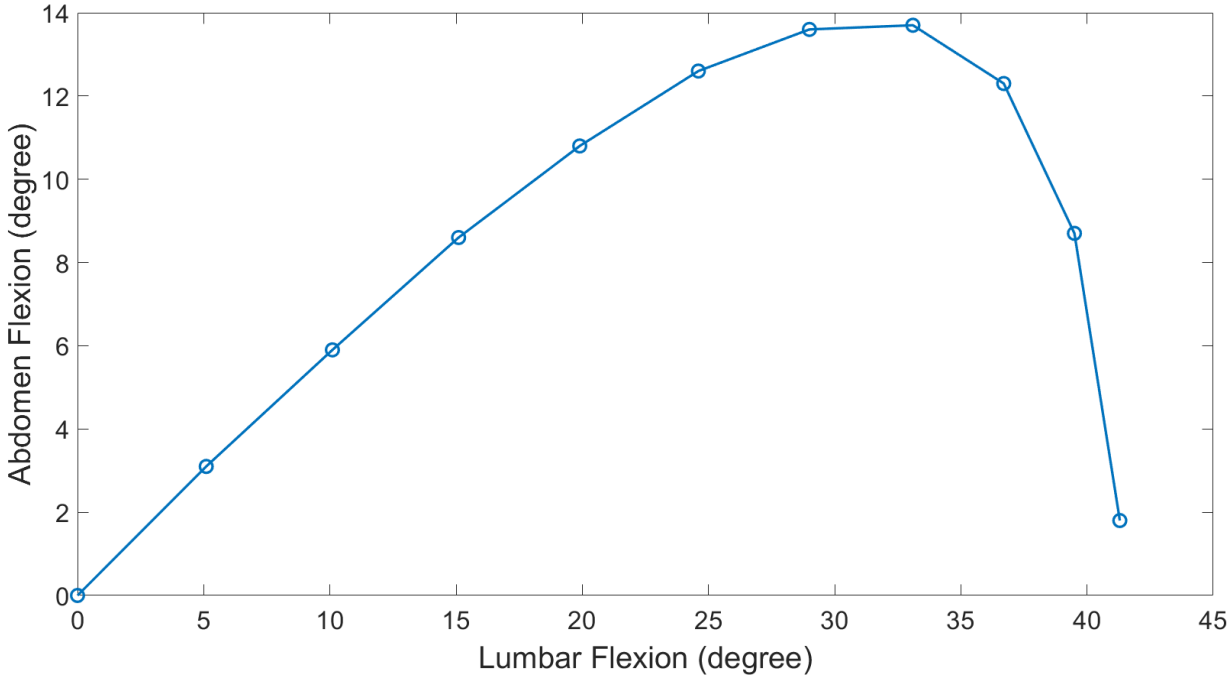


Fig. D.3. The abdomen and lumbar flexion data points that were used to define the piecewise-linear function for coupling $L_5S_1$ and abdomen coordinates.

## D–SI. 4

### *D–SI. 4.1 Normalizing Spinal Forces*

Among personalized factors, body weight is known to have the greatest effect on spinal forces (Akhavanfar et al., 2018). Therefore, to better compare spinal forces across a population, previous experimental and modelling studies have often normalized measured and estimated spinal forces by dividing these forces by body weight (Bruno et al., 2017; Malakoutian et al., 2018) or dividing them by the intervertebral load during a neutral, unloaded, standing posture (Actis et al., 2018; Beaucage-Gauvreau et al., 2019). We recently demonstrated that these common procedures for normalizing spinal forces do not adequately remove the effect of body weight on spinal forces during tasks involving trunk flexion (e.g., the stoop and squat tasks examined in the present study) (Akhavanfar et al., 2023). Our results suggested that the most appropriate normalization technique to remove the effect of body weight is offset normalization. For offset normalization, we first derived equations of the form $y = ax + b$, which describe spinal forces ($y$) estimated by our enhanced FATLS model as a function of body weight ($x$) during static symmetric trunk flexion tasks (0–120° in increments of 10°). The normalized forces ($y_n$) were then calculated as $y_n = {(y - b)}/{x}$. Coefficient $b$ in the offset normalization function was found to depend on the flexion angle (Table D.1). Therefore, to normalize the estimated $L_1L_2$ resultant forces during the dynamic trials in the present study, the following steps were taken to determine the appropriate coefficient $b$ for normalization at each instant of the simulation: i) the total trunk flexion of the model at each instant was determined by computing the T1 orientation with respect to the ground using a Body Kinematics analysis in OpenSim, and ii) the nearest range of static trunk flexion angle for which coefficient $b$ is known was determined. For instance, if the flexion angle at an instant of the dynamic simulation was 44°, the nearest static trunk flexion range would be 40–50°. Coefficient

*b* at each instant of the dynamic simulation was then calculated by assuming coefficient *b* varies linearly in the corresponding static trunk flexion range. To normalize implant data, first, the total trunk flexion during the motion cycle was calculated using the video of each trial (https://orthoload.com/) and Kinovea (Puig-Diví et al., 2019), which is a free and easy-to-use 2D motion analysis software. The same procedure as that described above for normalizing estimated forces was then employed to normalize the implant data.

Table 0.1. Coefficient *b* in the offset normalization function during various static trunk flexion tasks.

| *Total static trunk flexion angle (°)* | *Coefficient b for offset normalization (N)* |
|---|---|
| 0 | 4.4 |
| 10 | -90.9 |
| 20 | -174.4 |
| 30 | -252.4 |
| 40 | -334.4 |
| 50 | -414.1 |
| 60 | -476.4 |
| 70 | -522.2 |
| 80 | -566.3 |
| 90 | -611.4 |
| 100 | -697.6 |
| 110 | -701.4 |
| 120 | -591.0 |

### *D–SI. 4.2 References*


Actis, J.A., Honegger, J.D., Gates, D.H., Petrella, A.J., Nolasco, L.A., Silverman, A.K., 2018. Validation of lumbar spine loading from a musculoskeletal model including the lower limbs and lumbar spine. J. Biomech. 68, 107–114.

Akhavanfar, M., Kazemi, H., Eskandari, A.H., Arjmand, N., 2018. Obesity and spinal loads; a combined MR imaging and subject-specific modelling investigation. J. Biomech. 70, 102–112.

Akhavanfar, M., Uchida, T.K., Graham, R.B., 2023. Evaluation of spinal force normalization techniques. J. Biomech. 147, 111441.

Beaucage-Gauvreau, E., Robertson, W.S.P., Brandon, S.C.E., Fraser, R., Freeman, B.J.C., Graham, R.B., Thewlis, D., Jones, C.F., 2019. Validation of an OpenSim full-body model with detailed lumbar spine for estimating lower lumbar spine loads during symmetric and asymmetric lifting tasks. Comput. Methods Biomech. Biomed. Engin. 22, 451–464.

Bruno, A.G., Burkhart, K., Allaire, B., Anderson, D.E., Bouxsein, M.L., 2017. Spinal loading patterns from biomechanical modelling explain the high incidence of vertebral fractures in the thoracolumbar region. J. Bone Miner. Res. 32, 1282–1290.

Malakoutian, M., Street, J., Wilke, H.-J., Stavness, I., Fels, S., Oxland, T., 2018. A musculoskeletal model of the lumbar spine using ArtiSynth–development and validation. Comput. Methods Biomech. Biomed. Eng. Imaging Vis. 6, 483–490.

Puig-Diví, A., Escalona-Marfil, C., Padullés-Riu, J.M., Busquets, A., Padulles-Chando, X., Marcos-Ruiz, D., 2019. Validity and reliability of the Kinovea program in obtaining angles and distances using coordinates in 4 perspectives. PLoS One 14, e0216448.

**D–SI. 5**

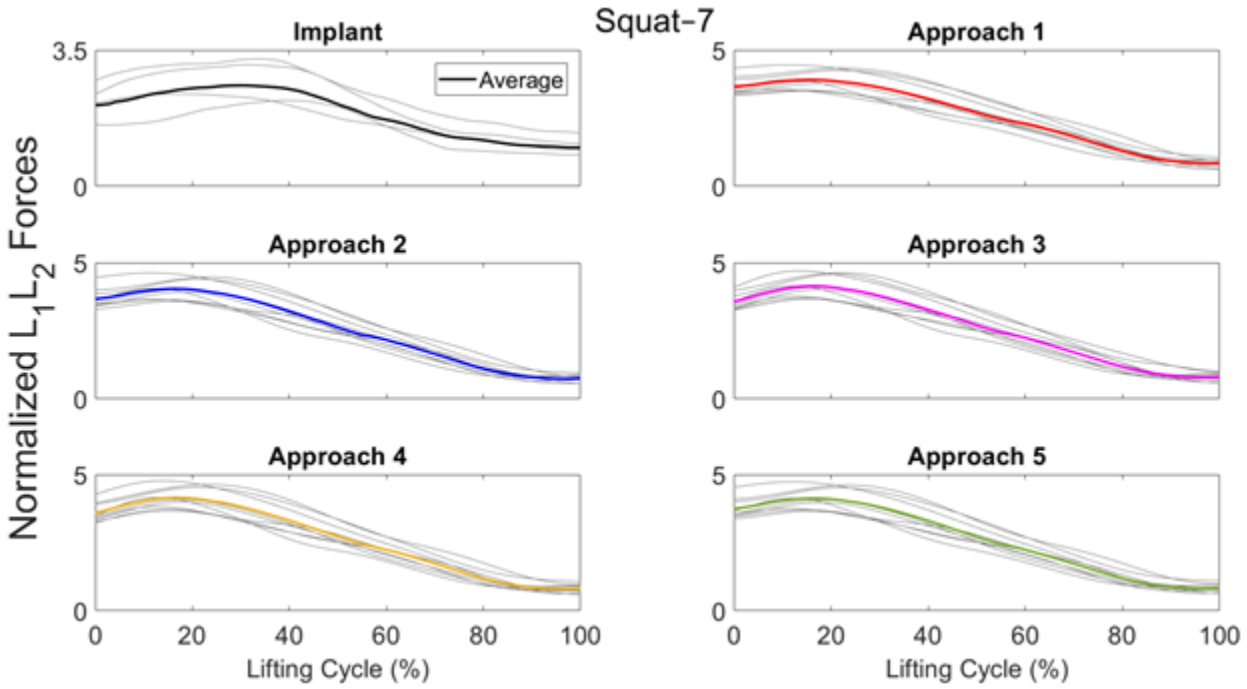


Fig. D.4. Raw and average normalized curves during the **lifting** motion cycle of the **Squat–7** task. $L_1L_2$ intervertebral forces were normalized using the body weight offset normalization technique (D–SI. 4). Raw estimated and measured normalized forces are shown in gray. The raw normalized forces were first averaged across the trials for each individual and then across all individuals. The final average curves for measured implant data and forces estimated using EHF&M Approaches 1–5 are shown as coloured solid lines.

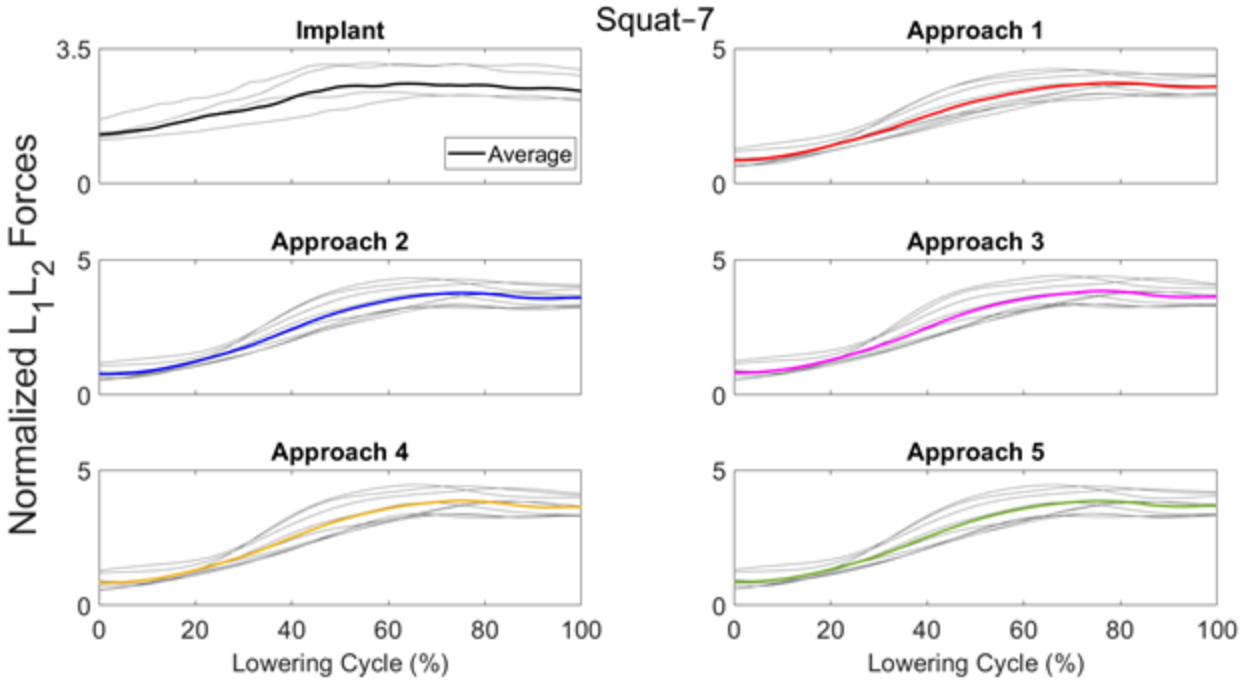


Fig. D.5. Raw and average normalized curves during the **lowering** motion cycle of the **Squat–7** task. $L_1L_2$ intervertebral forces were normalized using the body weight offset normalization technique (D–SI. 4). Raw estimated and measured normalized forces are shown in gray. The raw normalized forces were first averaged across the trials for each individual and then across all individuals. The final average curves for measured implant data and forces estimated using EHF&M Approaches 1–5 are shown as coloured solid lines.

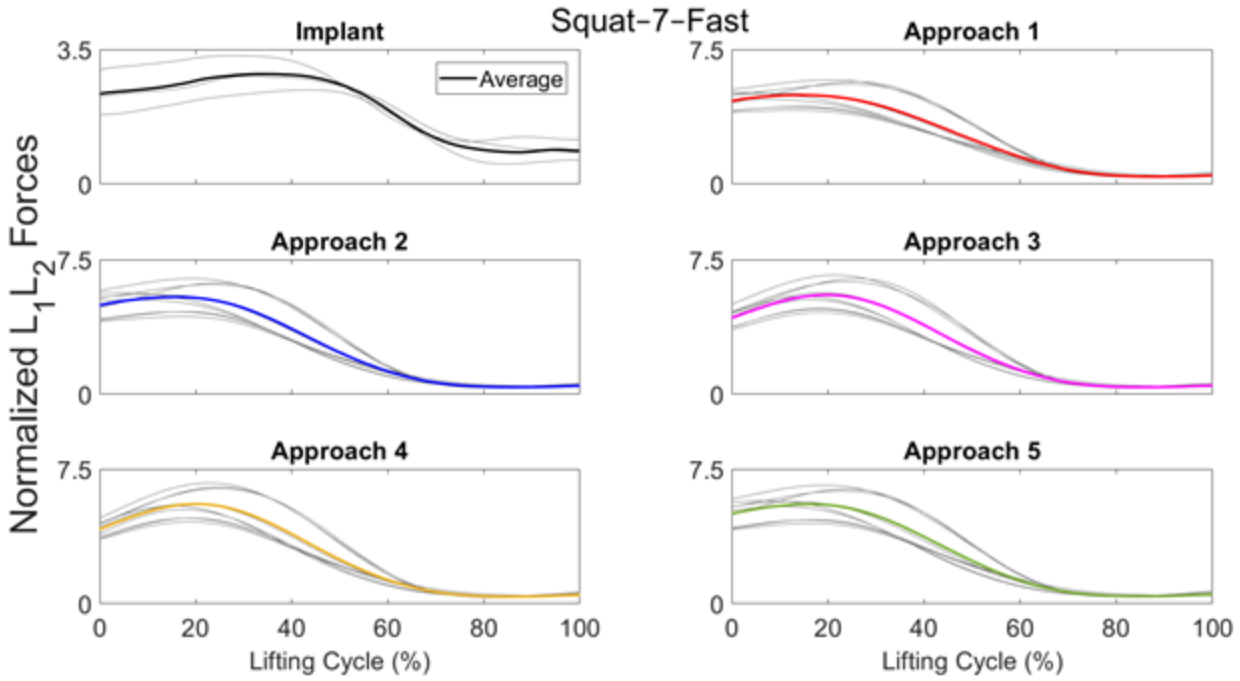


Fig. D.6. Raw and average normalized curves during the **lifting** motion cycle of the **Squat–7–Fast** task. $L_1L_2$ intervertebral forces were normalized using the body weight offset normalization technique (D–SI. 4). Raw estimated and measured normalized forces are shown in gray. The raw normalized forces were first averaged across the trials for each individual and then across all individuals. The final average curves for measured implant data and forces estimated using EHF&M Approaches 1–5 are shown as coloured solid lines.

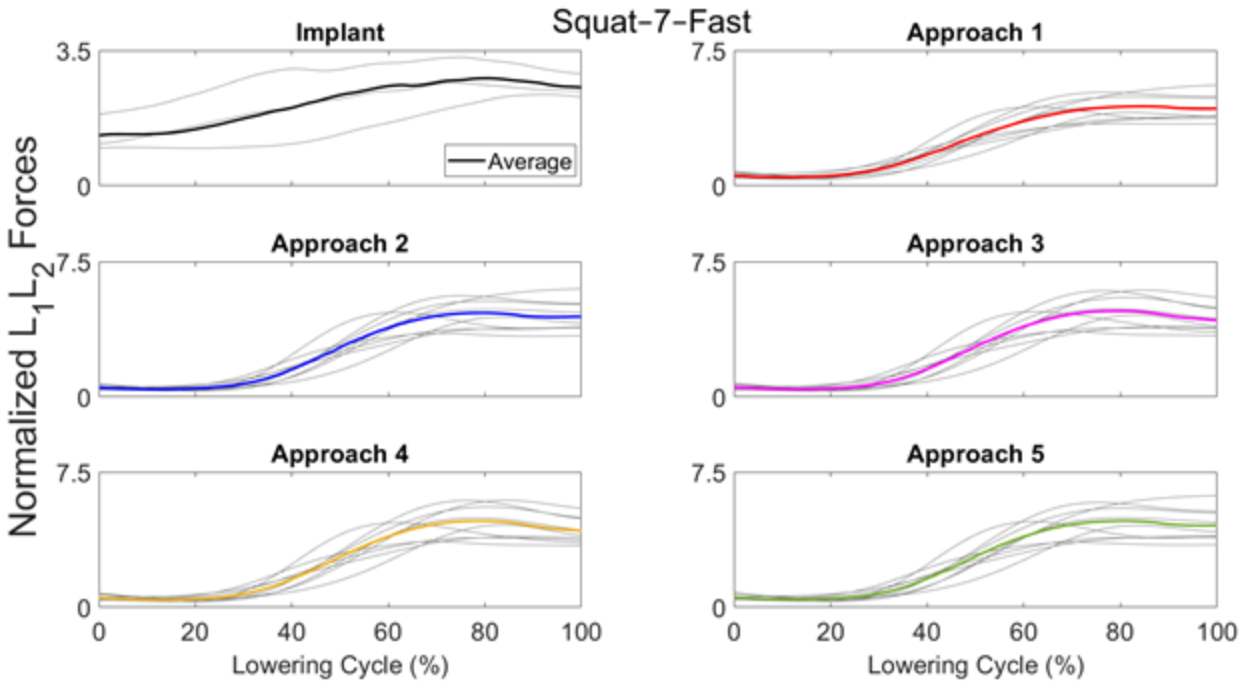


Fig. D.7. Raw and average normalized curves during the **lowering** motion cycle of the **Squat–7–Fast** task. $L_1L_2$ intervertebral forces were normalized using the body weight offset normalization technique (D–SI. 4). Raw estimated and measured normalized forces are shown in gray. The raw normalized forces were first averaged across the trials for each individual and then across all individuals. The final average curves for measured implant data and forces estimated using EHF&M Approaches 1–5 are shown as coloured solid lines.

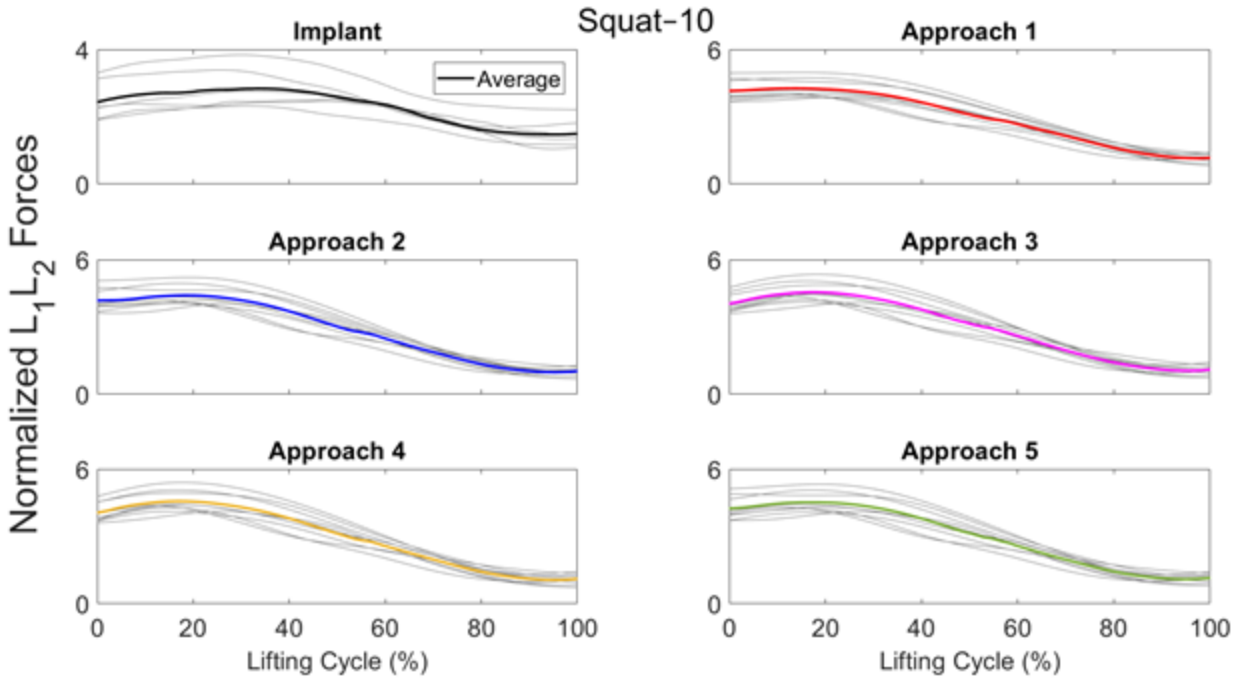


Fig. D.8. Raw and average normalized curves during the **lifting** motion cycle of the **Squat–10** task. $L_1L_2$ intervertebral forces were normalized using the body weight offset normalization technique (D–SI. 4). Raw estimated and measured normalized forces are shown in gray. The raw normalized forces were first averaged across the trials for each individual and then across all individuals. The final average curves for measured implant data and forces estimated using EHF&M Approaches 1–5 are shown as coloured solid lines.

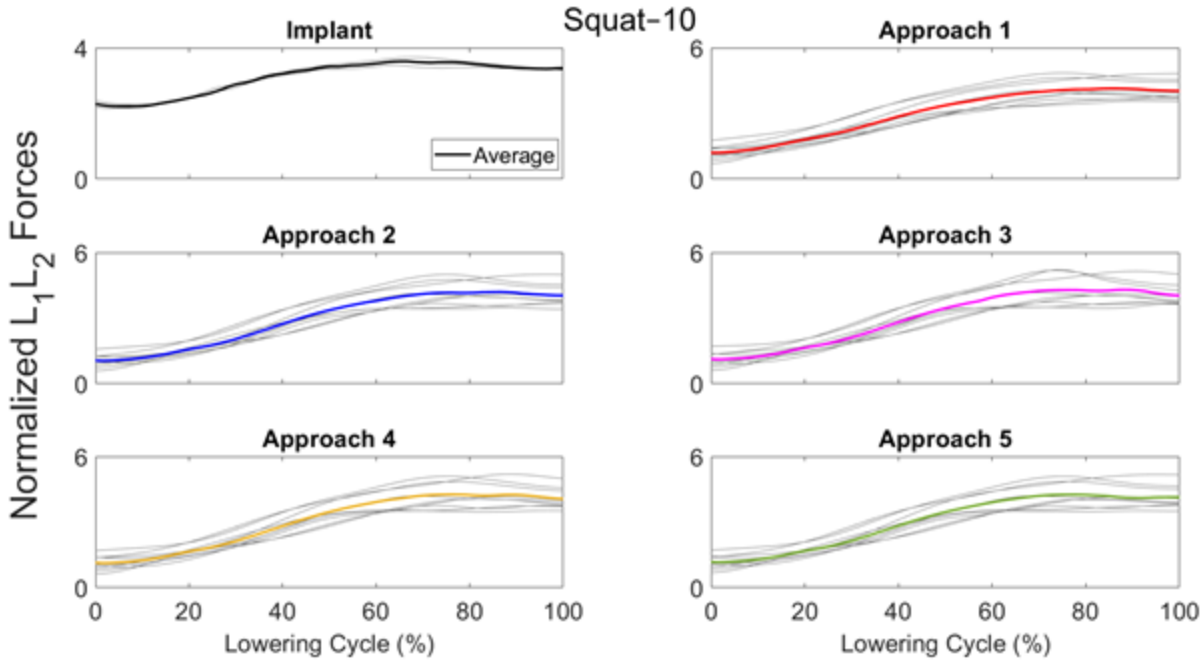


Fig. D.9. Raw and average normalized curves during the **lowering** motion cycle of the **Squat–10** task. $L_1L_2$ intervertebral forces were normalized using the body weight offset normalization technique (D–SI. 4). Raw estimated and measured normalized forces are shown in gray. The raw normalized forces were first averaged across the trials for each individual and then across all individuals. The final average curves for measured implant data and forces estimated using EHF&M Approaches 1–5 are shown as coloured solid lines.

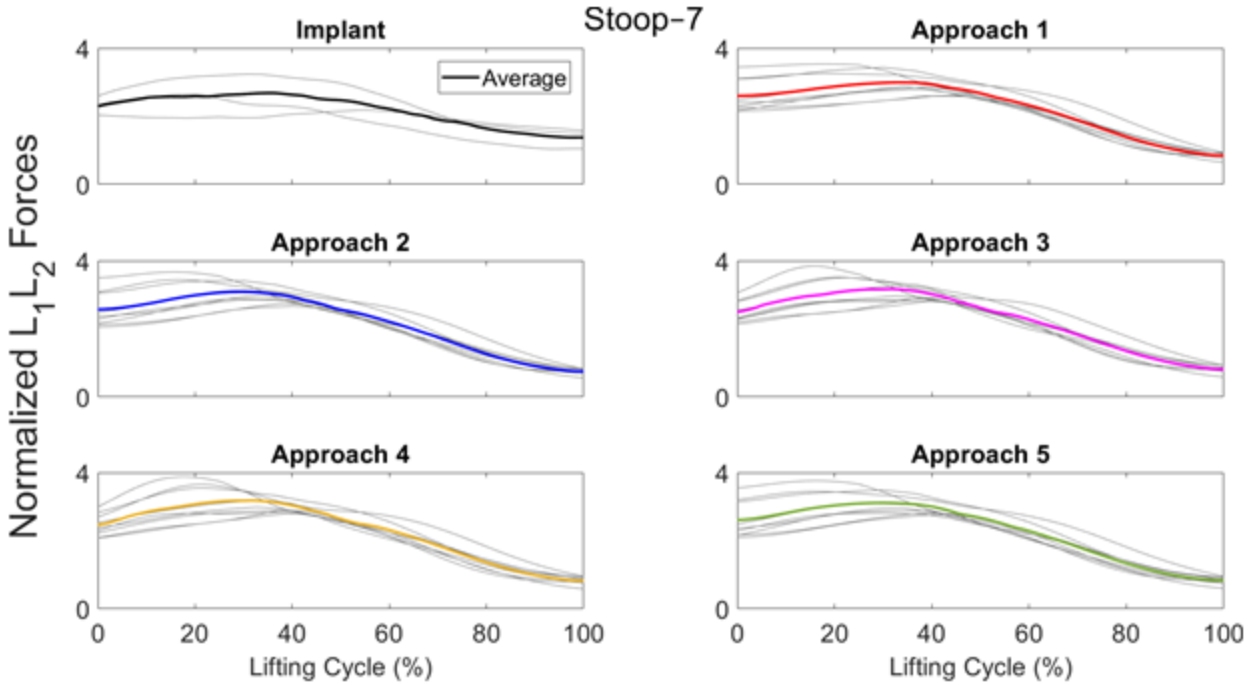


Fig. D.10. Raw and average normalized curves during the **lifting** motion cycle of the **Stoop–7** task. $L_1L_2$ intervertebral forces were normalized using the body weight offset normalization technique (D–SI. 4). Raw estimated and measured normalized forces are shown in gray. The raw normalized forces were first averaged across the trials for each individual and then across all individuals. The final average curves for measured implant data and forces estimated using EHF&M Approaches 1–5 are shown as coloured solid lines.

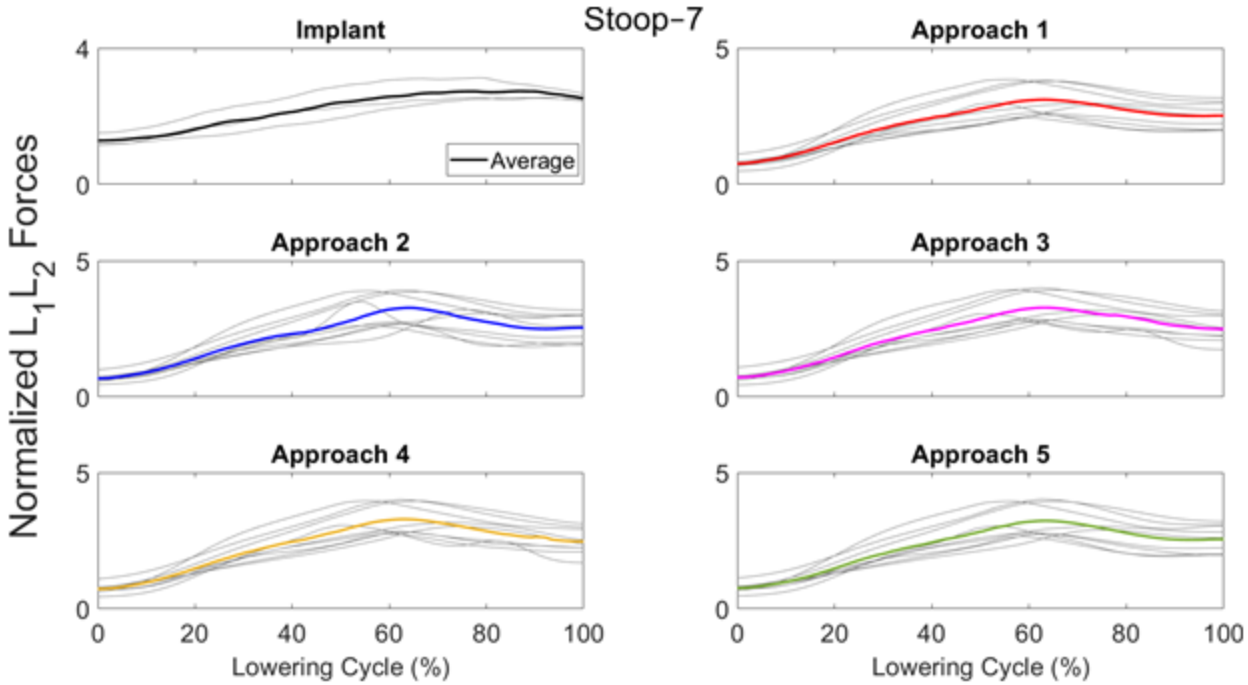


Fig. D.11. Raw and average normalized curves during the **lowering** motion cycle of the **Stoop–7** task. $L_1L_2$ intervertebral forces were normalized using the body weight offset normalization technique (D–SI. 4). Raw estimated and measured normalized forces are shown in gray. The raw normalized forces were first averaged across the trials for each individual and then across all individuals. The final average curves for measured implant data and forces estimated using EHF&M Approaches 1–5 are shown as coloured solid lines.

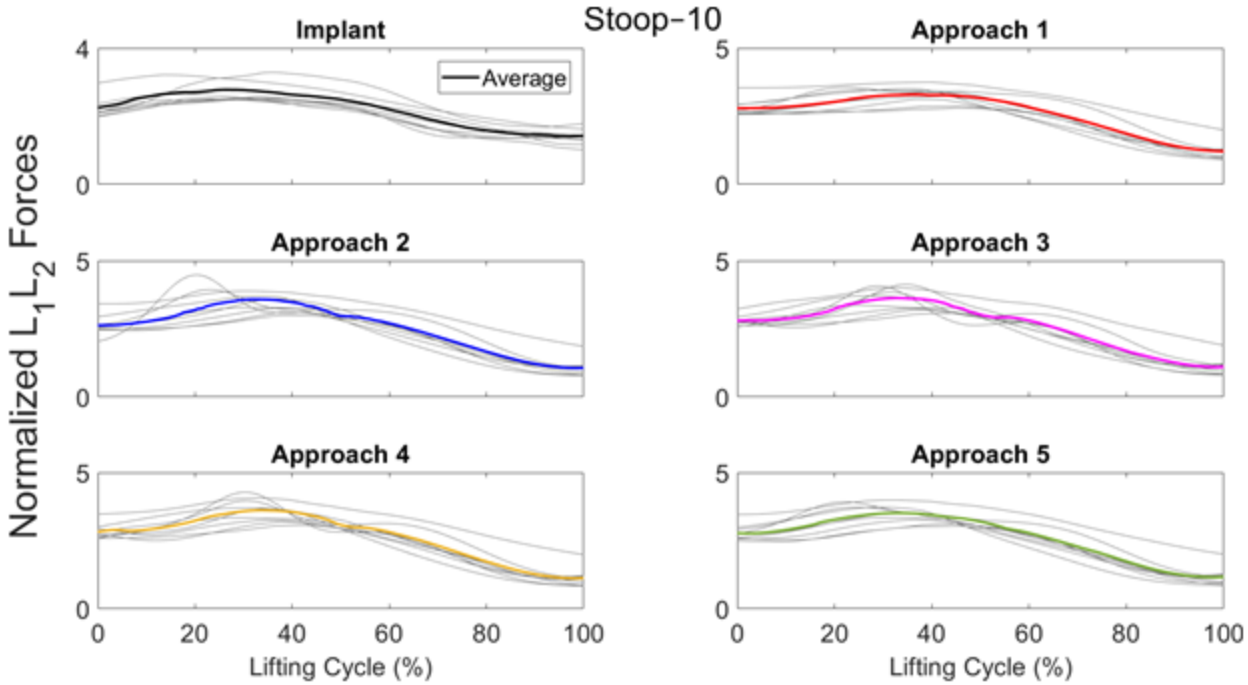


Fig. D.12. Raw and average normalized curves during the **lifting** motion cycle of the **Stoop–10** task. $L_1L_2$ intervertebral forces were normalized using the body weight offset normalization technique (D–SI. 4). Raw estimated and measured normalized forces are shown in gray. The raw normalized forces were first averaged across the trials for each individual and then across all individuals. The final average curves for measured implant data and forces estimated using EHF&M Approaches 1–5 are shown as coloured solid lines.

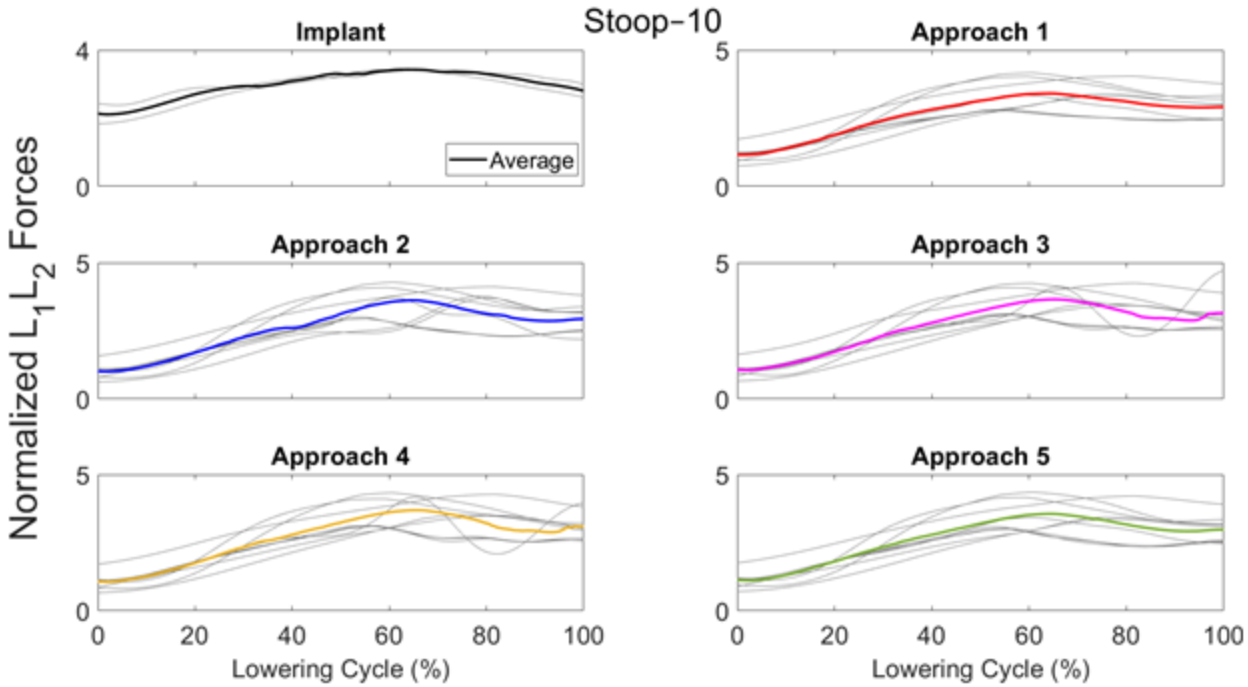


Fig. D.13. Raw and average normalized curves during the **lowering** motion cycle of the **Stoop–10** task. $L_1L_2$ intervertebral forces were normalized using the body weight offset normalization technique (D–SI. 4). Raw estimated and measured normalized forces are shown in gray. The raw normalized forces were first averaged across the trials for each individual and then across all individuals. The final average curves for measured implant data and forces estimated using EHF&M Approaches 1–5 are shown as coloured solid lines.

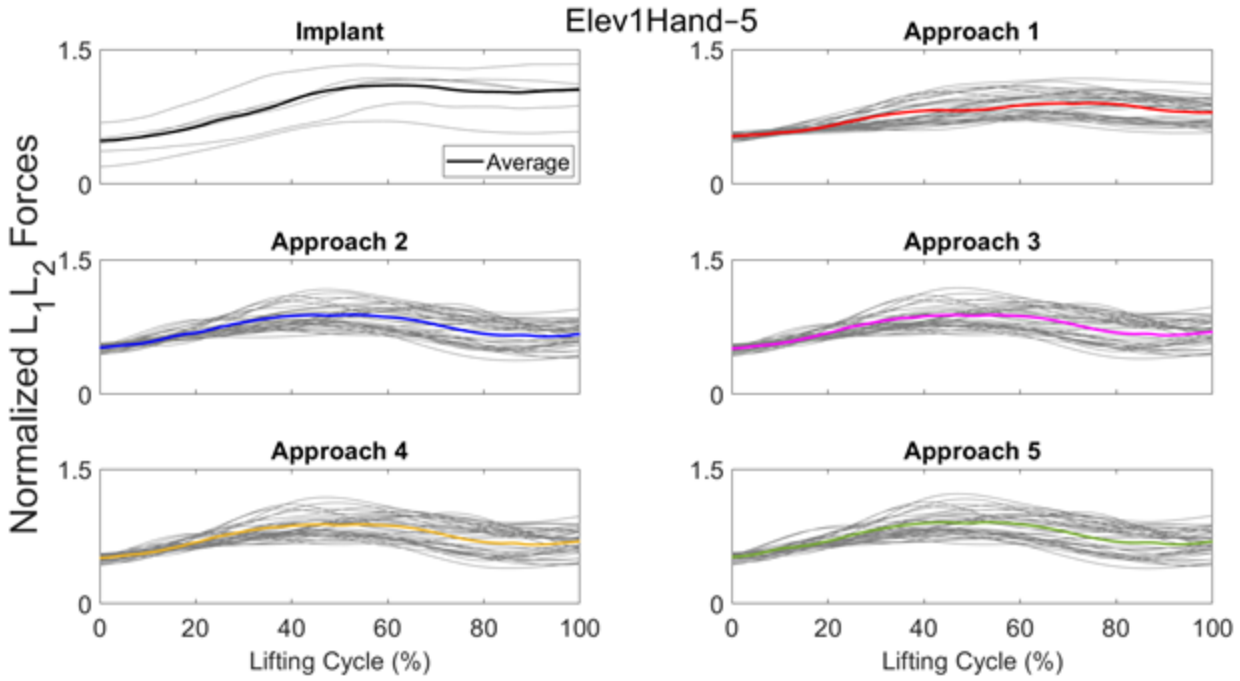


Fig. D.14. Raw and average normalized curves during the **lifting** motion cycle of the **Elev1Hand–5** task. $L_1L_2$ intervertebral forces were normalized using the body weight offset normalization technique (D–SI. 4). Raw estimated and measured normalized forces are shown in gray. The raw normalized forces were first averaged across the trials for each individual and then across all individuals. The final average curves for measured implant data and forces estimated using EHF&M Approaches 1–5 are shown as coloured solid lines.

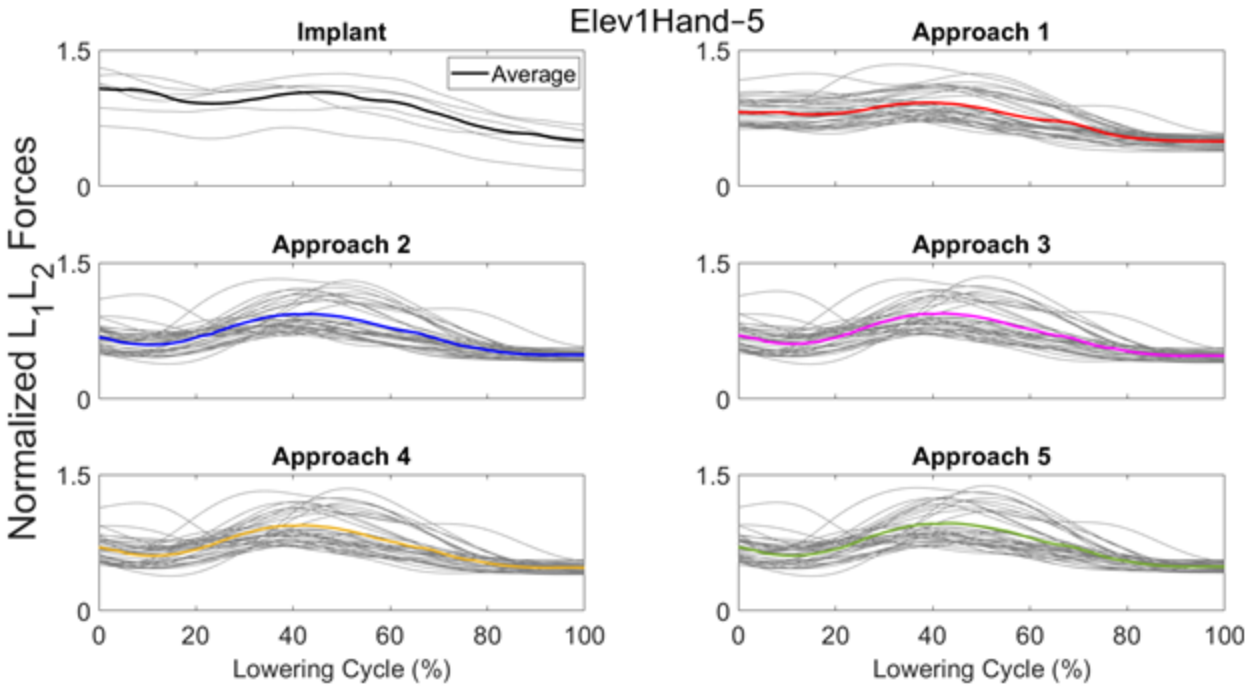


Fig. D.15. Raw and average normalized curves during the **lowering** motion cycle of the **Elev1Hand–5** task. $L_1L_2$ intervertebral forces were normalized using the body weight offset normalization technique (D–SI. 4). Raw estimated and measured normalized forces are shown in gray. The raw normalized forces were first averaged across the trials for each individual and then across all individuals. The final average curves for measured implant data and forces estimated using EHF&M Approaches 1–5 are shown as coloured solid lines.

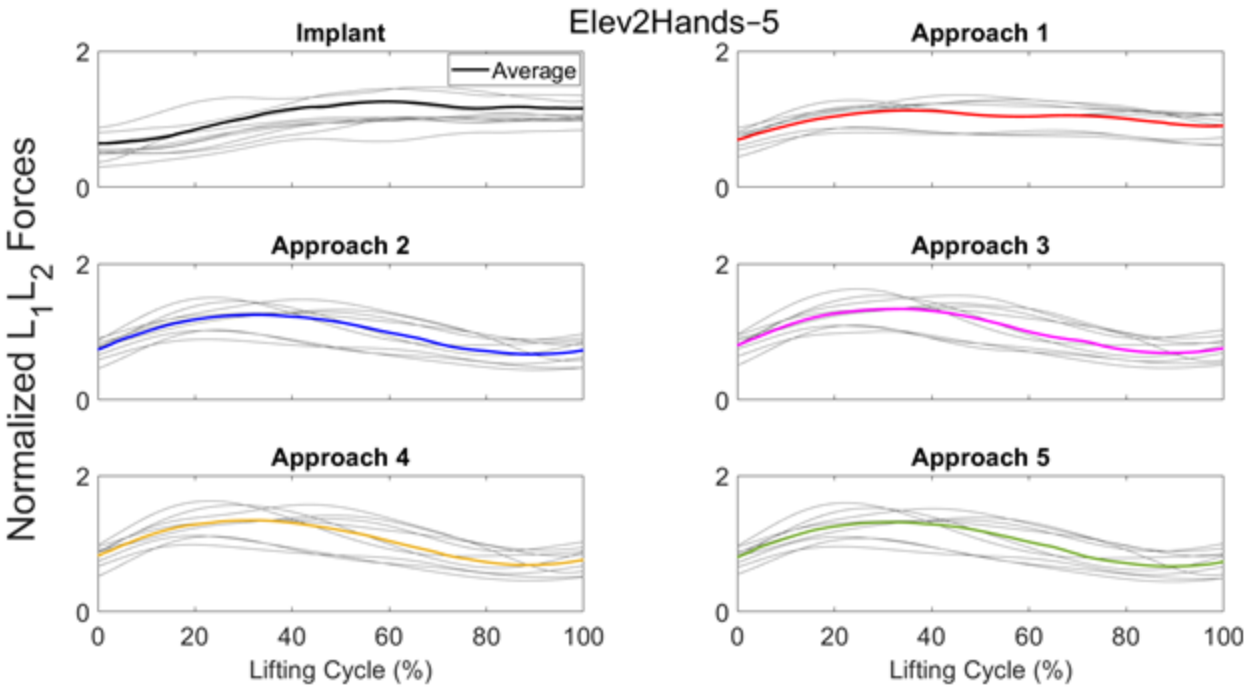


Fig. D.16. Raw and average normalized curves during the **lifting** motion cycle of the **Elev2Hands–5** task. $L_1L_2$ intervertebral forces were normalized using the body weight offset normalization technique (D–SI. 4). Raw estimated and measured normalized forces are shown in gray. The raw normalized forces were first averaged across the trials for each individual and then across all individuals. The final average curves for measured implant data and forces estimated using EHF&M Approaches 1–5 are shown as coloured solid lines.

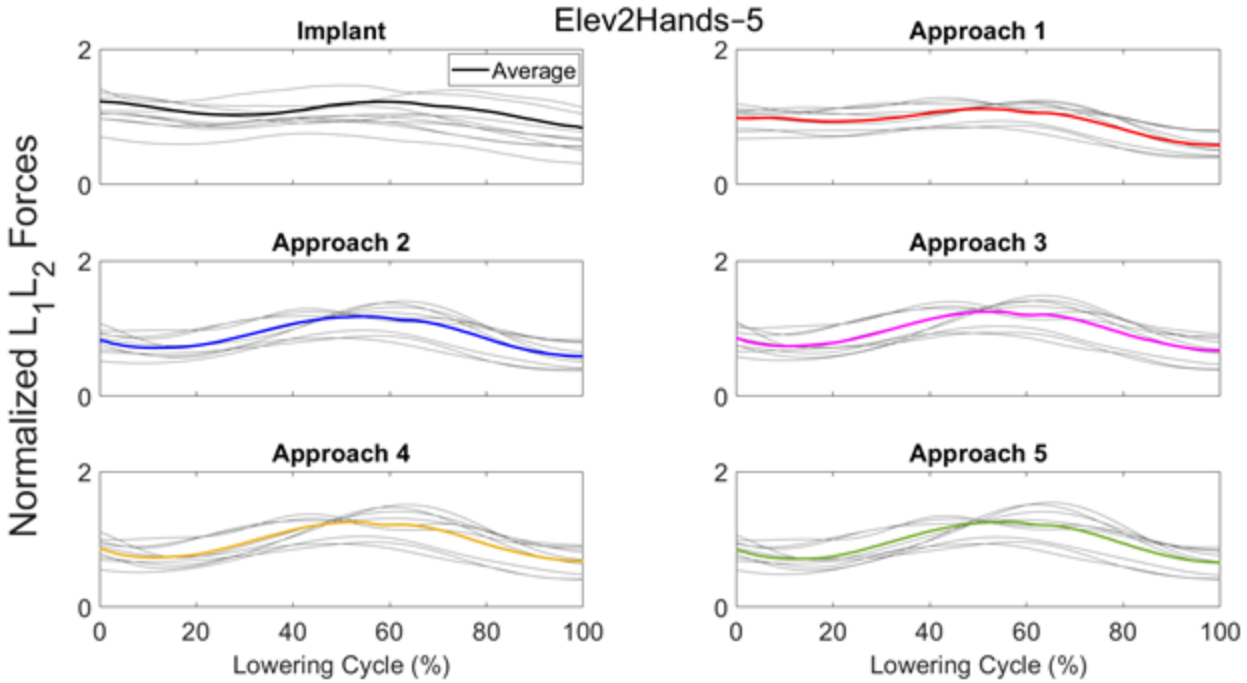


Fig. D.17. Raw and average normalized curves during the **lowering** motion cycle of the **Elev2Hands–5** task. $L_1L_2$ intervertebral forces were normalized using the body weight offset normalization technique (D–SI. 4). Raw estimated and measured normalized forces are shown in gray. The raw normalized forces were first averaged across the trials for each individual and then across all individuals. The final average curves for measured implant data and forces estimated using EHF&M Approaches 1–5 are shown as coloured solid lines.

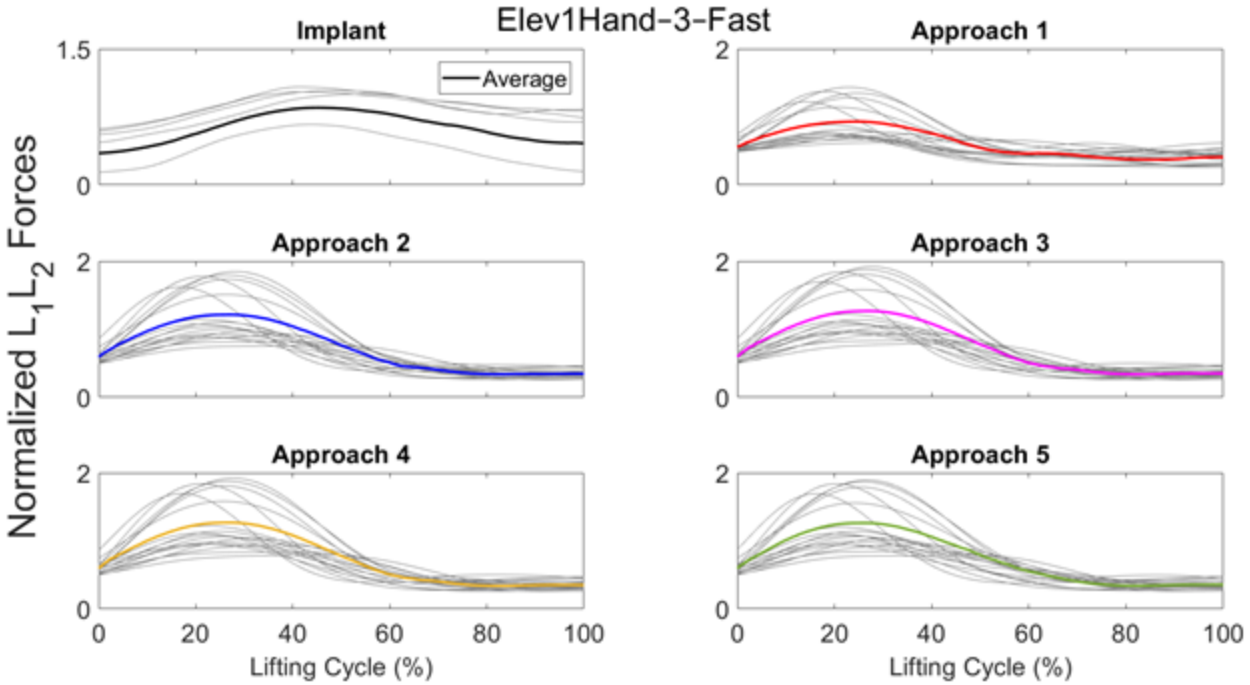


Fig. D.18. Raw and average normalized curves during the **lifting** motion cycle of the **Elev1Hand–3–Fast** task. $L_1L_2$ intervertebral forces were normalized using the body weight offset normalization technique (D–SI. 4). Raw estimated and measured normalized forces are shown in gray. The raw normalized forces were first averaged across the trials for each individual and then across all individuals. The final average curves for measured implant data and forces estimated using EHF&M Approaches 1–5 are shown as coloured solid lines.

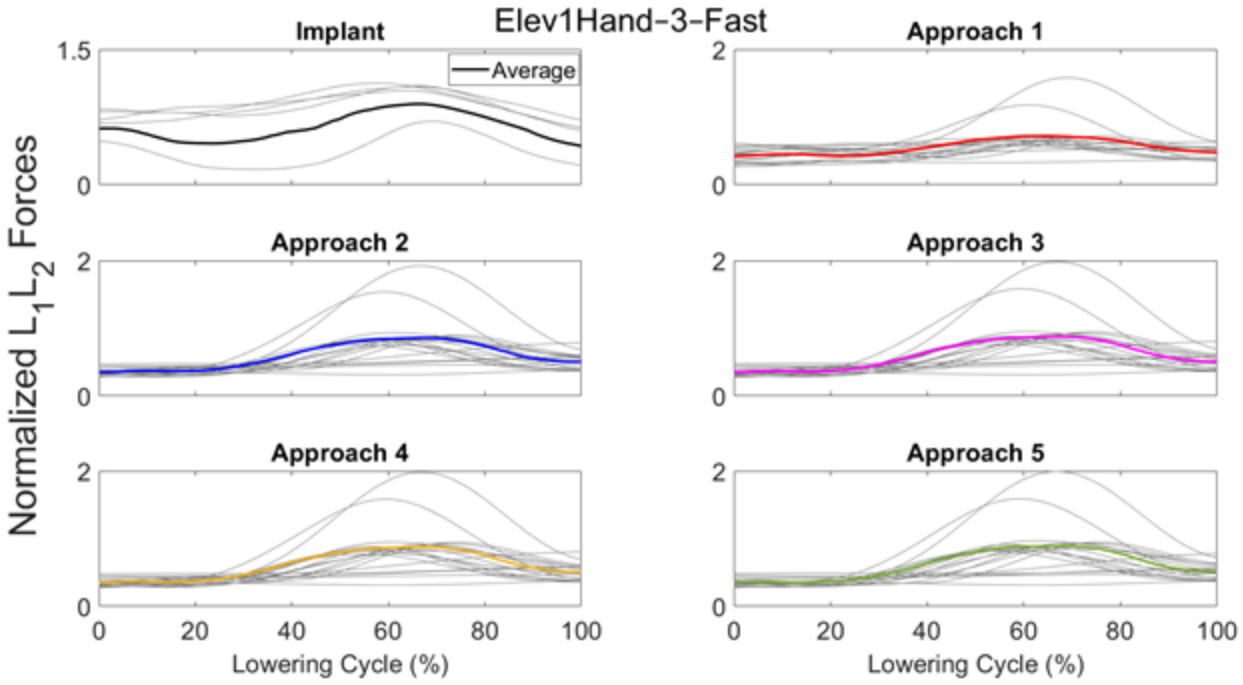


Fig. D.19. Raw and average normalized curves during the **lowering** motion cycle of the **Elev1Hand–3–Fast** task. $L_1L_2$ intervertebral forces were normalized using the body weight offset normalization technique (D–SI. 4). Raw estimated and measured normalized forces are shown in gray. The raw normalized forces were first averaged across the trials for each individual and then across all individuals. The final average curves for measured implant data and forces estimated using EHF&M Approaches 1–5 are shown as coloured solid lines.

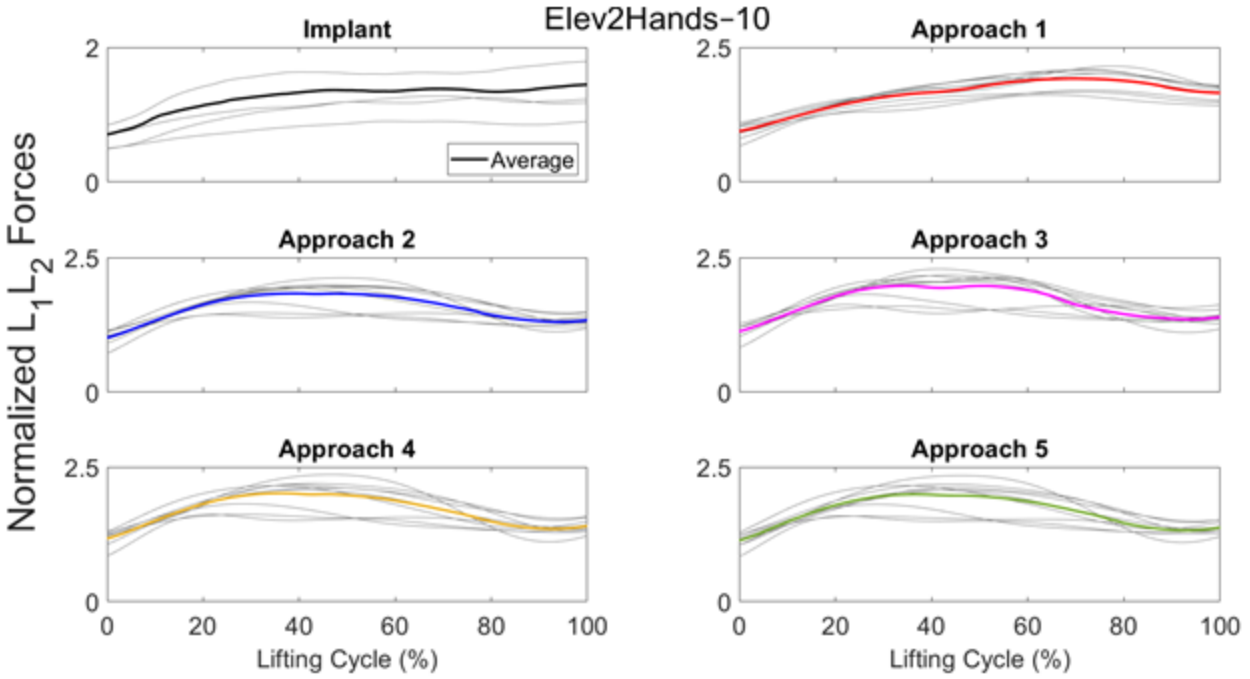


Fig. D.20. Raw and average normalized curves during the **lifting** motion cycle of the **Elev2Hands–10** task. $L_1L_2$ intervertebral forces were normalized using the body weight offset normalization technique (D–SI. 4). Raw estimated and measured normalized forces are shown in gray. The raw normalized forces were first averaged across the trials for each individual and then across all individuals. The final average curves for measured implant data and forces estimated using EHF&M Approaches 1–5 are shown as coloured solid lines.

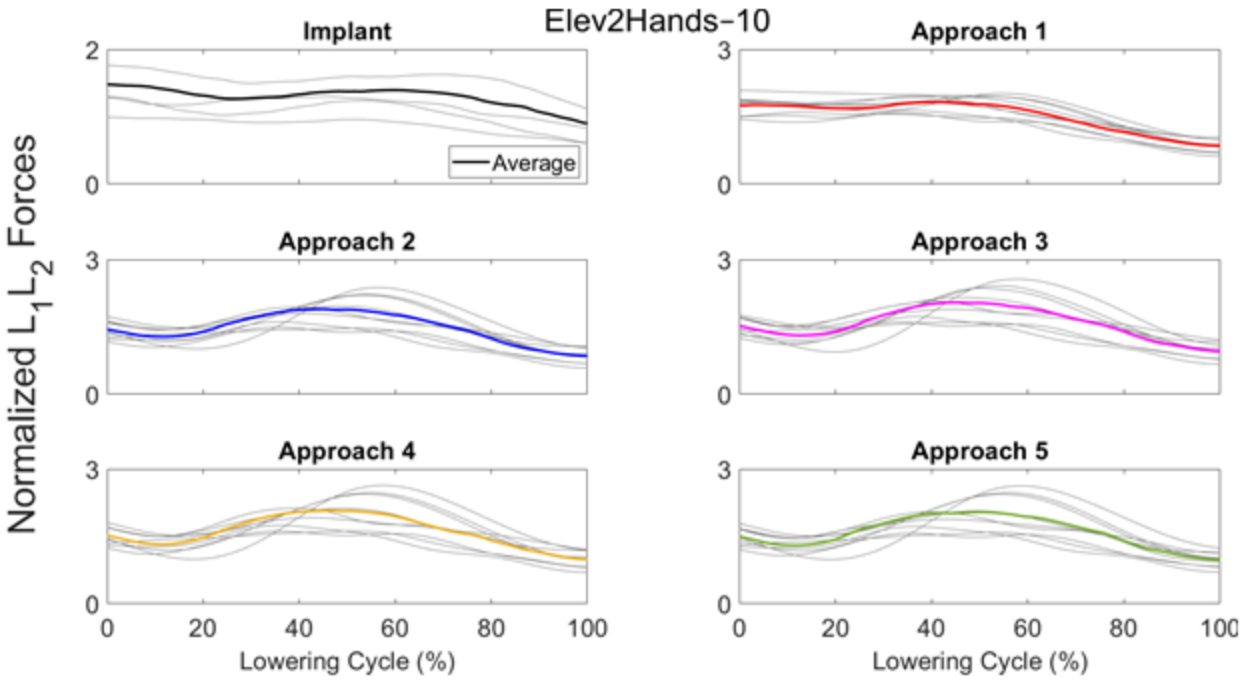


Fig. D.21. Raw and average normalized curves during the **lowering** motion cycle of the **Elev2Hands–10** task. $L_1L_2$ intervertebral forces were normalized using the body weight offset normalization technique (D–SI. 4). Raw estimated and measured normalized forces are shown in gray. The raw normalized forces were first averaged across the trials for each individual and then across all individuals. The final average curves for measured implant data and forces estimated using EHF&M Approaches 1–5 are shown as coloured solid lines.

**D–SI. 6**

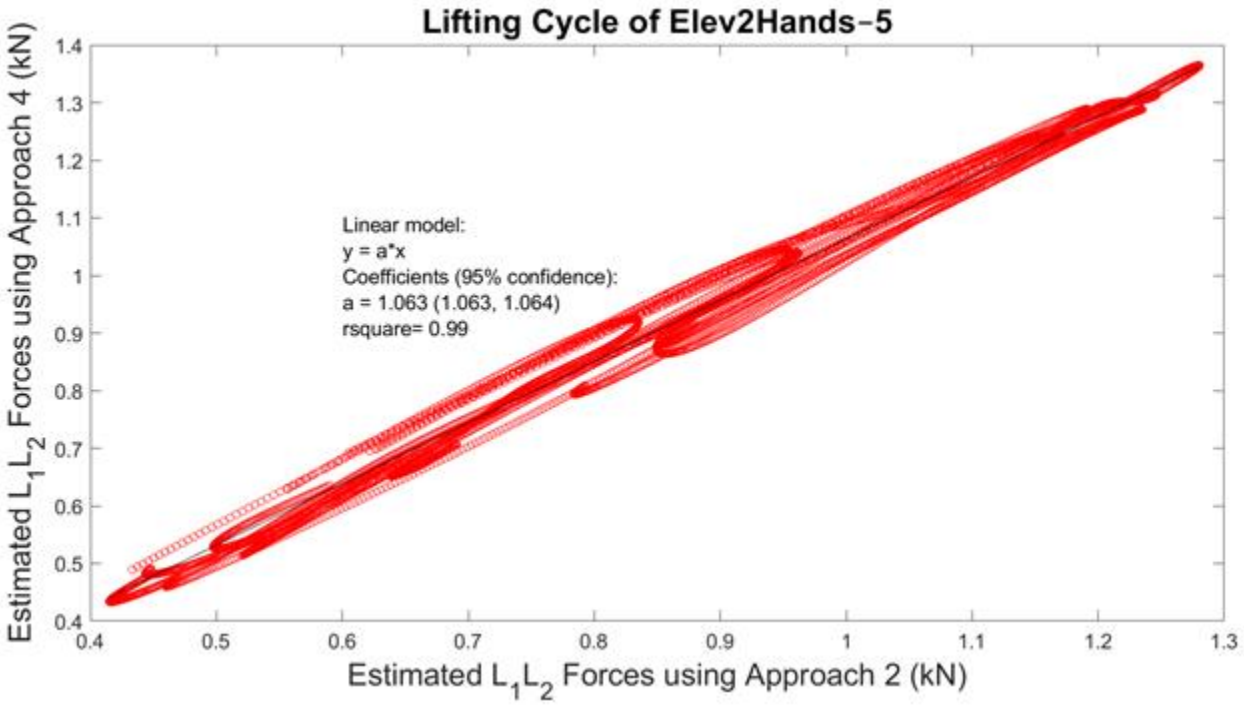


Fig. D.22. The linear trend line ($y = ax$) between the estimated $L_1L_2$ forces using EHF&M Approaches 2 and 4 during the lifting cycle of the Elev2Hands–5 task. This is one example; similar trend lines were fit for all studied tasks, for other intervertebral levels, and between other EHF&M approaches. The results of these trend lines (i.e., the slope and $R^2$ values) for the estimated $L_1L_2$ spinal forces were reported in Chapter 6 (Fig. 6.6), and the implications of these trend lines for estimated $L_4L_5$ and $L_5S_1$ forces are discussed in D–SI. 7.

## D–SI. 7

### *D–SI. 7.1 Uncertainty in Predicted Spinal Forces*

Considering the validity of the FATLS model demonstrated in this study and in previous research, we recommend its use for predicting intervertebral forces at different levels during lifting/lowering tasks. However, it is essential to consider that while the forces predicted by the various EHF&M modelling approaches showed considerable differences, all approaches resulted in equally valid intervertebral forces. As a result, reporting the uncertainty in the model's predictions is critical.

To support users in drawing informed conclusions about the impact of hand–load modelling decisions, we conducted a post hoc analysis focused on $L_4L_5$ and $L_5S_1$ spinal forces, which are of great interest in musculoskeletal modelling studies. Intervertebral forces estimated using Approach 2 were selected as the independent variables in this analysis as Approach 2 was recommended in this study due to its ease of setup and application. Additionally, in our previous study (Akhavanfar et al., 2022), we found that if the computational expense of the inverse kinematic analysis in Approach 4 is a concern, Approach 2 is a better alternative than Approach 1 as Approach 2 leads to fewer dynamic inconsistencies in the model.

In this post hoc analysis, we employed linear trend lines ($y = ax$) to fit the $L_4L_5$ and $L_5S_1$ spinal forces estimated using EHF&M Approach 2 ($x$) and those estimated using EHF&M Approaches 3–5 ($y$). The resulting $R^2$ value for all curve fits was greater than 0.97 (see D–SI. 6 for an example of this curve fitting). The maximum slope ($a$) among the linear trend lines (Table D.2) represents the upper limit used to quantify the uncertainty of the estimated spinal forces using Approach 2. Notably, the values presented in Table D.2 are all significantly greater than 1.00.

These upper limits, as shown in Table D.2, have practical implications. For instance, in the context of designing injury prevention programs, many studies have assumed 3400 N as the biomechanical safety limit for compression forces (Ghezelbash et al., 2020). In the case of the lifting motion cycle of Elev2Hands–10, we recommend that if the $L_4L_5$ and $L_5S_1$ compression forces estimated using EHF&M Approach 2 exceed 3148 N (=3400/1.08) for a participant, this task should not be considered safe.

Table D.2. The maximum slope ($a$) among the linear trend lines ($y = ax$) that were fit to relate the spinal forces ($L_4L_5$ and $L_5S_1$) estimated using EHF&M Approaches 3–5 ($y$) to those estimated using Approach 2 during all tasks.

| | **$L_4L_5$** | | **$L_5S_1$** | |
|---|---|---|---|---|
| | Lifting | Lowering | Lifting | Lowering |
| **Squat–7** | 1.02 | 1.02 | 1.02 | 1.02 |
| **Squat–7–Fast** | 1.02 | 1.02 | 1.02 | 1.02 |
| **Squat–10** | 1.02 | 1.02 | 1.02 | 1.02 |
| **Stoop–7** | 1.02 | 1.01 | 1.02 | 1.01 |
| **Stoop–10** | 1.02 | 1.01 | 1.01 | 1.01 |
| **Elev1Hand–5** | 1.02 | 1.02 | 1.02 | 1.01 |
| **Elev2Hands–5** | 1.06 | 1.08 | 1.06 | 1.08 |
| **Elev1Hand–3–Fast** | 1.03 | 1.02 | 1.02 | 1.02 |
| **Elev2Hands–10** | 1.08 | 1.10 | 1.08 | 1.10 |

### *D–SI. 7.2 References*


Akhavanfar, M., Uchida, T.K., Clouthier, A.L., Graham, R.B., 2022. Sharing the load: modelling loads in OpenSim to simulate two-handed lifting. Multibody Syst. Dyn. 54, 213–234.

Ghezelbash, F., Shirazi-Adl, A., Plamondon, A., Arjmand, N., 2020. Comparison of different lifting analysis tools in estimating lower spinal loads–Evaluation of NIOSH criterion. J. Biomech. 112, 110024.

## D–SI. 8

### *D–SI. 8.1 Effect of Passive Moments on the Predicted Intervertebral Forces*

We have conducted an analysis to assess the influence of the passive moments on the predicted vertebral loads in our FATLS model. Specifically, we compared the $L_1L_2$ spinal force predictions with and without passive moments during the Stoop–10 and Squat–10 tasks for each participant (P1, P2, P3). Our findings demonstrate that the inclusion of passive moments has a substantial effect on the spinal forces predicted by the model (Fig. D.23). Ignoring the passive stiffness can lead to substantial overestimation of spinal forces during stoop and squat tasks, with overestimations of peak $L_1L_2$ resultant forces ranging from 45% to 61% (approximately 1000–1300 N) during stoop lifting and lowering, and from 17% to 37% (500–1000 N) during squat lifting and lowering. These results highlight the importance of including passive stiffness in the model.

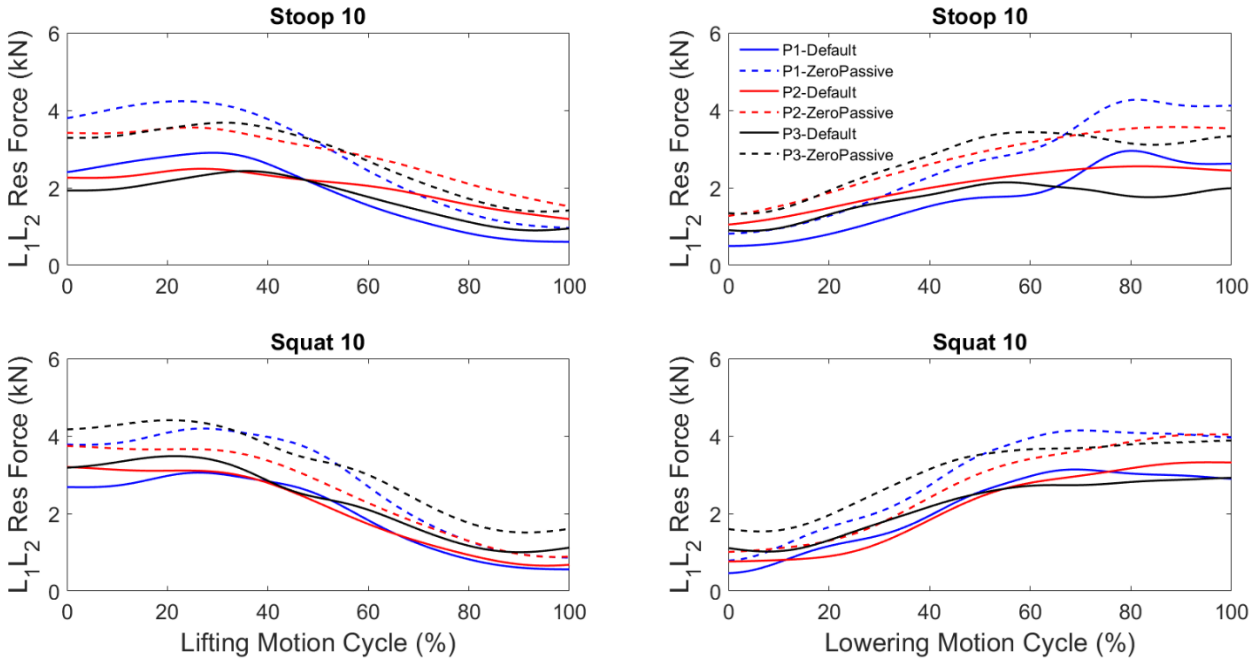


Fig. D.23. Estimated $L_1L_2$ spinal forces with and without passive moments during the Stoop–10 and Squat–10 tasks for each participant (P1, P2, P3).

# Appendix E: Ethics Approval

13/09/2022

Université d'Ottawa
Bureau d'éthique et d'intégrité de la recherche

University of Ottawa
Office of Research Ethics and Integrity

## CERTIFICAT D'APPROBATION ÉTHIQUE | CERTIFICATE OF ETHICS APPROVAL

| | |
|---|---|
| **Numéro du dossier / Ethics File Number** | H-06-21-7034 |
| **Titre du projet / Project Title** | Developing and validating new musculoskeletal models of the spine driven by two new marker-less technologies |
| **Type de projet / Project Type** | Thèse de doctorat / Doctoral thesis |
| **Statut du projet / Project Status** | Renouvelé / Renewed |
| **Date d'approbation (jj/mm/aaaa) / Approval Date (dd/mm/yyyy)** | 05/08/2021 |
| **Date d'expiration (jj/mm/aaaa) / Expiry Date (dd/mm/yyyy)** | 04/08/2023 |

### Équipe de recherche / Research Team

| Chercheur / Researcher | Affiliation | Role |
|---|---|---|
| Mohammadhossein AKHAVANFAR | École des sciences de l'activité physique / School of Human Kinetics | Chercheur Principal / Principal Investigator |
| Ryan GRAHAM | École des sciences de l'activité physique / School of Human Kinetics | Superviseur / Supervisor |
| Alexandre MIR-OREFICE | University of Ottawa | Assistant de recherche / Research Assistant |

**Conditions spéciales ou commentaires / Special conditions or comments**

13/09/2022

Université d'Ottawa

Bureau d'éthique et d'intégrité de la recherche

University of Ottawa

Office of Research Ethics and Integrity

Le Comité d'éthique de la recherche (CÉR) de l'Université d'Ottawa, opérant conformément à l'*Énoncé de politique des Trois conseils* (2014) et toutes autres lois et tous règlements applicables, a examiné et approuvé la demande d'éthique du projet de recherche ci-nommé.

L'approbation est valide pour la durée indiquée plus haut et est sujette aux conditions énumérées dans la section intitulée "Conditions Spéciales ou Commentaires". Le formulaire « Renouvellement ou Fermeture de Projet » doit être complété quatre semaines avant la date d'échéance indiquée ci-haut afin de demander un renouvellement de cette approbation éthique ou afin de fermer le dossier.

Toutes modifications apportées au projet doivent être approuvées par le CÉR avant leur mise en place, sauf si le participant doit être retiré en raison d'un danger immédiat ou s'il s'agit d'un changement ayant trait à des éléments administratifs ou logistiques du projet. Les chercheurs doivent aviser le CÉR dans les plus brefs délais de tout changement pouvant augmenter le niveau de risque aux participants ou pouvant affecter considérablement le déroulement du projet, rapporter tout évènement imprévu ou indésirable et soumettre toute nouvelle information pouvant nuire à la conduite du projet ou à la sécurité des participants.

The University of Ottawa Research Ethics Board, which operates in accordance with the *Tri-Council Policy Statement* (2014) and other applicable laws and regulations, has examined and approved the ethics application for the above-named research project.

Ethics approval is valid for the period indicated above and is subject to the conditions listed in the section entitled "Special Conditions or Comments". The "Renewal/Project Closure" form must be completedfour weeks before the above-referenced expiry date to request a renewal of this ethics approval or closure of the file.

Any changes made to the project must be approved by the REB before being implemented, except when necessary to remove participants from immediate endangerment or when the modification(s) only pertain to administrative or logistical components of the project. Investigators must also promptly alert the REB of any changes that increase the risk to participant(s), any changes that considerably affect the conduct of the project, all unanticipated and harmful events that occur, and new information that may negatively affect the conduct of the project or the safety of the participant(s).

Safaa LAMHOUJEB
Coordonnateur de l'éthique / Ethics Coordinator
Pour/For **Daniel LAGAREC** Président(e) du/ Chair of the **Comité d'éthique de la recherche en sciences de la santé et sciences / Health Sciences and Sciences Research Ethics Board**

# Appendix F: Informed Consents

uOttawa

Université d'Ottawa
Faculté des sciences de la santé
École des sciences de l'activité physique
University of Ottawa
Faculty of Health Sciences
School of Human Kinetics

☎ 613-562-5853
🖷 613-562-5149
125 University Private
Ottawa ON K1N 6N5 Canada
www.uOttawa.ca

# Research Consent Form

**Research Project Title:** **Developing and validating new musculoskeletal models of the spine driven by two new marker-less technologies**

**Thesis Supervisor:**
**Dr. Ryan Graham**
**613-562-5800 X 1025; ryan.graham@uottawa.ca**
**University of Ottawa**
**Faculty of Health Sciences**
**Department of Human Kinetics**
**200 Lees Ave (E020)**
**Ottawa, ON K1N6N5**

**Principal Investigator:**
**Mohammadhossein Akhavanfar**

**Funding information:**
This study is funded by the Natural Sciences and Engineering Research Council of Canada (RGPIN-2020-04748 [Dr. Ryan Graham], PGSD3-518358-2018 [Mohammadhossein Akhavanfar], the Ontario Early Researcher Award Program (ER17-13-007 [Dr. Ryan Graham]), and the University of Ottawa Research Chairs Program [Dr. Ryan Graham].

**COVID-19 Precautions:**
For the safety of both yourself and the researchers, precautions have been put in place to try and prevent the spread of COVID-19. Before arriving at the lab, you and the researchers will be screened for COVID-19 symptoms and will be asked to use hand sanitizer upon entering and exiting the lab. Both you and the researchers are required to wear a mask at all times during the data collection as well as protective eyewear. All equipment that is touched by either a participant or a researcher during the collection will be wiped down with disinfectant before and after the collection and all washable materials will be washed in between each participant starting. There will be a mandatory minimum of one day between data collections.

**Background and Purpose of the Study:**
This study is being conducted as part of a doctoral thesis. Marker-less technologies have been of great interest recently as they provide systems that can easily collect data in the field. Such technologies include inertial measurement units (IMUs) and marker-less motion capture systems. IMUs are small sensors that can record their orientation and acceleration about a coordinate system. Marker-less motion capture systems are able to calculate kinematic data from 2D RGB videos, such as those taken from a typical camera. Furthermore, these technologies can provide data able to drive musculoskeletal models and estimate muscle forces and

joint loads. To implement the use of these technologies in the field however, they must be deemed valid against a gold standard, that of stereophotogrammetric systems that use infrared cameras to locate the positions of reflective markers. Therefore, the purpose of this study is to develop new musculoskeletal models and drive them using two marker-less motion capture technologies, namely IMUs (DOT, Xsens, Netherlands) and marker-less motion capture systems (Theia3D, Theia Markerless, Inc., Kingston, Canada).

**Description of Study Procedures:**

You are invited to participate in a one-day motion analysis procedure for approximately 3.5 hours at the University of Ottawa Human Movement
Biomechanics Laboratory (200 Lees Avenue, E020). The study protocol consists of a series of tasks that comprise six load-free ranges of motions such as bending forwards and sideways; 45 dynamic symmetric lifting/lowering trials such as squats and stoops; 32 dynamic asymmetric lifting/lowering trials that involve moving weights from one side of you to a shelf located in front of you; six loaded walking trials; and 27 standing lifting trials that involve lifting a dumbbell in front of you (for a total of 116 dynamic trials). The maximum lifting load for the aforementioned tasks will be 20 kg, similar to the weight of a water cooler jug. You will be able to rest between each task and take breaks whenever needed to avoid onset of muscle fatigue.

Prior to data collection, anthropometric measures will be collected, namely, your height, weight, and the diameter of your thorax, pelvis, arm, and forearms. You will then be outfitted with 2 motion capture suits: an optical motion capture suit and an IMU suit. The optical motion capture suit is comprised of compressive leggings and a compressive shirt upon which we will place reflective marker clusters and individual markers will be placed on the upper and lower limbs, trunk, pelvis, and head. The IMU suit is comprised of X-treme straps that will hold the sensors and placed around the forearms, arms, trunk, and pelvis. Furthermore, two sensors will be placed on the back of your hands using double-sided adhesive tape. Before the experimental trials can begin, you will be asked to perform two five-second static reference calibration trials and a functional range of motion trial, which will both be used to create an individualized musculoskeletal model. Prior to the tasks, you will be asked to perform a small forward lean to orient the IMU sensors in space. In addition to the marker data and the IMU data, 8 video cameras will be capturing video data for the marker-less motion capture system; this system needs no special equipment.

**Possible Risks and Discomforts:**

There are no significant risks associated with participating in this study. You may experience pain and fatigue due to the nature of the tasks; however, sufficient rest will be given to reduce these effects. The tape used to attach the individual reflective markers may cause minor skin irritation; similar to what is experienced with a bandage and typically fades within 2 to 3 days.

Should you experience any major discomfort, please tell us immediately and seek primary care from a medical professional on campus (100 Marie Curie, Ottawa, Tel.: 613-564-3950) or a medical professional of your choosing.

**Possible Benefits:**

You will not directly benefit from participating in this study. However, the results of this study will greatly add to our knowledge of the validity of different motion capture systems.

**Voluntary Participation:**

You are not obliged to participate in this study; you participation is voluntary. You may also withdraw from the study at any time with no penalty or coercion. If chosen to withdaw, your data will be destroyed (i.e. it will not be used in the study).



**Confidentiality:**

All personal information is kept confidential. Information gained from this study will be stored electronically and will need a password to access, which will only be known to Dr. Ryan Graham and the research team. Paper study records are stored in a locked cabinet and will be destroyed after 5 years post publication; electronic records will be deleted and paper records will be shredded. You will not be identified by name in any reports of the completed study. Your anonymity will be strictly maintained – you will not be identified by your name but will be determined by an independent study number.

**Compensation:**
You will not be compensated for your participation in this study.

**Questions about the Study:**
You are free to ask questions at any time during the protocol and by contacting the principal investigator by email: Mohammadhossein Akhavanfar or the thesis supervisor: Dr. Ryan Graham (ryan.graham@uottawa.ca). The ethical components of this research project has been approved by the University of Ottawa research ethics board. If you have any questions regarding the ethical conduct of this study, you may contact the Protocol Officer for Ethics in Research, University of Ottawa, Tabaret Hall, 550 Cumberland Street, Room 154, Ottawa ON, K1N 6N5. Tel.: (613) 562-5387 Email: ethics@uottawa.ca. There are two copies of the consent form, one of which is yours to keep.

**Research Project Title:** **Developing and validating new musculoskeletal models of the spine driven by two new markerless technologies**

**Consent:**
I have read this consent form, and I agree to participate in the procedures of this study.

_____
Printed Name of Participant

_____ _____
Signature of Participant Date

**Investigator Statement (or Person Explaining the Consent):**
I have carefully explained to the research participant the nature of the above research study. To the best of my knowledge, the research participant signing this consent form understands the nature, demands, risks and benefits involved in participating in this study. I acknowledge my responsibility for the care and well-being of the above research participant, to respect the rights and wishes of the research participant, and to conduct the study according to applicable Good Clinical Practice guidelines and regulations.

_____
Name of Investigator/Delegate (printed)

_____ _____
Signature of Investigator/Delegate Date

**Informed Consent to have Videos Taken:**
I consent to have video footage taken during the protocol. I understand that these videos are being used as part of the analysis and if any of these videos are used in a subsequent presentation or publication, that my face and any other identifiers will be blurred. You cannot participate in the research study without consenting to having video footage taken.

| | |
|---|---|
| _____ | _____ |
| Name | Date |
| _____ | |
| Signature | |
| _____ | _____ |
| Witness Name | Witness Signature |

**Future Participation:**

- ☐ I am interested in being contacted to participate in future research performed by this laboratory (your email information will be saved in a password protected file).

uOttawa

Université d'Ottawa
Faculté des sciences de la santé
École des sciences de l'activité physique
University of Ottawa
Faculty of Health Sciences
School of Human Kinetics

# Formulaire de consentement à la recherche

**Titre du projet de recherche:** **Developing and validating new musculoskeletal models of the spine driven by two new marker-less technologies**

**Superviseur de Thèse:**
**Dr. Ryan Graham**
**613-562-5800 X 1025; ryan.graham@uottawa.ca**
**Université d'Ottawa**
**Faculté des sciences de la santé**
**École des sciences de l'activité physique**
**200 Lees Ave (E020)**
**Ottawa, ON K1N6N5**
**Chercheur Principal :**
**Mohammadhossein Akhavanfar**

## Financement de l'étude

Cette étude est financée par le Conseil de recherches en Sciences Naturelles et en Génie du Canada (RGPIN-2020-04748 [Dr. Ryan Graham], PGSD3-518358-2018 [Mohammadhossein Akhavanfar], le Programme de Bourse de Nouveaux Chercheurs (ER17-13-007 [Dr. Ryan Graham]), et le programme de chaire de recherche de l'Université d'Ottawa [Dr. Ryan Graham].

## Précautions pour la COVID-19

Pour votre sécurité et la sécurité des chercheurs, des précautions ont été mises en place afin d'essayer de prévenir la propagation de la COVID-19. Avant d'arriver au laboratoire, les chercheurs et vous allez être filtrer pour des symptômes de COVID-19 et allez être demander d'utiliser du désinfectant pour les mains lorsque vous arrivez et partez du laboratoire. Les chercheurs et vous-même êtes requis de porter un masque en plus de lunettes de protection en tout temps lors de la collection de données. Tout équipement qui sera touché par soit le participant ou le chercheur lors de la collection sera essuyer avec du désinfectant avant et après la collection de données et tout matériel nettoyable sera lavé entre chaque participant. Il y aura un minimum de un jour entre la collection chaque collection de données.

## Contexte et objectif de l'étude:

Cette étude est faite dans le contexte d'une thèse doctorale. Les technologies sans marqueurs sont de grands intérêts récemment car elles fournies des systèmes qui peuvent facilement collectées des données à l'extérieure. Ses technologies inclues les unités de mesures inertielles (IMUs) et les systèmes de capture de mouvements sans marqueurs. Les

☎ 613-562-5853
🖷 613-562-5149
125 University Private
Ottawa ON K1N 6N5 Canada
www.uOttawa.ca

IMUs sont de petits senseurs capables de mesurer leurs orientation et accélération dans un système de coordonnées. Les systèmes de capture de mouvements sans marqueurs sont capables de mesurer les données cinématiques à partir de vidéos RGB en 2D, tel que celle prises avec des caméras vidéo normales. De plus, ces technologies peuvent fournir des données capables de contrôlées des modèles musculosquelettiques et d'estimées les forces musculaires et les charges aux jointures. Pour implémenter l'utilisation de ces technologies sur le terrain par contre, il faut qu'elles soient considérées valides en comparaison avec le médaillon d'or, les systèmes de stéréophotogrammétries qui utilisent des caméras infrarouges pour localiser la position de marqueurs réfléchissants. Pour cette raison, l'objectif de cette étude est de développés des nouveaux modèles musculosquelettiques et de les contrôler avec deux technologies sans marqueurs, précisément les IMUs DOT, Xsens, Pays-Bas) et un systèmes de capture sans marqueurs (Theia3D, Theia Markerless, Inc., Kingston, Canada).

**Description des procédures d'étude:**
Vous êtes invité à participer à une procédure d'analyse de mouvement sur de un jour qui durera a peu près trois heures et demi au Laboratoire de biomécanique du mouvement humain de l'Université d'Ottawa (200, avenue Lees, E020). Le protocol consiste d'une séries de tâches qui compreenent six tâches sans charges mesurant votre amplitude de mouvements tel que des flexions avant et de côté, 45 tâches de levages symmetriques tel que des squats, 32 tâches de levages assymmétriques qui consistent de déplacé un poids de votre côté à une étagère placé devant vous, 6 tâches de marcher avec un poids et 27 tâches de levage debout qui consistent à lever un poids devant soi (pour un total de 116 mouvements). La charges maximale utilisée sera de 20kg, un poids similaire à un bidon d'eau. Vous serez capable de prendre du repos enter chaque tâches et de prendre des pauses quand vous le souhaiter.

Avant de commencer la collection de données, des mesures anthropométriques seront collectés, précisément votre taille, poids, et le diamètre de votre torso, bassin, bras et avant-bras. Vous allez ensuite mettre deux costumes de captures de mouvements : un costumes optiques et un pour les IMUs. Le costumes pour le systèmes optique comprendra des leggings et un chandail de compression sur lequel on placera des groupes de marqueurs réfléchissants et des marqueurs individuels sur vos membres supérieurs et inférieurs, votre torso, bassin et tête. Le costumes de IMUs comprends des strappes X-treme qui tiendront les senseurs et seront placées autour des avant-bras, bras, torso et bassin. De plus, deux senseurs seront placés sur le dos de vos mains avec un ruban adhésif. Avant de commencés les tâches expérimentales, vous allex devoir faire un calibration statique et une séries de mouvements dans l'ensemble de vos amplitudes de mouvements qui seront utilisées pour créer un modèle musculosquelettique personallisé. Avant le début de chaque tâches, vous allez devoir vous incliner légèrement vers l'avant pour orienter les IMUs. En plus des données des marqueurs et des IMUs, 8 caméras vidéos vont filmés vos mouvements pour le système de capture de mouvement sans marqueurs, qui ne nécéssite aucun équipement.

**Risques possibles et inconforts:**
Il n'y a pas de risques significatifs associés à la participation à cette étude. Vous pourriez ressentir de la douleur et de la fatigue en raison de la nature des tâches; cependant, suffisamment de repos sera donné pour réduire ces effets. Le ruban adhésif utilisée pour attacher les marqueurs réfléchissants individuels peut causer une légère irritation de la peau; similaire à ce qui est ressentis avec un bandage et disparaîtra généralement dans les 2 à 3 jours suivants.

Si vous ressentez un inconfort majeur, veuillez-nous en informer immédiatement et demander des soins primaires auprès d'un professionnel de la santé sur le campus (100 Marie Curie, Ottawa, 613-664-3950) ou d'un professionnel de la santé de votre choix.

**Avantages possibles:**
Vous ne bénéficierez pas directement de votre participation à cette étude. Cependant, les résultats de cette étude ajouteront beaucoup à notre connaissance de la validité des systèmes de capture de mouvement lors de mouvements militaires chargés.

**Participation Volontaire:**

Vous n'êtes pas obligé de participer à cette étude; Votre participation est volontaire. Vous pouvez également vous retirer de l'étude à n'importe quel moment, sans pénalité ni coercition. Vous serez compensé jusqu'au moment du retrait et vos données seront détruites (c'est-à-dire qu'elles ne seront pas utilisées dans l'étude).

**Confidentialité:**
Toutes les informations personnelles sont gardées confidentielles. Les informations tirées de cette étude seront stockées électroniquement et nécessiteront un mot de passe pour y accéder, qui ne sera connu que par Dr. Ryan Graham et l'équipe de recherche. Les dossiers d'étude sur papier sont stockés dans une armoire verrouillée et seront détruits 5 ans après leur publication; les dossiers électroniques seront supprimés et les dossiers papier seront déchiquetés. Vous ne serez pas identifié par nom dans les rapports finaux de l'étude. Votre anonymat sera strictement maintenu - vous ne serez pas identifié par votre nom, mais sera déterminé par un numéro d'étude indépendant.

**Compensation:**
Vous ne recevrez aucune compensation pour votre participation dans cette étude

**Questions sur l'étude:**
Vous êtes libre de poser des questions à tout moment pendant le protocole et en communiquant avec le chercheur principal par courriel: Mohammadhossein Akhavanfar ou le superviseur de thèse : Dr Ryan Graham (ryan.graham@uottawa.ca). Les composantes éthiques de ce projet de recherche ont été approuvées par le comité d'éthique de la recherche de l'Université d'Ottawa. Si vous avez des questions concernant la conduite éthique de cette étude, vous pouvez communiquer avec l'agente de protocole pour l'éthique de la recherche, Université d'Ottawa, Pavillon Tabaret, 550, rue Cumberland, pièce 154, Ottawa (Ontario) K1N 6N5. Tél .: (613) 562-5387 Courriel: ethics@uottawa.ca. Il y a deux copies du formulaire de consentement, dont l'une est à vous de conserver.

**Titre du projet de recherche: Developing and validating new musculoskeletal models of the spine driven by two new marker-less technologies**

**Consentement:**
J'ai lu ce formulaire de consentement et j'accepte de participer aux procédures de cette étude.

_____
Nom imprimé du participant

_____ _____
Signature du participant Date

**Déclaration de l'investigateur (ou personne expliquant le consentement):**
J'ai soigneusement expliqué au participant à la recherche la nature de l'étude de recherche ci-dessus. À ma connaissance, le participant à la recherche qui signe ce formulaire de consentement comprend la nature, les exigences, les risques et les avantages de participer à cette étude. Je reconnais ma responsabilité pour les soins et le bien-être du participant à la recherche ci-dessus, pour respecter les droits et les souhaits du participant à la recherche, et pour mener l'étude conformément aux directives et règlements applicables en matière de bonnes pratiques cliniques.

Nom de l'enquêteur / délégué (imprimé)

_____ _____
Signature de l'enquêteur / délégué Date

**Consentement pour la prise de photos:**
Je consens à la prise de photos en complétant l'expérience, et je comprends qu'aucune photo ne sera prise à aucun moment sans que je le sache. Je comprends également que si l'une de ces images est utilisée dans une présentation ou une publication ultérieure, mon visage et tous les autres identifiants seront flous. Vous pouvez toujours participer à l'étude de recherche sans consentir à la prise de photos.

_____ _____
Nom Date

_____
Signature

_____ _____
Nom du témoin Signature du témoin

**Participation future:**

- ☐ Je suis intéressé à être contacté pour participer à de futures recherches effectuées par ce laboratoire (vos informations d'email seront sauvegardées dans un fichier protégé par mot de passe).

# uOttawa Consent Information Addendum- COVID-19 Risks

**Principal Investigator**: Mohammadhossein Akhavanfar

**Study Title**: Developing and validating new musculoskeletal models of the spine driven by two new marker-less technologies

**Please note that a Word version of this form can be requested to the Office of the Vice-Dean, Research of your faculty.**

Please read the following statements carefully and feel free to ask questions if anything seems unclear.

We are putting in place safety precautions to reduce exposure to COVID-19, but the risk of exposure can still exist. COVID-19 can result in severe illness, medical expenses, and loss of income and in some cases, death.

If you are considered vulnerable to the effects of COVID-19 (e.g., an older adult; underlying medical conditions or a compromised immune system), please discuss your participation with the research team before consenting to participate.

**If you are feeling unwell or experiencing any potential COVID-19 symptoms leading up to the research session, please stay home and notify the research team that you cannot attend. Should you experience symptoms in days following the session, please also notify the research team.**

Potential COVID-19 symptoms include: new or worsening cough, shortness of breath or difficulty breathing, temperature equal to or over 38C (100.4F), feeling feverish, chills, fatigue or weakness, muscle or body aches, new loss of smell or taste, headache, gastrointestinal symptoms (abdominal pain, diarrhea, vomiting), or feeling very unwell.

**To reduce the possibility of COVID-19, we have implemented the following safety procedures.**

- Regular handwashing
- Using hand sanitizer when handwashing is not possible.
- Wearing of face masks/face coverings
- Physical distancing (as recommended by the local health authority)
- Limiting shared material and documents (pens, paper)
- Sanitizing surfaces and shared equipment
- Waiting 24h between each session
- Using face shields or goggles
- Using lab coats
- Collecting personal contact information for contact-tracing purposes

Please advise a researcher if you believe a safety measure is not being taken, or that your safety is atrisk.

**Considerations for the Participant:**

We ask that you:

- Wear a mask or face covering. Masks will be provided by the researcher if you do not have one. If you feel that you are unable to wear a mask, discuss your participation with the research team.
- Complete a screening assessment before each research session.
- Wash or sanitize your hands upon arrival. Hand sanitizer will be provided or a washing station will be available.
- Maintain physical distancing to the extent possible during the in-person research activities.

We ask that you follow the health-related directives above for your safety and the safety of the researchers.

**Information for Contact Tracing**

We are collecting personal contact information for contact-tracing purposes, in the event that you may have been exposed to COVID-19 at the research site.

Your name and contact information:

- Will not be stored with the research data.
- Will always be securely stored.
- Will only be used if requested by Public Health authorities for COVID-19 contact tracing purposes.
- Will be held only for the time required by Public Health authorities.

**Right to Withdraw**

You are under no obligation to participate. You can stop participating or withdraw from the study at any time by notifying the researcher using the contact information above.

Thank you for your interest and participation.

**Information for Contact Tracing (to be kept separately from research documents)**

This information:

- will not be stored with the study data;
- will always be securely stored;
- will be used only if requested by public health to provide this information for COVID-19 contact tracing purposes; and
- will be held only for the time required by public health authorities.

Name (please print):_____(required)

Phone:_____(required)

Email:_____(optional)

Name (please print):_____(required)

Phone:_____(required)

Email:_____(optional)

Date: _____

# Advenant au formulaire de consentement pour la COVID-19

**Chercheuse ou chercheur principal :** Mohammadhossein Akhavanfar, Département de l'activité physique

**Titre du projet :** Developing and validating new musculoskeletal models of the spine driven by two new marker-less technologies

Veuillez lire attentivement les informations contenues dans ce document et veuillez poser toute question de clarification.

Nous mettons en place des mesures de sécurité pour réduire l'exposition à la COVID-19, mais le risque d'exposition peut toujours exister. La COVID-19 peut entraîner une maladie grave, des frais médicaux, une perte de revenu et, dans certains cas, la mort.

Si vous considérez que vous appartenez à un groupe vulnérable par rapport à la COVID-19 (p. ex. une personne âgée, des conditions médicales sous-jacentes, un système immunitaire affaibli), veuillez discuter de votre participation avec l'équipe de recherche avant d'accepter.

**Si, avant la session, vous ne vous sentez pas bien ou si vous présentez des symptômes potentiels de la COVID-19, restez à la maison et informez l'équipe de recherche que vous ne pouvez pas vous présenter. Veuillez également informer l'équipe de recherche si vous avez des symptômes dans les jours qui suivent votre participation.**

Les symptômes de la COVID-19 peuvent inclure : l'apparition ou l'aggravation d'une toux, l'essoufflement ou des difficultés respiratoires, une température égale ou supérieure à 38°C, une sensation de fièvre, des frissons, de la fatigue ou des faiblesses, des douleurs musculaires ou des courbatures, la perte de l'odorat ou du goût, le mal de tête, des symptômes gastro-intestinaux (douleur abdominale, diarrhée, vomissements), ou des malaises intenses.

**Afin de réduire le risque de contracter la COVID-19, nous avons mis en place les mesures suivantes :**

- ☐ Lavage régulier des mains
- ☐ Utilisation d'un désinfectant à mains s'il est impossible de se laver les mains
- ☐ Port d'un masque/couvre-visage
- ☐ Distanciation physique (selon les recommandations de la Santé publique locale)
- ☐ Limitation du partage de matériel et de documents (stylos, documents papier)
- ☐ Désinfection des surfaces et de l'équipement

- ☒ Période tampon de 1440 minutes entre chaque séance
- ☒ Utilisation d'écrans faciaux ou de lunettes de protection
- ☒ Port du sarrau
- ☐ Installation de barrières de plexi-verre
- ☒ Obtention de coordonnées personnelles pour fins de recherche de contacts
- ☐ Autre :

Veuillez aviser un chercheur si vous croyez que les mesures appropriées ne sont pas en place, ou si vous croyez que vous n'êtes pas en sécurité.

**Considérations pour le participant :**

Nous vous demandons de :

- Veiller à porter un masque ou un couvre-visage. Si vous n'avez pas un masque, le chercheur vous en fournira un. Si vous croyez que vous ne pouvez pas porter de masque, veuillez discuter de votre participation avec l'équipe de recherche.
- Remplir un questionnaire d'évaluation de la santé avant chaque visite.
- Laver ou désinfecter vos mains à l'arrivée. Un désinfectant pour les mains sera fourni ou une station de lavage sera disponible.
- Maintenir la distanciation physique dans la mesure du possible pendant les activités de recherche en personne.

Nous vous demandons de suivre ces directives liées à la santé pour votre sécurité et celle des chercheurs.

**Information pour recherche de contacts**

Nous recueillons des informations personnelles pour des fins de recherche de contacts, dans l'éventualité où vous aurez été exposé au virus de la COVID-19 sur le lieu de la recherche.

Votre nom et vos coordonnées :

- Ne seront pas conservés avec les données de recherche
- Seront conservés de façon sécuritaire
- Seront partagés seulement s'il y a une demande de la part de la Santé publique, pour des fins de recherche de contacts
- Seront détruits dès que ceci est permis par la Santé publique.

**Droit de se retirer de la recherche**

Vous n'êtes pas obligé de participer à cette recherche. À tout moment, vous pouvez cesser de participer ou vous retirer de l'étude en informant le chercheur (coordonnées ci-dessus).

Merci pour votre intérêt et votre participation.

**Information pour recherche de contacts** [Instructions : détacher cette section et la conserver séparée des données de recherche]

Cette information :

- Sera conservée de façon sécuritaire
- Ne sera pas conservée avec les données de recherche
- Sera partagée seulement s'il y a une demande de la part de la santé publique, pour des fins de recherche de contacts
- Sera détruite dès que la santé publique le permet

Nom (écrire en lettres moulées) : _____

Numéro de téléphone : _____

Courriel : _____

Date : _____